



THE HONG KONG
POLYTECHNIC UNIVERSITY

香港理工大學

Pao Yue-kong Library
包玉剛圖書館

Copyright Undertaking

This thesis is protected by copyright, with all rights reserved.

By reading and using the thesis, the reader understands and agrees to the following terms:

1. The reader will abide by the rules and legal ordinances governing copyright regarding the use of the thesis.
2. The reader will use the thesis for the purpose of research or private study only and not for distribution or further reproduction or any other purpose.
3. The reader agrees to indemnify and hold the University harmless from and against any loss, damage, cost, liability or expenses arising from copyright infringement or unauthorized usage.

If you have reasons to believe that any materials in this thesis are deemed not suitable to be distributed in this form, or a copyright owner having difficulty with the material being included in our database, please contact lbsys@polyu.edu.hk providing details. The Library will look into your claim and consider taking remedial action upon receipt of the written requests.

Development of a Geographic Information System (GIS) for Managing and Predicting Coastal Water Quality in the Pearl River Estuary (South China)

Sandy Man-Yi Ng

A thesis

submitted in partial fulfilment of the requirements
for the Degree of Master of Philosophy

Department of Civil and Structural Engineering
The Hong Kong Polytechnic University
July 2006



Pao Yue-kong Library
PolyU · Hong Kong

Certificate of Originality

I hereby declare that this thesis is my own work and that, to the best of my knowledge and belief, it reproduces no material previously published or written nor material which has been accepted for the award of any other degree or diploma, except where due acknowledgement has been made in the text.

Signed

Sandy Man-Yi Ng

Abstract

The Pearl River Estuary (PRE), in recent decades, has experienced serious water quality deterioration due to the massive economic and industrial developments in the nearby regions. Mitigation of this situation begins with a good quantitative understanding of the existing hydrodynamic and environmental conditions. Geographic Information System (GIS), with its ability to handle large quantities of geographically-referenced hydrodynamic and water quality information as well as to visualize spatial relationships, has been identified as a plausible tool for this task. However, limited research has been conducted on the development of a GIS for hydrodynamic and water quality applications, particularly for integrations with models which facilitate three-dimensional (3D), dynamic simulations. This has provided the motivation for the development of a tool using GIS technology in 3D hydrodynamic-water quality modelling to assist engineers and decision makers in managing and predicting water quality in the PRE.

The GIS-based hydrodynamic-water quality tool for the PRE in this study is developed using the ArcView GIS software package. The developed GIS consists of three main components. The first component involves the compilation of a GIS database of hydrodynamic and water quality data and the development of a set of data retrieval and visualization functions. The compilation of the GIS database has unified hydrodynamic and water quality field-collected data into a single management platform for efficient retrieval and query of information for the PRE. The developed data display tools have resolved the challenge of dealing with 3D, dynamic marine data in a GIS environment by supplementing the time series, profile, as well as dynamic display. In addition, the interpolation functions combining both spatial and one-dimensional (1D) data-fitting techniques adopted in this study have accounted for the typically temporally and spatially scattered field data.

The second component involves the integration of the GIS with a 3D finite element hydrodynamic-water quality coupled model based on the *interface integration* method. A pre-processor component is developed for analyzing and exporting GIS data to model input files, while a post-processor component is for importing the model output and displaying it in the GIS interface. Similar data displaying functionality for field data is extended for visualization of model input and results. In addition, the integrated-GIS is also customized for generating the setup of model mesh grid and for carrying out

refinements. Successful integration of the GIS with the hydrodynamic-water quality coupled model has allowed the mutual exchange of field-collected and model data, and thus provides support for various useful applications, such as setting of model initial conditions, calibration and verification of the model, and assessment of quality of the collected data.

The third component involves the incorporation of an environmental impact assessment (EIA) module into the system for evaluation of water quality conditions based on either field-collected data or model-predicted results. This module makes use of the GIS *Map Algebra* functions to combine raster layers of different parameters into a single raster of water quality index. The resulting spatial layer provides an overall picture of the areas potentially at risk.

This newly developed integrated-GIS is a comprehensive tool for coastal management, research, and decision-making. This system provides a wide range of applications including retrieval and visualization of 3D, dynamic marine data, viewing and modification of model input, display of model output, estimation of unknown points in space and time, investigation of temporal and spatial trends, assessment of quality of the collected data, and management of wastewater disposal. In the future, the system can be shared with other domains in the field and thus promote better understanding and management of the PRE.

Acknowledgements

I would like to express my sincere gratitude to my chief supervisor Dr. Onyx W. H. Wai for his guidance throughout this research. His insights and encouragement in conducting independent scientific research are important to the success of this project. I would also like to thank my co-supervisor Prof. Y. S. Li for giving me the opportunity to study at The Hong Kong Polytechnic University.

Special thanks are extended to Dr. Y.W. Jiang not only for his assistance in helping me learn the usage of the hydrodynamic model, but also for his hospitality during my stay in Xiamen. Thanks are also due to Xu Zhan Hua, who has provided all the technical programming support I desperately needed for the development of the GIS. I would also like to express special thanks to Mrs. Anson for perfecting my thesis to “elegant” technical form.

Thanks also go to the Hong Kong Research Grants Council and the Hong Kong Polytechnic University for the financial support. I am also grateful to all colleagues and friends who have given me support and help during my study. I wish them success in the future years.

Above all, I am deeply thankful to my family for their endless love, care, and support in no matter what I choose to pursue in life.

TABLE OF CONTENTS

Certificate of Originality	ii
Abstract	iii
Acknowledgements.....	v
List of Figures	ix
List of Tables	xvi
List of Abbreviations.....	xvii
1 Introduction	1
1.1 Background.....	1
1.2 Research Motivation	2
1.3 Objectives	3
1.4 Scope of Work	3
1.5 Outline of Thesis	5
2 Literature Review.....	7
2.1 Overview.....	7
2.2 Applications of GIS in Marine and Coastal Environment.....	7
2.3 Study Area.....	14
2.4 Summary	15
3 Development of an Integrated-GIS for the PRE	16
3.1 GIS Software.....	16
3.2 Concept of PRE_WAGIS.....	17
3.3 Summary	23
4 GIS Database	24

4.1	Collected Data.....	24
4.1.1	CEDD Project – Agreement no. CE32/96	27
4.1.2	EPD Marine Water and Sediment Quality Monitoring.....	28
4.1.3	EPD Project – Agreement no. CE 42/97	29
4.1.4	PREPP	30
4.1.5	WAHMO 1990 Data Collection	31
4.1.6	WAHMO 1992 Data Collection	31
4.1.7	HKO	33
4.2	Database System	33
4.2.1	Application of Relational Database System for GIS.....	33
4.2.2	Structure of Database System.....	34
4.3	Summary	35
5	Development of Data Retrieval and Visualization Tools	36
5.1	Marine Data Retrieval and Visualization.....	36
5.2	Data Retrieval.....	37
5.2.1	Application of OLE Technology.....	37
5.2.2	Data Framework for Database Metadata Management.....	37
5.3	Station Display	38
5.4	Data Displays	39
5.4.1	Spatial Layer	40
5.4.2	Time Series and Profile	42
5.5	Data Interpolation	43
5.5.1	Spatial Interpolation.....	43
5.5.2	Temporal and Profile Interpolation	44
5.5.3	Tempo-spatial and Profile-spatial Interpolation.....	50
5.6	Interactive Data Display Tools.....	51
5.6.1	Dynamic Time Series Display	53
5.7	Find Tables Function.....	54
5.8	Summary	55
6	Integration with a Hydrodynamic-Water Quality Coupled Model	56
6.1	GIS-Model Integration	56
6.2	3D Hydrodynamic-Water Quality Coupled Model	56
6.2.1	Governing Equations	57
6.2.1.1	Base Model.....	57
6.2.1.2	Cohesive Sediment Transport Model	59
6.2.1.3	Heavy Metal Transport Model.....	60
6.2.2	Operational Platform.....	62
6.3	Integration Method	62
6.4	Model Pre-processing	63
6.4.1	Retrieval and Editing of Model Input Data	63
6.4.2	Setting Initial Conditions from Spatial Layer.....	65
6.4.3	Model Input Display.....	67
6.4.3.1	Spatial Layer.....	67
6.4.3.2	Time Series and Profile	70
6.4.4	Mesh Grid Configuration.....	72
6.5	Model Post-processing.....	78

6.6	Extensibility of Interpolation Functions and Interactive Tools for Model Data	81
6.7	Summary	82
7	Applications of the Integrated-GIS.....	83
7.1	System Applications	83
7.2	Estimation of Values at Unknown Points in Space and Time.....	83
7.3	Evaluation of Interpolation Methods.....	87
7.3.1	1D Interpolation Methods.....	87
7.3.1.1	Time series	87
7.3.1.2	Profile.....	92
7.3.2	Spatial Interpolation Methods.....	98
7.4	Investigation of Temporal and Spatial Trends.....	101
7.5	Assessment of Quality of the Collected Data	109
7.6	Calibration and Verification of the Hydrodynamic-Water Quality Coupled Model.....	113
7.7	Setting of Model Initial Conditions	116
7.8	Management of Wastewater Disposal	118
7.9	Summary	120
8	Development of an EIA Module for Water Quality Assessment	123
8.1	Application of GIS in EIA for Water Quality Evaluation	123
8.1.1	WQI	124
8.1.2	Deriving WQI Using Aggregation Function.....	124
8.1.2.1	Water Quality Variables and Rating Curves.....	127
8.1.2.2	Aggregation Functions	139
8.2	Identification of Areas Most Vulnerable to Environmental Impact.....	140
8.3	Assessment of the Relative Importance of Parameters	148
8.4	Investigation of Temporal Patterns and Trends	154
8.5	Prediction of Future Hydrodynamics and Water Quality.....	163
8.6	Summary	163
9	Conclusions and Recommendations	165
9.1	Conclusions	165
9.2	Recommendations	167
	References.....	170

List of Figures

Figure 2.1 The Pearl River Estuary.	14
Figure 3.1 Conceptual diagram of the GIS-hydrodynamic integrated system.....	18
Figure 3.2 Customized ArcView interface incorporated with five new menus.	20
Figure 3.3 Menu structure: Data.....	20
Figure 3.4 Menu structure: Interpolate.	21
Figure 3.5 Menu structure: Model.....	22
Figure 3.6 Menu structure: Results.	23
Figure 3.7 Menu structure: EIA.	23
Figure 4.1 Database relationship diagram - field data.....	35
Figure 5.1 Data framework diagram.	38
Figure 5.2 Dialog box for creating a station layer.	39
Figure 5.3 Station layer for station_Water_EPD station table.....	39
Figure 5.4 Data display.....	40
Figure 5.5 Dialog box for creating single spatial layer.	41
Figure 5.6 System procedures for creating a spatial layer.	41
Figure 5.7 Dialog box for creating time series.	42
Figure 5.8 Dialog box for creating profile.	43
Figure 5.9 Temporal and profile interpolation.....	44

Figure 5.10	Dialog box for fitting of time series tidal data by input of tidal constituents.....	48
Figure 5.11	Tempo-spatial and profile-spatial interpolation.	51
Figure 5.12	Profile plot display tool.	52
Figure 5.13	Section plot display tool.	53
Figure 5.14	Dynamic time series display tool.	54
Figure 5.15	Dialog box for <i>Find Tables By Parameter</i> function.	54
Figure 5.16	Dialog box for <i>Find Tables By Time</i> function.....	55
Figure 6.1	Computation flow of the three-dimensional hydrodynamic sediment and heavy transport numerical model (Jiang, 2003).....	57
Figure 6.2	Data flow diagram for model input retrieval and editing.....	64
Figure 6.3	Dialog box for initial conditions of velocity.	64
Figure 6.4	Dialog box for updating input files.....	65
Figure 6.5	Dialog box for setting initial conditions from existing spatial layer.....	66
Figure 6.6	System procedures for setting initial conditions from spatial layer.....	66
Figure 6.7	A spatial layer overlaying the model mesh of nodal points.	67
Figure 6.8	Dialog box for creating single spatial layer – model input.....	68
Figure 6.9	System procedures for creating a spatial layer – model input.	68
Figure 6.10	Database relationship diagram – model input data.	69
Figure 6.11	Display of a spatial point layer of water depth from model input in GIS.....	70
Figure 6.12	Dialog box for creating time series – model input.	71
Figure 6.13	Dialog box for creating profile – model input.	72
Figure 6.14	Typical configuration for a triangular element.....	73
Figure 6.15	Dialog box for configuring mesh grid.	73
Figure 6.16	Mesh grid generation.	74
Figure 6.17	System procedure for generating a mesh grid setup.	75
Figure 6.18	Mesh grid shapefiles in GIS interface.....	75
Figure 6.19	Procedure for editing mesh grid.	77
Figure 6.20	Mesh grid edit session.	77
Figure 6.21	End of mesh grid edit session.	78
Figure 6.22	Re-configured mesh grid after edit session.	78

Figure 6.23 Data flow diagram for model result retrieval	79
Figure 6.24 Dialog box for updating output file.....	79
Figure 6.25 Dialog box for creating a single spatial layer.....	80
Figure 6.26 System procedures for creating a spatial layer – model results.....	80
Figure 6.27 System procedures for creating a time series – model results.....	81
Figure 7.1 Repulse Bay Beach and fixed stations for measurement table WQ2_Water_EPD.....	85
Figure 7.2 Time Series for E. coli from measurement table WQ2_Water_EPD - station ID: SM2 – depth: surface - fitted using Linear Spline method.	85
Figure 7.3 Interpolate time series for station SM2 – surface, August 5, 2003.....	86
Figure 7.4 Tempo-spatial layer of E. coli from measurement table WQ2_Water_EPD - August 5, 2003 – depth level: surface.	86
Figure 7.5 Tempo-spatial layer of E. coli from measurement table WQ2_Water_EPD - August 5, 2003 - classified based on Hong Kong beach water quality standards.....	87
Figure 7.6 Time series for tidal level from measurement table tide_dry_CEDD_CE3296 – station ID: 1 – fitted using trigonometric (four principal constituents: M2, S2, O1, and K1) function.	88
Figure 7.7 Time series for tidal level from measurement table tide_wet_CEDD_CE3296 – station ID: 1 – fitted using trigonometric (four principal constituents: M2, S2, O1, and K1) function.	88
Figure 7.8 Time series for current speed from current_dry_spring_CEDD_CE3296 – station ID: 3 – depth: 1 m below surface – fitted using trigonometric (four principal constituents: M2, S2, O1, and K1) function.....	89
Figure 7.9 Time series for current direction from current_dry_spring_CEDD_CE3296 – station ID: 3 – depth: 1 m below surface.....	89
Figure 7.10 Time series for temperature from measurement table WQ1_wet_spring_CEDD_CE3296 - station ID: 1 – depth: surface – fitted using 6 th polynomial and trigonometric (three tidal constituents: M2, S2, and K2) functions.....	89
Figure 7.11 Time series for temperature from measurement table WQ2_Water_EPD – station ID: DM1 – depth: surface – fitted using 4 th polynomial and trigonometric (one frequency: 1 degree/day) functions.	90
Figure 7.12 Time series for salinity from measurement table WQ1b_dry_neap_CEDD_CE3296 – station ID: 2 – depth: surface – fitted using 6 th polynomial and trigonometric (three tidal constituents: M2, S2, and K2) functions.....	90
Figure 7.13 Time series for salinity from measurement table WQ2_Water_EPD – station ID: DM1 – depth: surface – fitted using 6 th polynomial and trigonometric (one frequency: 1 degree/day) functions.....	90
Figure 7.14 Time series for DO from measurement table WQ2_Water_EPD - station ID: DM1 – depth: surface -fitted using Linear and Natural Neighbour Spline methods.....	91

Figure 7.15	Time series for turbidity from measurement table WQ2_Water_EPD - station ID: DM1 – depth: surface -fitted using Linear and Natural Neighbour Spline methods. .91	.91
Figure 7.16	Time series for pH from measurement table WQ2_Water_EPD - station ID: DM1 – depth: surface -fitted using Linear and Natural Neighbour Spline methods.....91	.91
Figure 7.17	Time series for chlorophyll a from measurement table WQ2_Water_EPD - station ID: DM1 – depth: surface -fitted using Linear and Natural Neighbour Spline methods. 91	91
Figure 7.18	Time series for total nitrogen from measurement table WQ2_Water_EPD - station ID: DM1 – depth: surface -fitted using Linear and Natural Neighbour Spline methods. .92	.92
Figure 7.19	Time series for total phosphorus from measurement table WQ2_Water_EPD - station ID: DM1 – depth: surface -fitted using Linear and Natural Neighbour Spline methods.....92	92
Figure 7.20	Time series for BOD from measurement table WQ2_Water_EPD - station ID: DM1 – depth: surface -fitted using Linear and Natural Neighbour Spline methods.92	92
Figure 7.21	Time series for E. coli from measurement table WQ2_Water_EPD - station ID: DM1 – depth: surface -fitted using Linear and Natural Neighbour Spline methods.92	92
Figure 7.22	Profile for current speed from measurement table ADP_wet_CEDD_CE3296 – station ID: 1 – time: 7/14/1998 5:30:00 PM – fitted using 6th degree polynomial, logarithmic, exponential, and power functions.93	93
Figure 7.23	Profile of current direction from measurement table ADP_wet_CEDD_CE3296 – station ID: 1 – time: 7/14/1998 5:30:00 PM – fitted using 6 th degree polynomial function.93	93
Figure 7.24	Profile of temperature from measurement table CTD_dry_CEDD_CE3296 – station ID: 1 – time: 3/9/1998 5:00:06 PM – fitted using 6 th degree polynomial, logarithmic, exponential, and power functions.94	94
Figure 7.25	Profile of salinity from measurement table CTD_dry_CEDD_CE3296 – station ID: 1 – time: 3/9/1998 8:01:31 PM – fitted using 3 rd degree polynomial and exponential functions.94	94
Figure 7.26	Profile of turbidity from measurement table CTD_dry_CEDD_CE3296 – station ID: 1 – time: 3/9/1998 5:00:06 PM – fitted using 3 rd degree polynomial function.95	95
Figure 7.27	Profile of DO from measurement table DO_dry_spring_CEDD_CE3296 – station ID: 1 – time: 3/19/1998 12:00:00 PM – fitted using 3 rd degree polynomial function, and Linear Spline and Natural Neighbour Spline methods.....95	95
Figure 7.28	Profile of pH from measurement table WQ1_wet_neap_CEDD_CE3296 – station ID: 1 – time: 7/4/1998 12:00:00 PM – fitted using 3 rd degree polynomial function, and Linear Spline and Natural Neighbour Spline methods.....96	96
Figure 7.29	Profile of chlorophyll a from measurement table WQ4_wet_neap_CEDD_CE3296 – station ID: 1 – time: 7/4/1998 12:00:00 PM – fitted using 4 th degree polynomial function, and Linear Spline and Natural Neighbour Spline methods.....96	96
Figure 7.30	Profile of total nitrogen from measurement table WQ2_dry_spring_CEDD_CE3296 – station ID: 1 – time: 3/13/1998 7:30:00 AM – fitted using 2 nd degree polynomial function, and Linear Spline and Natural Neighbour Spline methods.....96	96

Figure 7.31 Profile of total phosphorus from measurement table WQ2_dry_spring_CEDD_CE3296 – station ID: 1 – time: 3/13/1998 7:30:00 AM – fitted using 2 nd degree polynomial function, and Linear Spline and Natural Neighbour Spline methods.....	97
Figure 7.32 Profile of BOD from measurement table WQ4_wet_neap_CEDD_CE3296 – station ID: 1 – time: 7/4/1998 12:00:00 PM – fitted using 3 rd degree polynomial function, and Linear Spline and Natural Neighbour Spline methods.....	97
Figure 7.33 Profile of E. coli from measurement table WQ4_wet_neap_CEDD_CE3296 – station ID: 1 – time: 7/4/1998 12:00:00 PM – fitted using 3 rd degree polynomial function, and Linear Spline and Natural Neighbour Spline methods.....	97
Figure 7.34 Cross validation analysis using ArcGIS Geostatistical Analyst extension.	98
Figure 7.35 Dynamic display of spatial layers for pH at water level: surface.	104
Figure 7.36 Dynamic display of spatial layers for pH at water level: middle.....	105
Figure 7.37 Dynamic display of spatial layers for pH at water level: bottom.	106
Figure 7.38 Dynamic display of time series for pH at water level: surface.....	107
Figure 7.39 Dynamic display of time series for pH at water level: middle.....	107
Figure 7.40 Section display of pH in Deep Bay.....	108
Figure 7.41 Fixed stations for measurement table WQlab_BW_PkgB_EPD_CE4297.....	110
Figure 7.42 Predicted spatial layers for suspended solids for datasets WQ2_Water_EPD and WQlab_BW_PkgB_EPD_CE4297, and percentage difference.	112
Figure 7.43 Tidal stations for model calibration and model mesh grid configuration.....	114
Figure 7.44 Procedure for adjusting nodal point for WAG station.....	115
Figure 7.45 Identification of node number 5793 for WAG station.....	116
Figure 7.46 Tempo-spatial layer of salinity from measurement table WQ2_Water_EPD – November 1, 2003 – depth level: surface.	117
Figure 7.47 Dialog box for setting initial conditions for salinity – layer 1 from an existing layer.....	117
Figure 7.48 A spatial layer of salinity after setting initial condition from an existing layer.....	118
Figure 7.49 Tempo-spatial layer of turbidity from measurement table WQ2_Water_EPD – December 1, 2003 – depth level: surface.	120
Figure 8.1 Application of <i>Map Algebra</i> operations for deriving a WQI spatial layer.	124
Figure 8.2 Rating curve for dissolved oxygen in mg/L.....	130
Figure 8.3 Rating curve for dissolved oxygen in %.....	131
Figure 8.4 Rating curve for biochemical oxygen demand in mg/L.	132
Figure 8.5 Rating curve for nitrogen in mg/L.	133

Figure 8.6 Rating curve for phosphorus in mg/L.....	133
Figure 8.7 Rating curve for faecal coliform in no/100 mL.....	134
Figure 8.8 Rating curve for pH.....	135
Figure 8.9 Rating curve for temperature in degree Celsius.....	136
Figure 8.10 Rating curve for turbidity in NTU.....	137
Figure 8.11 Rating curve for suspended solids in mg/L.....	137
Figure 8.12 Rating curve for toxicants.....	138
Figure 8.13 Rating curve for chlorophyll in mg/m ³	139
Figure 8.14 Tempo-spatial layers from measurement table WQ2_Water_EPD - August 1, 2003 – depth level: surface.....	142
Figure 8.15 Dialog box for creating WQI layer.....	144
Figure 8.16 WQI spatial layer – August 1, 2003 - Weighted Arithmetic Mean.....	145
Figure 8.17 WQI spatial layer - August 1, 2003 - Weighted Geometric Mean.....	145
Figure 8.18 WQI spatial layer - - August 1, 2003 - Harmonic Mean of Square.....	146
Figure 8.19 WQI spatial layer - - August 1, 2003 - Minimum Operator.....	146
Figure 8.20 WQI spatial layer - - August 1, 2003 - Swamee and Tyagi.....	147
Figure 8.21 Water quality subindex spatial layer – August 1, 2003 – DO.....	149
Figure 8.22 Water quality subindex spatial layer – August 1, 2003 – BOD.....	149
Figure 8.23 Water quality subindex spatial layer – August 1, 2003 – total nitrogen.....	150
Figure 8.24 Water quality subindex spatial layer – August 1, 2003 – total phosphorus.....	150
Figure 8.25 Water quality subindex spatial layer – August 1, 2003 – F. coli.....	151
Figure 8.26 Water quality subindex spatial layer – August 1, 2003 – pH.....	151
Figure 8.27 Water quality subindex spatial layer – August 1, 2003 – temperature.....	152
Figure 8.28 Water quality subindex spatial layer – August 1, 2003 – turbidity.....	152
Figure 8.29 Water quality subindex spatial layer – August 1, 2003 – suspended solids.....	153
Figure 8.30 Water quality subindex spatial layer – August 1, 2003 – chlorophyll a.....	153
Figure 8.31 WQI spatial layer – February 1, 1998 – Harmonic Mean of Square.....	155
Figure 8.32 WQI spatial layer – August 1, 1998 – Harmonic Mean of Square.....	155
Figure 8.33 WQI spatial layer – February 1, 1999 – Harmonic Mean of Square.....	156
Figure 8.34 WQI spatial layer – August 1, 1999 – Harmonic Mean of Square.....	156

Figure 8.35 WQI spatial layer – February 1, 2000 – Harmonic Mean of Square.	157
Figure 8.36 WQI spatial layer – August 1, 2000 – Harmonic Mean of Square.....	157
Figure 8.37 WQI spatial layer – February 1, 2000 – Harmonic Mean of Square.	158
Figure 8.38 WQI spatial layer – August 1, 2000 – Harmonic Mean of Square.....	158
Figure 8.39 WQI spatial layer – February 1, 2001 – Harmonic Mean of Square.	159
Figure 8.40 WQI spatial layer – August 1, 2001 – Harmonic Mean of Square.....	159
Figure 8.41 WQI spatial layer – February 1, 2002 – Harmonic Mean of Square.....	160
Figure 8.42 WQI spatial layer – August 1, 2002 – Harmonic Mean of Square.....	160
Figure 8.43 WQI spatial layer – February 1, 2003 – Harmonic Mean of Square.	161
Figure 8.44 WQI spatial layer – August 1, 2003 – Harmonic Mean of Square.....	161
Figure 8.45 Selected fixed stations for extracting values from WQI layers.....	162
Figure 8.46 WQI at selected fixed stations for dry season (February 1).....	163
Figure 8.47 WQI at selected fixed stations for dry season (August 1).	163

List of Tables

Table 2.1 Literature review in application of GIS in coastal and marine environment.	11
Table 2.2 Coastal-related GIS software.	13
Table 4.1 Variables included in the collected hydrodynamic and water quality data.	25
Table 5.1 Summary of tidal constituents, descriptions, and frequencies included in module.	49
Table 7.1 Standards for water quality control at bathing beaches in Hong Kong.	86
Table 7.2 Selected datasets for spatial interpolation method evaluation.	99
Table 7.3 Results of prediction error mean and root-mean square from cross validation.	100
Table 7.4 Recommended spatial interpolation method(s).	101
Table 7.5 Water control zone.	101
Table 7.6 Measurement tables selected for model calibration of tidal data.	113
Table 8.1 Summary of Water Quality Objectives (WQOs) for marine waters of Hong Kong – Environmental Protection Department (EPD) of Hong Kong.	126
Table 8.2 Summary of water quality variables and their respective rating curves included in the EIA module.	128
Table 8.3 Aggregation functions.	140
Table 8.4 Selected rating curves for sample application.	144
Table 8.5 WQI at sample location on upper end of the Deep Bay.	147
Table 8.6 WQI at selected fixed stations for dry season.	162
Table 8.7 WQI at selected fixed stations for dry season.	162

List of Abbreviations

1D	One-dimensional
2D	Two-dimensional
3D	Three-dimensional
ADCIRC	ADvanced CIRCulation Multi-dimensional Hydrodynamic Model
ADCP	Acoustic Doppler Current Profiler
ASA	Applied Science Associates, Inc.
BASINS	Better Assessment Science Integrating point and Nonpoint Sources
CEDD	Civil Engineering and Development Department
COM	Component Object Model
CTD	Cell Transfer Delay
DBF	Database File
DDE	Dynamic Data Exchange
DHI	Danish Hydraulic Institute
DLL	Dynamic Link Library
EGS	Electronic and Geophysical Services Limited
EIA	Environmental Impact Assessment
EMSI	Environmental Modelling Systems, Incorporated
EPD	Environmental Protection Department
EPM	Efficient Parallel Numerical Model
ESRI	Environmental Systems Research Institute, Inc.
FESWMS	Finite Element Surface Water Modelling System
GIS	Geographic Information System

GQA	Geo-data Quality Analysis
HEC-RAS	Hydrologic Engineering Centers River Analysis System
HKO	Hong Kong Observatory
HKUST	Hong Kong University of Science and Technology
IAC	Inter Application Communication
IDW	Inverse Distance Weighted
OLE	Object Linking and Embedding
MGIS	Marine Geographic Information System
MS	Microsoft
MPI	Message Passing Interface
POM	Princeton Ocean Model
PRD	Pearl River Delta
PRE	Pearl River Estuary
PRE_WAGIS	Pearl River Estuary Water Geographic Information System
PREPP	Pearl River Estuary Pollution Project
RMS	Root-Mean-Square of deviation
SMS	Surface Water Modelling System
SOA	State Oceanic Administration People's Republic of China
SQL	Structure Query Language
TXT	Text
US EPA	US Environmental Protection Agency
VB	Visual Basic
VBA	Visual Basic for Application
WCZ	Water Control Zone
WQI	Water Quality Index
WQOs	Water Quality Objectives

1 Introduction

1.1 Background

The Pearl River Estuary (PRE), in recent decades, has experienced serious water quality deterioration due to the massive economic and industrial developments in the nearby regions. Understanding of the existing hydrodynamic and environmental conditions is the first step to mitigating this situation. This will require a huge quantity of geographically-referenced information gathered from various sources. Geographic information system (GIS), with its capability to store, organize, manipulate, retrieve, and display geographically-referenced information, can unify the different kinds of data into one manageable database system, providing efficient access and mapping of data for engineers and researchers. By putting spatial data in a GIS environment, various spatial analysis techniques can be employed to find patterns and relationships previously not recognized (Bernhardsen, 2002; Clark, 2001; Delaney, 1999; Demers, 2000). In addition, by linking a GIS with a hydrodynamic numerical model for wastewater discharge, the integrated system will be an efficient tool not only for predicting and evaluating potential environment impacts due to coastal wastewater disposal activities, but also for assessing the accuracy of the numerical model by comparing field-collected data and model-generated results.

Although GIS is demonstrated to be an invaluable asset in hydrodynamics, there are relatively few such applications, particularly for integrations with models which facilitate three-dimensional (3D) simulations. Perhaps one of the reasons behind this is the difficulty in establishing a rigorous model to represent the ever-changing nature of marine environment. Marine environmental data exhibit variation not only in both location and depth, but also through time (Lucas, 2000). Most of the current hydrodynamic-GIS models so far are limited to two-dimensional (2D) capabilities. An example is the IDOR 2D which is a closely-coupled depth-averaged model for simulation of pollutant transports (Tsanis and Boyle, 2001). Since hydrodynamics is intrinsically 3D and dynamic, such models oversimplify the real situations and generate results with limited accuracy. While the fundamental concept of GIS is mapping of information in 2D ground, there is considerable challenge in unfolding this two dimensionality for application into the three and four-dimensional world.

Another aspect which inhibits greater use of GIS in hydrodynamics is the difficulty of collecting marine and coastal data. In general, two approaches are used to obtain marine-related data. One involves performing actual field surveys and measurements, from deploying shipboard instrument, or by means of automatic data loggers at fixed monitoring stations. However, such means of data collection, requiring expertise in both equipment and skills, are inevitably costly and time-consuming. A second approach is to gather data from existing sources. This may include data derived from published or archived materials, such as maps and graphs, on-site observations, and satellite images, provided by public and commercial domains. Although acquisition of these data is usually less costly, very often, due to the lack of comprehensive data documentation and metadata, the reliability of these data is in question (Bartlett, 2000).

1.2 Research Motivation

The value of applying GIS technology in hydrodynamics and water quality is mentioned in the previous section. However, its application in this field is still relatively limited. The obvious reason is the challenge in representing the 3D, dynamic marine environment with 2D GIS. The shortcoming of other research efforts in comprehensively applying GIS for coastal water quality management represents the motivation of the current research.

1.3 Objectives

The overall aim of this research project is to develop a preliminary tool to assist engineers and decision makers in managing and predicting coastal water quality in the PRE by applying GIS technology in 3D hydrodynamic-water quality modelling. The following are the subsidiary objectives:

- a) To develop a GIS database for efficient retrieval and display of field-collected hydrodynamic and water quality data
- b) To integrate the GIS with a hydrodynamic-water quality coupled model
- c) To apply the integrated system for Environmental Impact Assessment (EIA) in assessing water quality conditions

These three objectives work together in mitigating the water quality problems in the PRE. The purpose of the first objective is to improve our understanding of past trends and patterns of hydrodynamics and water quality in the PRE using historical information. On the other hand, the second objective serves to provide insights in the future conditions using predictive results. By relating what happen in the past and that in the future, better coastal management decisions can be made for the present time. Finally, the third objective offers the necessary tools to quantify the environmental impact for different situations.

1.4 Scope of Work

GIS is suggested as a potential means of dealing with the critical water quality deterioration situation in the PRE. The main scope of work is the development of a GIS-based tool for evaluating and predicting coastal water quality issues in the PRE. The work is divided into the following parts:

1) Development of a database for field-collected hydrodynamic and water quality data

Hydrodynamic and water quality information is acquired from a number of public domains and compiled into a GIS database. The sources of hydrodynamic and water quality information include large-scale field survey data collected by the Hong Kong Government. The data collection process encompasses evaluating data

quality and accuracy, and screening of what data to include and exclude in the GIS database. The GIS database is created for efficient retrieval, query, manipulation, and management of the collected data. The development of database first involves the selection of a suitable database software, followed by the design of database structure and the actual import of collected data into the database system.

2) Selection of GIS development software package

There is a wide variety of GIS development and application software products available in the market. Selecting the most suitable GIS software package begins with an assessment of the needs of this project, followed by a comparison of how the capabilities of each GIS software package may meet these needs. Other factors to consider include flexibility of the system and the cost of purchase, operation, and maintenance.

3) Customization of GIS software for data retrieval and display.

The selected GIS software is customized to adopt a new set of functions to meet the needs of this project. The additional functions include retrieval and display of collected data, temporal and spatial interpolation of data, input of required parameters and boundary conditions for model simulation, display of model results, and application for EIA.

4) Integration of the GIS with a hydrodynamic-water quality coupled model.

Before integrating the GIS with a hydrodynamic-water quality coupled model, the fundamental concepts and basic usage of the model is learnt. The methods of GIS modelling integration – the *interchange* method, the *interface integration* method, and the *total integration* method (Shamsi, 2002) – are reviewed to determine which is best-suited for this project. The integration enables the handling of pre-processing and post-processing procedures within the GIS interface. Once the GIS is linked with the hydrodynamic-water quality model, the collected data can be applied for model calibration and verification.

5) Application of the integrated system for EIA.

The collected hydrodynamic and water quality data together with the model-integrated system is an invaluable resource for conducting EIA. The GIS is further

customized to incorporate an EIA module for water quality evaluation. In the application for EIA, various techniques such as data interpolation, overlay, and *Map Algebra* are applied to the collected data for analysis of water quality trends, development of cause-effect relationships between various parameters, evaluation of the relative importance of the physical and chemical parameters, and identification of the most critical regions in the study area. Furthermore, the GIS-model integrated system can be used as a predictive tool to simulate different pollutant disposal scenarios and to evaluate whether the impacts due to the proposed coastal activity are within the environmentally acceptable limit.

1.5 Outline of Thesis

This thesis consists of nine chapters.

Chapter 2 provides a review of literature on the application of GIS in marine and coastal environment. A brief description of the study area, the PRE, is presented and a past GIS-related project on the PRE is mentioned.

Chapter 3 presents the general setup of the development of an integrated-GIS for hydrodynamics. In doing so, one of the most important procedures is to select a suitable GIS development software package. The selected software and the reasons for selection are discussed. The integrated-GIS consists of three key system components: data, model, and EIA. The conceptual configuration of the integrated-GIS as well as the new menus incorporated into the GIS are also described.

Chapters 4 and 5 present in detail the first component (i.e. data) of the integrated-GIS. The hydrodynamic and water quality data used in this thesis has been gathered from a number of public sources, and stored into a database system. The data as well as the selected software for creating a GIS database are examined in Chapter 3. After compilation of the GIS database, a linkage is established between the database and the GIS for data retrieval and display. The implementation of data retrieval and the framework for managing database metadata are discussed in Chapter 4. Different approaches developed for visualizing 3D and dynamic coastal data are also explored.

Chapter 6 presents the second component (i.e. model) of the integrated-GIS. The GIS is integrated with a hydrodynamic-water quality coupled model using the *interface*

integration method (Shamsi, 2002) for carrying out the pre-processing and post-processing tasks within the GIS interface. Modelling functionalities, including model input data retrieval, editing, and display, mesh grid configuration, model output display are considered.

Chapter 7 brings together the work done in Chapters 3, 4, and 5, by providing demonstrations on how the integrated-GIS can be applied for conducting spatial-based analysis of hydrodynamic and water quality data in a number of ways. These include estimation of values at unknown points in space and time, evaluation of the interpolation methods, investigation of temporal and spatial trends, assessment of quality of the collected data, calibration and verification of the hydrodynamic-water quality coupled model, setting of model initial conditions, and management of wastewater disposal.

Chapter 8 centres on the third component of the integrated-GIS (i.e. EIA). An EIA module is developed to evaluate the overall water quality condition based on the concept of Water Quality Index (WQI). The background theory of WQI and the previous work done in this area are reviewed. Sample applications are given for the four approaches to conducting EIA in this study. These include identification of areas most vulnerable to environmental impact, assessment of the relative importance of parameters, investigation of temporal patterns and trends, and prediction of future hydrodynamics and water quality.

Finally, Chapter 9 concludes the entire thesis and gives recommendations for future work.

Note that the integrated-GIS developed in this project is referred as the **Pearl River Estuary Water Geographic Information System (PRE_WAGIS)** throughout this thesis.

2 Literature Review

2.1 Overview

This chapter provides a review of literature relevant to the development of a GIS for coastal water quality management in the present study. As discussed in Chapter 1, there are still relatively few applications of GIS in hydrodynamics primarily due to the limitation of representing the dynamic, 3D marine environment using a fundamentally 2D mapping technology. A review of the applications of GIS, not strictly in hydrodynamics, but in a broader scope of marine and coastal environment is covered. In addition, the environmental condition of the study area, the PRE, and a past GIS-related project on the PRE are reviewed.

2.2 Applications of GIS in Marine and Coastal Environment

GIS plays an important role in deepening our understanding of the global environment with its ability to store, organize, manipulate, retrieve, and display huge quantities of geographically-referenced information. However, despite more than 70 percent of the Earth's surface is covered by water bodies, the applications of GIS so far are predominantly confined to terrestrial-based (Wright and Goodchild, 1997). One of the

main challenges in dealing with marine and coastal information using GIS is to represent the dynamic, 3D characteristic of marine environment. As Lucas (2000) suggested, marine environmental data exhibit variation not only in both location and depth, but also through time. Wright and Goodchild (1997) has also identified the other plausible reasons for the impediment of the use of GIS in oceanography including the high cost in the collection of oceanographic data, the difficulty to establish geo-referencing points during field data collection, and the sparseness of oceanographic data in one or two dimensions in compared to others.

Various GIS-based hydrodynamic models have been proposed previously; however, most of these models are limited to 2D representation. An example is the IDOR 2D, a 2D depth-averaged hydrodynamic/pollutant transport model developed by Tsanis and Boyle (2001). This model is integrated with a GIS using a closely-coupled method for data input, management and display, model processing and execution, and results presentation. Although the efficient use of GIS for handling and displaying of model inputs and outputs is demonstrated, such models with only 2D capabilities hinder the visualization and understanding of the actual dynamic, 3D hydrodynamic environment.

GIS has been applied to 3D hydrodynamic models but only specifically for the generation of bathymetric and shoreline grids, and result display rather than for complete integrations. For example, a module has been developed for IDOR3D (Tsanis et al., 2002; Naoum et al., 2003), a 3D hydrodynamic/pollutant transport model, to provide bathymetric and shoreline data input, grid generation, and result representation. Similar application has been carried out by French and Reed (1996) in their development of an environmental model system for assessing the impact of oil and chemical spills. A hydrodynamic environment consisting of 2D and 3D hydrodynamic/water quality models, a surface modelling system software, a mesh generation software, and a tidal calculation software for coastal environmental management developed by Pinho et al. (2004) has also made use of GIS for model result display. Another example is a marine geographic information system (MGIS) developed by Jiang et al. (2004). The MGIS integrates four main components - a database system, two 3D hydrodynamic numerical models, namely, the Princeton Ocean Model (POM) and the Efficient Parallel Numerical Model (EPM), a plot and query sub-system, and the MapInfo/MapBasic development platform - for handling of miscellaneous tasks such as coordinate conversion, auto-framing, display of multimedia files and photos, mesh grid generation, and display of

model results. These applications have evidently shown the benefit the use of GIS in hydrodynamics but have not exploited the full advantage of the technology.

Apart from the applications of GIS strictly in hydrodynamics, there has been quite a few studies which are extended to examine other marine features such as algae, nutrient, sea organisms and sediment quality. One example is a GIS module MODESTIS developed by Harnett and Nash (2004) to link GIS with DIVAST, a hydrodynamic/water quality and solute model based on a 2D depth-integrated approach, for investigation of nutrient and chlorophyll a dynamics. In addition, Runca et al. (1996) has applied GIS overlay technique to evaluate the relative impact of various physical and chemical factors in order to identify the region in the Lagoon of Venice most at risk of macroalgae bloom. GIS has also been applied by Bergamasco et al. (2003) to exploit and manage both in situ measurements and models results of various parameters involving hydrodynamics, sediments, nutrients, light, and phytobenthic biomass for coastal zone management in estuaries.

Other marine and coastal-related uses of GIS include integration of GIS and environmental data for EIA (Goodwin and Palerud, 2003), design of spatial sampling strategy for sediment quality in estuaries (Caeiro et al., 2003), and sensitivity of spatial data quality in a GIS-environmental model integrated system (Li et al., 2000). In another case, GIS has been applied for the interfacing of a numerical river water quality model, developed in Matlab with a GIS using a simple Inter Application Communication (IAC) such as Dynamic Data Exchange (DDE) procedure, which is supported by both environments (Marsilli-Libelli et al., 2001). These multi-facet applications demonstrate the diversified potential for marine and coastal disciplines to benefit from GIS.

A number of specialized software products have also incorporated GIS technology into coastal environmental modelling system, with Applied Science Associates, Inc. (ASA) being one of the leading groups in this field. The environmental software of this group covers an extensive range of applications, from real-time monitoring of coastal environmental to predictions of current and water level, and from analysis of the effects of sediment plumes to aquatic organisms to modelling of coastal wave fields. The surface water modelling system (SMS) developed by the Environmental Modelling Systems, Incorporated (EMSI) has also included a GIS module for importing, creating, and manipulating GIS vector and raster data pertinent to hydrodynamics, pollutant and sediment transport, and wave modelling. The SMS is integrated with a number of

models for different applications. These include two coastal circulation models, ADvanced CIRCulation Multi-dimensional Hydrodynamic Model (ADCIRC) and M2D; two wave models, STeady WAVE (STWAVE) and CGWAVE; four river models, Finite Element Surface Water Modelling System (FESWMS), RMA2, HIVE2D, and Hydrologic Engineering Centers River Analysis System (HEC-RAS); and two water quality/sediment transport models, SED2D and RMA4. Although SMS is a largely comprehensive GIS, its prediction for water quality/sediment transport (i.e. using SED2D and RMA4) is still limited to 2D computation. Another coastal-related GIS software is the MIKE INFO Coast developed by the Danish Hydraulic Institute (DHI). This software has been integrated with a GIS to monitor morphological evolution in coastal zone. Furthermore, the US Environmental Protection Agency (US EPA) has integrated environmental databases, water quality stream models, and associated assessment tools with a GIS as part of the development of the Better Assessment Science Integrating point and Nonpoint Sources (BASINS). The BASINS system allows efficient access to large quantity of point and non-point source data and can be extended to simulate environmental fate and ecological effects in aquatic ecosystems using AQUATOX.

A summary of the literature reviewed and a list of the existing marine and coastal-related GIS software are shown, respectively, in Table 2.1 and 2.2.

Table 2.1 Literature review in application of GIS in coastal and marine environment.

Applications of GIS in Coastal and Marine Environment	Scope of Work
Development of IDOR2D , a 2D hydrodynamic/pollutant transport GIS software	<ul style="list-style-type: none"> integrated a 2D depth-averaged hydrodynamic/pollutant transport model with a GIS (ArcView) using closely-coupled method for data input, management and display, model processing and execution, and results presentation (Tsanis and Boyle, 2001)
GIS bathymetric model for pollutant transport modelling	<ul style="list-style-type: none"> developed GIS module in ArcView GIS to provide bathymetric and shoreline data input and grid generation and results presentation for a 3D hydrodynamic/pollutant transport model (IDOR3D) applied in number of coastal areas in Greece to demonstrate functionality of 3D model (Tsanis et al., 2002; Naoum et al., 2003)
Integration of GIS and Environmental Impact Model for Oil and Chemical Spills	<ul style="list-style-type: none"> developed two numerical models, NRDAM/CME and NRDAM/GLE, for oil and chemical spills assessments (Type A under the CERCLA) integrated the model system, which included 3D physical, biological, and economic damages components, with GIS to generate bathymetric and shoreline grids, represent coastal boundaries, and display results (French and Reed, 1996)
Hydroinformatic environment for coastal waters hydrodynamics and water quality modelling	<ul style="list-style-type: none"> developed a hydroinformatic environment consisting of a number of hydrodynamic/water quality models (TELEMAC2D, RMA2, POM, POM-UMH, POM-UMQ, RMA4, RMA4-UMQ, and PROCESSES), a surface modelling system (SMS) software, a mesh generation software TRIANGLE, a tidal calculation software SR95 and a GIS software ArcView GIS (Pinho et al., 2004)
Development of a MGIS	<ul style="list-style-type: none"> integrated four main components - a database system, two 3D hydrodynamic numerical models (i.e. POM and EPM), a plot and query sub-system, and the MapInfo/MapBasic development platform - for handling of miscellaneous tasks such as coordinate conversion, auto-framing, display of multimedia files and photos, mesh grid generation, and display of model results (Jiang et al., 2004)
Development of a georeferenced river quality model	<ul style="list-style-type: none"> interfaced a numerical river water quality model developed in Matlab with a GIS (i.e. ArcView GIS) based on a simple Inter Application Communication (IAC) such as Dynamic Data Exchange (DDE) procedure, which is supported by both environments (Marsilli-Libelli et al., 2001) conducted case study for a small river reach in Tuscany
Monitoring of Arctic coastal and marine environment – conducted by Akvaplan-niva (Norwegian)	<ul style="list-style-type: none"> built environmental database for the Arctic region linked database with ArcView GIS and customized for EIA and risk assessments of potential environmental pollutions (Goodwin and Palerud, 2003)
Modelling of nutrient and chlorophyll a dynamics in Wexford Harbor	<ul style="list-style-type: none"> collected and analyzed various water quality parameters in study area developed a chlorophyll a production model using DIVAST, a hydrodynamic/ water quality and solute model based on a 2D depth-integrated approach developed a GIS module MODESTIS to link GIS with DIVAST (Harnett and Nash, 2004)
Control of macroalgae bloom in the Lagoon of Venice	<ul style="list-style-type: none"> evaluated the relative impact of each physical or chemical factor and identified area subjected to most critical conditions using GIS overlay technique used a ecological model (consisted of three modules: hydrodynamic, dispersive, and ecological) to predict high-risk areas and compared with GIS result simulated different pollution reduction scenarios to estimate which level of nutrient reduction will achieve most effective results (Runca et al., 1996)

Table 2.1 Continued.

Applications of GIS in Coastal and Marine Environment	Scope of Work
Analysis and modelling of interactions among phytobenthos, hydrodynamics, nutrient cycling, and sediment transport in the Lagoon of Venice	<ul style="list-style-type: none"> • conducted field survey to measure various parameters involving hydrodynamics, sediments, nutrients, light, and phytobenthic biomass • developed feedback model, which combined suspended particulate matter transport/erosion mechanisms, nutrient and macroalgae dynamics, and hydrodynamics • applied GIS to exploit and manage both in situ measurements and model results for the coastal zone management in estuaries (Bergamasco et al., 2003)
Design of spatial sampling strategy for sediment quality in estuaries	<ul style="list-style-type: none"> • developed systematic spatial sampling strategy based on semi-variogram analysis • applied sampling strategy to define boundaries of environmental management area of the Sado Estuary in Portugal (Caeiro et al., 2003)
Sensitivity analysis of quality of spatial data in GIS and environmental modelling	<ul style="list-style-type: none"> • studied the effects of spatial data quality on environmental model results and propagation of errors • proposed an approach which is to incorporate a geo-data quality analysis (GQA) engine into GIS/model integrated system (Li et al., 2000)

Table 2.2 Coastal-related GIS software.

Coastal-related GIS software	Developer	Description
Surface Water Modelling System (SMS)	Environmental Modelling Systems, Incorporated (EMSI)	<ul style="list-style-type: none"> • a comprehensive environment for hydrodynamics, pollutant and sediment transport, and wave modelling - consisting of 2D finite-element, 2D finite-difference, 3D finite-element and 1D backwater modelling tools • supports a number of models including USACE-ERDC supported TABS-MD (GFGEN, RMA2, RMA4, SED2D-WES), ADCIRC, CGWAVE, STWAVE, M2D, HIVEL2D, and HEC-RAC models • allows the construction of 2D and 3D finite element meshes and finite difference grids of rivers, estuaries, bays, or wetland areas • includes GIS module for importing, creating, and manipulating GIS vector and raster data (Environmental Modelling System, Incorporated)
COASTMAP	Applied Science Associates, Inc. (ASA) and the Ocean Engineering Department at the University of Rhode Island	<ul style="list-style-type: none"> • an integrated system which combines real-time and historical observations, data analysis, GIS, predictive modelling, and internet-based distribution • includes pollutant, marine spill, atmospheric plume and water quality models (Applied Science Associates, Inc., 2003a)
HYDROMAP	ASA	<ul style="list-style-type: none"> • predicts currents and water level for coastal waters using a gridding approach to allow for a wide range of spatial scales (Applied Science Associates, Inc., 2003b)
SSDOSE	ASA and the US Army Engineering Research and Development Center at Vicksburg	<ul style="list-style-type: none"> • evaluates exposures of various aquatic organisms to suspended sediment plumes (based on output from SSFATE) to examine alternatives for dredging activities (Applied Science Associates, 2003c)
SSFATE	ASA and the US Army Engineering Research and Development Center at Vicksburg	<ul style="list-style-type: none"> • an integrated GIS with a computational model to predict transport, dispersion, and settling of suspended sediments released to water column from dredging operations (Applied Science Associates, Inc., 2003d)
WAVEMAP	ASA	<ul style="list-style-type: none"> • an integrated wave-modelling software with a GIS to predict wave fields in coastal environment (Applied Science Associates, Inc., 2003e)
WQMAP	ASA	<ul style="list-style-type: none"> • integrated with GIS to examine surface water quality issues – includes grid generation, hydrodynamic model, pollutant transport model, and eutrophication model (Applied Science Associates, Inc., 2003f)
MIKE INFO Coast	Danish Hydraulic Institute (DHI) Water & Environment	<ul style="list-style-type: none"> • integrated with a GIS to monitor morphological evolution in coastal zone based on ArcView GIS (Danish Hydraulic Institute (DHI))
IDOR 2D GIS	The Water Resource Environmental Information Systems Laboratory, Department of Civil Engineering McMaster University	<ul style="list-style-type: none"> • integrated with ArcView GIS with 2D depth-averaged hydrodynamic/pollutant transport model for lakes, impoundments, coastal and estuarine waters (Water Resources Environmental Information Systems Laboratory, Department of Civil Engineering, McMaster University)
Better Assessment Science Integrating point and Nonpoint Sources (BASINS)	US Environmental Protection Agency	<ul style="list-style-type: none"> • integrated environmental databases and water quality stream models, and associated assessment tools with ArcView 3.1 GIS for watershed and water quality-based studies (U.S. Environmental Protection Agency, 2004a) • system allows efficient access to large quantity of point and non-point source data and can be extended to simulate environmental fate and ecological effects in aquatic ecosystems using AQUATOX (U.S. Environmental Protection Agency, 2004b)

2.3 Study Area

The PRE, with an area of about 2110 km², is a triangular-shaped estuary which receives freshwater from the Pearl River Delta (PRD) and drains into the South China Sea (see Figure 2.1). The estuary is exposed to effluent from four major river outlets at the northwest side, namely, Humen, Jiaomen, Hongqilimen, Hengmen, resulting in a total average annual freshwater runoff and sediment discharge of 1.742×10^8 m³ and 2757×10^4 tons respectively (Wai, O. W. H.). The estuary is about 5 km wide at the northern end and widens to about 35 km at the southern end, with a longitudinal (north-south) length of approximately 70 km. The water depth increases from north to south and decreases from east to west at the southern end. With the exception of two major natural water channels with water depth varying from 20 m to 30m, most of the estuary is quite shallow with a water depth between 2 m and 10 m (Chen and Heinke, 2001).

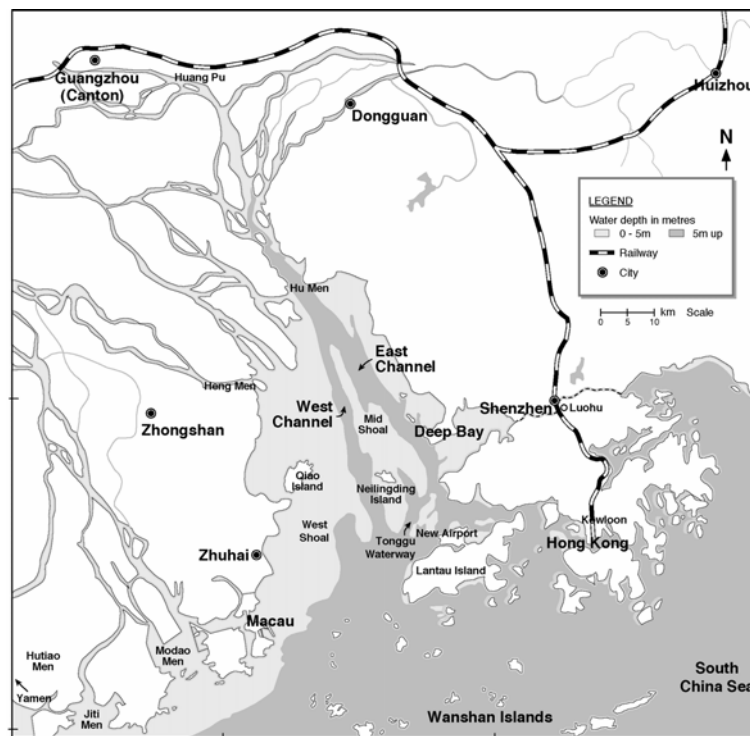


Figure 2.1 The Pearl River Estuary.

The huge economic and industrial development in the PRD region during the recent decades has led to serious degradation of water quality from the increased loadings of pollutants discharged into the PRE system. In order to mitigate this situation, it is essential to gain a good quantitative understanding of the hydrodynamic and water

quality characteristics of the estuary system. An efficient approach is to make use of numerical models combined with water quality monitoring programs. So far the Pearl River Estuary Pollution Project (PREPP), conducted by the Hong Kong University of Science and Technology (HKUST) between 1999 and 2002, is publicly known by far “the most comprehensive cross-boundary study on the Pearl River Estuary to date”. According to the PREPP summary report, the scope of this project encompasses collection of field data using shore-based, shipboard, and satellite remote sensing techniques as well as development of an integrated mathematical model system, which interlinked a hydrodynamic model (i.e. POM), a tracer sediment transport model, and a water quality model. Although GIS technology was also implemented for management and display of both collected and model data, the project did not extend the use of GIS for integration with numerical models (Chen and Heinke, 2001; Chen et al., 1999; Institute for the Environmental (IENV), the Hong Kong University of Science and Technology (HKUST)). Furthermore, no documentation giving details of how GIS was applied in this project is publicly available.

2.4 Summary

A review of the literature on GIS in marine context has found that a number of reasons, including the sparseness of oceanographic data as well as the high cost and the georeferencing difficulty in data collection, contribute to the relatively limited GIS applications in hydrodynamics and water quality. Yet, the most crucial factor for such thwarted advance is the challenge in exceeding the two dimensionality of GIS for representations in the three and four-dimensional world. Most integration between GIS and hydrodynamic models are constraint to 2D capabilities although there have been applications for 3D models supporting specific tasks such as generation of bathymetric and shoreline data input, and result representation. Besides applications of GIS in hydrodynamics, quite a few studies have been extended to examine other marine features such as algae nutrient, sea organism and sediment quality. In addition, the environmental condition of the study area, the PRE, and a past GIS-related project on the PRE are reviewed. While this chapter focuses on a review of the applications of GIS in marine and coastal environment as well as the study area, detailed reviews of other relevant subjects are presented in the corresponding chapters throughout this thesis.

3 Development of an Integrated-GIS for the PRE

3.1 GIS Software

ArcView Version 9, developed by the Environmental Systems Research Institute, Inc. (ESRI), is selected as the GIS software for developing PRE_WAGIS in this study. The system exploits the basic functionality of ArcView as well as three additional extensions: 3D Analyst, Spatial Analyst, and Geostatistical Analyst for advance GIS capabilities.

ArcView is an integrated GIS software package for visualization, management, query, and analysis of geographic data. One of the reasons for using ArcView for this project is its advanced raster-based modelling capabilities. Since field data are typically collected at a limited number of sample points, it is necessary to have the spatial interpolation function for deriving values at the unsampled locations. The ArcGIS Spatial Analyst extension not only allows for interpolation of spatial data but also provides an extensive set of cell-based analysis tools such as raster overlay, query, and *Map Algebra* calculation. These functions are particularly useful for assessing the spatial trend of water quality in the study area.

In addition, ArcView offers a comprehensive developer environment to customize or extend applications using industry-standard programming languages such as Visual Basic for Application (VBA) and C++. Using the ArcGIS Desktop Developer Kit, it is

possible to configure user interface, incorporate new GIS tools, and build custom functions to fit the needs of the integrated system. ArcView also supports any Component Object Model (COM)-compliant programming languages such as Visual Basic (VB), .NET C++, and Delphi for advance customization tasks.

Other advantages of ArcView for developing the tool are as follows (Booth and Environmental Systems Research Institute, 2000; Environmental Systems Research Institute, 2006; Johnston and Environmental Systems Research Institute, 2001; McCoy and Johnston, 2001):

- Fully interoperable with Microsoft Office and other Windows applications
- User-friendly graphic interface with easy-to-access command menus and comprehensive layer-managing operations
- High-quality display of information with an extensive array of symbols and cartographic capabilities
- Ability to connect with other relational databases using Object Linking and Embedding (OLE) Database providers. For the case of this project, information stored in the Microsoft (MS) Access database system can be directly retrieved through ArcView Interface.
- Graphical representation of attribute data. Types of graphs include Area, Bar and Column, Bubble, High-Low-Close, Line, Pie, Polar, and Scatter.
- 3D Analyst – 3D perspective display of data and animation tool for examining temporal trend in water quality data
- Geostatistical Analyst - combines spatial and statistical techniques to characterize error and variability of data and allows for generating of more accurate continuous surfaces from limited sampling datasets

3.2 Concept of PRE_WAGIS

A customized GIS-based tool is developed to support retrieval, display, and interpretation of both field-collected and model-simulated datasets as well as for EIA. Figure 3.1 is a conceptual diagram of the GIS-hydrodynamic integrated system - PREWAGIS. The integrated-GIS links together three key system components: 1) a

database for storing field-collected data, 2) a pair of connections with a hydrodynamic-water quality coupled model, one for data exchange with model inputs and the other for retrieval of outputs, and 3) an EIA module for water quality evaluation, to a single operation platform.

First, datasets of field data are gathered and compiled into a GIS database, which is further linked with the GIS. This enables efficient retrieval and display of raw data through the GIS interface, and enhancing the user's understanding of information. Likewise, a database for storage of model input as well as a specified directory for model output files are both connected with the GIS. In this way, the GIS links together the collected field information, and the model inputs and results. This linkage of information is useful for many applications, for examples, the use of field-collected data for setting model boundary conditions and the comparisons of field-collected and model-simulated results to verify accuracy of model results. Finally, an EIA module for water quality evaluation is incorporated to evaluate potential environmental impact based on field-collected or model-generated information.

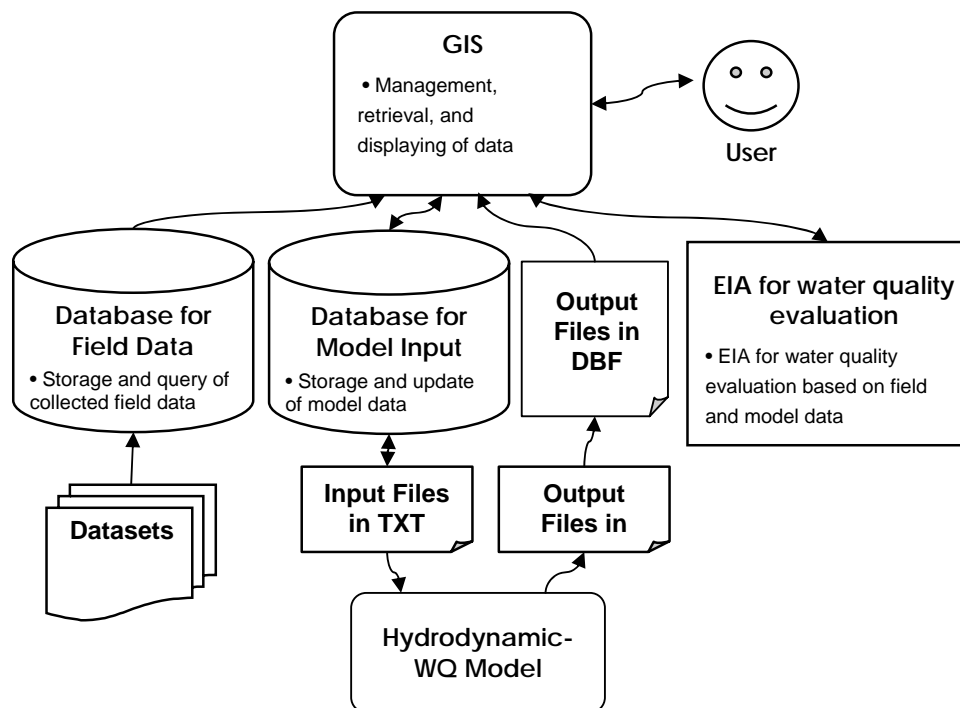


Figure 3.1 Conceptual diagram of the GIS-hydrodynamic integrated system.

The customization process is carried out using ArcView's built-in VBA scripting capabilities for manipulation of ArcObjects (Chang, 2005; Razavi, 2002; Zeiler, 2001). Other more advance tools are also developed from Active Dynamic Link Library (DLL) in VB and registered into the system. Using a COM-compliant programming language (i.e. VBA) in ArcView in the development of the GIS allows for a window-based operational platform, and thus maximizes the user-friendliness. The operation is carried out through the use of an interactive graphic interface and intelligible dialog boxes. The data retrieval methods for the data and model components, which are discussed in respectively in Chapters 5 and 6, follow similar procedure to enhance the ease of usage. Furthermore, each of the three components as shown in Figure 3.1 can run independently with one another or together as an integrated whole for more complicated analysis. This structure gives the system great adaptability and flexibility.

A menu-driven interface is used to conduct GIS-related hydrodynamic analysis (see Figure 3.2). The developed interface of PRE_WAGIS introduces five new menus to the current ArcView window display (see Figure 3.3-3.7): 1) Data, 2) Interpolate, 3) Model, 4) Results, and 5) EIA. The *Data* menu is primarily for retrieval and display of field data. The *Interpolate* menu is similar to the *Data* menu, but including interpolation functionality to derive values at the time and space in which no measurements were taken. The *Model* menu provides a linkage with the model database for viewing and editing model inputs. The *Results* menu is for displaying model output through the GIS interface. Finally, the *EIA* menu consists of a set of tools for evaluating environmental impacts based on either field-collected or model-generated data.

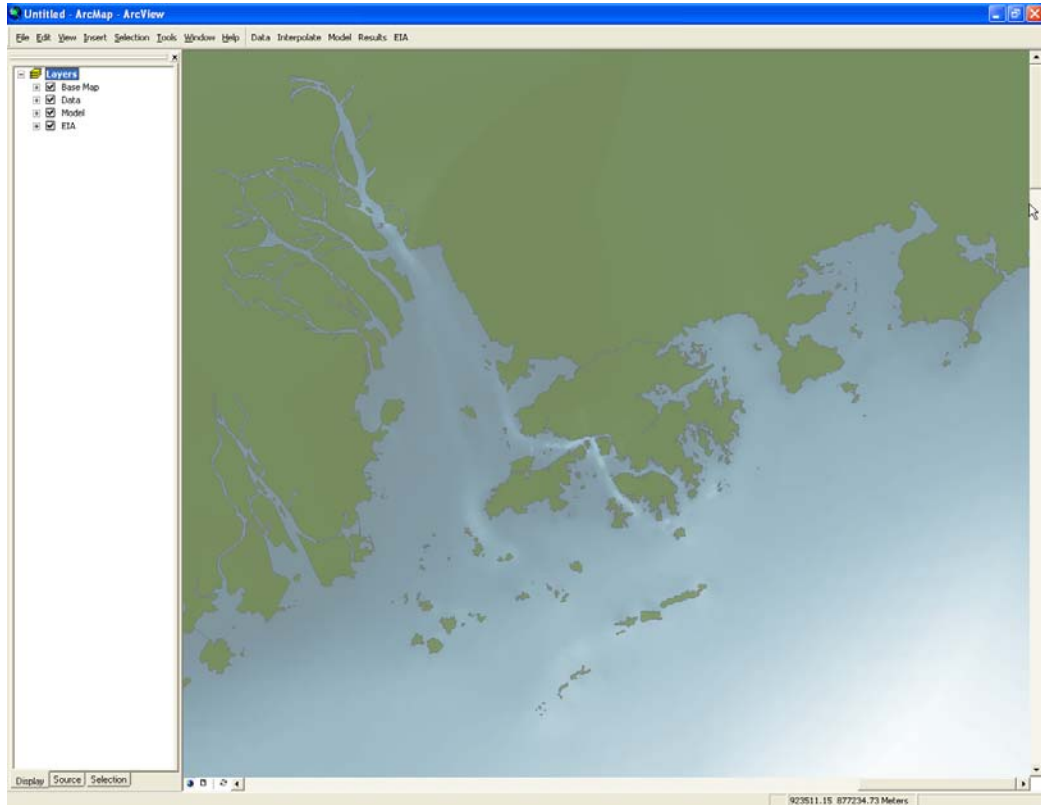


Figure 3.2 Customized ArcView interface incorporated with five new menus.

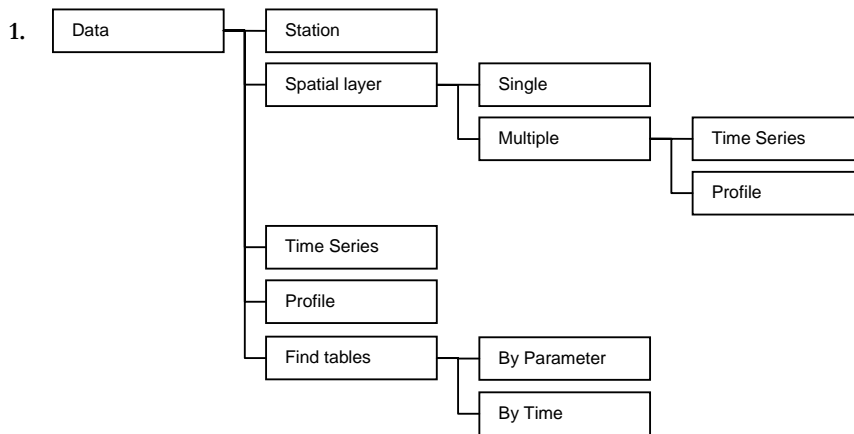


Figure 3.3 Menu structure: Data.

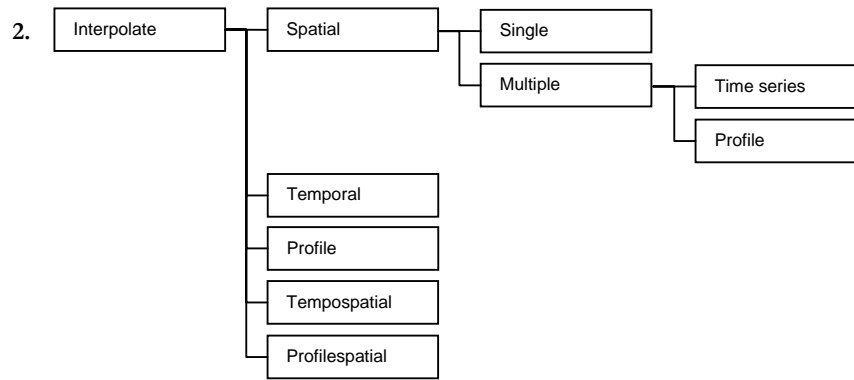


Figure 3.4 Menu structure: Interpolate.

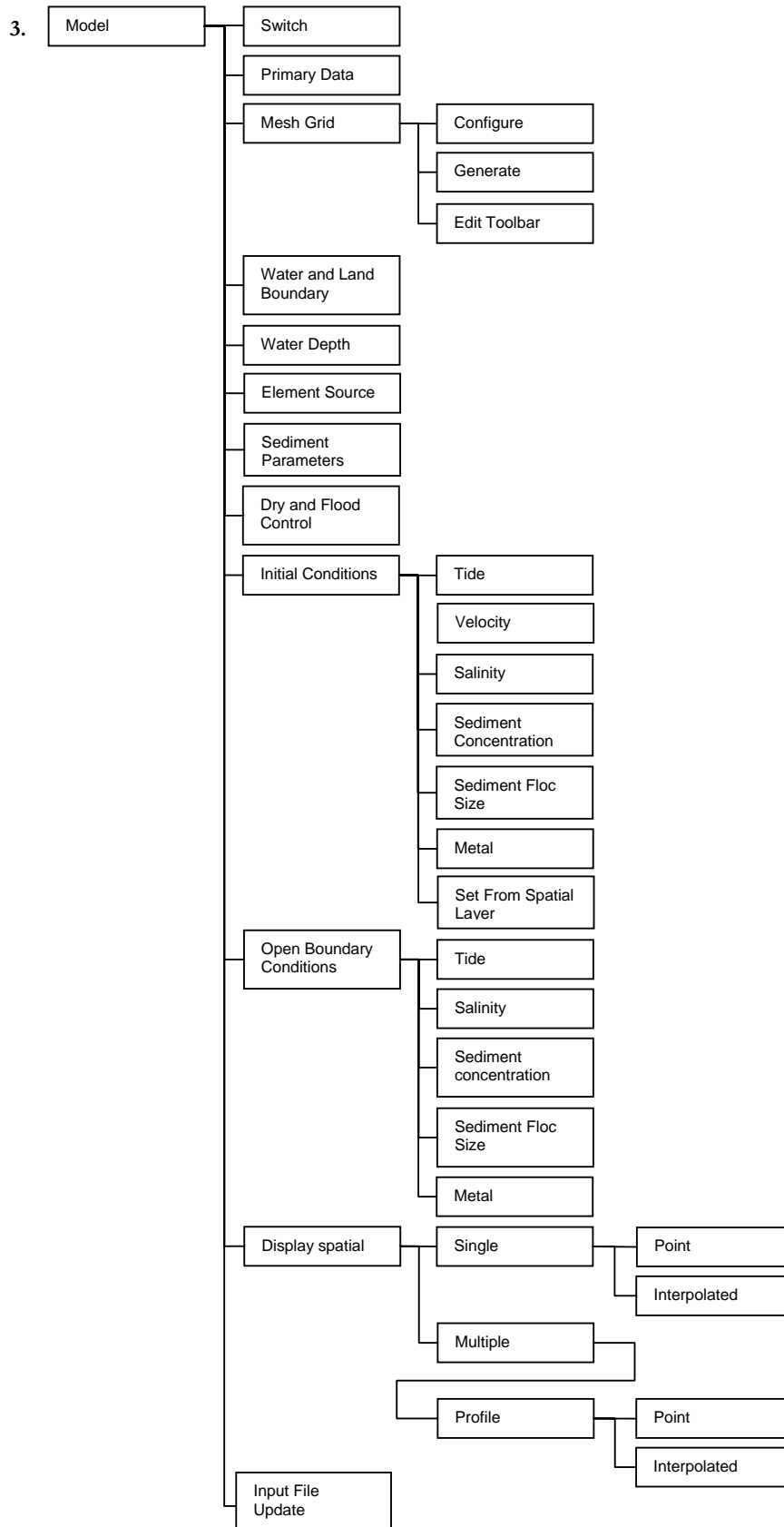


Figure 3.5 Menu structure: Model.

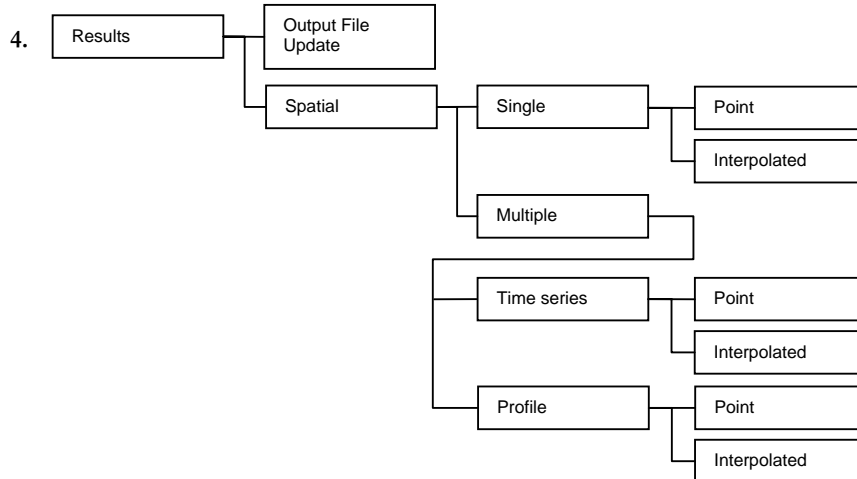


Figure 3.6 Menu structure: Results.

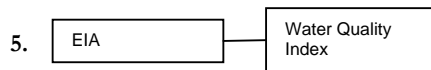


Figure 3.7 Menu structure: EIA.

3.3 Summary

This chapter has been devoted to providing the general setup in the development of an integrated-GIS for hydrodynamics - PRE_WAGIS. The three main components include a database for field data, integration with a hydrodynamic-water quality coupled model, and an EIA module for water quality evaluation. In addition, the new set of menus incorporated into the GIS interface has been presented. The development of each component along with the highlights of the customized function is discussed in detail in the following chapters.

4 GIS Database

4.1 Collected Data

In this study, a GIS database of hydrodynamic and water quality data is developed as part of the first component of PRE_WAGIS (see Figure 3.1). The collected data encompass various physical, chemical, and biological – organic and inorganic variables, as summarized in Table 4.1. These data have been gathered from a number of different sources, including a Civil Engineering and Development Department (CEDD) Project – AGREEMENT NO. CE32/96 (Study on Tonggu Waterway), the Enhancement of WAHMO Mathematical Models project, Environmental Protection Department (EPD) on-going marine water and sediment quality monitoring, an EPD Project – AGREEMENT NO. CE42/97, the PREPP conducted by the HKUST, and the Hong Kong Observatory (HKO).

Table 4.1 Variables included in the collected hydrodynamic and water quality data.

Variables	Abbreviation
General variables	
temperature	temp
salinity	
conductivity	cond
electrochemical potential	
dissolved oxygen	DO
saturated oxygen	OXSAT
secchi depth	sec depth
turbidity	turb
pH	pH
chlorophyll a	chl a
Wave variables	
wave height	wave ht
wave period	wave T
wave direction	wave dir
wave height above sensor	WHA
average wave height	HAV
significant wave height	HS
maximum wave height	HMAX
average height of the height 1/10 of the wave	H_10
period of peak wave energy	TP
zero crossing period	TZ
significant wave period	TS
crest wave period	TC
period of the maximum wave height	TMAX
mean wave direction vs frequency	DIR
standard deviation of the surface elevation	STD
spectral band width	EPSI
Hydrodynamic variables	
current speed	m/s
current direction	degree
tidal level	m
Ambient variables	
air temperature	air temp
wind speed	wind v
wind direction	wind dir
Sediment-related variables	
suspended solids	SS
total solids	TS
total volatile solids	TVS
volatile suspended solids	VSS
silt concentration	silt conc
dry wet ratio	
particle size fraction < 63 micrometer	
Nutrients: Nitrogen compounds	
ammonium	NH ₄
ammonia	NH ₃
unionized ammonia	unionized NH ₃
nitrite	NO ₂
nitrate	NO ₃
total inorganic nitrogen	TIN
total dissolved nitrogen	TDN
total dissolved kjeldahl nitrogen	TDKN
total kjeldahl nitrogen	TKN
total nitrogen	TN
Nutrients: Phosphorus compounds	
orthophosphate phosphorus	PO ₄
reactive (ortho) phosphorus	R(O)P
total dissolved phosphorus	TDP
total phosphorus	TP

Table 4.1 Continued.

Variables	Abbreviation
Organic matter	
total organic carbon	TOC
dissolved organic carbon	DOC
total carbon	TC
chemical oxygen demand	COD
chemical oxygen demand on magnesium	CODMn
biochemical oxygen demand	BOD
biochemical oxygen demand (5-day)	BOD5
Inorganic variables	
argon	Ar
boron	B
silica	SiO2
silicate	SiO3
sulphide	S
Metals	
aluminum	Al
barium	Ba
cadmium	Cd
chromium	Cr
copper	Cu
copper-soluble	CuS
copper-total	CuT
iron	Fe
magnesium	Mg
mercury	Hg
nickel	Ni
lead	Pb
silver	Ag
tin	Sn
vanadium	V
zinc	Zn
Microbiological indicators	
Escherichia coliform	E. coli
Faecal coliform	F. coli
Phaeo-pigments	Ppigments
Other toxic substances	
dibenzo(ah)anthracene	
benzo(k)fluoranthene	
chrysene	
pyrene	
phenanthrene	
acenaphthene	
indeno(1,2,3-cd)pyrene	
benzo(ghi)perylene	
benzo(a)pyrene	
benzo(b)fluoranthene	
benzo(a)anthracene	
fluoranthene	
anthracene	
fluorene	
acenaphthylene	
total polychlorinated biphenyls	
total cyanide	

4.1.1 CEDD Project – Agreement no. CE32/96

As part of the “Agreement No. CE32/97 – Study on Tonggu Waterway” project, a hydrographic and water quality survey was conducted by the CEDD in the PRE region. This extensive survey, which covered on-site field measurements as well as water samplings at more than 13 monitoring stations for both wet and dry seasons in 1998, is divided into two parts: the hydrographic survey and the water quality survey.

i) Hydrographic Survey

Each seasonal hydrographic survey consisted of the followings:

- a 30-day fixed station continuous monitoring of tidal level taken at 10-minute interval at 5 specified stations;
- a 10-hour fixed station measurement of current velocity taken using 1-hour time intervals at 5 depths for 5 specified stations carried out during both neap and spring tide period;
- a 10-hour fixed station measurement of DO (refer to Table 4.1 for the full names of all water quality variables) profiles taken using a time interval of approximately 3 hours and a depth interval of 1 m at 12 specified stations for dry season and at 8 specified stations for wet season;
- a 15-day fixed station continuous measurement of current velocity profiles taken using a time interval of 30-minute and a depth interval of 1 m at 2 specified stations;
- a 15-day fixed station continuous measurement of conductivity, temperature, salinity, and turbidity profiles taken using a time interval of 30 minute and a depth interval of 1 m at 13 specified stations for dry season and 15 specified stations for wet season;
- a 15-day fixed station continuous measurement of turbidity at seabed, and DO at two water depths taken at 30-minute interval at specified stations;
- a 15-day fixed station continuous monitoring of wind velocity and direction at 2 specified stations;

- a 10-hour ship-based measurement of current velocity, conductivity, temperature, turbidity, salinity, and DO profiles along specified survey line carried out during both neap and spring tide period;
- a 30-day fixed station continuous wave measurements for wet season only at 1 specified station to account for the rough wave climate that might occur during a tropical storm or a typhoon event.

ii) Water Quality Survey

For the water quality survey, water samplings as well as in situ monitoring of DO, temperature, salinity, and turbidity were conducted for a neap tide and a spring tide in the wet season and the dry season.

Water samples were collected at 5 depths (at equal vertical interval from seabed to surface) for the wet season and at 3 depths (surface, mid-depth, and seabed) for the dry season. Each sampling period was approximately 28 hours and the sampling intervals were 3 to 3.5 hours, resulting in a total of 8 samples for each sampling station per sampling period. This timing was concurrent with the 28-period ship-based line surveys.

The collected water samples were brought to the laboratory for analysis of various water quality parameters. The tested parameters included SS, pH, TOC, DOC, BOD5, CODMn, NH₃-N, NO₃, NO₂, TIN, TKN, TDKN, TN, TDN, TP, TDP, PO₄, SiO₃, E. coli, chlorophyll-a, and heavy metals (Cd, Cr, Cu, Hg, Ni, Pb, Zn) Test of heavy metals was conducted only for samples taken at surface and mid-depth.

4.1.2 EPD Marine Water and Sediment Quality Monitoring

On-going monitoring of marine water and sediment quality for 90 water and 60 sediment sampling stations within the Hong Kong water region was obtained from the EPD. The sampling stations were grouped into 10 water control zones. For each water control zone, water quality monitoring was generally conducted once a month while sediment quality monitoring was done twice a year. In addition to in situ measurements of various physical and chemical parameters, including temperature, pH, salinity, turbidity, and DO, water and sediment samples were also collected and sent to laboratories for analysis of more than 40 parameters such as nutrients, metals, organics, and coliform bacteria.

4.1.3 EPD Project – Agreement no. CE 42/97

As part of the “AGREEMENT NO. CE42/97 – Update of Cumulative Water Quality and Hydrological Effects of Coastal Developments and Upgrading of Assessment Tool” Project, in situ water quality monitoring and sampling were carried out by EPD within Hong Kong waters. This comprehensive set of data, covering water quality and hydrodynamic measurements taken over a six-month period from July 1998 to Jan 1999, comprises the following parts:

i) **Package A**

Three surveys were conducted to obtain spatial distribution and tidal variation of hydrological and water quality: 1) during 24 to 27 July 1998 – a spring tide in the wet season, 2) during 25 to 28 September 1998 – a neap tide in the transitional period, and 3) during 21 to 25 November 1998 – dry season.

For the spatial distribution survey, 33 monitoring stations were selected in the survey area. These stations were grouped according to the tidal condition at which field measurements/ water samples were to be taken: 1) one hour before a high high water, 2) at high high water, 3) one hour after a high high water within the survey period, and 4) at anytime. In situ and on-site measurements of water depth, temperature, salinity, DO, and turbidity were conducted once per survey at its specified tidal condition for a duration of 2 to 30 minutes at 10 depths for locations where water depth greater than 10 m, or at every one meter interval otherwise. Meteorological parameters including air temperature, wind speed and direction, wave height and period were also recorded. Water samples were also collected at each station for three depths: 1 m below surface, mid-depth, and 1 m above seabed. The water samples were taken for laboratory analysis of various water quality parameters including SS, Cu-S, Cu-T, SiO₃, NH₄, NO₂⁻, NO₃⁻, TKN, TP, R(O)P, TOC, chlorophyll a, BOD, and E. coli (Refer to Table 4.1 for the full names of each water quality parameter).

For the tidal cycle survey, 7 fixed monitoring stations were selected. Water samples and on-site measurements were taken every 3 hours. Tests for copper were conducted twice for each station using samples taken at high high water and low low water. On-site measurement and water sampling setup (i.e. measurement and water

sampling depths) as well as the sampled and on-site monitored parameters are the same as those for spatial distribution survey.

In addition, Acoustic Doppler Current Profiler (ADCP) was used along nine transverses to record current velocity in 1 m bins from seabed to sea surface. The locations of the transverses were chosen where current flows are known to be concentrated. On-site measurements of water depth, temperature, salinity, DO, and turbidity as well as other meteorological parameters were also taken at 5 equal depths along the same transverses.

ii) Package B

Similar to the tidal cycle survey in Package A, each of the 19 stations for Package B has a designated tidal condition at which on-site water quality monitoring and sampling were to be carried out: 1) one hour before high water, 2) at high water, 3) one hour after high water, 4) one hour before low water, 5) at low water, 6) one hour after low water, and 7) at anytime. Water sampling along with on-site measurement was carried out at the stations on a bi-weekly basis. The on-site measurement and water sampling setup (i.e. measurement and water sampling depths) as well as the measured/ sampled water quality and recorded meteorological parameters are same as those for Package A.

iii) Long-term measurements

Long-term measurements were carried out at three selected positions: 1) C1-1 Siu Ho Wan, 2) C1-2 Tsing Yi, and 3) C1-3 Fan Lau. Sea water current velocity measurements were taken using ADCP at these locations, for every 1 m vertically along the water column at 10-minute time intervals, while temperature, salinity, and conductivity measurements were recorded with Cell Transfer Delay (CTD) at the bottom, middle, and top of the water column at the same time interval. Additionally, tidal levels were also measured at three EGS (Electronic and Geophysical Services Limited) tide gauge positions.

4.1.4 PREPP

A series of cruise surveys was conducted under the PREPP in 2000-2001 throughout the PRE region. Different from the surveying approaches mentioned previously, this is a

vessel-based survey in which measurements were taken at numerous different points within the study area rather than at several pre-defined fixed monitoring locations. The information gathered from this project includes profiles of current velocity, chlorophyll a, salinity, turbidity, and SS with various measurement periods in January and July of 2000. Other parameters such as upwelling spectral radiance, absorption coefficient of colored dissolved oxygen matter, absorption coefficient of particles, downwelling irradiance, surface irradiance, and upwelling spectral radiance taken in March and April of 2001 were also obtained.

4.1.5 WAHMO 1990 Data Collection

From the WAHMO 1990 data collection, a set of on-site measurements of current, temperature, salinity, conductivity, silt concentration and DO profiles was obtained. These measurements were taken once every minute using 2 m water depth intervals at 7 EGS fixed stations, located within the Hong Kong waters, for a neap and a spring tide in the wet and dry season:

- | | |
|---------------|---|
| 1) dry season | <ul style="list-style-type: none"> ▪ spring tide: 08 Feb 1990 8:30pm to 09 Feb 1990 10:30pm ▪ neap tide: 13 Feb 1990 5:30am to 14 Feb 1990 7:30pm |
| 2) wet season | <ul style="list-style-type: none"> ▪ spring tide: 21 Jun 1990 2:30pm to 22 Jun 1990 4:30pm ▪ neap tide: 28 Jun 1990 4:00pm to 29 Jun 1990 6:00pm |

4.1.6 WAHMO 1992 Data Collection

From the WAHMO 1992 data collection project, a set of field measurements of current and water quality was obtained. The monitoring stations in this dataset can be divided into two groups: EGS - stations within Hong Kong waters and State Oceanic Administration People's Republic of China (SOA) - stations outside Hong Kong waters.

For the EGS group, on-site continuous measurements of current velocity, temperature, salinity, conductivity, silt concentration, and DO were collected at 2 m water depth interval at 6 fixed stations for a neap tide and a spring tide in the wet and dry seasons:

- | | |
|---------------|---|
| 1) wet season | <ul style="list-style-type: none"> ▪ neap tide: 04 Aug 1992 11am to 05 Aug 1992 1pm
for stations WQ2, WQ3, and WQ5 05 Aug 1992 5pm to 06 Aug 1992 7pm |
|---------------|---|

for stations WQ1, WQ4, WQ7

- spring tide: 09 Aug 1992 5pm to 10 Aug 1992 7pm
for stations WQ2, WQ3, WQ5

11 Aug 1992 4am to 12 Aug 1992 6am
for stations WQ1, WQ4, WQ7

- 2) dry season
- neap tide: 13 Jan 1993 10pm to 15 Jan 1993 12am
for stations WQ1, WQ2, WQ3
- 15 Jan 1993 6am to 16 Jan 1993 8am
for stations WQ4, WQ5, WQ7
- spring tide: 06 Jan 1993 10pm to 08 Jan 1993 12am
for stations WQ1, WQ2, WQ3
- 08 Jan 1993 6am to 09 Jan 1993 8am
for stations WQ4, WQ5, WQ7

In addition, tidal data were recorded at 10-minute time intervals at three locations:

- 1) Lamma Island
- wet season 04 Aug 1992 9am to 12 Aug 1992 7am
 - dry season 13 Jan 1993 5pm to 16 Jan 1993 8:30am
- 2) Tung Lung Chau
- wet season 04 Aug 1992 9am to 12 Aug 1992 8am
 - dry season 03 Jan 1993 2pm to 16 Jan 1993 9am
- 3) Tap Mun Chau
- wet season 05 Aug 1992 4pm to 12 Aug 1992 6:30am
 - dry season 06 Jan 1993 12pm to 15 Jan 1993 1am

For the SOA group, 12 fixed monitoring stations were selected within the PRE region for on-site measurements of temperature, salinity, and velocity profiles for a neap tide and a spring tide in the wet and dry seasons:

- 1) wet season
- neap tide: 03 Aug 1992 4am to 04 Aug 1992 5am
for stations WF3, WF4, WF5, WF6, WF7
- 04 Aug 1992 11am to 05 Aug 1992 12pm
for stations WF1, WF2, WQ9, WQ10, WQ11
- 05 Aug 1992 6pm to 06 Aug 1992 7pm
for stations WQ6, WQ8
- spring tide: 09 Aug 1992 1pm to 10 Aug 1992 2pm
for stations WQ6, WQ8
- 10 Aug 1992 8pm to 12 Aug 1992 5am
for stations WF1, WF2, WQ9, WQ10, WQ11
- 12 Aug 1992 10am to 13 Aug 1992 12pm

for stations WF3, WF4, WF5, WF6, WF7

- 2) dry season
- neap tide: 13 Jan 1993 8pm to 14 Jan 1993 10pm
for stations WF6, WQ6, WF7, WF5, WF5, WF4
 - 16 Jan 1993 10am to 17 Jan 1993 10am
for stations WQ11, WQ8, WF1, WF2, WQ9, WQ10
 - spring tide: 06 Jan 1993 8pm to 07 Jan 1993 10 pm
for stations WF6, WQ6, WF7, WF5, WF5, WF4
 - 08 Jan 1993 10am to 09 Jan 1993 12 pm
for stations WQ11, WQ8, WF1, WF2, WQ9 WQ10

It is noted that the measurements were taken at 10-minute time intervals and at water depths which varied at different stations and measurement periods.

4.1.7 HKO

Two sets of tidal data, one for Quarry Bay and the other for Waglan Island, were obtained from the HKO. Both of these tidal elevation records span from Jan 1995 to Feb 2000 and were taken on an hourly basis. Information on the times and tide heights of high and low tides was also provided in the datasets.

4.2 Database System

The application of a relational database system is an effectual approach to store, organize, and manage the collected data of different formats. The MS Access software is the selected relational database system for this study.

4.2.1 Application of Relational Database System for GIS

The reason for storing data in a relational database rather than directly in a GIS program is that a relational database is generally more flexible and efficient in managing, relating, and querying tabular attribute data. A large quantity of data was collected in this project. However, for most applications, only a selection of the entire collected dataset is usually needed. A relational database program is equipped with data manipulation and query functions for efficient retrieval of necessary information. The performance of the GIS program is enhanced by importing only the information as needed into the GIS program.

There are several reasons why MS Access was chosen as the database system in this project. Firstly, MS Access is already available with the MS Office Professional suite of products. MS Access, though being a simpler database software when compared with more sophisticated database system such as Oracle or SQL Server is still capable of performing complex query tasks. In addition, because of its simplicity, MS Access has a shorter learning curve and its cost for implementation and maintenance is significantly lower. Although MS Access can only support databases of size up to 2GB, the required data storage capacity for the collected text-based data is well below this limit. When dealing with such relatively low data volume, MS Access typically performs faster than other larger database systems.

4.2.2 Structure of Database System

Data from various sources of different formats has been organized into a collection of tables for the GIS database developed in this study. These tables can be broadly categorized into two types: 1) station and 2) measurement. For most of the field surveys, measurement data were taken at several monitoring stations of fixed locations. The station tables store the geographic positions of the fixed stations, referenced using either the geographic coordinate system (i.e. latitude and longitude) or the projected coordinate system (i.e. northing and easting). The measurement tables contain the actual measurement records. Each measurement record of a particular set of hydrodynamic or water quality parameters contains: 1) a date/time, 2) a water depth (i.e. distance from water surface or water depth level (e.g. surface, middle, etc.)), and 3) a fixed station ID, to identify from where the data were taken.

For each field survey, there are typically one station table and several measurement tables and “one-to-many” relationships are established between the core station table and each subordinate measurement table (see Figure 4.1).

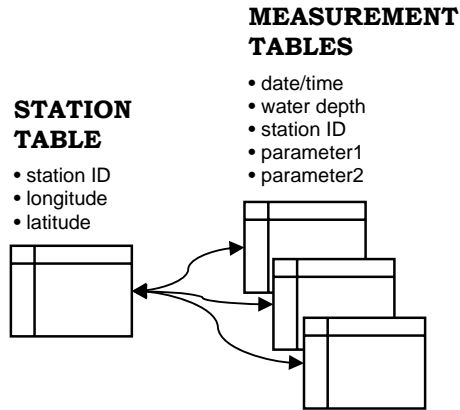


Figure 4.1 Database relationship diagram - field data.

4.3 Summary

In this study, hydrodynamic and water quality data has been acquired from different public domains and is compiled into a database system. This chapter has described the types of collected data as well as the setup of sampling time/depth and spatial distribution for each survey from the different data sources. All data sources contain information largely within the Hong Kong water region with the exception of the CEDD Project – AGREEMENT NO. CE32/96 (Study on Tonggu Waterway). The reasons for choosing the MS Access software for GIS database development has also been examined. This is mainly due to the fact that a smaller database system generally works more efficiently for storing the collected low-memory consumption text-based information. The methods for retrieving the data as well as displaying them through the GIS interface are presented in the next chapter.

5 Development of Data Retrieval and Visualization Tools

5.1 Marine Data Retrieval and Visualization

Also as part of the first component of PRE_WAGIS is the development of a set of marine data retrieval and visualization tools (see Figure 3.1). As mentioned in Chapter 1, the two key challenges when applying GIS technology for marine information are that: 1) it is difficult to visualize the intrinsic 3D and dynamic nature of marine environment using 2D mapping technology; and 2) data are typically collected from a limited number of sampling locations. In this study, the development of a set of data retrieval and visualization tools focuses particularly on addressing these two issues. This chapter covers three basic data display approaches, namely (i) display of a spatial snapshot at a specified time, (ii) display of a vertical profile at a specified time, and (iii) graphical plot of temporal variation at a specified location. In addition, the interpolation tools to account for temporally and spatially-scattered marine-collected data as well as a set of more advance data visualization methods which break through the two-dimensionality of GIS for three and four-dimensional data visualization are discussed. Furthermore, a data framework, implemented to manage metadata for the database system and thus enhance data retrieval process, is discussed. Finally, two additional functions, one for station display and the other for table querying, are also presented.

5.2 Data Retrieval

5.2.1 Application of OLE Technology

All the data retrieval processes from the MS Access database to the GIS interface make use of the OLE technology inherited in the MS COM architecture. In definition, OLE is a compound document technology which enables objects such as spreadsheet, table, and graphic to be embedded into the customized software document (i.e. ArcView in the case of this project). For example, in this project, the MS Access database system can be embedded into the ArcView interface menu, such that scripts can be written to extract data from the MS Access database for GIS display. The development of the time series and profile functions also employs two important application components, charts and spreadsheets, for graphic data display (Chappell, 1996; Puopolo, 1997).

5.2.2 Data Framework for Database Metadata Management

The database system for field data currently contains a total of 118 measurement tables and 28 station tables. A data framework has been defined for management of the metadata of these tables to enhance the data retrieval process. Figure 5.1 is a structure diagram showing how data sources, datasets, and measurement tables are organized. It can be seen from this diagram that a specific measurement table can be identified first by specifying its data source, followed by its dataset. Each measurement table, in turn, contains a set of hydrodynamic or water quality parameters. To characterize the relationship among these components (i.e. data source, dataset, measurement table, parameter, etc.) as well as other properties for querying purposes, each of these components is defined as an object variable (Burke, 2003). For example, all measurement tables are declared using the measurement table class. The measurement table class contains a list of properties, such as the name of the measurement table, the name of the dataset to which the measurement table belongs, an array of parameter names which the measurement table contains, the measurement time and depth, and the coordinate system (e.g. geographic or projected), for geographic definition of the specified measurement table. This data structure gives the flexibility of enabling new tables to be added into the database system in the future. The retrieval of a new table can be implemented by simply declaring variables for each of the components: data source, dataset, and measurement table, and then specifying the required properties accordingly.

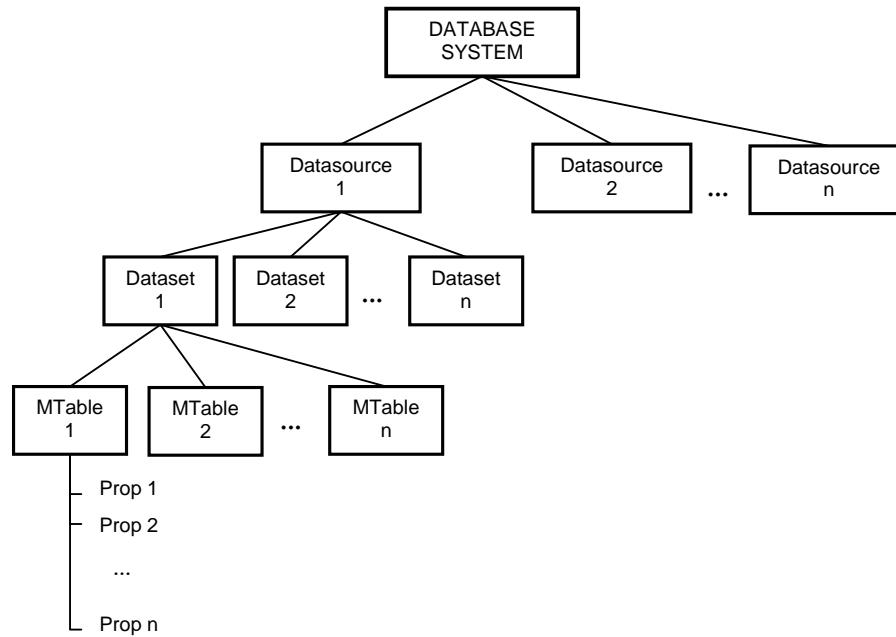


Figure 5.1 Data framework diagram.

5.3 Station Display

Before the actual retrieval of hydrodynamic or water quality information, the user may want to examine the geographic location of the fixed monitoring stations for certain datasets. The station display is developed specifically for this task. Figure 5.2 is the dialog box for creating a station layer. The input requirement is first the data source, followed by the station table. Upon execution of this command (i.e. clicking of the *Add* button), the system links with the selected station table from the GIS database, and creates a station layer based on the station coordinates and the coordinate system for the station table. The coordinate system, that is, the projected coordinate system (northing and easting) or the geographic coordinate system (latitude and longitude) in which the station is displayed is pre-defined within the system (i.e. a property of the station table class). As shown in Figure 5.3, the created station layer provides an overall picture of the geographic locations of each monitoring station for the station_Water_EPD station table.

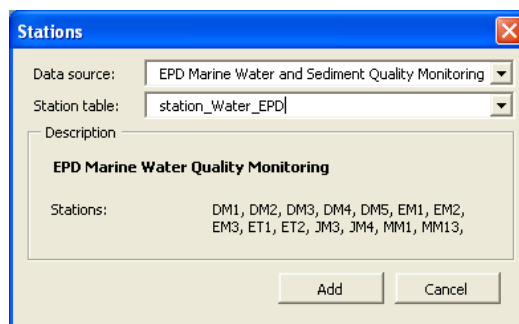


Figure 5.2 Dialog box for creating a station layer.



Figure 5.3 Station layer for station_Water_EPDI station table.

5.4 Data Displays

There are three basic methods to display raw measurement data (see Figure 5.4). The simplest data display method using GIS is a spatial snapshot in the horizontal direction at a specified time and depth. Two other data displaying functions, time series plot and vertical profile display, are also incorporated into the system for examining temporal and depth variation.

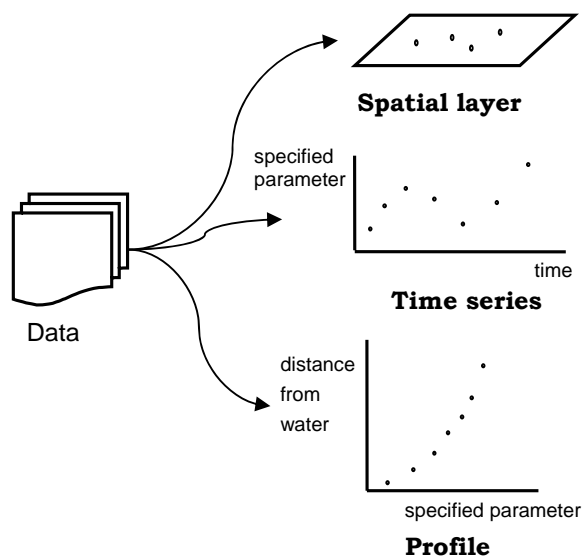


Figure 5.4 Data display.

5.4.1 Spatial Layer

As shown in the single spatial layer dialog box in Figure 5.5, a spatial layer can be created by specifying a list of input parameters including the data source, the dataset, the measurement table, the hydrodynamic or water quality parameter, the measurement depth level (e.g. surface, middle, bottom) or depth range (i.e. from a specific distance from water surface to another), and the measurement time period. When the user chooses among the measurement tables, the dialog box provides a description detailing the station table name, the entire measurement time period, time interval between samplings, the measurement depth, and the measurement depth interval.

Based upon the selection criteria, the GIS performs two Structured Query Language (SQL) queries: the first creates a spatial table containing all data for geographic referencing and the selected parameter; the second queries the information for the specified measurement depth and time, for creating a point feature layer (see Figure 5.6). The system identifies the station table to which the selected measurement table is related, determines its coordinate system (i.e. geographic or projected), and extracts and displays the data correspondingly. The main reason for having this two-step querying process is that high computational effort (i.e. takes quite a bit of time) is required for querying information from the database and attaching the data obtained to the GIS. In this way, if retrieval of information for the same parameter and measurement table is repeated, the first querying step is automatically bypassed and thus enhances retrieval speed. For

efficiency in creating multiply layers, this data retrieval process can also be done using batch mode. In this case, either a block of time series spatial layers or a block of profile spatial layers can be created.

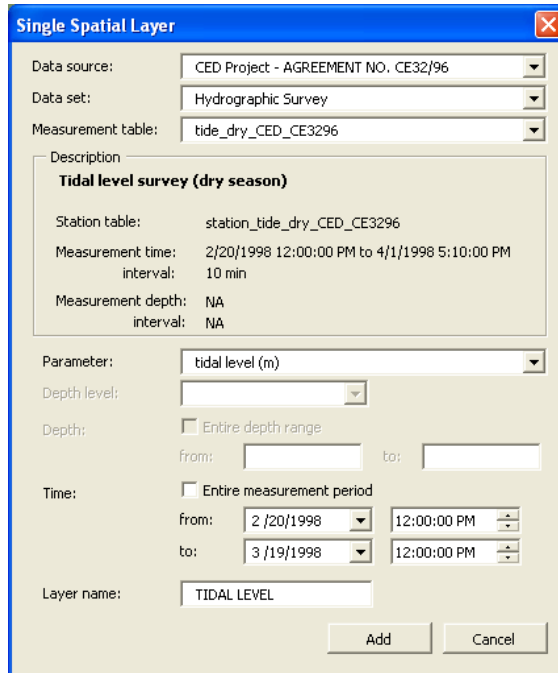


Figure 5.5 Dialog box for creating single spatial layer.

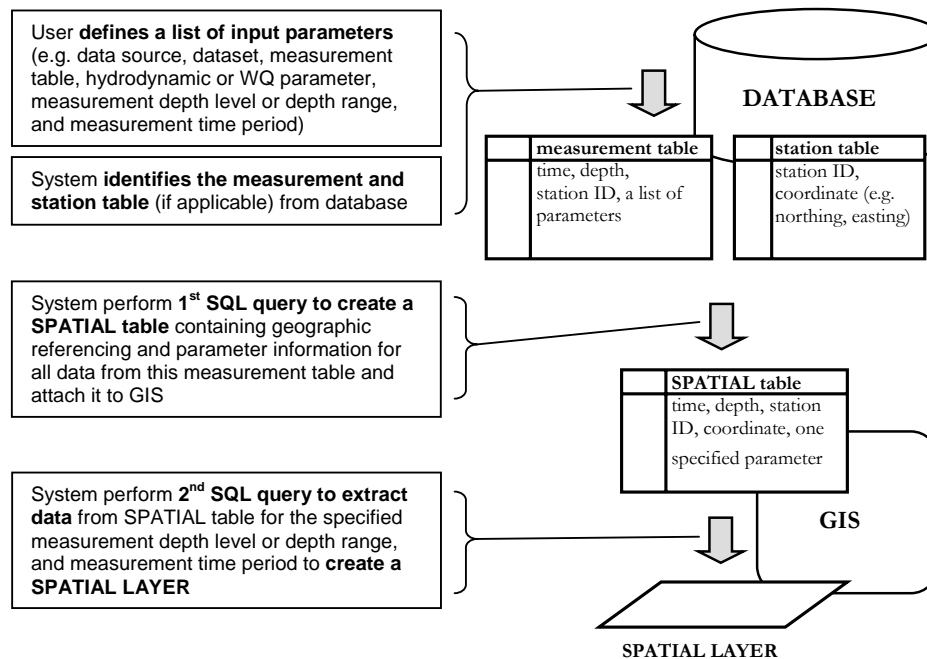


Figure 5.6 System procedures for creating a spatial layer.

5.4.2 Time Series and Profile

Similar querying operation for spatial layer is applied for creating time series and profile plots. Note that profile plot developed in this system is referred as a vertical profile along a water column. The exception is that a NON-SPATIAL table (i.e. excluding coordinates and requiring only station ID) instead of a SPATIAL table is attached into the system. The graphing displays for the time series and profile are developed using the MS Office Chart Component. The retrieved data is first placed into a spreadsheet (invisible in the dialog box) and then plotted into a chart. For the time series, the output is an x-y scatter plot with time given in the x-axis and the specified hydrodynamic or water quality parameter in the y-axis (see Figure 5.7). The profile is for a display of parameter along a vertical water column (see Figure 5.8). Additional options of the time series and profile include the display of more than one curve for comparison of the same parameter at different survey stations, time instants, or depth levels, manual adjustment of graph scales and units, and addition of trendlines to enhance visibility of information.

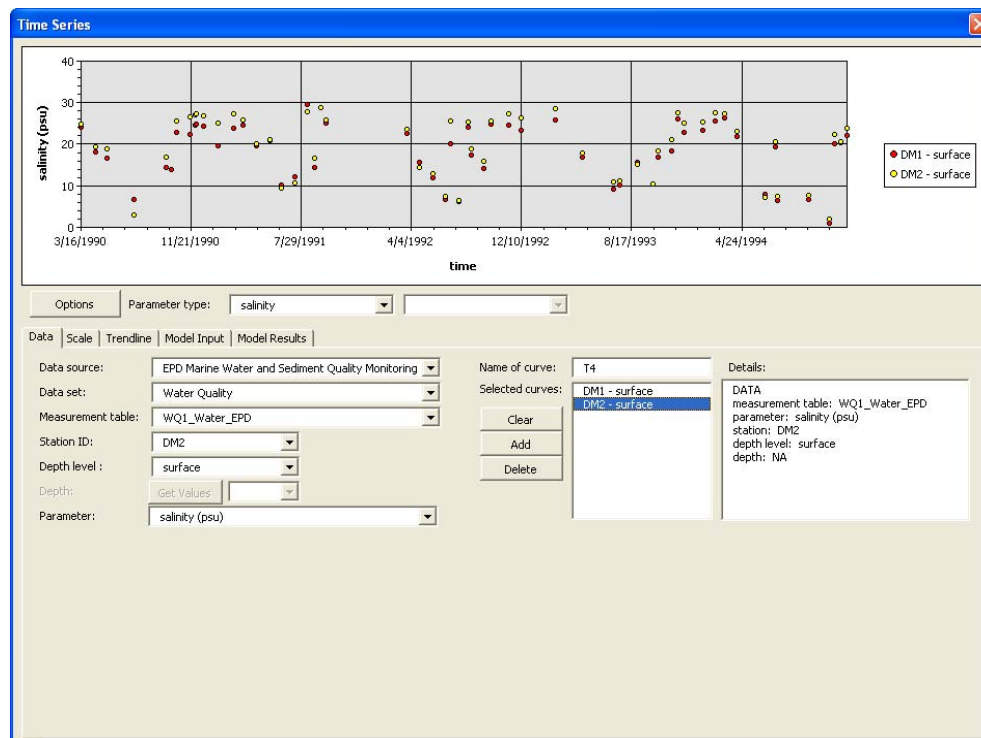


Figure 5.7 Dialog box for creating time series.

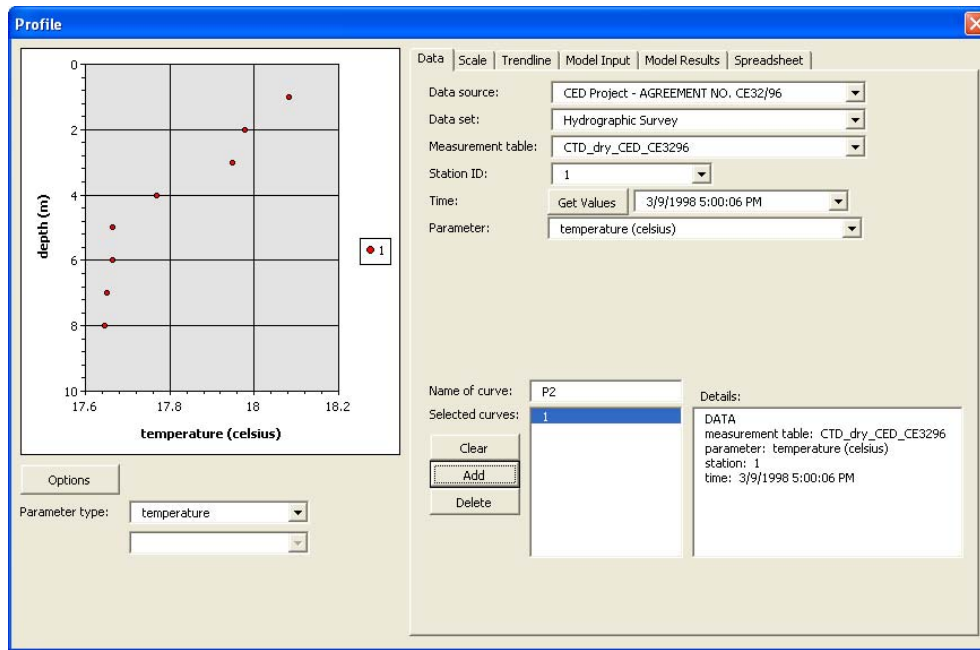


Figure 5.8 Dialog box for creating profile.

5.5 Data Interpolation

Both spatial and one-dimensional (1D) interpolation techniques are used for estimating values at points in space and time for which no measurement was taken. This section discusses the methods available for spatial interpolation and 1D interpolation as well as how the methods are selected for applications.

5.5.1 Spatial Interpolation

For spatial interpolation, five basic methods are used to create continuous predictions from sampled point values: 1) Inverse Distance Weighted (IDW), 2) Spline, 3) Kriging, 4) Natural Neighbours, and 5) Trend. Which of the above interpolation methods to be applied depends largely on the type and characteristics of the specific sampling dataset. While IDW is best for creating variables that diminish influence with distance from sampled location, Natural Neighbours is a good general interpolation method for situations where sample data points are unevenly distributed. Spline and Trend are suitable for interpolating tidal variation as they work best for generating smooth, gradually changing surface. Finally, since Kriging accounts for distance or directional bias in the data, it is best-suited for exploring pollutants dispersed from a single point source (McCoy and Kevin, 2001). Additionally, further analysis on the accuracy of predicted surfaces can be validated using geostatistical techniques (i.e. ArcGIS

Geostatistical Analyst extension) (Johnston and Environmental Systems Research Institute, 2001).

5.5.2 Temporal and Profile Interpolation

Temporal interpolation is for deriving values at unsampled points in time for a specified fixed station, while profile interpolation is for deriving values at unknown points along a vertical water column (see Figure 5.9).

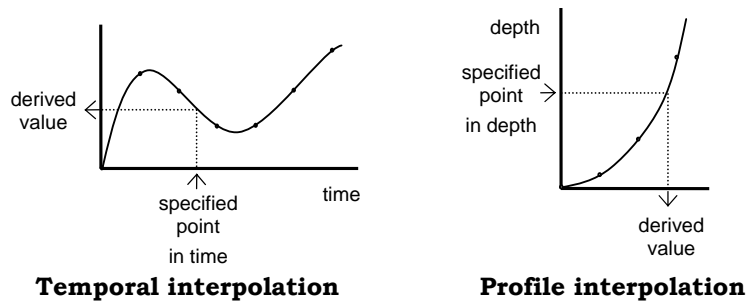


Figure 5.9 Temporal and profile interpolation.

For both temporal and profile interpolation, a wide range of mathematic functions are available for curve fitting:

- a) Polynomial of n-degree (n= 1 to 6)
- b) $f(x) = a_0 + a_1x + a_2x^2 + \dots + a_nx^n$ where $a_0, a_1, a_2, \dots, a_n$ are coefficients
- c) Spline (Linear and Natural Cubic)
- d) Logarithmic

$$f(x) = a \ln(x) + b$$
 where a and b are coefficients
- e) Exponential

$$f(x) = a \exp(b)$$
 where a and b are coefficients
- f) Power

$$f(x) = ax^b$$
 where a and b are coefficients
- g) Trigonometric of i-freq component

$f(x) = a_0 + \sum_{i=1}^n b_i \cos(\omega_i x) + \sum_{i=1}^n c_i \sin(\omega_i x)$ where a_0 is an coefficients, b_i and c_i are coefficients of the i -th angular frequency, ω_i is the i -th angular frequency, and n is the number of frequency

Data are fitted with the above equations based on the least-square method, with the exception of the Spline method. Suppose that the data points are (x_1, y_1) , (x_2, y_2) , ..., (x_n, y_n) where x is the independent variable and y is the dependent variable; the residual error between the fitted curve $f(x)$ and each data point is given as $d_1 = y_1 - f(x_1)$, $d_2 = y_2 - f(x_2)$, ..., $d_n = y_n - f(x_n)$; and the best fitting curve $f(x)$ has the property in which sum of the squares of the residual error is minimum.

$$R^2 = \sum_{i=1}^n [y_i - f(x_i)]^2 = \min \quad (5.1)$$

The unknown coefficients of $f(x)$ can be solved by setting the first derivative of R^2 in respect to each coefficient to zero (Lancaster and Šalkauskas, 1986).

$$\frac{\partial(R^2)}{\partial a_i} = 0 \quad (5.2)$$

To allow examination of the goodness-of-fit of the selected interpolation function, the interpolation module also evaluates and displays the root-mean-square of the deviation (RMS):

$$RMS = \sqrt{\frac{1}{N} \sum_{i=1}^n [y_i - f(x_i)]^2} \quad (5.3)$$

For a set of ordered (x_1, y_1) , (x_2, y_2) , ..., (x_n, y_n) input points, the Linear Spline interpolation method derives values simply by connecting each pair of points, (x_j, y_j) and (x_{j+1}, y_{j+1}) , with a linear segment. Linear interpolation in that segment satisfies the following formula:

$$y = Ay_j + By_{j+1} \quad (5.4)$$

$$\text{where } A \equiv \frac{x_{j+1} - x}{x_{j+1} - x_j} \text{ and } B \equiv 1 - A = \frac{x - x_j}{x_{j+1} - x_j}$$

Since equation (5.4) is linear, the fitted curve has zero derivative between the interval and undefined or infinite second derivative at the boundary points. For the Cubic Spline interpolation method, a cubic equation is fitted between each interval. In addition, the interpolation formula must be smooth in the first derivative, and continuous in the second derivative, both within the segment and at the end points. Spline cubic interpolation complies with the following formula:

$$y = Ay_j + By_{j+1} + Cy_j'' + Dy_{j+1}'' \quad (5.5)$$

where A and B are same as for linear interpolation from equation (5.4) and

$$C \equiv \frac{1}{6}(A^3 - A)(x_{j+1} - x_j)^2 \quad D \equiv \frac{1}{6}(B^3 - B)(x_{j+1} - x_j)^2$$

By taking the derivatives of equation (5.5) with respect to x the following results are derived

$$\frac{dy}{dx} = \frac{y_{j+1} - y_j}{x_{j+1} - x_j} - \frac{3A^2 - 1}{6}(x_{j+1} - x_j)y_j'' + \frac{3B - 1}{6}(x_{j+1} - x_j)y_{j+1}'' \quad (5.6)$$

for the first derivative, and

$$\frac{d^2y}{dx^2} = Ay'' + By_{j+1}'' \quad (5.7)$$

for the second derivative. Since the first derivative is continuous at the end points, the following equation can be obtained by setting equation (5.6) for interval (x_{j-1}, x_j) equals to that of the interval (x_j, x_{j+1}) .

$$\frac{x_j - x_{j-1}}{6} y_{j-1}'' + \frac{x_{j+1} - x_{j-1}}{3} y_j'' + \frac{x_{j+1} - x_j}{6} y_{j+1}'' = \frac{y_{j+1} - y_j}{x_{j+1} - x_j} - \frac{y_j - y_{j-1}}{x_j - x_{j-1}} \quad (5.8)$$

for $j = 2, \dots, n-1$. A unique solution can be derived by setting the boundary conditions at the endpoints x_1 and x_n . For the case of Natural Cubic Spline method, the second derivatives y_1'' and y_n'' are set to zero. Note that the computation algorithm is taken directly out of the book *Numerical Recipes in Fortran 77 The Art of Scientific Computing* by Press et al. (1992) and translated to VB for the development of this module.

Although the application of which 1D interpolation methods is controlled essentially by the user, the GIS program advises the interpolation method for hydrodynamic parameters which conform particularly well with certain mathematical functions in accordance with hydrodynamic and sediment transport theories. For instance, trigonometric function is suggested for fitting tidal data since tidal level generally varies in a harmonic manner according to the following equation:

$$h(t) = h_0 + \sum_{j=1}^M A_j \cos(\omega_j t + \delta_j) \quad (5.9)$$

where $h(t)$ is the tidal level at time t , h_0 is the mean sea level above datum of reference, ω_j is the angular frequency of the j -th harmonic constituent, A_j is the amplitude of the j -th constituent, and δ_j is the phase lag of the j -th constituent. Note that Equation (5.9) can be rewritten as:

$$h(t) = h_0 + \sum_{j=1}^M C_j \cos(\omega_j t) + \sum_{j=1}^M S_j \sin(\omega_j t) \quad (5.10)$$

where C_j and S_j are coefficients for the cosine and sine functions respectively. h_0 , C_j , and S_j can be solved using the least-square method.

In specifying the frequency of the fitting curve, a list of tidal constituents (e.g. M_2 for semi-diurnal species, principal lunar constituent) is available for selection (See Figure 5.10). As shown in Table 5.1, this module includes all the major constituents for accurate estimations of tidal level. The program allows a selection of up to a maximum of twenty-five tidal constituents. This accounts for all the major harmonic constituents of semi-diurnal, diurnal, and quarter-diurnal conditions. Since each set of the collected tidal measurements is of considerable length N , for most cases the criteria for separation of harmonic constants, as shown in the following equation, is satisfied:

$$N > T_j \quad \text{and} \quad N > \frac{360^\circ}{|\omega_i - \omega_j|} \quad \text{for any constituent pair } (i, j) \quad (5.11)$$

where T_j is the period of the j -th harmonic constituent (Ip and Wai, 1990).

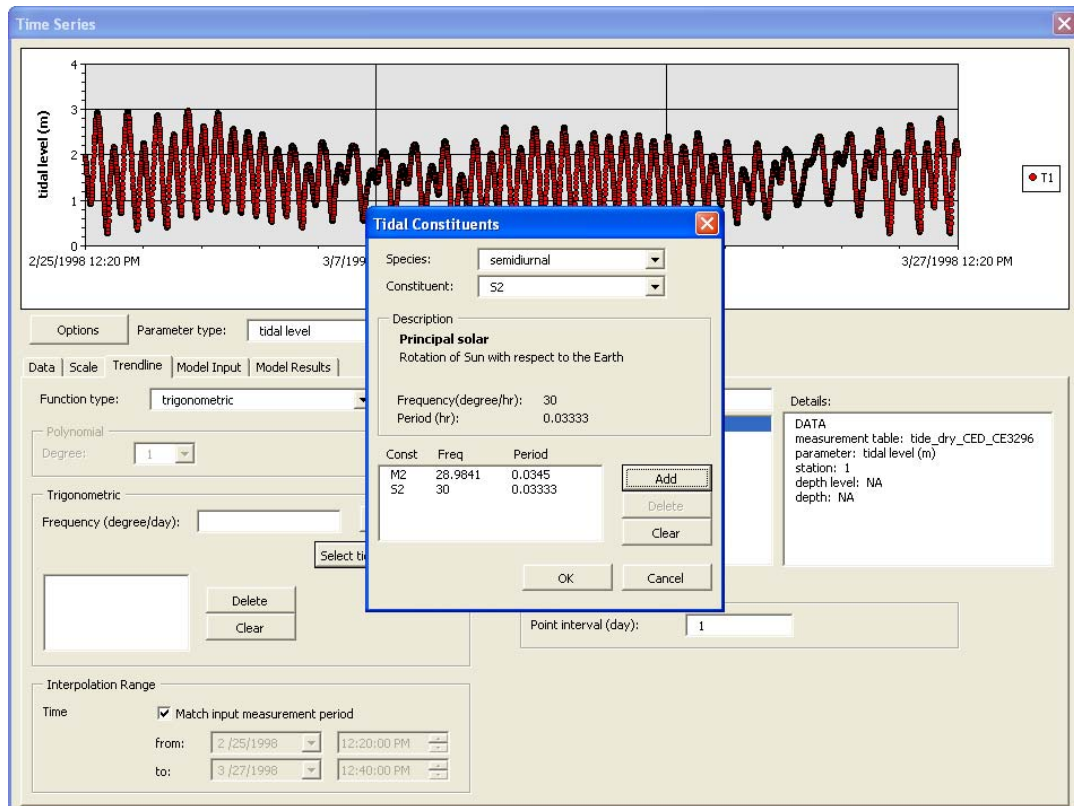


Figure 5.10 Dialog box for fitting of time series tidal data by input of tidal constituents.

Table 5.1 Summary of tidal constituents, descriptions, and frequencies included in module.

Constituent		Description	Frequency (degree/hr)
Semidiurnal			
Principal lunar	M2	Rotation of Earth with respect to Moon	28.9841042
Principal solar	S2	Rotation of Sun with respect to Earth	30
Lunisolar	K2	Effect of declination of the Moon and Sun	30.0821373
Larger lunar elliptic	N2	N2 & L2 - Effect of variation in Moon's orbital speed due to its elliptical orbit around Earth	28.4397295
Smaller lunar elliptic	L2	N2 & L2 - Effect of variation in Moon's orbital speed due to its elliptical orbit around Earth	29.5284789
Larger solar elliptic	T2	T2 & R2 - Effect of variation in Earth's orbital speed due to its elliptical orbit around Sun	29.9589333
Smaller solar elliptic	R2	T2 & R2 - Effect of variation in Earth's orbital speed due to its elliptical orbit around Sun	30.0410667
Variational	mu2	mu2, 2N2, nu2, & lambda2 - Perturbations of the Moon's orbit by the Sun	29.97
Lunar elliptic second-order	2N2	mu2, 2N2, nu2, & lambda2 - Perturbations of the Moon's orbit by the Sun's attraction for the	27.8953548
Larger lunar evectional	nu2	mu2, 2N2, nu2, & lambda2 - Perturbations of the Moon's orbit by the Sun's attraction for the	28.5125831
Smaller lunar evectional	lambda2	mu2, 2N2, nu2, & lambda2 - Perturbations of the Moon's orbit by the Sun's attraction for the	29.4556253
Variational	2MS2	Same speed as mu2 produced by interaction of M2 and S	27.9682084
Diurnal			
Lunisolar	K1	K1 & P1 - Effect of Sun's declination K1 & O1 - Effect of Moon's declination	15.0410686
Solar	P1	K1 & P1 - Effect of Sun's declination	14.9589314
Lunar	O1	K1 & O1 - Effect of Moon's declination	13.9430356
Solar	S1		15
Larger lunar elliptic	Q1	M1 & Q1 - Effect of the Moon's elliptical orbit on	13.3986609
Smaller lunar elliptic	M1	M1 & J1 - Effect of the Moon's elliptical orbit on K1	14.4966939
Smaller lunar elliptic	J1	M1 & J1 - Effect of the Moon's elliptical orbit on	15.5854333
Lunar second-order	OO1	Lunar second-order	16.1391017
Lunar elliptic second-order	2Q1	Lunar elliptic second-order	12.8542862
Larger lunar evectional	rho	Larger lunar evectional	13.4715145
Terdiurnal			
Compound of principal lunar	M3	Compound of principal lunar	43.4761563
Shallow water			
Overtides of principal lunar	M4	Shallow water overtides of M2 with a speed twice as that of M2	57.9682084
Overtides of principal lunar	M6	Shallow water overtides of M2 with a speed three times that of M2	86.9523127
Overtides of principal lunar	M8	Shallow water overtides of M2 with a speed four times that of M2	115.9364169
Overtides of M2 and S2	MS4	Shallow constituent produced by the interaction of M2 and S2	58.98
Overtides of principal solar	S4	Shallow water overtides of S2 with a speed twice as that of S2	60
Overtides of principal solar	S6	Shallow water overtides of S2 with a speed three times that of S2	90
Long period			
Lunar fortnightly	Mf	Effect of departure from a sinusoidal declination	1.0980331
Lunar monthly	Mm	Effect of irregularities in the Moon's rate of change of distance and speed in orbit	0.5443747
Lunisolar synodic fortnightly	MSf		1.0158958
Solar Semi-annual	Ssa	Ssa & Sa - Nonuniform changes in Sun's declination and distance	0.0821373
Solar annual	Sa	Ssa & Sa - Nonuniform changes in Sun's declination and distance	0.04106864

Another example for which an interpolation method is recommended is current velocity profile. Since it is known that velocity distribution in a boundary layer follows the log-law profile, the program suggests fitting velocity data based on the following logarithmic function:

$$u = \frac{1}{u_* K} \ln \frac{y}{\delta} + \frac{u_\delta}{u_*} \quad (5.12)$$

where u is the current velocity at y measured from the lowest point of the bed surface upwards, u_* is the shear velocity, K is the Von Karman constant, δ is the thickness of laminar (or viscous) sublayer, and u_δ is the current velocity at boundary layer (Yalin, 1977).

5.5.3 Tempo-spatial and Profile-spatial Interpolation

Two other interpolation functions, tempo-spatial and profile-spatial, both of which combine 1D and spatial interpolation techniques, are also included into the system (see Figure 5.11). Any data group to be placed in the same spatial layer must be collected at the same time instant. However, often the sampling time of each survey station is not simultaneous with one another, hence the tempo-spatial interpolation function is intended to deal with this problem. Using this function, a fitted curve is first obtained from the time series at each sampling station. Values at certain specified time instants can be estimated based on such curves to create a set of point feature spatial layers, which can be further converted into rasters using spatial interpolation methods. The result is a time series interpolated block. The profile-spatial function is designed to account for different measurement depth levels among stations and the interpolation concept behind it is much the same as that for tempo-spatial interpolation.

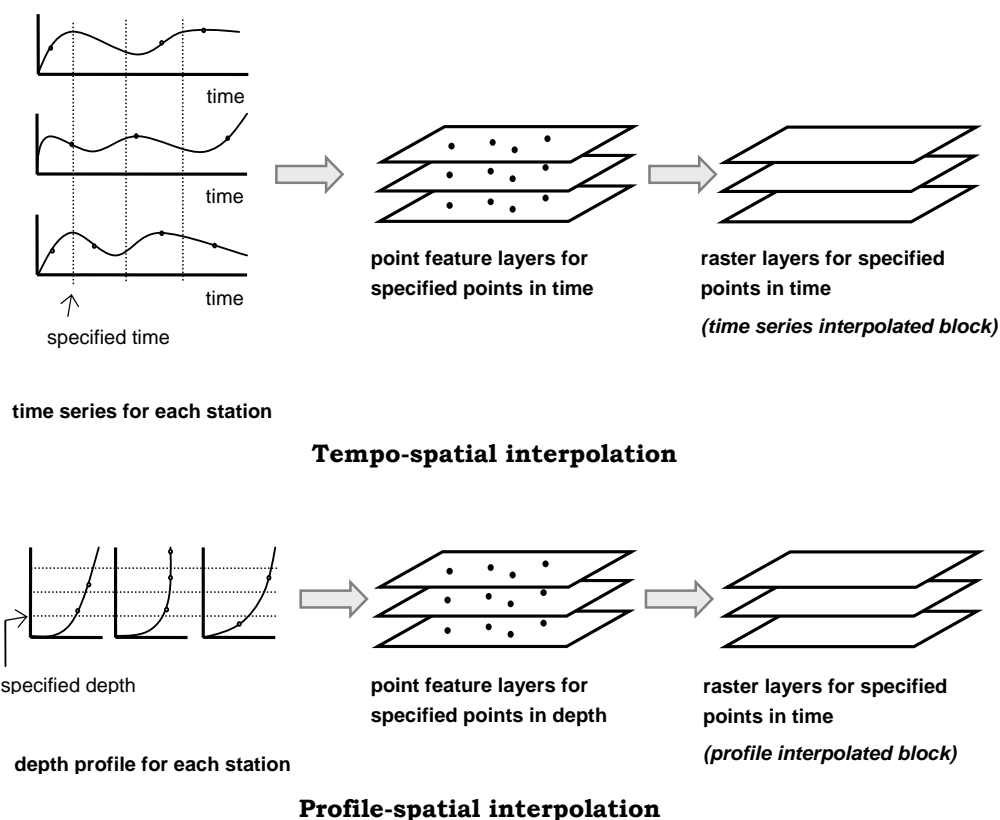


Figure 5.11 Tempo-spatial and profile-spatial interpolation.

5.6 Interactive Data Display Tools

Two interactive tools: 1) the profile and section display tool and 2) the dynamic time series display tool, are included in the GIS program to enhance comprehensiveness of information from the interpolated blocks.

To facilitate the profile display tool, the procedure involves first specifying the name of the interpolated block for which the profile plot will be created, and then clicking a location within the map region. A module is written, which extracts value at the selected point from each of the raster layers in the interpolated block and generates a profile plot using the extracted values (see Figure 5.12). Similar data extraction technique is used for creating a section display (see Figure 5.13). However, instead of clicking a single point, selection of two points is required to generate a section color map plot. The GIS, when creating a section plot, first identifies the ocean bathymetry along the line from a raster depth layer in order to draw a polygon object representing the seabed. Several discrete values are then taken out along the specified line from each layer, and plotted into a shapefile accordingly. Since ArcView provides the essential capability for spatial

interpolation, this point feature shapefile can be further interpolated into a raster layer. With the seabed polygon object overlapping a rectangular raster image, the result resembles a colormap of the sectional view of the specified parameter.

Note that for plotting the section point feature shapefile, the representation has been stretched vertically (i.e. the distance between layers has been magnified). The vertical scaling of the section plot is necessary in order to avoid spatial interpolation operation error in ArcView and to enhance the visibility of the section display. Since the value for each cell in spatial interpolation is determined primarily by the values of the input points and its distance from the points, the directional stretching of the plot will induce a certain degree of error into the interpolated result; and this error is likely to have a greater influence when vertical dispersion of the parameter of interest is significant. Nevertheless, the interpolated result at cells close to the input layers will be relatively stable and thus provides a rough estimate of the spatial distribution in vertical section.

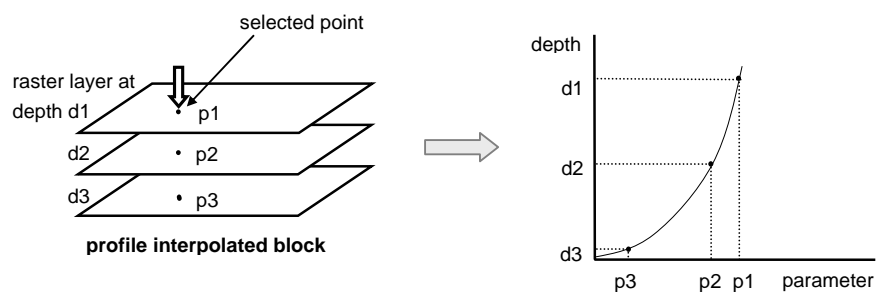


Figure 5.12 Profile plot display tool.

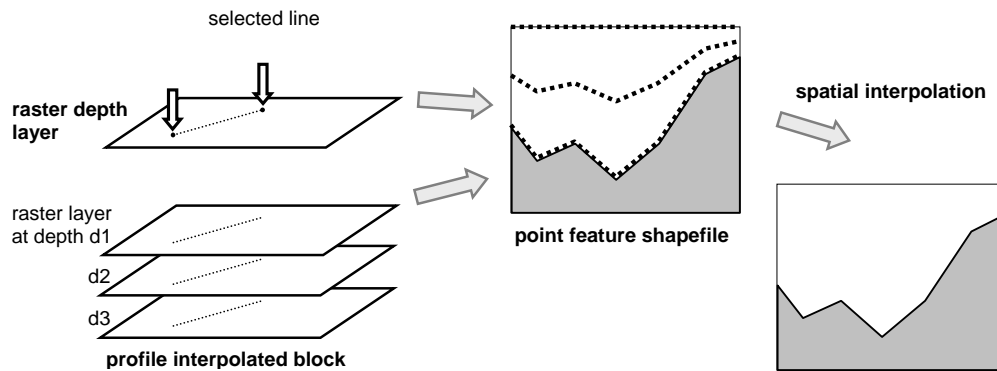


Figure 5.13 Section plot display tool.

5.6.1 Dynamic Time Series Display

As the hydrodynamic characteristic of marine environment is endlessly changing, dynamic display is an important tool for examining and analyzing temporal variation of coastal data. Dynamic display can be implemented with a time series interpolated block. The idea for creating an interactive display of time series is similar to that for profile (see Figure 5.14). The procedure is to select any point within the map region, and values at selected point are then extracted to create a time series plot. A module for dynamic display of the map layers is developed using the VB Timer control. An animated simulation of the spatial layers can be generated by adjusting the visibility of the raster layer with time (i.e. layer 1 is visible only at time t_1 , layer 2 is visible only at time t_2 , and so on). At the same time, a cursor dynamically moves along the time series curve to the position (i.e. time) corresponding to that of the visible layer. Additional features in the tool are playback controls such as pause, stop buttons, and play speed adjustment.

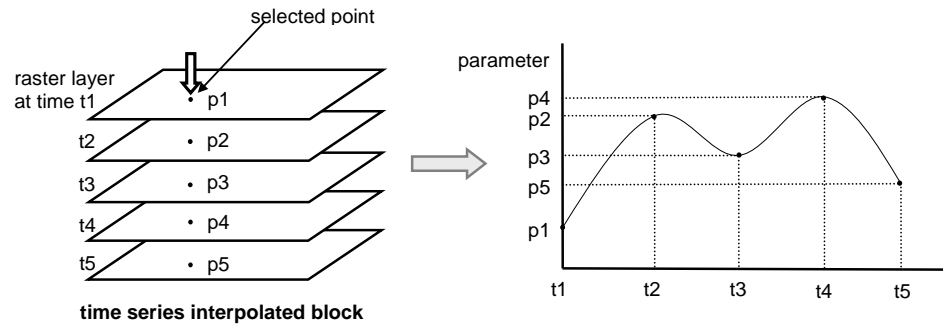


Figure 5.14 Dynamic time series display tool.

5.7 Find Tables Function

When conducting analysis with this GIS program, the user may be interested in retrieving data for a certain hydrodynamic or water quality parameter, or measurement time period. The *Find Tables* function is implemented specifically for this purpose. Figure 5.15 shows the dialog box for the *Find Tables By Parameter* function. The input requirement is simply the parameter of interest. By clicking the *Find* command button, the program automatically searches and lists all tables which contain the specified parameters. A similar function is also developed for searching for tables containing information for a certain measurement period (see Figure 5.16).

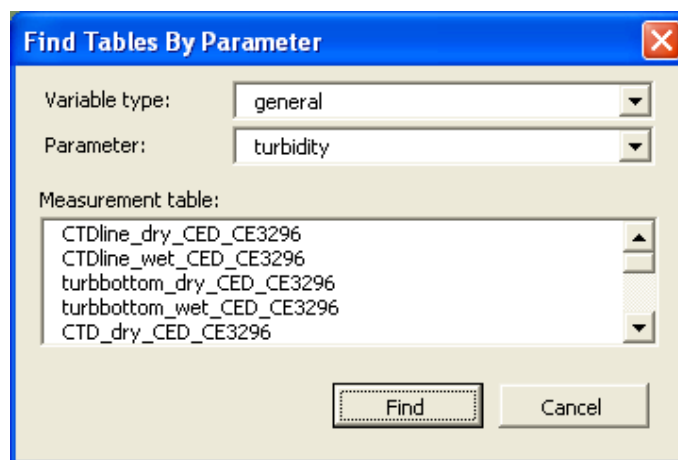


Figure 5.15 Dialog box for *Find Tables By Parameter* function.

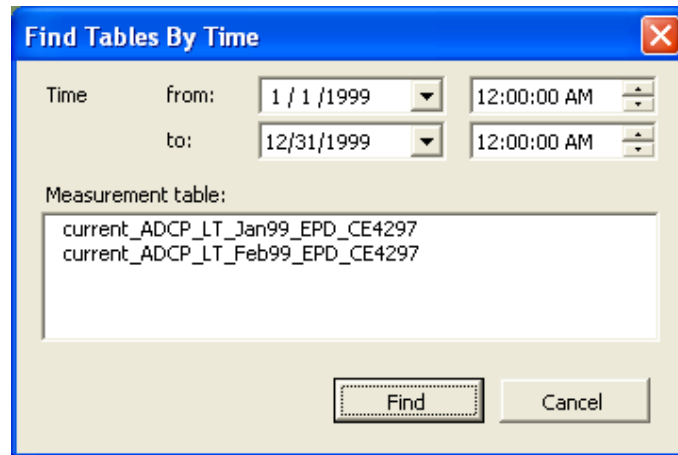


Figure 5.16 Dialog box for *Find Tables By Time* function.

5.8 Summary

This chapter has been concerned with the development of tools for retrieval and visualization of data from the field database. Data retrieval is implemented using the OLE technology inherited in the MS COM architecture. In addition, a data framework making use of object variables for defining data source, dataset, measurement table, and parameter is developed for efficient management of database metadata. For data visualization, there are three basic methods – spatial layer, time series, and profile. Interpolation functions combining spatial and 1D data-fitting techniques are also incorporated into the system to account for the fact that collected data are typically sparsely-distributed in both space and time. In addition, two interactive data display tools: the sectional display tool and the dynamic display tool, are developed to extend the 2D and static entity of GIS for 3D and dynamic applications. The *Find Tables* Function which is developed for querying measurement tables based on input of measurement time or parameter has also been presented.

6 Integration with a Hydrodynamic-Water Quality Coupled Model

6.1 GIS-Model Integration

The second component of PRE_WAGIS is the integration of the GIS with a 3D hydrodynamic-water quality coupled finite element model (refer to Figure 3.1). This chapter presents the fundamental governing equations as well as the operational platform of this model. The methods for integrating GIS and environmental models are examined to determine which is the most suitable for the current study. In addition, the development of the GIS-modelling functionalities, including retrieval and editing of model input data, setting initial conditions from spatial layer, model input and output displays, and mesh grid configuration, are discussed.

6.2 3D Hydrodynamic-Water Quality Coupled Model

The 3D hydrodynamic-water quality coupled finite element model was initially developed by Wai and Lu (2000) to simulate sediment-water transport processes using an efficient parallel-processing algorithm, and was later modified by Jiang (2003) to include the fate and transport of cohesive sediment and heavy metals modelling. Jiang (2003) also adopted more advance algorithms, such as the parallelized Eulerian-Lagrangian operator splitting strategy for solving large linear equation system, the level 2.5 turbulence closure sub-model to improve the accuracy of the vertical eddy viscosity

coefficient estimation, and the finite element method for solving vertical diffusion term, and successfully applied it for simulating the PRE situation. Note that the following description of the 3D hydrodynamic-water quality coupled model is referenced from Jiang (2003).

6.2.1 Governing Equations

The model is made of a set of sub-components as shown in Figure 6.1. The hydrodynamic model together with the turbulence and salinity modules forms the base model. Variables are passed through two auxiliary models for predictions of cohesive sediment and heavy metal.

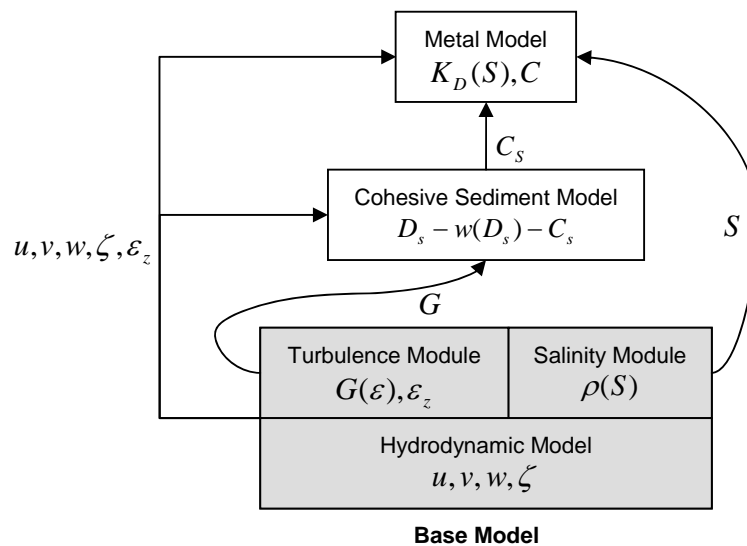


Figure 6.1 Computation flow of the three-dimensional hydrodynamic sediment and heavy transport numerical model (Jiang, 2003).

6.2.1.1 Base Model

The base model is built upon the Navier-Stokes equations with the assumption that hydrodynamics in estuaries and coasts is isothermal; and the vertical acceleration is negligible in comparison with gravitational acceleration, resulting in hydrostatic pressure distribution. In the hydrodynamic module, important phenomenon including turbulence and salinity are also considered. The governing equations are given as follow:

Continuity equation

$$\frac{\partial \zeta}{\partial t} + \frac{\partial H u_j}{\partial x_j} = 0 \quad (6.1)$$

Momentum equation (Navier-Stokes equations)

$$\frac{d u_i}{d t} + f \beta_{ij} u_j + P_i^* + g \frac{\partial \zeta}{\partial x_i} = \frac{\partial}{\partial x_j} \left(\varepsilon_j \frac{u_i}{x_j} \right) \quad (6.2)$$

Salinity transport equation

$$\frac{\partial S}{\partial t} = \frac{\partial}{\partial x_j} \left(\varepsilon_{sali,j} \frac{S}{x_j} \right) \quad (6.3)$$

Level 2.5 turbulence closure model (Mellor et al., 1998; Mellor and Yamada, 1982)

$$\frac{d q^2}{d t} = \frac{\partial}{\partial x_j} \left(\varepsilon_{q,j} \frac{q^2}{x_j} \right) + \frac{2 \varepsilon_{q,z}}{H^2} \left(\frac{\partial u_i}{\partial \sigma} \right)^2 + \frac{2 g \varepsilon_{sali,z}}{\rho_o H} \frac{\partial \rho}{\partial \sigma} - \frac{2 q^3}{B l} \quad (6.4)$$

$$\frac{d q^2 l}{d t} = \frac{\partial}{\partial x_j} \left(\varepsilon_{q,j} \frac{q^2 l}{x_j} \right) + \frac{E_1 l \varepsilon_z}{H^2} \left(\frac{\partial u_i}{\partial \sigma} \right)^2 + E_1 E_3 l \frac{g \varepsilon_{sali,z}}{\rho_o H} \frac{\partial \tilde{\rho}}{\partial \sigma} - (1 + E_2 (l / k L)^2) \frac{q^3}{B_1} \quad (6.5)$$

$$\text{where } u_j = \{u, v, \omega\}, \omega = \frac{1}{H} \left[w + (1 - x_3) u_i \frac{\partial h}{\partial x_i} - x_3 \left(\frac{\partial \zeta}{\partial t} + u_i \frac{\partial \zeta}{\partial x_i} \right) \right];$$

$$\varepsilon = [\varepsilon_x, \varepsilon_y, \varepsilon_z H^{-2}]; \varepsilon_{sali,j} = [\varepsilon_{sali,x}, \varepsilon_{sali,y}, \varepsilon_{sali,z} H^{-2}]; x_j = [x, y, (z + h) H^{-1}];$$

$$H = h + \zeta; \beta_{ij} = \begin{bmatrix} 0 & -1 & 0 \\ 1 & 0 & 0 \end{bmatrix}; i = 1, 2; j = 1, 2, 3;$$

$$\varepsilon_{q,j} = [\varepsilon_{q,x}, \varepsilon_{q,y}, \varepsilon_{q,z} H^{-2}]; L = [(\eta - z)^{-1} + (H - z)^{-1}]^{-1}; \frac{\partial \tilde{\rho}}{\partial \sigma} \equiv \frac{\partial \rho}{\partial \sigma} - \frac{1}{v_s^2} \frac{\partial \rho}{\partial \sigma};$$

t is time; h is the water depth relative to the minimum water level; ζ is the water level from the minimum water level; x_1, x_2, x_3 are the spatial coordinates in sigma σ coordinates; u, v, ω are the velocity components along the x, y, z directions, respectively, in σ coordinates; w is the vertical velocity in Cartesian coordinate; $\varepsilon_x, \varepsilon_y, \varepsilon_z$ are the eddy viscosity coefficients for water in the x, y, z directions, respectively;

$\varepsilon_{sali,x}, \varepsilon_{sali,y}, \varepsilon_{sali,z}$ are the eddy diffusion coefficients for salinity in the x, y, z directions, respectively; g is the gravity acceleration; f is the Coriolis coefficient; S is the water salinity; ρ is the water density; ρ_o is the constant reference water density; $q^2/2$ is the turbulence energy; l is the master turbulence length scale; $\varepsilon_{q,x}, \varepsilon_{q,y}, \varepsilon_{q,z}$ are the eddy diffusion coefficients for turbulence energy in the x, y, z directions, respectively; p is the water pressure; v_s is the speed of sound; the constant coefficients are $E_1 = 1.8, E_2 = 1.33, E_3 = 1.0, B_1 = 0.74$ and $k = 0.4$; and P_i^* is the baroclinic term with Boussinesq assumption in the x_i direction given by the following equation:

$$P_i^* = \frac{gH}{\rho} \int_{\sigma}^1 \frac{\partial \rho}{\partial x_i} d\sigma - \frac{g}{\rho} \frac{\partial H}{\partial x} \int_{\sigma}^1 (\sigma - 1) \frac{\partial}{\partial \sigma} d\sigma \quad (6.6)$$

The water density ρ is a function of temperature T and chlorinity Cl :

$$\rho = 1000 + 1.455Cl - 0.0065(T - 4 + 0.4Cl)^2 \quad (6.7)$$

and Cl relates to salinity by:

$$Cl = (S - 0.03)/1.805 \quad (6.8)$$

The Smagorinsky formula is used to obtain the horizontal viscosity and coefficients, ε_i and $\varepsilon_{sali,i}$:

$$\varepsilon_i, \varepsilon_{sali,i} = \frac{1}{2} CA \left[\left(\frac{\partial u_1}{\partial x_1} \right)^2 + \frac{1}{2} \left(\frac{\partial u_1}{\partial x_2} + \frac{\partial u_2}{\partial x_1} \right)^2 + \left(\frac{\partial u_2}{\partial x_2} \right)^2 \right]^{1/2} \quad (6.9)$$

where C is a constant ranging from 0.1 to 0.2, A is the area of the triangular elements. The Level 2.5 turbulence closure model adopted by Mellor and Yamada (1982) is applied for computation of vertical eddy viscosity and diffusion coefficients.

6.2.1.2 Cohesive Sediment Transport Model

The fate of cohesive sediment is heavily influenced by flocculation as the floc settling velocity can be several orders of magnitude greater than that of primary particles. In this model, the floc size equation is coupled with the sediment concentration equation for computation of the transport and fate of cohesive suspended sediment concentration.

Sediment Concentration Equation

$$\frac{\partial C_s}{\partial t} - \frac{\partial w_s C_s}{H \partial x_3} = \frac{\partial}{\partial x_j} \left(\varepsilon_{sed,j} \frac{C_s}{x_j} \right) \quad (6.10)$$

Floc Size Transport Equation

$$\frac{\partial D_s}{\partial t} - w_s \frac{\partial D_s}{H \partial x_3} = \frac{\partial}{\partial x_j} \left(\varepsilon_{sed,j} \frac{D_s}{x_j} \right) + K_A C_s G D_s^2 - K_B G^{3/2} D_s^2 (D_s - D_p) \quad (6.11)$$

where $\varepsilon_{sed,j} = [\varepsilon_{sed,x}, \varepsilon_{sed,y}, \varepsilon_{sed,z} H^{-2}]$; C_s is the cohesive sediment concentration; w_s is the apparent sediment settling velocity; $\varepsilon_{sed,x}, \varepsilon_{sed,y}, \varepsilon_{sed,z}$ are the eddy diffusion coefficients for sediment in the x, y, z directions, respectively; D_s is the diameter of floc; K_A and K_B are the break-up parameters; D_p is the diameter of primary particle; and G is the turbulence shear stress.

The turbulence shear stress G is calculated by substituting the turbulence energy equation according to Mellor and Yamada (1982):

$$G = \sqrt{\frac{\varepsilon}{\nu}} = \sqrt{\frac{q^3}{Bl\nu}} \quad (6.12)$$

where ε is the turbulence energy dissipation rate; ν is the kinetics viscosity; and B is a constant set to 16.6.

6.2.1.3 Heavy Metal Transport Model

The computation of the fate and transport of heavy metal is based on the one-stage and two-stage adsorption and desorption mechanism. The one-stage equation assumes that the concentration of metal remains constant as the dissolved metal is adsorbed onto surface of sediment. The equations for the two-stage mechanism is adopted based on the theory by Jannasch et al. (1988), which assumes that the dissolved metal particle is adsorbed “quickly” onto the surface of sediment, and then deposit “slowly” into the inner part of sediment.

One-stage Model:

Adsorbed Metal Concentration Equation

$$\frac{dP}{dt} = k(K_D C_d - P) + w_s \frac{\partial P}{\partial z} + \frac{\partial}{\partial x_j} \left(\varepsilon_{p,j} \frac{\partial P}{\partial x_j} \right) \quad (6.13)$$

Dissolved Metal Concentration Equation

$$\frac{dC_d}{dt} = -C_s k(K_D C_d - P) + \frac{\partial}{\partial x_j} \left(\varepsilon_{m,j} \frac{\partial C_d}{\partial x_j} \right) \quad (6.14)$$

Two-stage Model:
First Stage (Fast Process) Metal Sorption Equation

$$\frac{dP_1}{dt} = k(K_{D,1} C_d - P_1) - k_2(K_{D,2} P_1 - P_2) + w_s \frac{\partial P_1}{\partial x_3} + \frac{\partial}{\partial x_j} \left(\varepsilon_{p,j} \frac{\partial P_1}{\partial x_j} \right) \quad (6.15)$$

Second Stage (Slow Process) Metal Sorption Equation

$$\frac{dP_2}{dt} = k_2(K_{D,2} P_1 - P_2) + w_s \frac{\partial P_2}{\partial x_3} + \frac{\partial}{\partial x_j} \left(\varepsilon_{p,j} \frac{\partial P_2}{\partial x_j} \right) \quad (6.16)$$

Dissolved Metal Concentration Equation

$$\frac{dC_d}{dt} = -C_s k_1(K_{D,1} C_d - P_1) + \frac{\partial}{\partial x_j} \left(\varepsilon_{m,j} \frac{\partial C_d}{\partial x_j} \right) \quad (6.17)$$

$$P = P_1 + P_2, j = 1, 2, 3 \quad (6.18)$$

where P is the adsorbed/particulate metal concentration in ug/g; K_D is the partition coefficient in l/g; k is the forward or reverse transfer rate in 1/s; w_s is the particle setting velocity; $\varepsilon_{p,j} = [\varepsilon_{p,x}, \varepsilon_{p,y}, \varepsilon_{p,zH^{-2}}]$, $\varepsilon_{p,x}, \varepsilon_{p,y}, \varepsilon_{p,z}$ are the eddy diffusion coefficients for adsorbed/particulate metal; C_d is the dissolved sediment concentration; C_s is the suspended sediment concentration; $\varepsilon_{m,j}$ is the dissolved metal diffusivity coefficient in j direction. The subscript “1” denotes the parameter of the first equilibrium partition at the sediment surface, where “2” denotes the interactive process in the inner sediment.

6.2.2 Operational Platform

Because of the high computational effort required in solving the complex equations as discussed, this model runs on an efficient parallel computing system of ten computer units using Message Passing Interface (MPI) scripting. The parallelized system is implemented using a LINUX operating system, in which its user-friendliness is incomparably lower than that of proprietary operating systems such as Windows or MacOS.

The 3D hydrodynamic-water quality coupled finite element model, being operated in a command line interpreter system, achieves its ultimate function in solving the complex hydrodynamic problems. However, in terms of pre-processing and post-processing capabilities, the existing 3D hydrodynamic-water quality coupled finite element model is not equipped with any tools to handle spatial analysis and visualization. This constraint marks the necessity to provide the essential graphical tools for preparations and displays of model inputs and output; and the integration of the model with a GIS is identified as an efficient approach.

6.3 Integration Method

According to Shamsi (2002), there are three basic methods of integrating GIS with environmental models. They are the *interchange* method, the *interface integration* method, and the *integration* method. In the *interchange* method, the GIS and the model run independently and separately and there is no direct linkage between the two systems. This method requires manual batch processing of data interchange between the GIS and the model. The *interface integration* automates batch transfer of information process using a pre-processor and a post-processor component. The pre-processor is for analyzing and exporting GIS data to the model input files, while the post-processor is for importing the model output and displaying it through the GIS interface. The *integration* method resembles the closest relationship between the GIS and the model. This method not only includes the automation of data transfer, but also allows the execution of the model, such that the GIS and the model become a tightly-coupled system offering both GIS and modelling capabilities.

In this study, the *interface integration* method is applied for integrating the GIS with the hydrodynamic-water quality coupled model. One of the main advantages for using this

method is that the automation of data transfer eliminates the hassle to deal with manual transfer of data and thus avoids the potentials of data entry errors. As for why not extending this integration further, using the *integration* method lies upon the model operational scheme and the requirement of GIS capabilities for the model. The procedural implementation of the model consists of three sequential steps: 1) preparation of input file, 2) execution of model, and 3) retrieval of result from output. Note that the model does not provide any real-time generation of results, that is, results are outputted in a batch after model simulation is fully complete. The actual execution of the model is a single, distinct procedure that does not require any GIS capabilities. So the application of a simpler approach of the *interface integration* method is sufficient to meet the goal of integration, that is, to allow pre-processing and post-processing procedures to be carried out entirely within the GIS interface, for this study.

6.4 Model Pre-processing

The pre-processing component is designed for retrieval, manipulation, editing, display, and export of model input data through the GIS interface. The data input requirements for the model include bathymetry of the study area, inflow and outflow for source elements, suspended and bed sediment parameters, tidal flat drying and flooding control variables, initial conditions and boundary conditions of tidal elevation, salinity, current velocity, sediment concentration, and metal (or water quality) concentration, as well as mesh grid configuration.

6.4.1 Retrieval and Editing of Model Input Data

All model inputs are primarily stored in forms of text file. A separate relational database is developed specifically for model inputs (refer to Figure 3.1) also using the MS Access software. The placement of model input into a relational software is essential not only for efficient management of data but also for establishing a direct linkage between the model input and the GIS user interface using OLE. The tables of input data in the database can be embedded into the pivot tables in the user input dialog boxes. In this way, the user not only can view the data from the database, but also can update input data through the dialog boxes (see Figure 6.1). Figure 6.2 shows the dialog box for retrieval and editing of initial conditions of velocity. Similar dialog boxes are implemented for all other model inputs including switch and primary data; mesh grid

configuration; water and land boundary; water depth; element source; sediment parameters; dry and flood control parameters; and initial and open boundary conditions of tide, salinity, sediment concentration, sediment floc size, and metal. Finally, to complete the entire pre-processing implementation, an *Update Input Files* function is incorporated into the software. This function takes the data from the database and creates input files based on the data. As shown in the dialog box in Figure 6.4, the user can specify the directories for model input database and input files and all or a selection of the input files for update. In doing so, only the files for model inputs previously changed are created to avoid extraneous computational efforts.

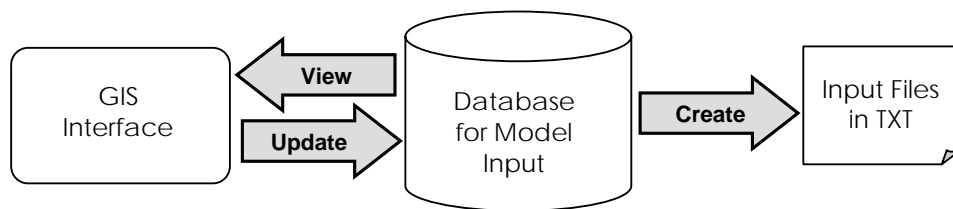


Figure 6.2 Data flow diagram for model input retrieval and editing.

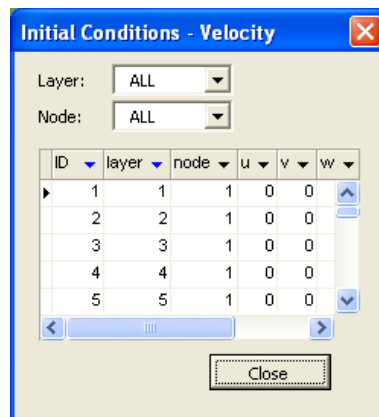


Figure 6.3 Dialog box for initial conditions of velocity.

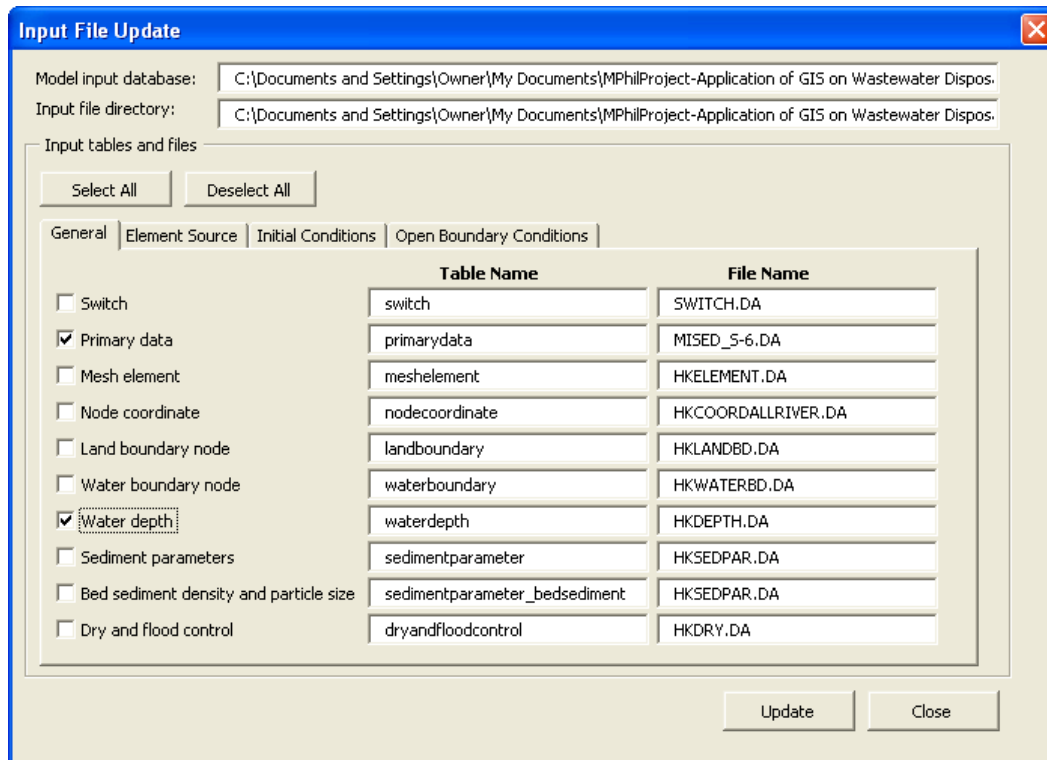


Figure 6.4 Dialog box for updating input files.

6.4.2 Setting Initial Conditions from Spatial Layer

In addition to manually adjusting the numeric figures through the pivot tables in the input dialog boxes, a second approach to set initial conditions is by exploiting information from the spatial interpolated layer created from the collected data. A module is developed, which extracts values (at locations of nodal points) from an existing layer and updates accordingly in the model input table. As shown in the dialog box in Figure 6.5, the input requirements are simply the name of an existing spatial layer, and the parameter and depth layer for which initial conditions are to be set. Figure 6.6 shows the procedural diagram for this function. Upon execution, the system first identifies the locations of nodal points by reading their corresponding geographic coordinates. The system then runs through a loop for each nodal point, checking whether the nodal point is within the boundaries of the spatial layer. If this is the case, values are extracted and placed into the initial conditions table. This procedure is repeated for each node until the last node number (i.e. 11342) for the mesh grid is reached. The verification of the nodal point locations is significant because in general, the created spatial layer covers only a portion of the entire mesh grid (see Figure 6.7).

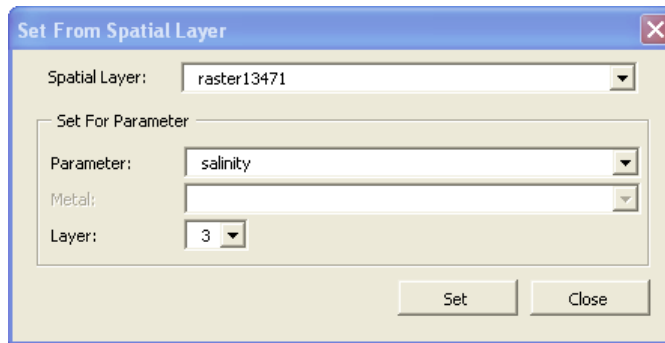


Figure 6.5 Dialog box for setting initial conditions from existing spatial layer.

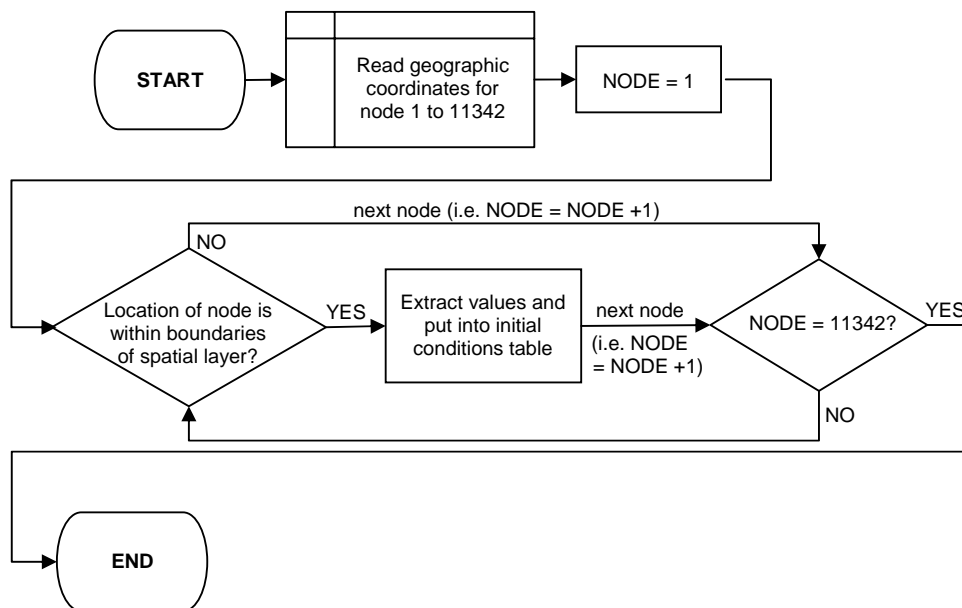


Figure 6.6 System procedures for setting initial conditions from spatial layer.

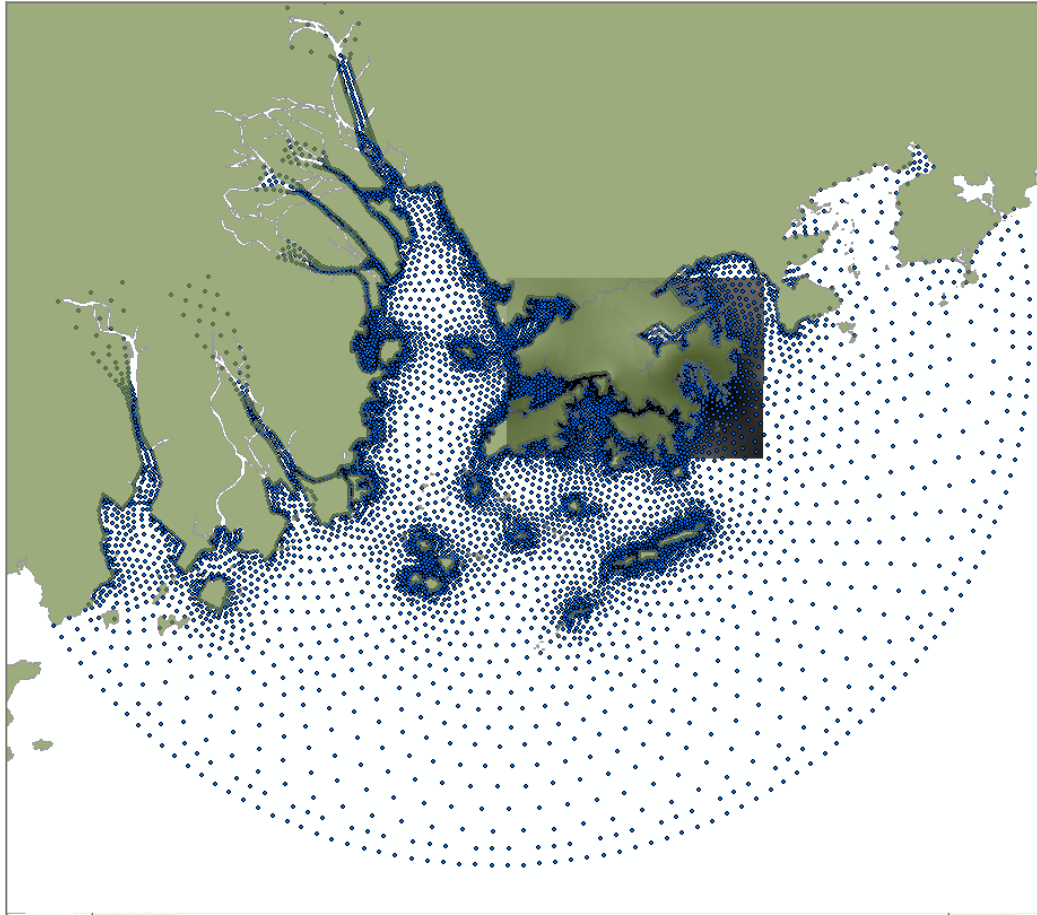


Figure 6.7 A spatial layer overlaying the model mesh of nodal points.

6.4.3 Model Input Display

6.4.3.1 Spatial Layer

In addition to examine the model input in numerical text formats, a more imperative purpose for integrating model input with the GIS is to visualize the information in spatial forms through the mapping window. Fundamentally, the types of model input which would make practical use through GIS display are initial conditions, water depths, and mesh grid configuration (discussed in the next section). The data displaying functions for model input are similar to that for field data (mentioned in Chapter 4). As shown in the dialog box in Figure 6.8, a spatial layer can be created simply by specifying the parameter and the layer number (not applicable for water depths and tidal data). Similar to the retrieval process for field data, the retrieval process for model input takes on a two-step SQL query procedure as shown in Figure 6.9. The system first creates a spatial table containing all data including geographic referencing information of the

selected parameter based on the input from the model database, and then further filters the data of the specified depth layer to create a spatial layer.

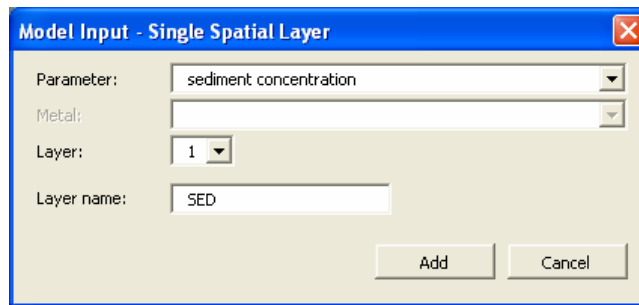


Figure 6.8 Dialog box for creating single spatial layer – model input.

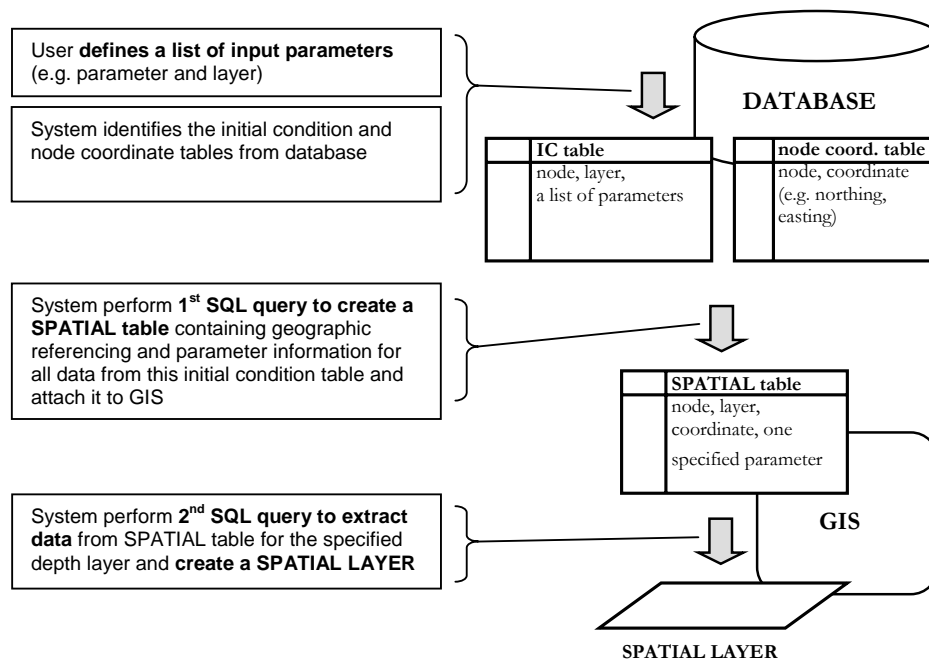


Figure 6.9 System procedures for creating a spatial layer – model input.

The setup of the model mesh grid consists of 11342 nodes horizontally and 7 layers in the vertical direction. The values for model input parameters are attributed to node and layer numbers. In order to display the information spatially, each nodal point must be referenced to a geographic coordinate. The nodal geographic coordinates are all stored in a data coordinate table, which is connected with the other tables, for geographical referencing. As shown in Figure 6.10, the relational structure (i.e. one-to-many) between the nodal coordinate table and the tables for initial conditions and water depths is an analogy to that of the field data (refer to Figure 4.1).

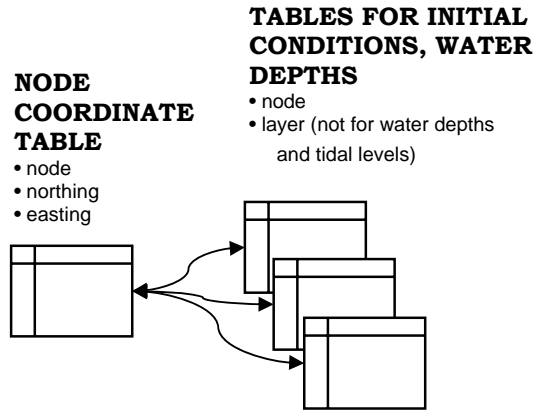


Figure 6.10 Database relationship diagram – model input data.

The incorporation of model input displays in PRE_WAGIS allows for quick and easy interpretation of information. Figure 6.11 is a single spatial point layer of water depth created using the model input display command. The colour of the nodal points gradates from light to dark as the water depth varies from shallow to deep. Hence, the user can acquire, at a glance, a comprehensive picture of a specified model input variable. Note that similar to the data display for field data, the spatial layer display function can also be implemented using batch mode (i.e. more than one spatial layer can be created upon a single execution of command) to generate a block of profile spatial layers.

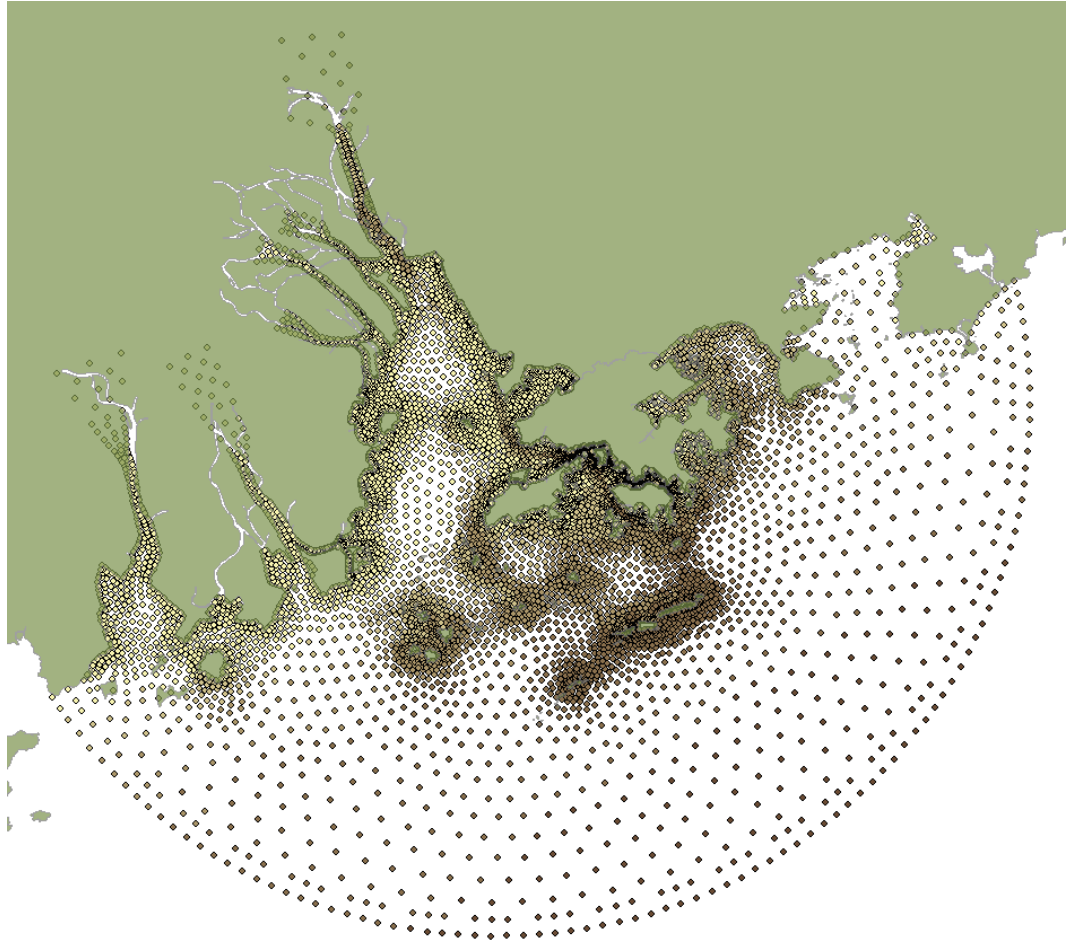


Figure 6.11 Display of a spatial point layer of water depth from model input in GIS.

6.4.3.2 Time Series and Profile

The only input variable at the open boundary which varies with time and thus requires time series display is tidal level. All other variables, such as sediment concentration, salinity, and metal concentration, are assumed to be constant with time. The time series display for tidal level is included as part of the same dialog box for the field data. This allows comparison of field-collected and model data through the same graphic display. Figure 6.12 is the time series dialog box showing the selection controls, namely, the measurement time period and the open boundary node number, for model input. The graphic display shows two tidal curves, one created from field data (i.e. from CEDD Project – AGREEMENT NO. CE32/96; Hydrographic Survey; tidal data for dry season; station ID: 1) and the other from model input at open boundary node number 1.

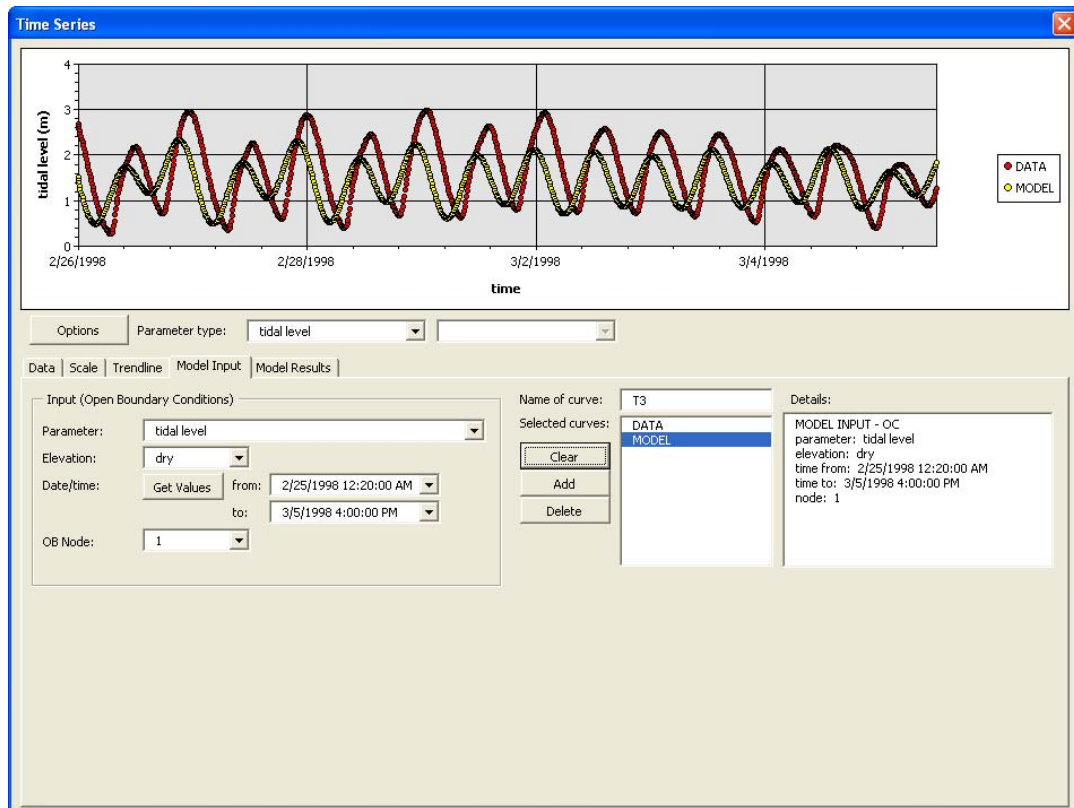


Figure 6.12 Dialog box for creating time series – model input.

The type of model input which can utilize the profile display function includes both initial and boundary conditions of all variables except tidal level and water depth. Similarly, the profile display for model input is incorporated into the same dialog box for field data to enable comparison of information. As shown in Figure 6.13, a profile for model input can be created by simply specifying the parameter and the node number or open boundary node number. The graphic display shows two salinity profile curves, one from field data (i.e. from CEDD Project – AGREEMENT NO. CE32/96; Hydrographic Survey; tidal data for dry season; station ID: 1; measurement time: 3/9/1998 5:00:06 PM) and the other from model input (i.e. initial conditions, node number 1).

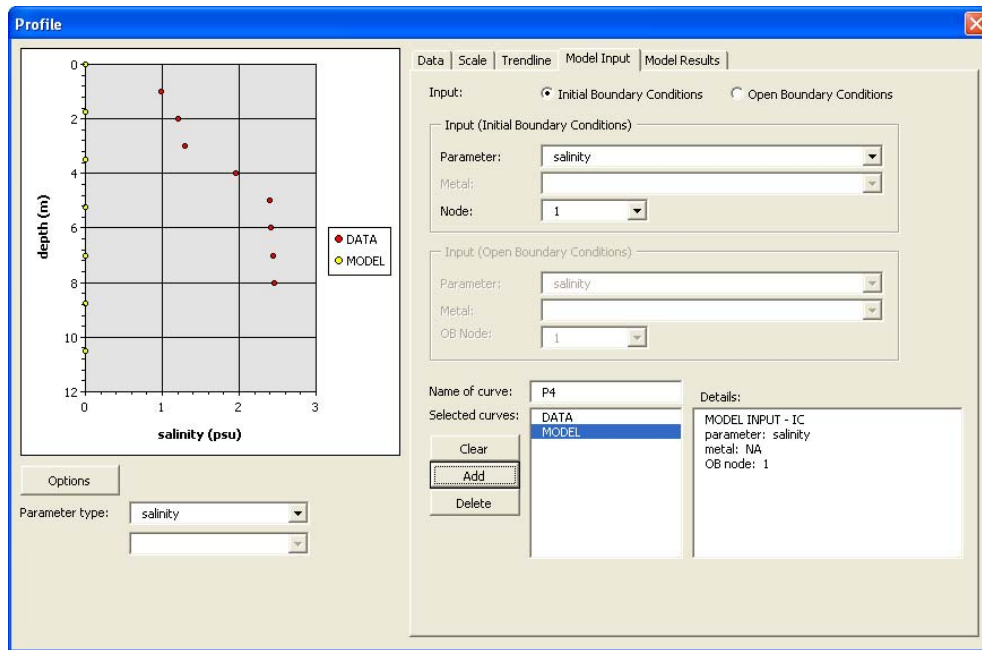


Figure 6.13 Dialog box for creating profile – model input.

The data retrieval process for creating a time series and profile plot is similar to that for creating a spatial layer. However, instead of creating a SPATIAL table, a NON-SPATIAL table (i.e. excluding coordinates, but including node number) is attached into the system. Information for the specified node number is extracted and placed into a spreadsheet for plotting.

6.4.4 Mesh Grid Configuration

Mesh grid configuration is another important procedure which can make efficient use of GIS. The mesh for this model is composed of 4853 triangular elements, and each triangular element is configured based on a set of six nodal points, three for corner points and three for middle points, as shown in Figure 6.14. This results in a total of 11342 nodes, of which 3229 are corner nodes and 8113 are middle nodes. A set of modules is developed not only for generating the mesh grid through the GIS interface, but also for editing the grid elements.

The setup of the mesh grid is derived primarily from two input tables, one identifies the six nodal numbers for each triangular element and the other provides the coordinates of nodal points. Figure 6.15 shows the dialog box for viewing the mesh grid configuration in numeric format.

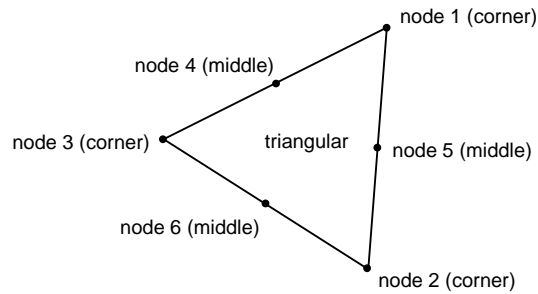


Figure 6.14 Typical configuration for a triangular element.

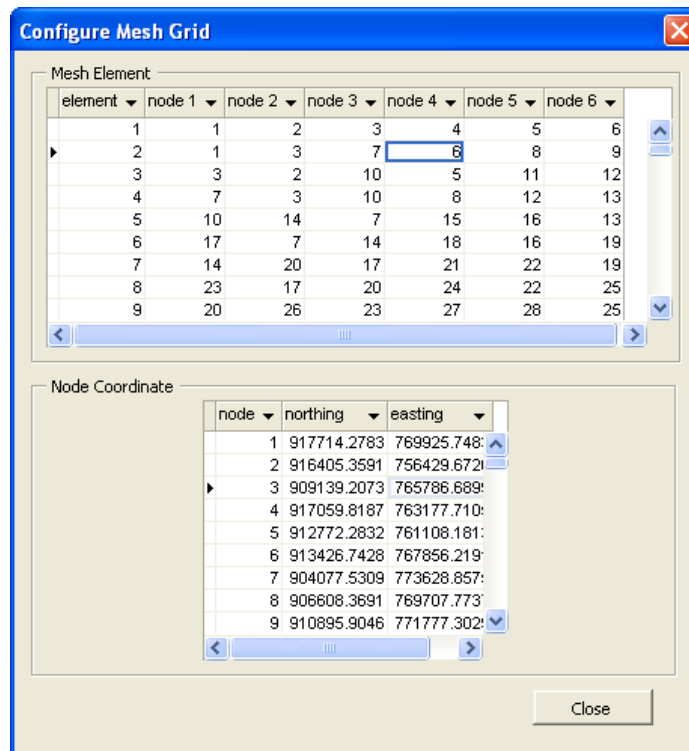


Figure 6.15 Dialog box for configuring mesh grid.

In order to allow spatial examination of the mesh grid in the mapping window, a module is developed for generating shapefiles resembling the mesh grid configuration. The mesh grid generation function is used for creating three types of shapefile: one polygon shapefile representing the triangular elements, one point shapefile for all nodes, and another point shapefile for the corner nodes only (see Figure 6.16).

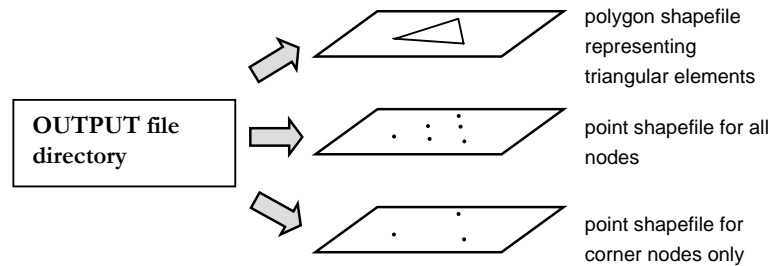


Figure 6.16 Mesh grid generation.

Note that in Figure 6.14 the arrangement of triangular elements relies merely on corner nodes; therefore, a separate corner node shapefile is essential for editing the mesh grid. For this purpose, a table which stores the nodal number for corner nodes is added into the model input database. In addition, another table is created for the middle nodes. This middle node table details the nodal number for all middles as well as the nodal numbers for the two corner nodes, between which each middle node lies. This referencing of middle node to corner nodes is needed for mesh grid editing as made clear in the later sections.

Figure 6.17 outlines the system procedure for generating the three shapefiles. In short, three tables (i.e. nodal coordinates, corner node, mesh element node) provide all the geo-referencing requirement for creating a mesh grid shapefile. The procedure simply involves creating a blank shapefile and then adding point or polygon features sequentially into the shapefile. Figure 6.18 shows the three generated shapefiles in the GIS interface. For better comprehension of the mesh grid setup, the user can add labels for numbering the mesh elements or nodes.

Integration with a Hydrodynamic-Water Quality Coupled Model

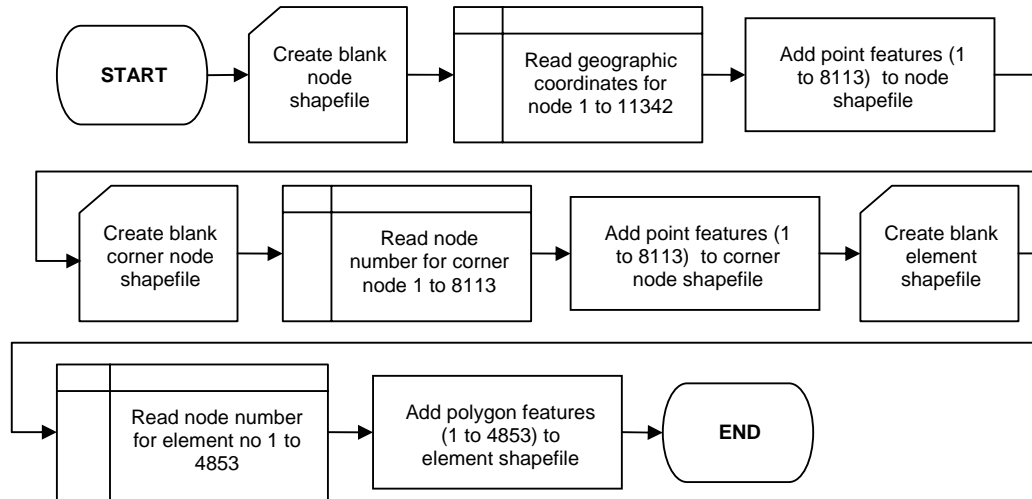


Figure 6.17 System procedure for generating a mesh grid setup.

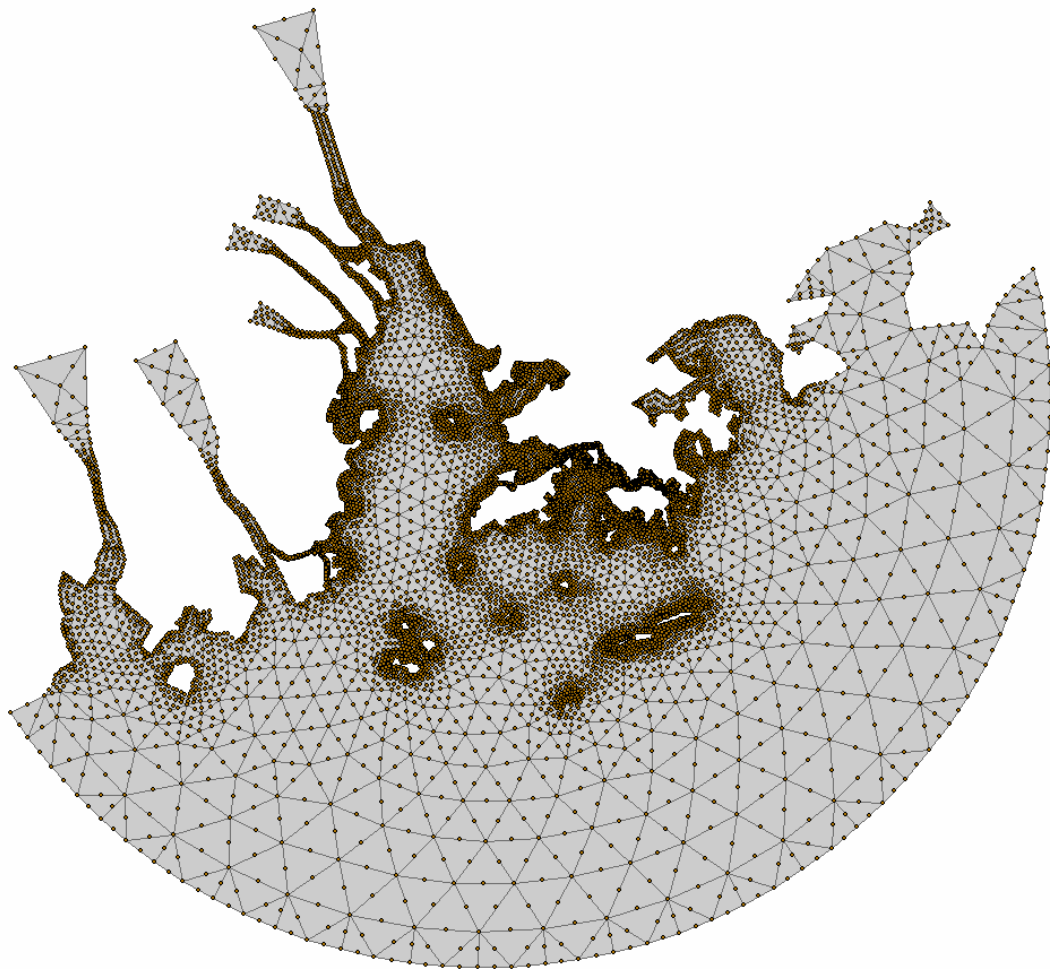


Figure 6.18 Mesh grid shapefiles in GIS interface.

A mesh grid edit toolbar is incorporated into PRE_WAGIS for carrying out element refinements. Using this toolbar, the position of the corner nodes can be modified by moving the nodal points through the GIS display. Figure 6.20 shows the mesh edit toolbar as well as a part of the mesh grid, while Figure 6.19 is an outline of the user-system interaction for a mesh grid edit session. Upon initialization of a mesh grid edit session, the GIS turns off (i.e. make invisible) the shapefile for all nodal points in order to reinforce that only the shapefiles for mesh element and corner points are allowed for selection and editing. The user can re-configure the mesh grid by moving the corner nodes. As shown in Figure 6.20, one of the corner nodes has been selected and moved from position A to B. At the end of the edit session, a message box appears to confirm the changes made within the session (see Figure 6.21). Given this confirmation, the system carries out two types of update, one for the coordinate tables in the model input database and the other for the shapefiles. The program keeps track, during the edit session, which corner node has been modified. Upon termination of the edit session, the new geographic coordinates of these modified corner nodes are acquired from the corner node shapefile. The middle nodes related to the modified corner nodes are identified. Since geometrically a middle node must lie halfway between the two corner nodes, the coordinate for each middle node (x_{middle}, y_{middle}) can be calculated simply by taking the average of the coordinates for the two corner nodes, $(x_{corner1}, y_{corner1})$ and $(x_{corner2}, y_{corner2})$:

$$x_{middle} = \frac{x_{corner1} + x_{corner2}}{2} \quad (6.19)$$

$$y_{middle} = \frac{y_{corner1} + y_{corner2}}{2} \quad (6.20)$$

Based the new coordinate values for middle and corner nodes, the system updates both the coordinate table and the three shapefiles. Figure 6.22 shows the re-configured elements and nodal points after the modification. Note that tracking of the adjusted points within the edit session is an important feature as it enables selected modification in the three shapefiles (i.e. instead of re-generation of entire shapefiles) and thus avoids extra computational load.

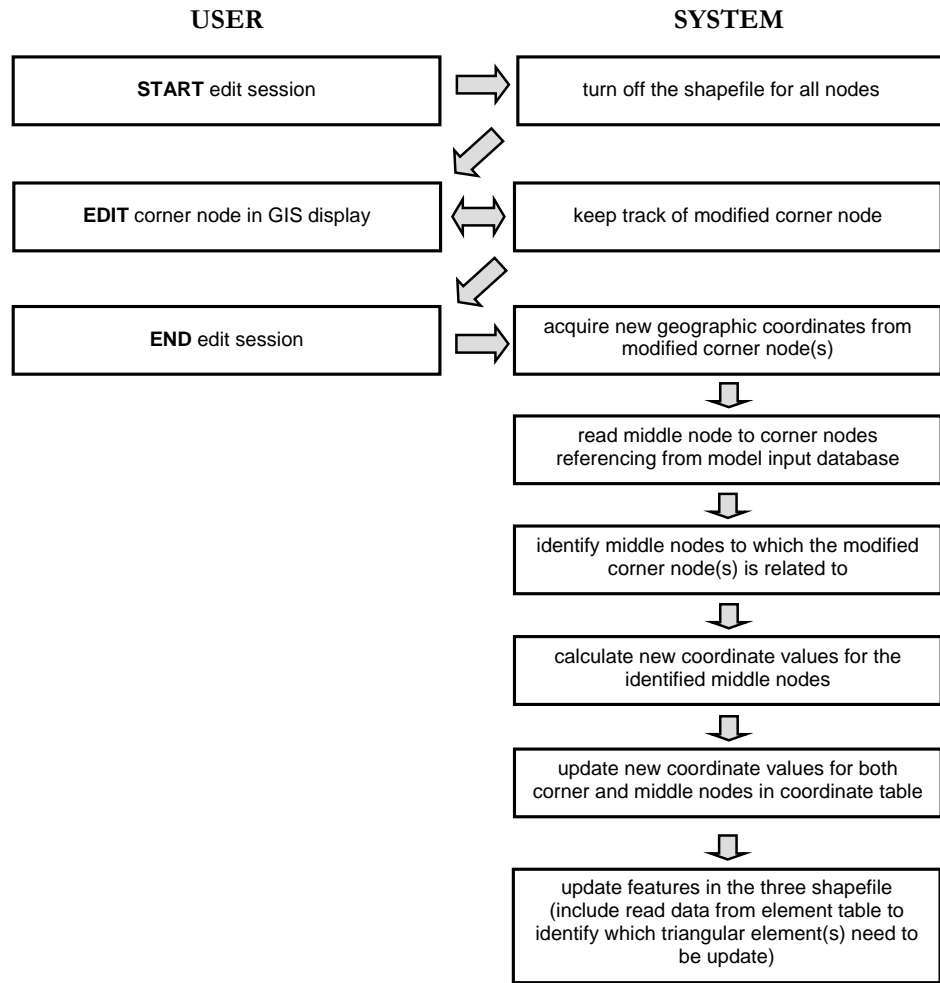


Figure 6.19 Procedure for editing mesh grid.

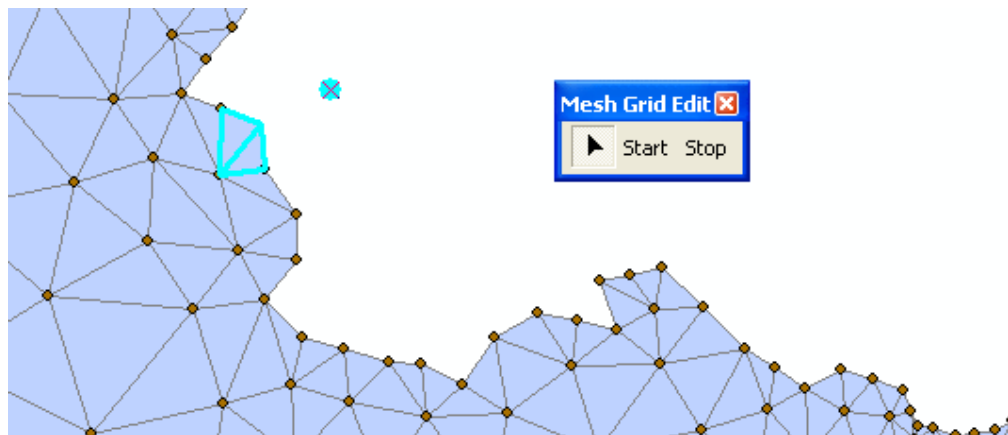


Figure 6.20 Mesh grid edit session.

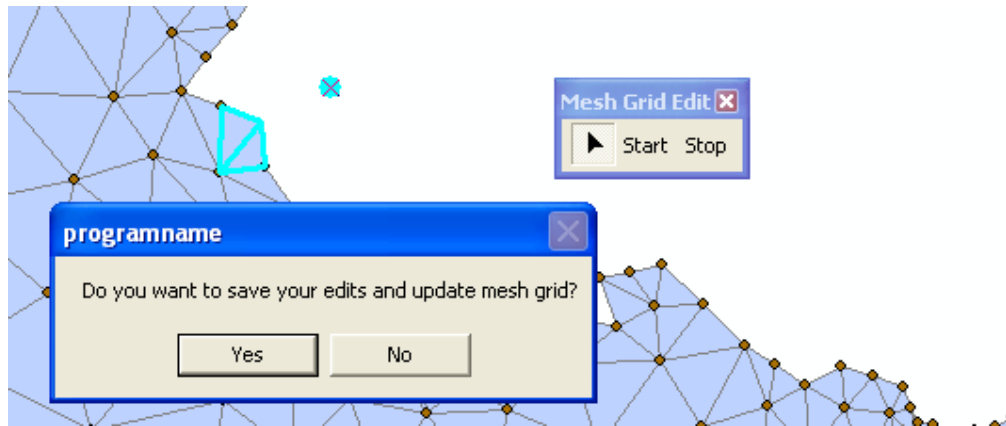


Figure 6.21 End of mesh grid edit session.

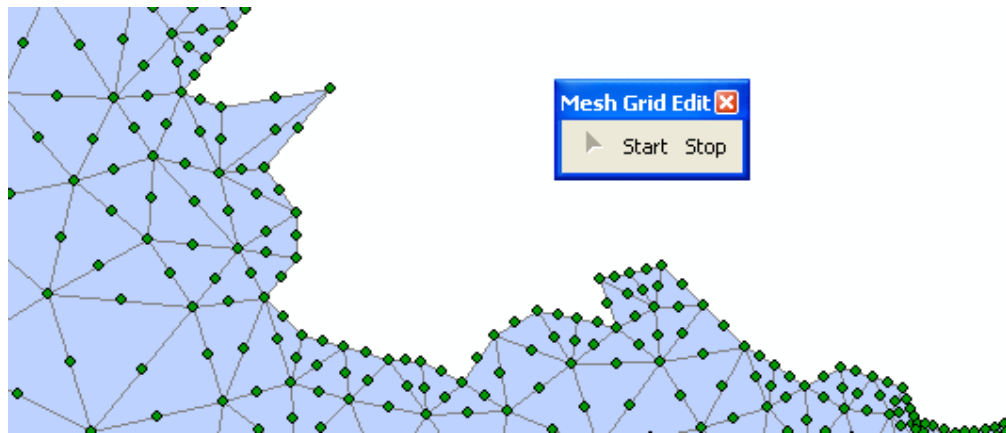


Figure 6.22 Re-configured mesh grid after edit session.

6.5 Model Post-processing

The main intention of the post-processing module is to take the model output data and display them in forms of spatial layer, time series, and profile. Similar to model input, the results consist of a set of text files. Each text file contains data for all output parameters for a specific depth layer, and time. The referencing of the depth layer and time is denoted using the file name. For example, the output file 06M20D01H00M01L.TXT holds the information for June 20, 1:00 am, depth layer 1. Each output file lists the coordinates of each node, and corresponding values for a list of 16 parameters: 1) sediment concentration, 2) sediment floc size, 3) salinity, 4) metal concentration dissolved in water, 5) metal concentration adsorbed on particle surface, 6) metal concentration adsorbed in inter particle, 7) tidal level, 8) depth from sea mean level, 9) horizontal viscosity by Smagorinsky formula, 10) vertical viscosity by turbulence module

for water, 11) vertical viscosity by turbulence module for salinity, 12) vertical viscosity by turbulence module for turbulence, 13) turbulence energy, 14) turbulence energy multiplied by character length, 15) bed shear stress, and 16) critical shear stress.

Two important procedures are undertaken to allow efficient retrieval of the model results in the GIS interface. Firstly, modification is made to model output algorithm such that the output results for each parameter are stored in an individual file, and a slight change is made to the file name format for referencing. For example, the revised output code generates a text file, named 06M20D01H00M01L04P.TXT. This file name denotes June 20, 1:00, depth layer 1, and parameter 4. Each of the output parameters is assigned to a number (i.e. 1 to 16), and parameter 4 refers to metal concentration dissolved in water. In this way, only the output file for the specified time, depth layer, and parameter is attached to the GIS for display, to avoid unnecessary system burden. Secondly, a module is written to convert these output text (TXT) files into Database File (DBF) format (see Figure 6.23). Although the text files can be directly attached to the system for GIS data display, it was observed to be slowing down the system notably. Adding the information in DBF format resolves this problem. A simple output file management dialog box for specifying the output file directories (for TXT and DBF), and for performing the file format conversion operation is shown in Figure 6.24.

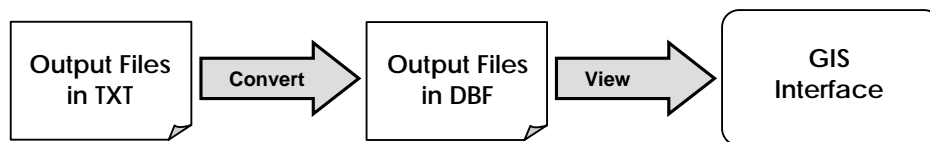


Figure 6.23 Data flow diagram for model result retrieval.

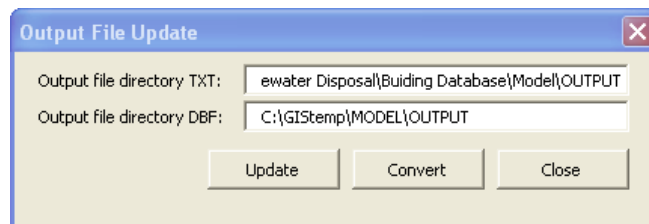


Figure 6.24 Dialog box for updating output file.

The spatial layer displaying procedure for model output is similar to that for initial conditions. However, as shown in the dialog box in Figure 6.25, in addition to the parameter and layer number, the date/time must also be specified. Note that the inputs

of *parameter*, *date/time*, and *layer* are all implemented using combobox controls (e.g. the type of control in which the users select from a given list of items). A module is added, which identifies the available outputs (i.e. for what parameter, date/time, and layer number) and prescribes for selection in the dialog menus. The identification of the available output is carried out by checking the name of each output file in the specified directory.

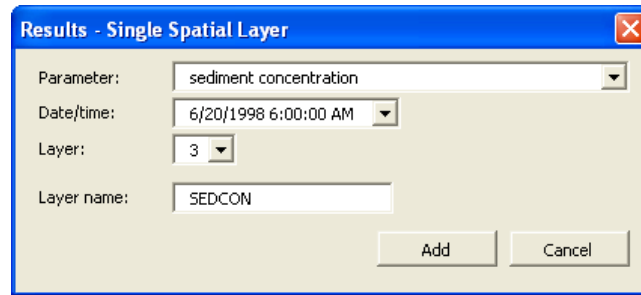


Figure 6.25 Dialog box for creating a single spatial layer.

Upon execution of this dialog box, the system, in turn, converts the specified inputs back into a file name for identification. For instance, the inputs shown in the dialog box in Figure 6.25 translate to the file name 06M20D06H00M01L01P.DBF (note that parameter 1 refers to sediment concentration). As shown in Figure 6.26, the system takes the identified DBF file from the output file directory, attaches it as a table into the GIS, and creates a spatial layer based on the data in the table.

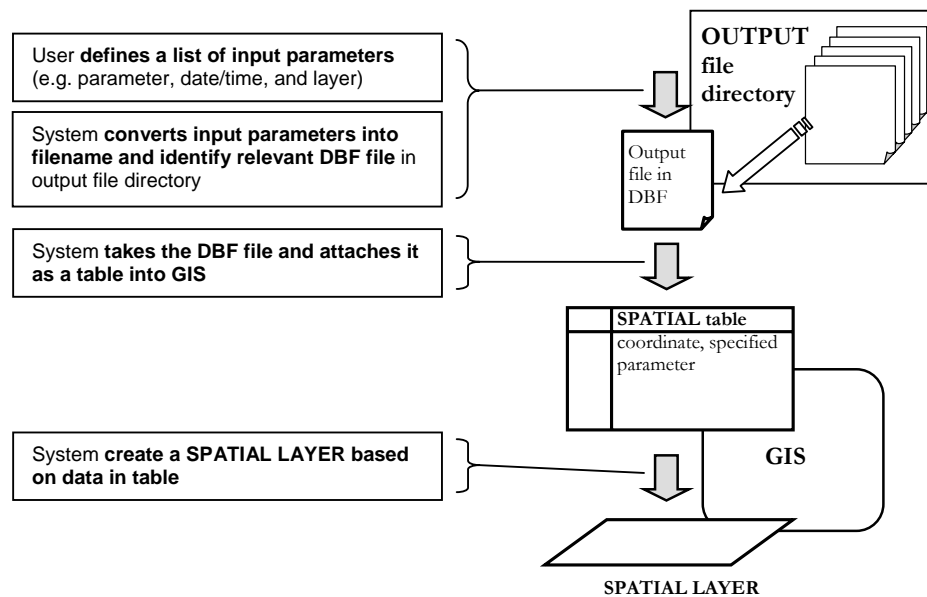


Figure 6.26 System procedures for creating a spatial layer – model results.

Time series and profile displays likewise are also available for model results and are designed as part of the same dialog boxes for field data and model input. The required data for plotting either a time series or a profile curve must be extracted from a group of output files, since each DBF output file contains data only for a particular time and depth layer. For instance, the data needed to create a time series for salinity (i.e. parameter 3) at node 567 and depth layer 2 come from all the files with names in this format: XXMXXDXXH02LM01L03P.DBF. In addition, the requirement to query information (e.g. values for node 567) from the output files demonstrates another reason for converting the initially text-based output files into DBF format. Figure 6.27 summaries the system procedure for creating a time series curve for model results. Similar procedure applies for creating a profile curve.

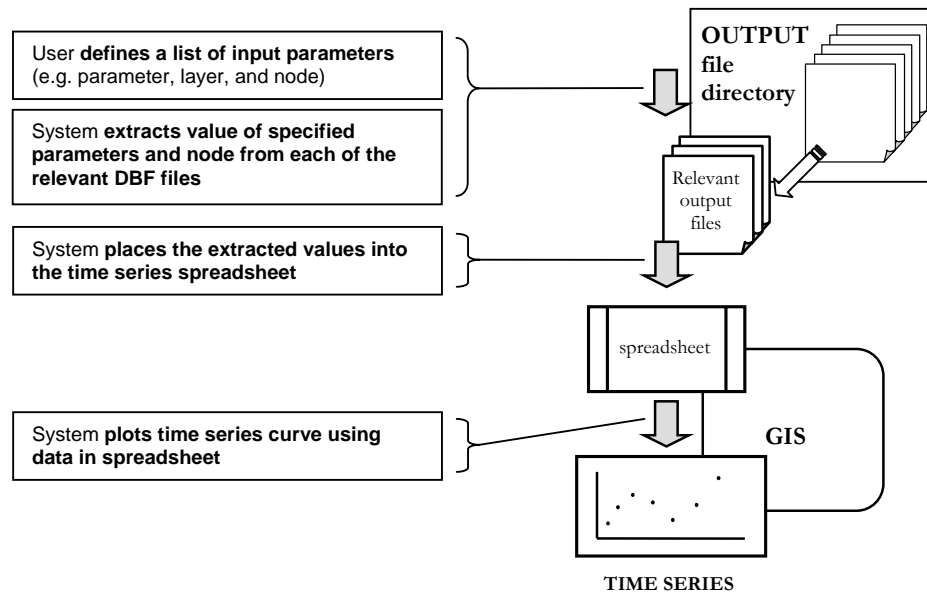


Figure 6.27 System procedures for creating a time series – model results.

6.6 Extensibility of Interpolation Functions and Interactive Tools for Model Data

As demonstrated, the data displays, whether derived from field data, model input, or model results, follow fundamentally the same retrieval framework. That is, three types of display – spatial layer, time series, and profile - are available; and the creating of spatial layers can be done in batch mode to generate a block of spatial layers. The spatial interpolation function also applies for both model input and results to produce single or multiple interpolated spatial layers. Profile interpolated blocks can be obtained from

model input, while both profile and time series interpolated blocks are applicable to model results. However, since the model is established using consistent depth and time interval, tempo-spatial and profile-spatial interpolation is not necessary and thus is not included for model input and results. Given that the functions for generating time series and profile blocks are available for model input and results, the interactive tools, namely, profile and section display and dynamic time series display, are completely interoperable.

6.7 Summary

The chapter has discussed the integration of the GIS with a 3D hydrodynamics-water quality coupled finite element model which was developed by Wai and Lu (2000), and was later modified by Jiang (2003). The main reason for implementing the integration is the lack of spatial analysis and visualization to handle model inputs and outputs in this LINUX-operated numerical model. Based on the *interface integration* method, the integration is carried out to include a pre-processor and a post-processor component. For the pre-processor component, a separate model input database is developed in order to support efficient access, retrieval, and update of information through the GIS interface. In addition, a module for model mesh grid configuration is incorporated to generate mesh grid for viewing in the GIS as well as to perform mesh element modifications. For the post-processing component, a module is developed to convert the original TXT output files to DBF format. In this way, the DBF output files can be attached into the GIS for more efficient data display. The three forms of data display for field data – spatial layer, time series, and profile – are in parallel for visualization of the model inputs and results. Since the model data display methods are in analogy with those for field data, the interpolation functions and interactive tools can easily be extended for application with the model data.

7 Applications of the Integrated-GIS

7.1 System Applications

As the central aim in developing PRE_WAGIS is to apply for spatial-based analysis in exploring hydrodynamic and water quality data, the purpose of this chapter is to demonstrate how the integrated-GIS can be utilized for a number of different applications. In addition to component-independent functionalities such as estimation of values at unknown points in space and time, evaluation of the interpolation methods, and investigation of temporal and spatial trends, other applications involving manipulation of information from both collected and model-generated sources will also be discussed. These include assessment of quality of the collected data, calibration and verification of the hydrodynamic-water quality coupled model, and setting of boundary conditions. Furthermore, how the management of wastewater disposal can be enhanced through the use of this integrated system is also examined.

7.2 Estimation of Values at Unknown Points in Space and Time

One of the applications of PRE_WAGIS is for deriving values in location and time for which no measurement is taken. For this example, the objective is to estimate the concentration of *E. coli* at the water surface of Repulse Bay Beach (see Figure 7.1) for

August 5, 2003. Since Repulse Bay Beach is one of the popular swimming areas in Hong Kong, maintaining a reasonably low *E. coli* level is crucial for public safety. Using the *Find Tables* functions, the measurement table WQ2_Water_EPD is chosen because it contains data for *E. coli* and the specified time falls in its measurement period. As shown in Figure 7.1, there are no monitoring stations anywhere here along the shoreline of the Repulse Bay Beach, but a few such as SM2, SM3, and SM4 are located in the nearby regions. The sampling times for this dataset are not simultaneous among the monitoring stations. Figure 7.2 shows a time series display for *E. coli* at SM2 – depth level: surface, fitted using the Linear Spline method. Values from fixed stations at any point in time within the measurement period can be derived using the *Interpolate Time Series* function. As shown in Figure 7.3, an *E. coli* concentration of 652 cfu/100 mL is derived for station SM2 for August 5, 2003. The tempo-spatial interpolation method is further used to examine the concentration of *E. coli* at Repulse Bay Beach for August 5, 2003. Figure 7.4 shows the tempo-spatial layer generated using the Linear Spline method for 1D interpolation and the IDW method for spatial interpolation. Also shown in this figure is the *Identify Results* dialog box showing that the *E. coli* concentration at Repulse Bay Beach is 500 cfu/100 mL.

Given the standards for water quality control at bathing beaches stipulated in the Hong Kong Yearbook 2004 (The Hong Kong Government, 2005) as shown in Table 7.1, the *E. coli* concentration at Repulse Bay Beach on August 5, 2003 is ranked as poor. The tempo-spatial layer is further classified based on the Hong Kong standard to identify all water regions not suitable for swimming (see Figure 7.5). Most water areas close to the urban centre such as Western Buffer and Victoria Harbour show extremely high concentrations of *E. coli* and thus are not appropriate for swimming. Other regions in which *E. coli* concentrations are of concern include Deep Bay and Mirs Bay. Port Shelter is the only coastal area that is ranked as of good water quality condition measured in terms of *E. coli*.



Figure 7.1 Repulse Bay Beach and fixed stations for measurement table WQ2_Water_EPD.

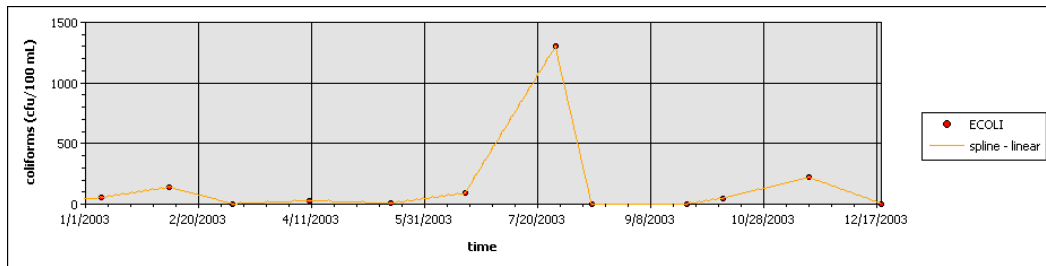


Figure 7.2 Time Series for E. coli from measurement table WQ2_Water_EPD - station ID: SM2 – depth: surface - fitted using Linear Spline method.

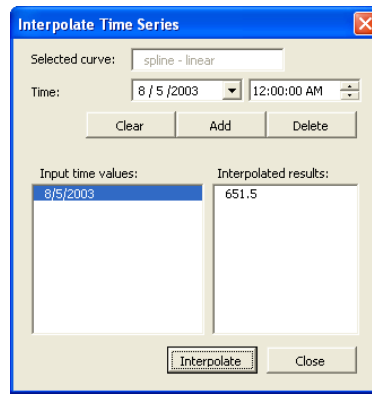


Figure 7.3 Interpolate time series for station SM2 – surface, August 5, 2003.

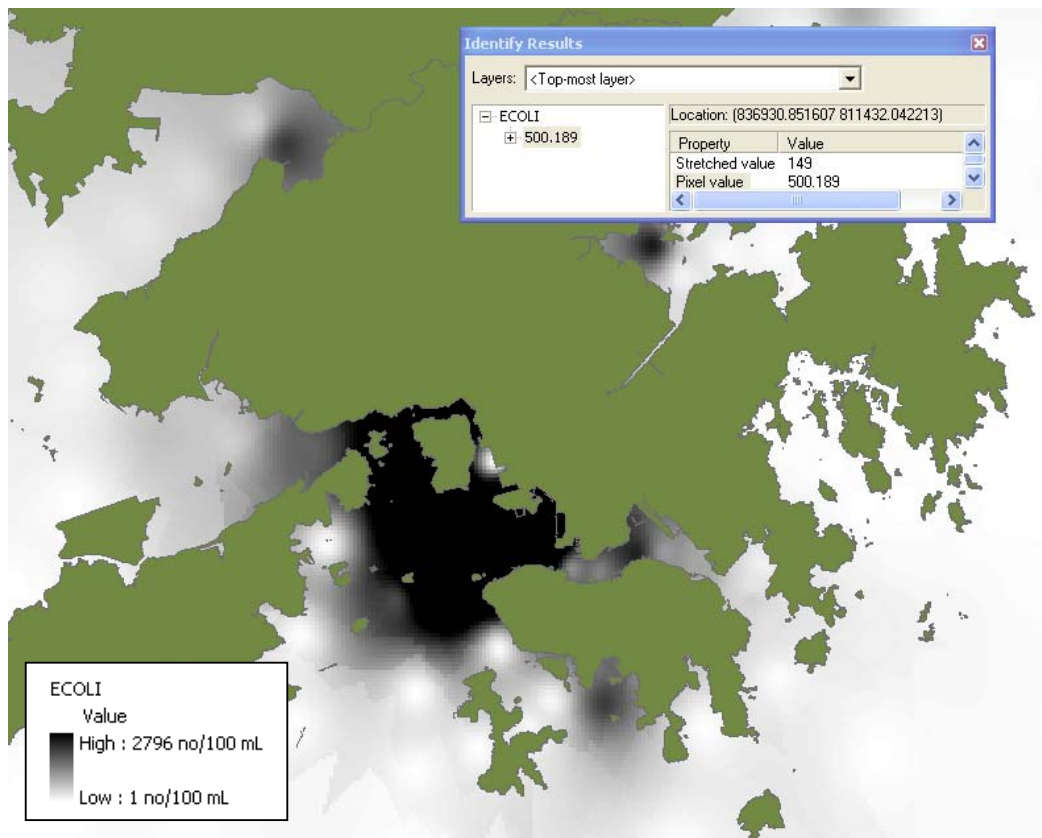


Figure 7.4 Tempo-spatial layer of E. coli from measurement table WQ2_Water_EPD - August 5, 2003 – depth level: surface.

Table 7.1 Standards for water quality control at bathing beaches in Hong Kong.

Beach water quality ranking	Bathing season geometric means of E. coli count per 100 mL of beach water	Minor health risk cases per 1000 swimmers
Good	Up to 24	Undetectable
Fair	25 to 180	10 or less
Poor	181 to 610	11 to 15

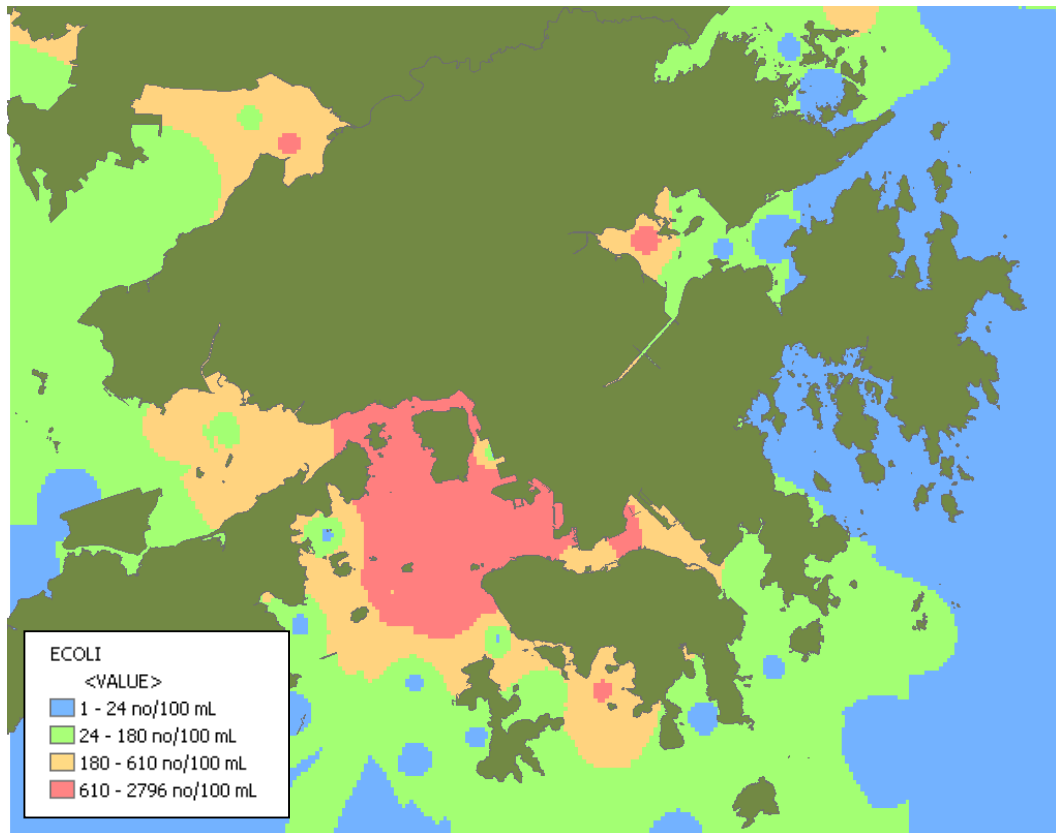


Figure 7.5 Tempo-spatial layer of E. coli from measurement table WQ2_Water_EPD - August 5, 2003 - classified based on Hong Kong beach water quality standards.

7.3 Evaluation of Interpolation Methods

The most reliable approach to determine the suitability of various interpolation methods for a specified dataset is to examine the goodness-of-fit individually. However, there are some parameters that are better fitted with certain interpolation methods. In this section, ten of the most common hydrodynamic/water quality parameters are selected to investigate the 1D and spatial interpolation methods that they are best fitted with. These include tidal level, current velocity (magnitude and direction), temperature, salinity, DO, turbidity, pH, chlorophyll a, total nitrogen, total phosphorus, BOD, and E. coli.

7.3.1 1D Interpolation Methods

1D interpolation methods are used for fitting time series as well as vertical profile.

7.3.1.1 Time series

Based on basic tidal theory, the best method to interpolate tidal data is by using trigonometric functions. Fundamentally, the goodness-of-fit for fitting tidal variation

with trigonometric function increases through the inclusion of more tidal constituents. However, in general, tidal data can be fitted reasonably well using the four principal tidal constituents, namely, M2, S2, O1, and K1. Figures 7.6 and 7.7 are the time series of tidal data for dry and wet seasons, respectively. In Figure 7.6, the fitting of tidal data using the four principal constituents results in a RMS value of 0.004181 m. The RMS value for the tidal curve in Figure 7.7 is 0.003543 m.

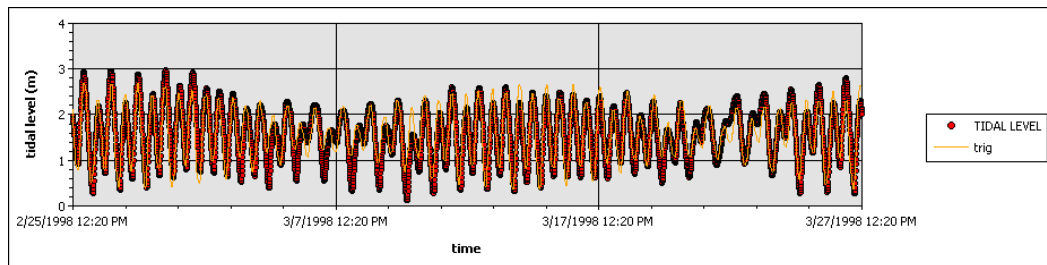


Figure 7.6 Time series for tidal level from measurement table tide_dry_CEDD_CE3296 – station ID: 1 – fitted using trigonometric (four principal constituents: M2, S2, O1, and K1) function.

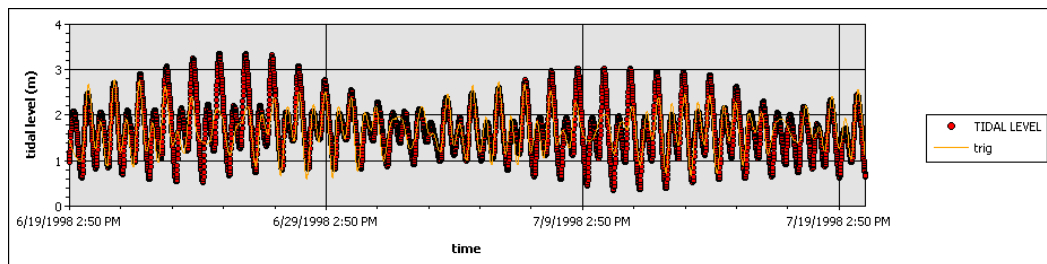


Figure 7.7 Time series for tidal level from measurement table tide_wet_CEDD_CE3296 – station ID: 1 – fitted using trigonometric (four principal constituents: M2, S2, O1, and K1) function.

It is also found that the magnitude of current velocity can also be fitted roughly using trigonometric function. This conforms to that fact that the major drive for current flow is tidal variation. As shown in Figure 7.8, the current speed data is fitted using a trigonometric function derived from the principal tidal constituents. The resulted RMS value is 4.049 mm/s. Although some patterns are also observed in current direction (see Figure 7.9), these variations do not appear to conform to any mathematical interpolation functions.

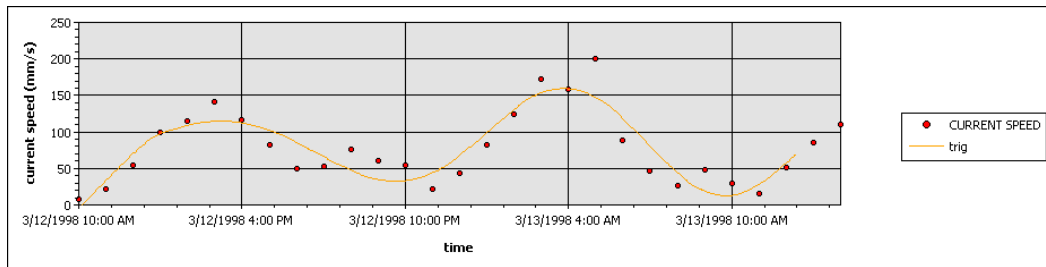


Figure 7.8 Time series for current speed from current_dry_spring_CEDD_CE3296 – station ID: 3 – depth: 1 m below surface – fitted using trigonometric (four principal constituents: M2, S2, O1, and K1) function.

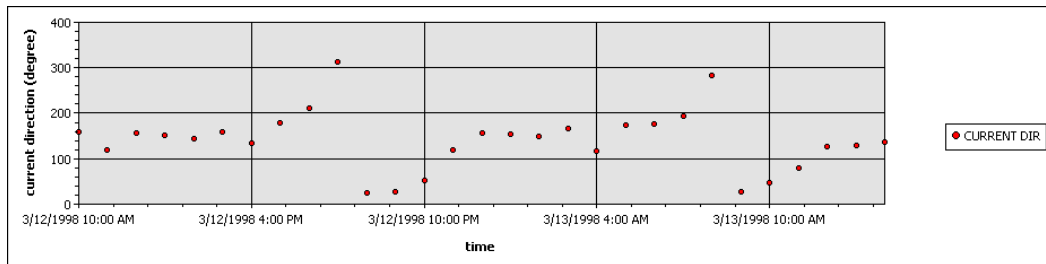


Figure 7.9 Time series for current direction from current_dry_spring_CEDD_CE3296 – station ID: 3 – depth: 1 m below surface.

Temperature and salinity both show daily as well as seasonal variations. The daily changes of temperature can be fitted well with either 6th degree polynomial or trigonometric functions. It has been shown, from trial-and-error, that the daily variation of temperature fits well with diurnal and semidiurnal tidal constituents. Figure 7.10 shows a time series with two interpolated curves, one derived from a 6th degree polynomial and the other from a trigonometric function with the application of three semidiurnal tidal constituents M2, S2, and K2. The RMS values of these two fitted curves are 0.02661 °C and 0.004635 °C, respectively. Figure 7.11 shows the variation of surface temperature throughout the year 2003. Similarly, seasonal variations of temperature can be fitted quite well with polynomial and trigonometric functions.

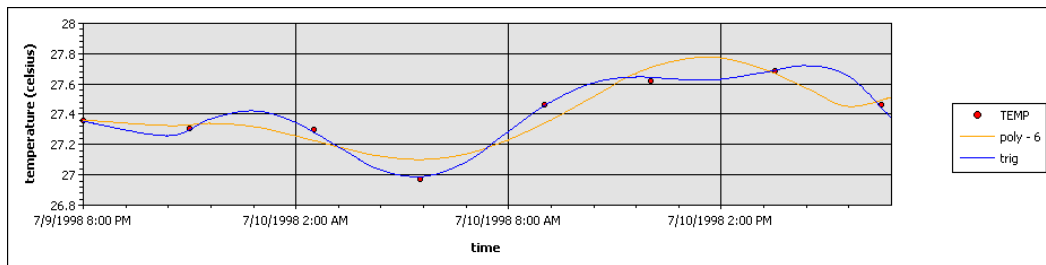


Figure 7.10 Time series for temperature from measurement table WQ1_wet_spring_CEDD_CE3296 - station ID: 1 – depth: surface – fitted using 6th polynomial and trigonometric (three tidal constituents: M2, S2, and K2) functions.

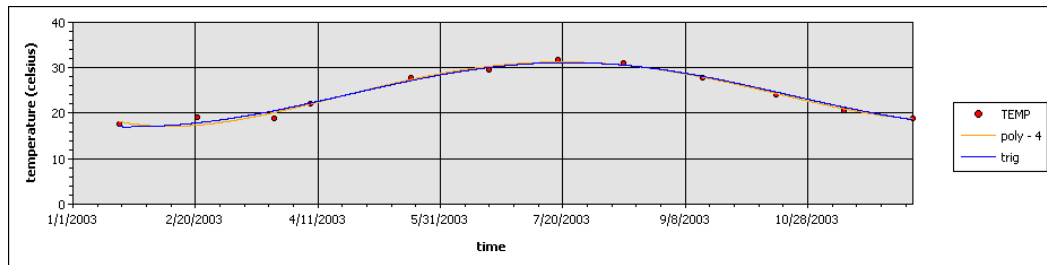


Figure 7.11 Time series for temperature from measurement table WQ2_Water_EPD – station ID: DM1 – depth: surface – fitted using 4th polynomial and trigonometric (one frequency: 1 degree/day) functions.

Similarly, both daily and seasonal variation of salinity can be represented using polynomial and trigonometric functions. As shown in Figure 7.12, salinity is fitted using two interpolated curves, one with a 6th polynomial function and the other with a trigonometric function using three semidiurnal tidal constituents, namely, M2, S2, and K2. The RMS values of these two fitted curves are 0.3648 psu and 0.3846 psu, respectively. An example of curve-fitting for the seasonal variations of salinity is shown in Figure 7.13. This time series is also fitted using polynomial and trigonometric functions, and the resulting RMS values are 0.4457 psu and 0.6624 psu, respectively.

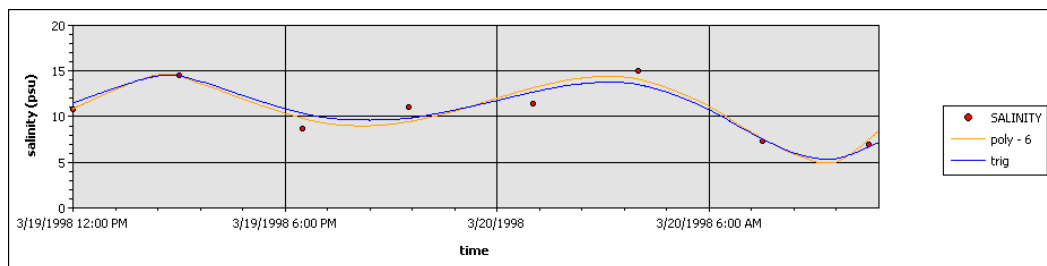


Figure 7.12 Time series for salinity from measurement table WQ1b_dry_neap_CEDD_CE3296 – station ID: 2 – depth: surface – fitted using 6th polynomial and trigonometric (three tidal constituents: M2, S2, and K2) functions.

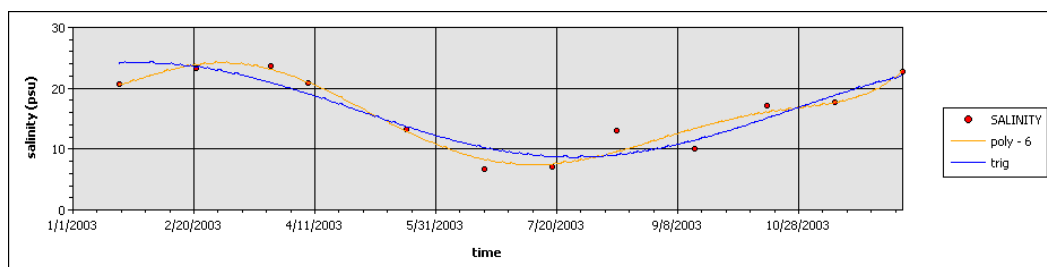


Figure 7.13 Time series for salinity from measurement table WQ2_Water_EPD – station ID: DM1 – depth: surface – fitted using 6th polynomial and trigonometric (one frequency: 1 degree/day) functions.

Other parameters, including DO, turbidity, pH, chlorophyll a, total nitrogen, total phosphorus, BOD, and E. coli, do not show any explicit trends which match with the

available mathematical functions. The time series of these parameters, however, can still be fitted using the Spline – Linear or Natural Neighbour – method. Examples of curve-fitting for these parameters using the Spline methods are shown in Figures 7.14 to 7.21.

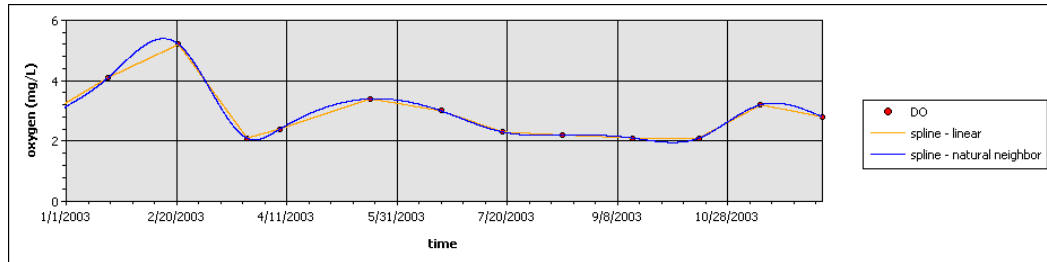


Figure 7.14 Time series for DO from measurement table WQ2_Water_EPD - station ID: DM1 – depth: surface -fitted using Linear and Natural Neighbour Spline methods.

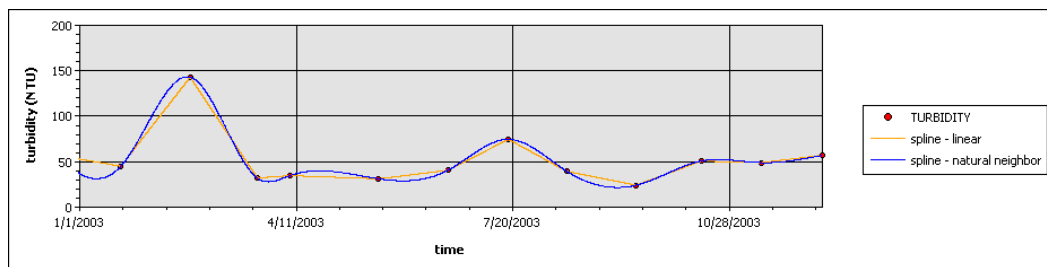


Figure 7.15 Time series for turbidity from measurement table WQ2_Water_EPD - station ID: DM1 – depth: surface -fitted using Linear and Natural Neighbour Spline methods.

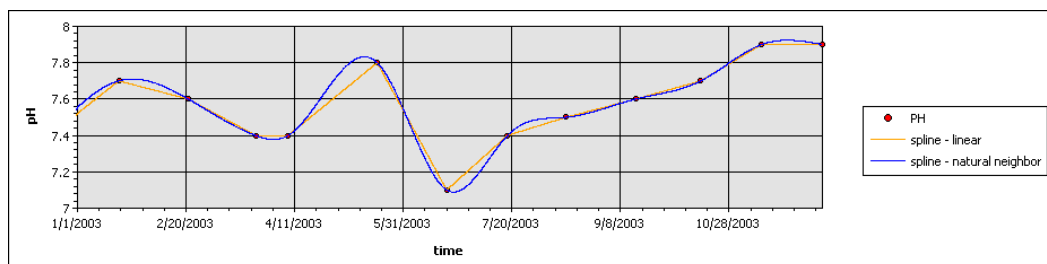


Figure 7.16 Time series for pH from measurement table WQ2_Water_EPD - station ID: DM1 – depth: surface -fitted using Linear and Natural Neighbour Spline methods.

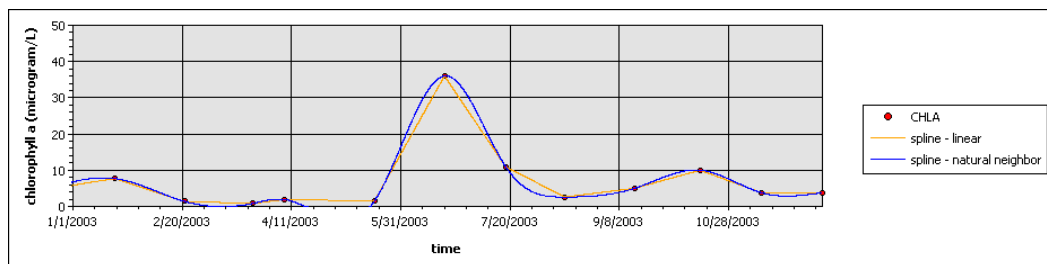


Figure 7.17 Time series for chlorophyll a from measurement table WQ2_Water_EPD - station ID: DM1 – depth: surface -fitted using Linear and Natural Neighbour Spline methods.

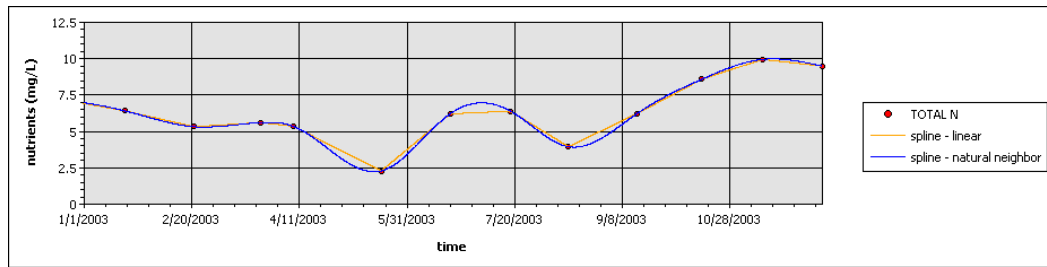


Figure 7.18 Time series for total nitrogen from measurement table WQ2_Water_EPD - station ID: DM1 – depth: surface -fitted using Linear and Natural Neighbour Spline methods.

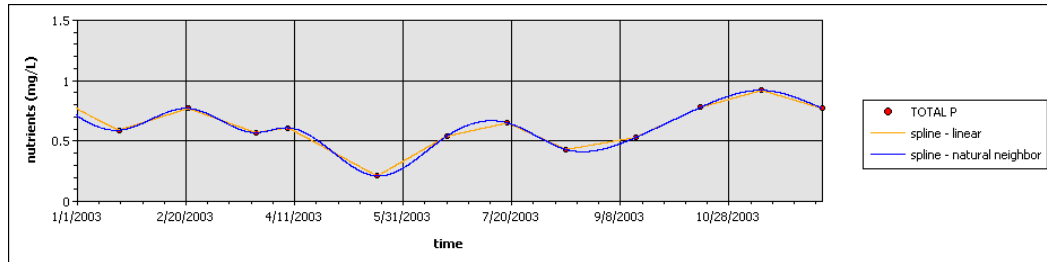


Figure 7.19 Time series for total phosphorus from measurement table WQ2_Water_EPD - station ID: DM1 – depth: surface -fitted using Linear and Natural Neighbour Spline methods.

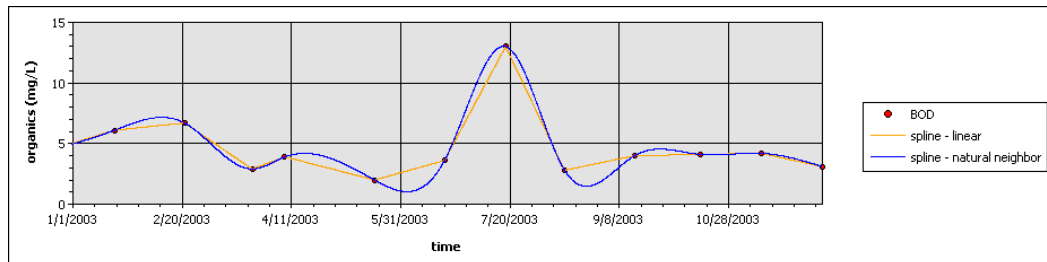


Figure 7.20 Time series for BOD from measurement table WQ2_Water_EPD - station ID: DM1 – depth: surface -fitted using Linear and Natural Neighbour Spline methods.

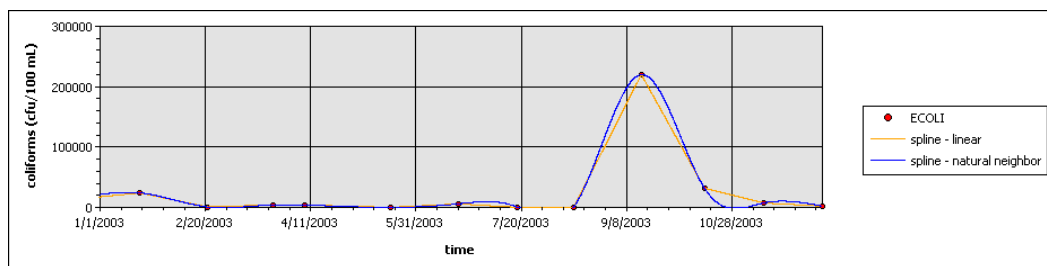


Figure 7.21 Time series for E. coli from measurement table WQ2_Water_EPD - station ID: DM1 – depth: surface -fitted using Linear and Natural Neighbour Spline methods.

7.3.1.2 Profile

The magnitude of current velocity typically decreases with water depth. Current speed profiles fit best with 6th degree polynomial functions. Other mathematical functions, including logarithmic, exponential, and power, also fit reasonably well. Figure 7.22

shows a current speed profile fitted with 6th degree polynomial, logarithmic, and exponential, and power functions; and the RMS values are 0.2281 mm/s, 2.249 mm/s, 3.638 mm/s, and 4.614 mm/s, respectively. Current direction profiles show less regular trends, and fit best using polynomial functions. Figure 7.23 shows a current direction profile fitted using a 6th degree polynomial function, and the RMS value is 0.4444 mm/s.

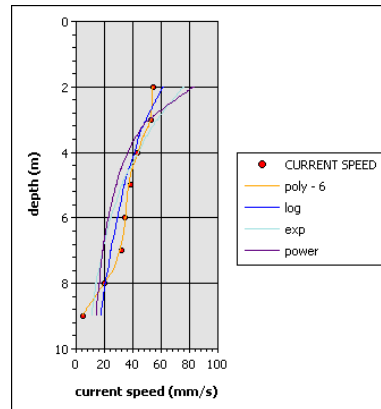


Figure 7.22 Profile for current speed from measurement table ADP_wet_CEDD_CE3296 – station ID: 1 – time: 7/14/1998 5:30:00 PM – fitted using 6th degree polynomial, logarithmic, exponential, and power functions.

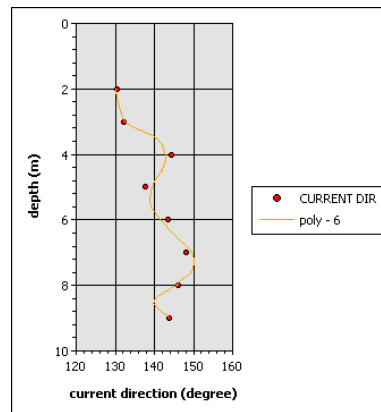


Figure 7.23 Profile of current direction from measurement table ADP_wet_CEDD_CE3296 – station ID: 1 – time: 7/14/1998 5:30:00 PM – fitted using 6th degree polynomial function.

Temperature, in general, decreases with depth along the water column. Profiles of temperature fit quite well using polynomial, logarithm, exponential, as well as power functions. Figure 7.24 is an example of a temperature profile interpolated using these four types of functions and the RMS values are 0.009122 degree celsius, 0.01626 degree celsius, 0.02048 degree celsius, and 0.01633 degree celsius, respectively.

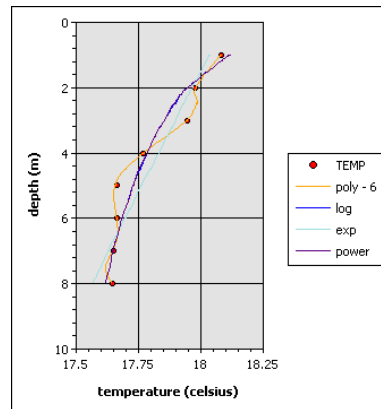


Figure 7.24 Profile of temperature from measurement table CTD_dry_CEDD_CE3296 – station ID: 1 – time: 3/9/1998 5:00:06 PM – fitted using 6th degree polynomial, logarithmic, exponential, and power functions.

Salinity generally increases with depth along the water column. Both polynomial and exponential functions fits quite well for salinity profiles. Figure 7.25 shows a salinity profile fitted using 3rd degree polynomial and exponential functions, and the RMS values are 0.01539 psu and 0.03299 psu, respectively.

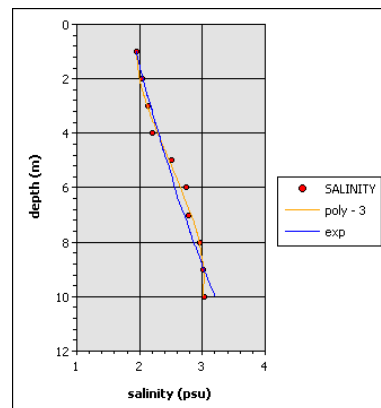


Figure 7.25 Profile of salinity from measurement table CTD_dry_CEDD_CE3296 – station ID: 1 – time: 3/9/1998 8:01:31 PM – fitted using 3rd degree polynomial and exponential functions.

Turbidity generally decreases with depth along the water column. Figure 7.26 is a turbidity profile fitted using 3rd degree polynomial and the RMS value is 0.2330 NTU.

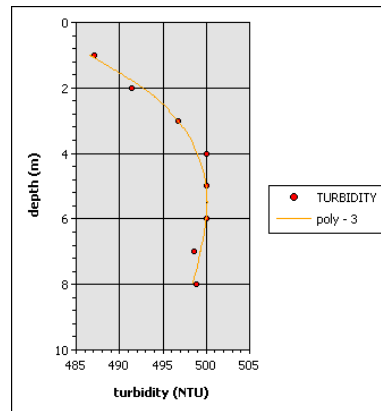


Figure 7.26 Profile of turbidity from measurement table CTD_dry_CEDD_CE3296 – station ID: 1 – time: 3/9/1998 5:00:06 PM – fitted using 3rd degree polynomial function.

All other parameters including DO, pH, chlorophyll a, total nitrogen, total phosphorus, biochemical oxygen demand, and E. coli, show no definable patterns in the profiles. However, since profiles are generally consisted of limited number of data points, they can be fitted easily using polynomial functions. Similar to time series, the Linear and Natural Neighbour Spline methods can be applied for profiles that do not match well with any mathematical equations. Figures 7.27 to 7.33 show examples of profiles fitted using polynomial function, and the Linear and Natural Neighbour Spline methods.

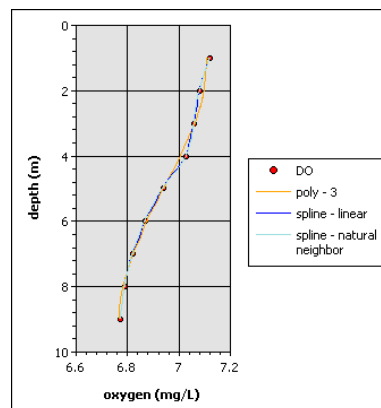


Figure 7.27 Profile of DO from measurement table DO_dry_spring_CEDD_CE3296 – station ID: 1 – time: 3/19/1998 12:00:00 PM – fitted using 3rd degree polynomial function, and Linear Spline and Natural Neighbour Spline methods.

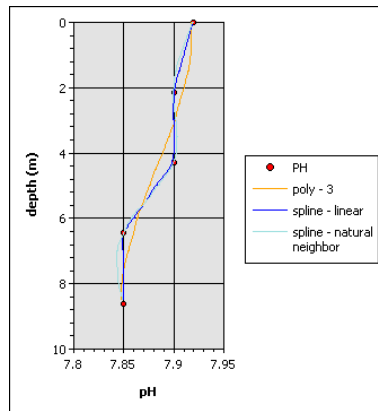


Figure 7.28 Profile of pH from measurement table WQ1_wet_neap_CEDD_CE3296 – station ID: 1 – time: 7/4/1998 12:00:00 PM – fitted using 3rd degree polynomial function, and Linear Spline and Natural Neighbour Spline methods.

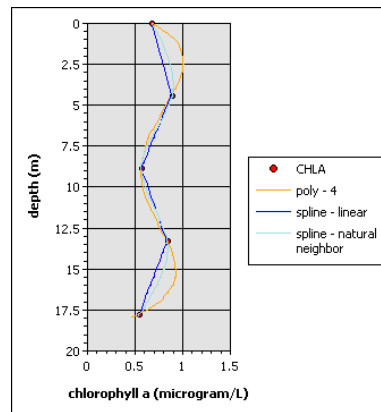


Figure 7.29 Profile of chlorophyll a from measurement table WQ4_wet_neap_CEDD_CE3296 – station ID: 1 – time: 7/4/1998 12:00:00 PM – fitted using 4th degree polynomial function, and Linear Spline and Natural Neighbour Spline methods.

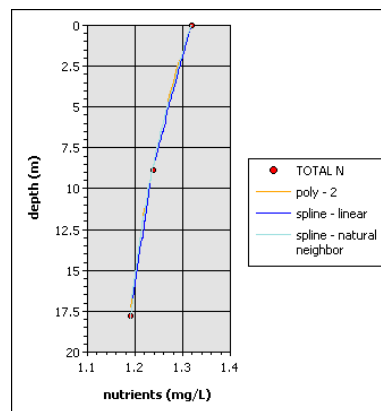


Figure 7.30 Profile of total nitrogen from measurement table WQ2_dry_spring_CEDD_CE3296 – station ID: 1 – time: 3/13/1998 7:30:00 AM – fitted using 2nd degree polynomial function, and Linear Spline and Natural Neighbour Spline methods.

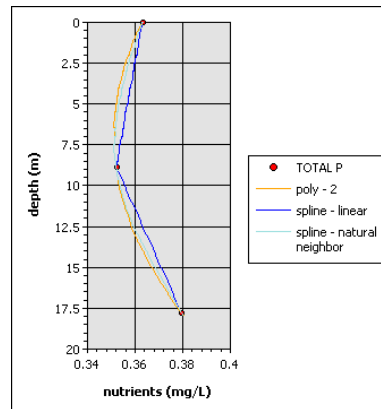


Figure 7.31 Profile of total phosphorus from measurement table WQ2_dry_spring_CEDD_CE3296 – station ID: 1 – time: 3/13/1998 7:30:00 AM – fitted using 2nd degree polynomial function, and Linear Spline and Natural Neighbour Spline methods.

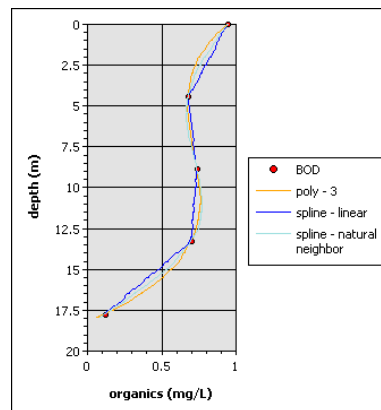


Figure 7.32 Profile of BOD from measurement table WQ4_wet_neap_CEDD_CE3296 – station ID: 1 – time: 7/4/1998 12:00:00 PM – fitted using 3rd degree polynomial function, and Linear Spline and Natural Neighbour Spline methods.

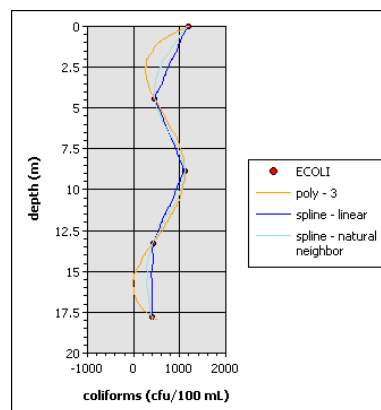


Figure 7.33 Profile of E. coli from measurement table WQ4_wet_neap_CEDD_CE3296 – station ID: 1 – time: 7/4/1998 12:00:00 PM – fitted using 3rd degree polynomial function, and Linear Spline and Natural Neighbour Spline methods.

7.3.2 Spatial Interpolation Methods

The approach to evaluate the suitability of spatial interpolation methods is by cross-validation. That is, for certain datasets, each sampling point is extracted individually and the interpolated layer is predicted using a specified spatial interpolation method selected from the interpolation process. The values from the predicted surface are then verified against the measured data (i.e. the extracted data point). The cross-validation analytical tool included in ArcGIS Geostatistical Analyst extension is applied in this evaluation process. Figure 7.34 shows the dialog box for displaying results of the cross validation analysis. Note that the unit of the displayed results is based on the parameter of the input spatial layer. The parameter of the input spatial layer in this example is pH, therefore, the generated results are unitless. At each point, the difference between the measured and predicted values is computed (i.e. error). Further, the errors for all points are summed up to generate a RMS prediction. The RMS thus provides a measure of how closely the interpolated layer predicts the measured data. Thus, a smaller value of RMS corresponds to better interpolated results.

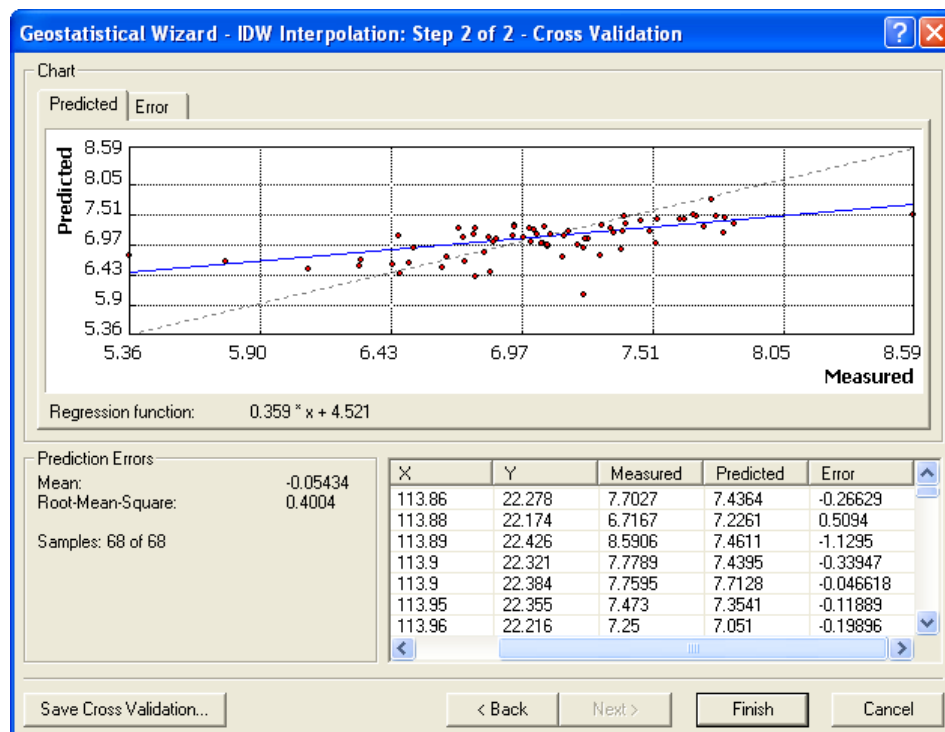


Figure 7.34 Cross validation analysis using ArcGIS Geostatistical Analyst extension.

In evaluating each of the designated parameters, four datasets have been taken from the available measurement tables. Table 7.2 summarizes the details for the selected

datasets. Note that tidal level and current velocity are not included as part of this analysis. This is because tidal level and current velocity are generally taken at a limited number of sampling locations (i.e. less than 6), and at least 10 input points are required for performing geostatistical data analysis.

Table 7.2 Selected datasets for spatial interpolation method evaluation.

parameters	dataset	measurement table	date/time	depth layer	number of stations
temperature	1	WQ2 Water EPD	1/1/2003	middle	68
	2	WQ2 Water EPD	6/1/2003	middle	68
	3	WQ1 wet neap CEDD CE3296	7/5/1998	surface	13
	4	WQ1 wet spring CEDD CE3296	7/10/1998	surface	13
salinity	1	WQ2 Water EPD	1/1/2003	middle	68
	2	WQ2 Water EPD	6/1/2003	middle	68
	3	WQ1 wet neap CEDD CE3296	7/5/1998	surface	13
	4	WQ1 wet spring CEDD CE3296	7/10/1998	surface	13
DO	1	WQ2 Water EPD	1/1/2003	middle	68
	2	WQ2 Water EPD	6/1/2003	middle	68
	3	WQ1 wet neap CEDD CE3296	7/5/1998	surface	13
	4	WQ1 wet spring CEDD CE3296	7/10/1998	surface	13
turbidity	1	WQ2 Water EPD	1/1/2003	middle	68
	2	WQ2 Water EPD	6/1/2003	middle	68
	3	WQ2 Water EPD	3/1/2003	middle	68
	4	WQ2 Water EPD	9/1/2003	middle	68
pH	1	WQ2 Water EPD	1/1/2003	middle	68
	2	WQ2 Water EPD	6/1/2003	middle	68
	3	WQ1 wet neap CEDD CE3296	7/5/1998	surface	13
	4	WQ1 wet spring CEDD CE3296	7/10/1998	surface	13
chlorophyll a	1	WQ2 Water EPD	1/1/2003	middle	68
	2	WQ2 Water EPD	6/1/2003	middle	68
	3	WQ2 Water EPD	3/1/2003	middle	68
	4	WQ2 Water EPD	9/1/2003	middle	68
total nitrogen	1	WQ2 Water EPD	1/1/2003	middle	68
	2	WQ2 Water EPD	6/1/2003	middle	68
	3	WQ2 Water EPD	3/1/2003	middle	68
	4	WQ2 Water EPD	9/1/2003	middle	68
total phosphorus	1	WQ2 Water EPD	1/1/2003	middle	68
	2	WQ2 Water EPD	6/1/2003	middle	68
	3	WQ2 Water EPD	3/1/2003	middle	68
	4	WQ2 Water EPD	9/1/2003	middle	68
BOD	1	WQ2 Water EPD	1/1/2003	middle	68
	2	WQ2 Water EPD	6/1/2003	middle	68
	3	WQ2 Water EPD	3/1/2003	middle	68
	4	WQ2 Water EPD	9/1/2003	middle	68
E. coli	1	WQ2 Water EPD	1/1/2003	middle	68
	2	WQ2 Water EPD	6/1/2003	middle	68
	3	WQ2 Water EPD	3/1/2003	middle	68
	4	WQ2 Water EPD	9/1/2003	middle	68

The results obtained from the cross validation analysis are summarised in Table 7.3. Four types of interpolation methods are considered, namely IDW, Global Polynomial (equivalent to Trend), Radial Basis Functions (equivalent to Spline), and Kriging. For

each dataset, cells are highlighted to indicate the best-fitted interpolation method (i.e. smallest value of RMS). In general, most of the parameters are shown to fit best with either the Radius Basis Functions or Kriging method. The Global Polynomial method is demonstrated to be the worst in predicting the parameters, while the IDW method is accurate in some cases. Based on these results, the recommended spatial interpolation methods for each parameter are listed in Table 7.4.

Table 7.3 Results of prediction error mean and root-mean square from cross validation.

parameter/ dataset		IDW		Global Polynomial		Radial Basis Functions		Kriging	
		mean	rms	mean	rms	mean	rms	mean	rms
temperature	1	0.03671	0.252	-0.00123	0.3031	0.01448	0.2366	0.0018	0.2297
	2	-0.00148	0.3595	-0.00169	0.4095	0.0007	0.3567	0.00129	0.3629
	3	-0.00177	0.5166	0.1165	1.203	-0.00288	0.5382	-0.02281	0.5796
	4	-0.00573	0.2709	0.00529	0.3891	-0.01032	0.2724	-0.00439	0.268
salinity	1	0.01063	0.1939	-2.43E-4	0.2128	0.00775	0.1779	0.00261	0.1555
	2	0.03159	1.96	-0.0261	2.047	0.02852	2.061	-0.00638	2.067
	3	0.08672	1.662	-0.08839	2.563	0.01108	1.622	0.07031	1.688
	4	0.2712	3.266	0.6042	4.438	0.2027	2.917	0.2312	2.824
DO	1	-0.04602	0.4061	0.00544	0.4671	-0.02658	0.4051	-0.00904	0.3907
	2	-0.00191	0.6534	0.00975	0.7742	0.03021	0.5885	0.00645	0.6342
	3	-0.1758	0.874	0.02449	1.258	-0.07982	0.8418	-0.06858	0.8092
	4	-0.1293	0.8108	-0.1433	0.9773	-0.06726	0.7987	-0.06878	0.8054
turbidity	1	-0.3012	3.111	-0.01491	3.442	-0.08672	3.179	-0.07719	3.281
	2	0.05304	1.435	-0.0225	1.569	0.0178	1.368	-0.0145	1.31
	3	-0.2399	1.974	0.0128	2.013	-0.1109	1.985	-0.00696	1.928
	4	0.04099	1.692	-0.00734	2.004	0.03812	1.653	0.00293	1.579
pH	1	-0.00933	0.05317	0.00108	0.08364	-0.00472	0.05261	-6.72E-4	0.05359
	2	-0.0049	0.05728	1.578E-4	0.06784	-0.00076	0.0563	-6.78E-4	0.05628
	3	0.03724	0.1819	0.02076	0.209	0.02054	0.1769	0.01223	0.1592
	4	-0.00885	0.1216	0.00375	0.1331	7.431E-4	0.09889	-0.00796	0.1208
chlorophyll a	1	0.01051	0.5582	-0.00384	0.9031	-0.00293	0.5057	0.00649	0.521
	2	0.05642	2.765	0.01494	3.24	0.03148	2.638	0.06682	2.945
	3	-0.07425	1.156	0.00746	1.881	-0.03243	1.007	0.00928	1.076
	4	-0.2001	3.926	-0.00395	4.932	-0.05239	3.797	-0.04833	3.701
total nitrogen	1	0.00670	0.08422	-0.00158	0.1109	-1.83E-4	0.07948	-3.08E-4	0.09241
	2	0.00231	0.1404	1.74E-5	0.136	-8.72E-4	0.142	-0.00221	0.1544
	3	0.00588	0.1024	-0.00226	0.1147	3.616E-4	0.09926	-9.87E-4	0.1005
	4	0.00246	0.1712	0.00114	0.1845	-8.38E-4	0.1759	-0.00148	0.1756
total phosphorus	1	6.326E-4	0.00989	-1.96E-4	0.01379	6.363E-5	0.00964	-2.38E-4	0.00988
	2	1.495E-4	0.00886	-9.22E-5	0.01074	-7.55E-5	0.00888	-8.81E-5	0.00879
	3	5.2E-4	0.00694	-1.59E-4	0.00929	-5.89E-5	0.00624	-1.81E-4	0.0061
	4	5.634E-4	0.00871	-8.18E-5	0.01141	4.516E-5	0.00847	-1.79E-4	0.0086
BOD	1	0.02946	0.2694	-1.32E-4	0.3036	0.00710	0.2623	0.00431	0.246
	2	0.01943	0.4074	0.00363	0.4757	0.01606	0.3833	0.01465	0.3703
	3	0.00579	0.3207	-9.73E-4	0.4432	0.00177	0.2789	7.51E-4	0.2985
	4	-0.00289	0.3631	-3.13E-4	0.437	0.00250	0.3626	0.00383	0.3784
E. coli	1	258	4096	-33.97	3740	104.7	3897	-49.94	3786
	2	394.8	4241	-48.88	4682	155.4	4102	8.682	4174
	3	312.6	3502	-37.32	3591	121.6	3334	3334	3348
	4	309.3	5757	-61.27	5843	171.8	5649	-31.66	5939

Table 7.4 Recommended spatial interpolation method(s).

parameter	recommended spatial interpolation method(s)
temperature	Kriging
salinity	Kriging
DO	Radial Basis Functions
turbidity	Kriging
pH	Kriging or Radial Basis Functions
chlorophyll a	Radial Basis Functions
total nitrogen	Radial Basis Functions
total phosphorus	Kriging or Radial Basis Functions
BOD	Kriging or Radial Basis Functions
E. coli	Radial Basis Functions

7.4 Investigation of Temporal and Spatial Trends

The intention of developing the dynamic time series and section display tools is to support data visualization in all physical dimensions, that is, spatially in both horizontal and vertical directions as well as temporally. This section presents a sample application of how the two interactive data display tools can be applied for investigating temporal and spatial trends in hydrodynamic or water quality geographic information.

The selected dataset for this example is obtained from the measurement table WQ2_Water_EPD (i.e. from EPD on-going marine water and sediment quality monitoring project), and the parameter of interest is pH. Referring to Figure 7.1, it is seen that the survey stations are quite uniformly distributed within the Hong Kong region. Table 7.5 provides the reference for the water control zones in Hong Kong.

Table 7.5 Water control zone.

station	water control zone
TM, TT	Tolo Harbour & Channel
SM, ST	Southern
PM, PT	Port Shelter
DM	Deep Bay
MM	Mirs Bay
NM	North Western
WM, WT	Western Buffer
EM	Eastern Buffer
VM, VT	Victoria Harbour

Since the measurement times among the stations are not concurrent, the tempo-spatial interpolation method is applied using the Spline – Natural Neighbour for 1D interpolation method and the IDW for spatial interpolation. The input measurement period is from Jan 5, 1998 to Dec 31, 1998 and the time interval is 10 days. In this example, pH taken at the water surface is first examined.

The result for the dynamic display of this time series interpolated block is shown as a series of slides in Figure 7.35. Note that for a succinct representation of results, slides taken at 30-day interval are shown in the figure. The pH value ranges from 5.7 to 9.7, with the lowest value represented by darkest shade and the highest with the lightest shade. It is clearly shown that the pH at outlying water remains relatively neutral during the entire year, and the areas close to the shore have a significantly lower pH. This suggests that the release of land source pollutants may possibly increase the acidity of the nearby water. As shown in the slides, one of the most vulnerable areas is Deep Bay. The lowering of pH in this region first took place between January and June, and eased off during July and August, and reoccurred during September and December. The time periods of pH decrease correspond closely with the time of reduced run-off in the PRE. The lack of flow circulation during this period may have led to the stagnancy of acidity in the Deep Bay region. Other areas of concern within the Hong Kong region are Tolo Harbour & Channel, Southern, Port Shelter, Mirs Bay, and Victoria Harbour. Although conditions at these areas are not as severe as that of Deep Bay, fluctuations of pH have been observed from time to time throughout the year.

The same tempo-spatial interpolation procedure has been repeated for the middle and bottom water level, and the results are shown in Figures 7.36 and 7.37, respectively. The pH varies from 5.8 to 9.2 for the middle layer and from 6.0 to 9.0 for the bottom layer. In contrast to the surface layer, the middle layer does not show any significant variation of pH in the Deep Bay region. Instead, a considerable decrease of pH is observed in the North Western zone from February to April, and a less severe condition reoccurred during July and December. Additionally, another region of concern is Mirs Bay, which shows a drop in pH during February and June. For the bottom layer, the time and location of the pH decrease is similar to those shown in the middle layer.

Using the interactive dynamic time series display, the user can click any location in the map region to generate a time series curve for the selected time series interpolated block. Figure 7.38 shows a time series extracted at a point in Deep Bay for the surface level and

Figure 7.39 shows a time series taken from a point in the North Western zone for the middle level. The map on the right for each of the two figures shows the location, indicated by a red dot, from which the time series is generated. It can be seen that both time series curves show that the first minimum of pH occurred at about the same time in early March. While the pH in Deep Bay continues to fluctuate throughout the year, the variation of pH in the North Western zone is not as severe after March.

To examine this further, the three time series blocks have been rearranged into a set of profile blocks (i.e. a set of thirty-seven blocks, one at each time instant and each with three layers), and a series of longitudinal sections are generated from the profile blocks along Deep Bay (see Figure 7.40). The map at the top of the figure shows the line, indicated by a red line, along which the section is taken. The pH value for the sections ranges from 6.6 to 8.5. It can be seen from the sections that, from January to June, the acidic water (indicated by the darkest shades) originating from the coastal region at the water surface disperses outward in both horizontal and vertical directions. A similar situation is observed between September and December. The downward dispersion of the acidic water may provide an explanation for the difference in the regions at which the lowering of pH is observed in the surface and middle layer. It is possible that by the time the acidic water from Deep Bay reaches the North Western zone, it has moved vertically downwards from the surface level to the middle/bottom level.

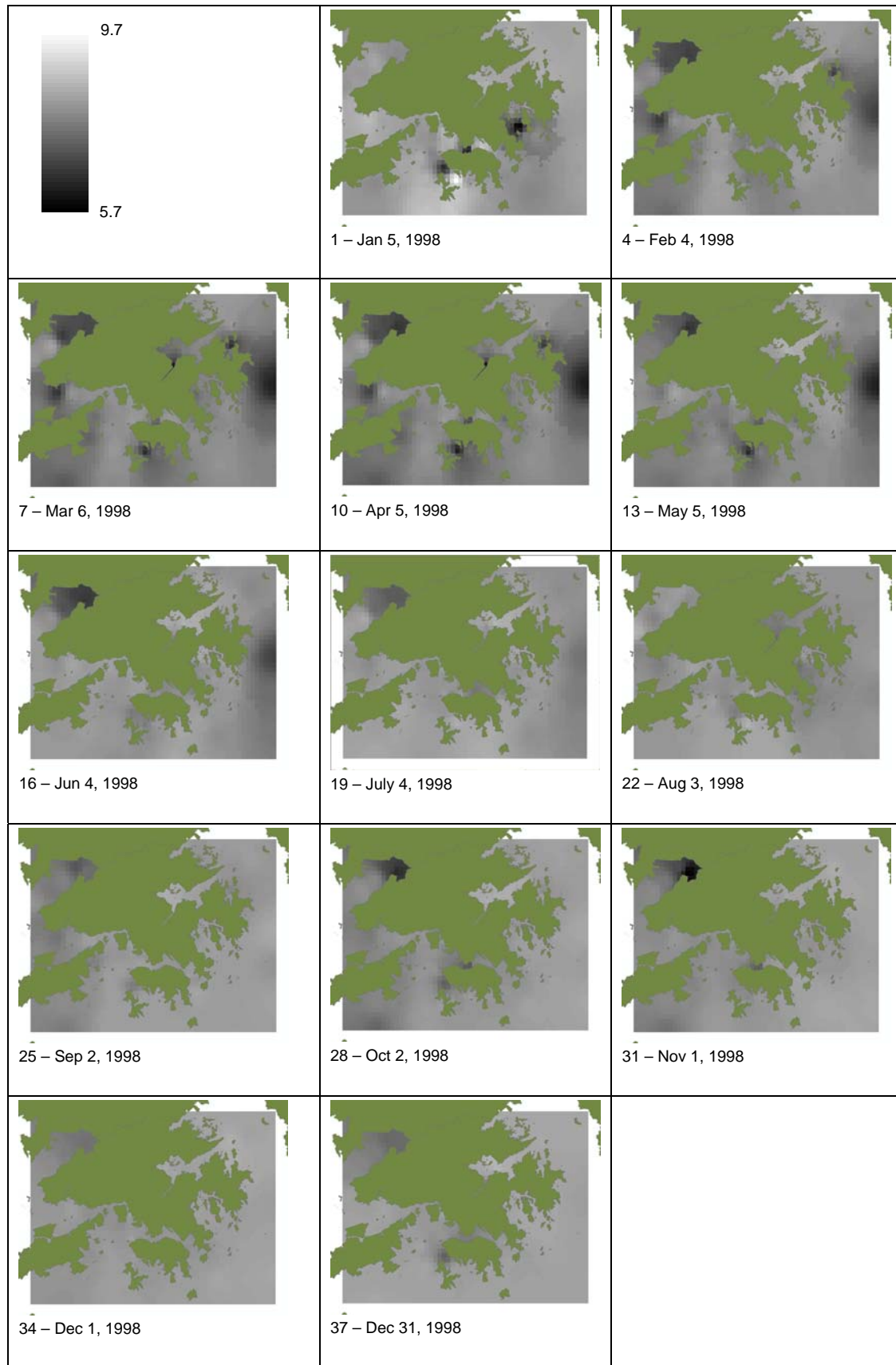


Figure 7.35 Dynamic display of spatial layers for pH at water level: surface.

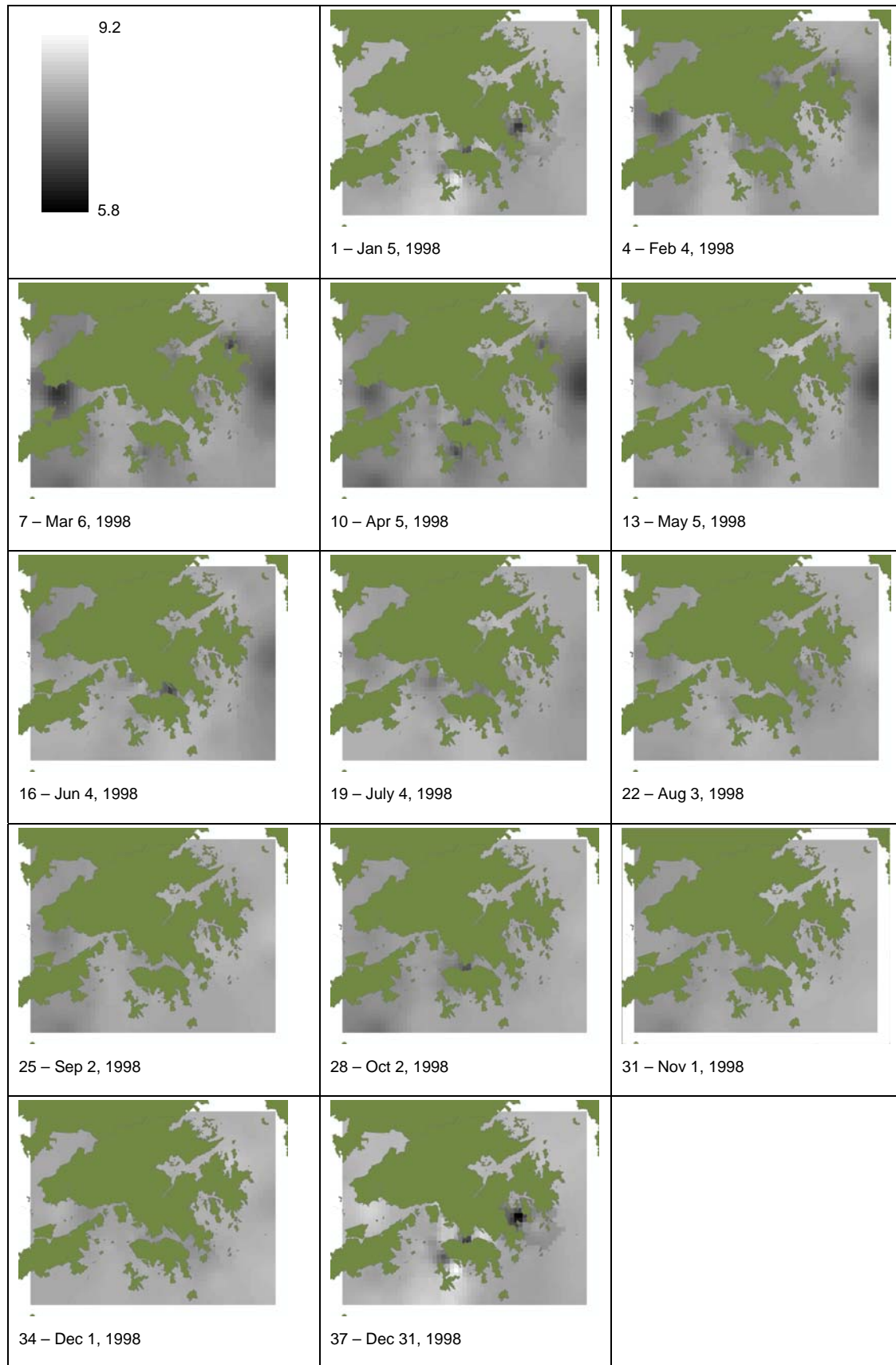


Figure 7.36 Dynamic display of spatial layers for pH at water level: middle.

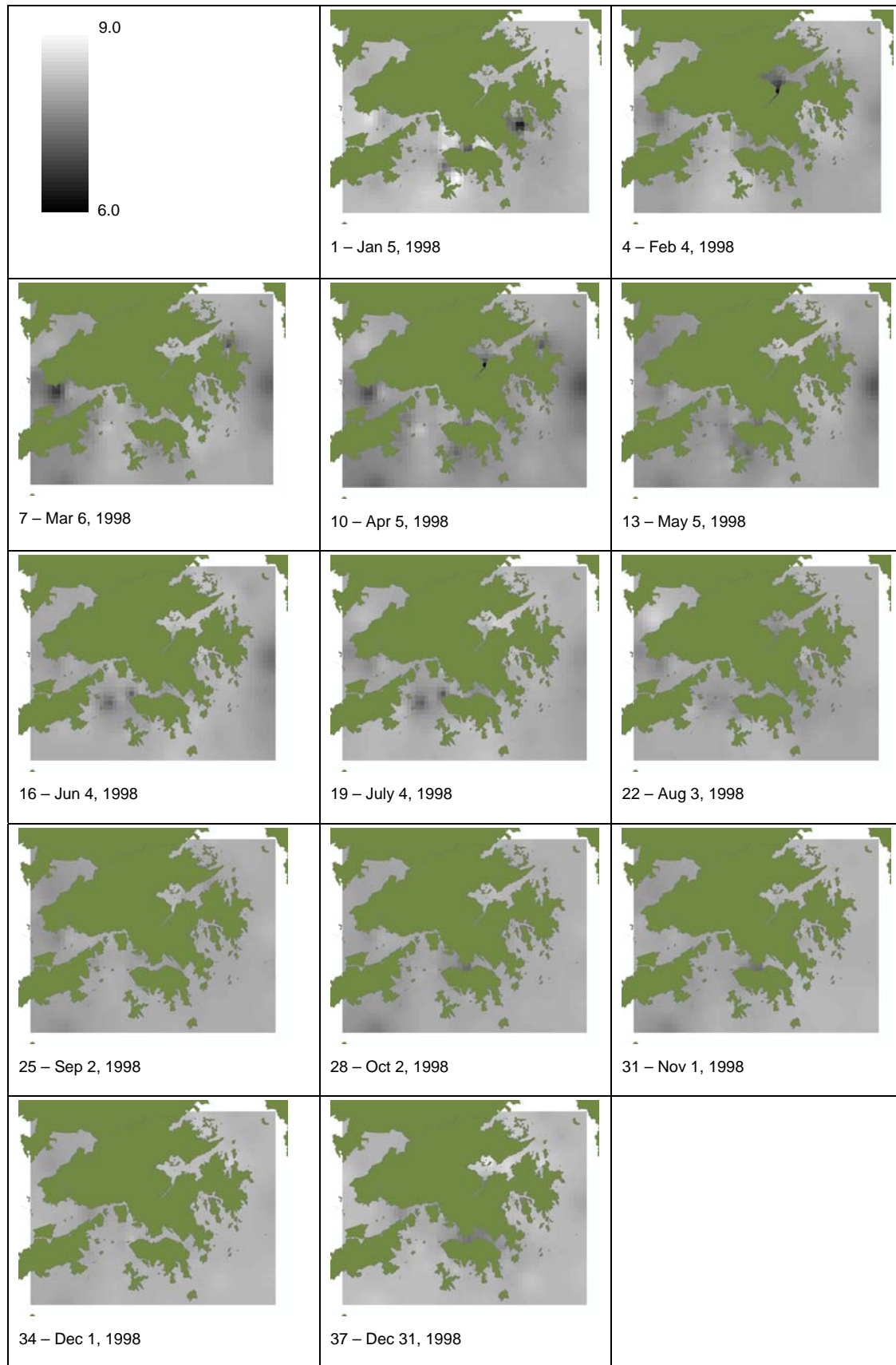


Figure 7.37 Dynamic display of spatial layers for pH at water level: bottom.

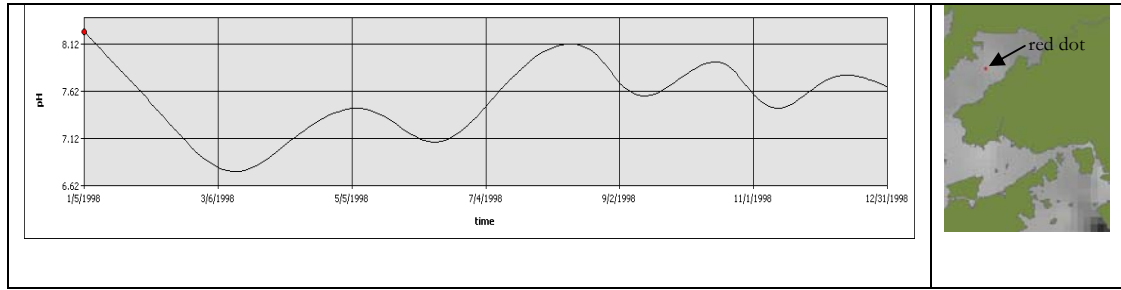


Figure 7.38 Dynamic display of time series for pH at water level: surface.

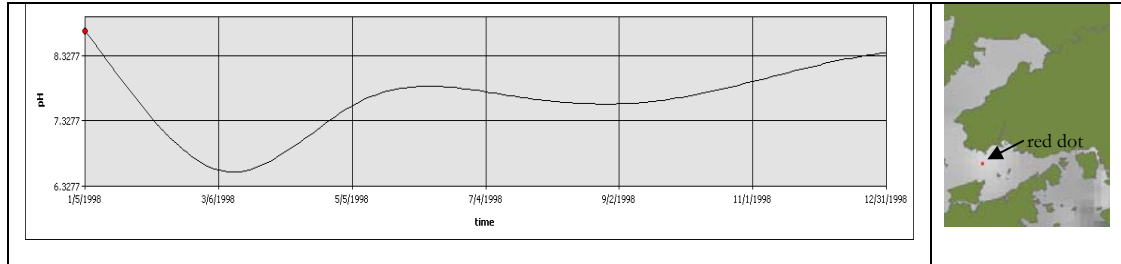


Figure 7.39 Dynamic display of time series for pH at water level: middle.

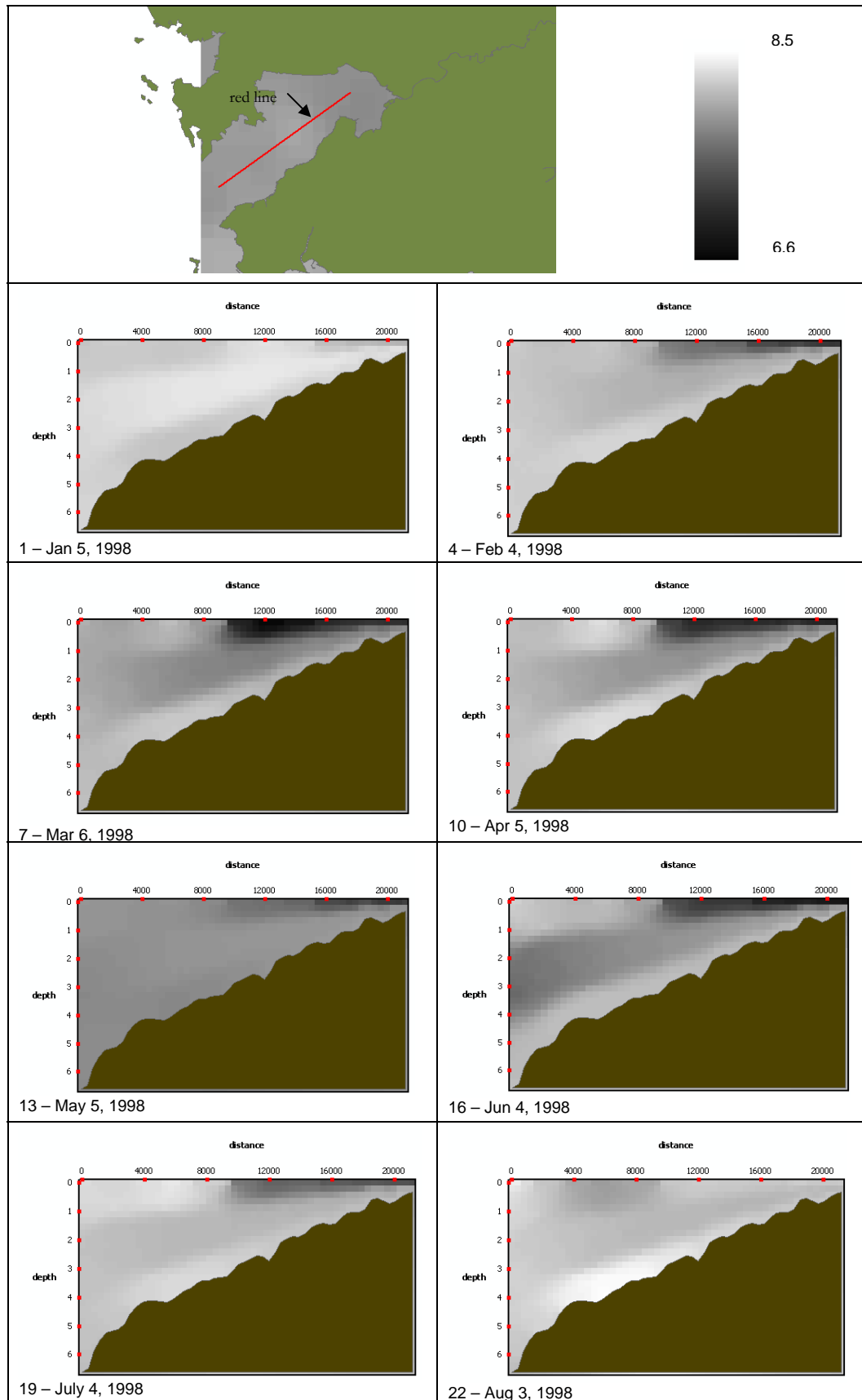


Figure 7.40 Section display of pH in Deep Bay.

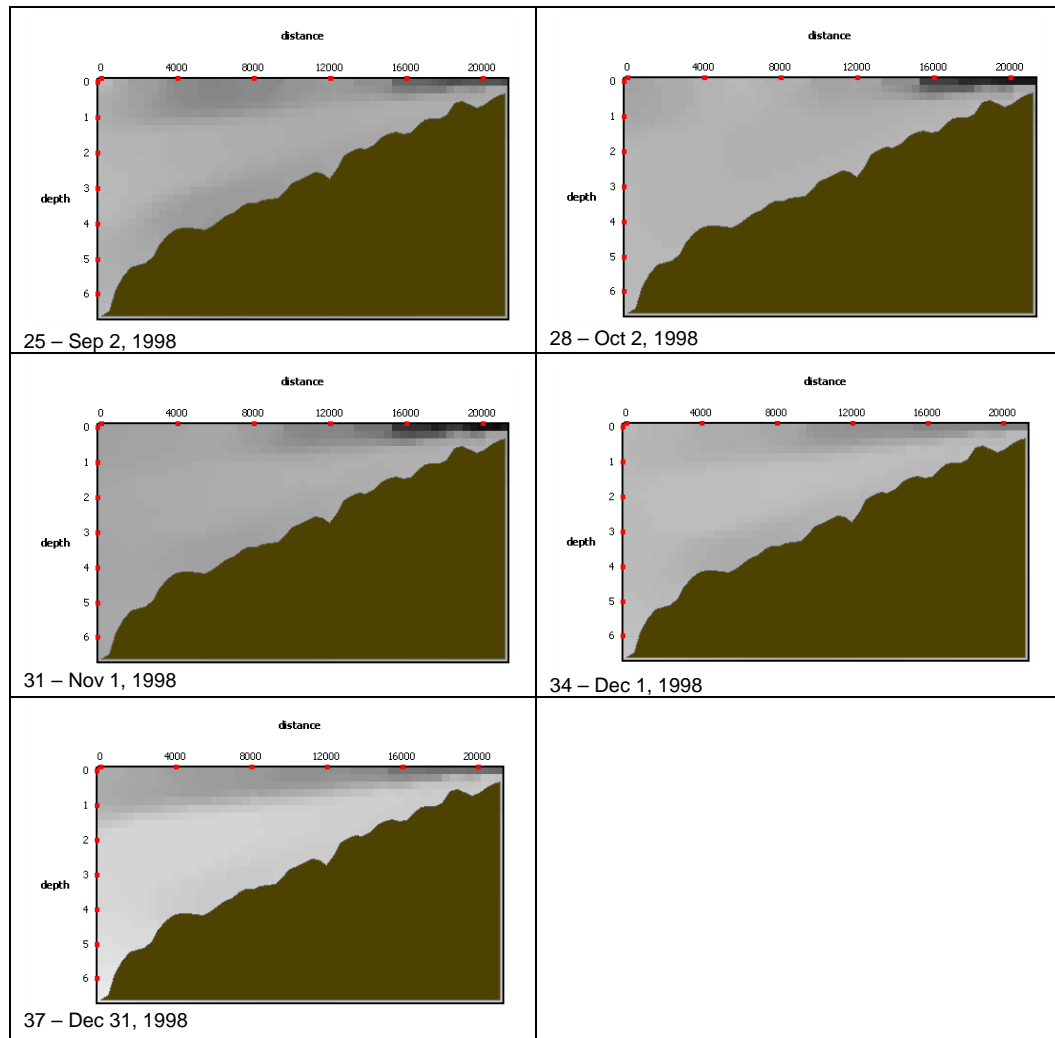


Figure 7.40 Continued.

7.5 Assessment of Quality of the Collected Data

The quality of the collected data can be assessed by comparing data of the same parameter taken within the same time measurement period and water region. In this example, datasets from the EPD Marine Water and Sediment Quality Monitoring are compared to those obtained from the EPD Project – Agreement no. CE 42/97. Both data sources contain information taken within the Hong Kong waters. The EPD Marine Water Sediment Quality Monitoring is a long-term water quality monitoring program, and thus contains data spanning from 1990 to 2003. Datasets from the EPD Project – Agreement no. CE 42/97 are collected during a six-month measurement interval from July 1998 to Jan 1999. The time frame for assessing quality of the collected data is set between July 1998 and Jan 1999, when the measurement times for both data sources coincide.

The method to assess the quality of the collected data is to compare the spatial layers from two datasets, one from the measurement table WQ2_Water_EPD, and the other from the measurement table WQlab_BW_PkgB_EPD_CE4297. The geographic locations of the fixed stations for the measurement table WQ2_Water_EPD and WQlab_BW_PkgB_EPD_CE4297 are shown in Figures 7.1 and 7.41, respectively.



Figure 7.41 Fixed stations for measurement table WQlab_BW_PkgB_EPD_CE4297.

The selected parameter of interest is suspended solids. From each of the two datasets, interpolated spatial layers for suspended solids at surface depth level are created for five instances in time using the Spline-Linear method for 1D interpolation and the Spline method for 2D interpolation. Additionally, using the Raster Calculator function from the ArcGIS Spatial Analyst extension, a spatial layer of percentage difference is derived for each pair of spatial layers compared. The results are summarized in Figure 7.42. The scale for suspended solids has been set to range from 0 to 20 mg/L to enhance visibility of the spatial layers. As the results of the spatial layer actually vary from -15 to 217 mg/L, any value less than 0 mg/L is set to the darkest shade, while any value greater than 20 mg/L is set to the lightest shade.

From the percentage difference spatial layers, huge differences between the two datasets are observed at regions closed to the domain boundaries, such as Deep Bay, Southern, and Mirs Bay. The discrepancies can be explained by examining the distribution of the monitoring stations for the first dataset (i.e. WQlab_BW_PkgB_EPD_CE4297). Referring to Figure 7.41, the first dataset contains either none or just a few stations at these regions. Quality of the predicted spatial layers is limited owing to the highly-scattered distribution of input data points.

In contrast, the quality of the predicted surfaces is quite stable at near-shore areas, such as North Western, Western Buffer, Victoria Harbour, Tolo Harbour and Channel, and Eastern Buffer. For the first and the last time instances, the percentage difference at these locations ranges from 0 to 60%. For the second, third, and fourth time instance, less accurate predictions are observed.

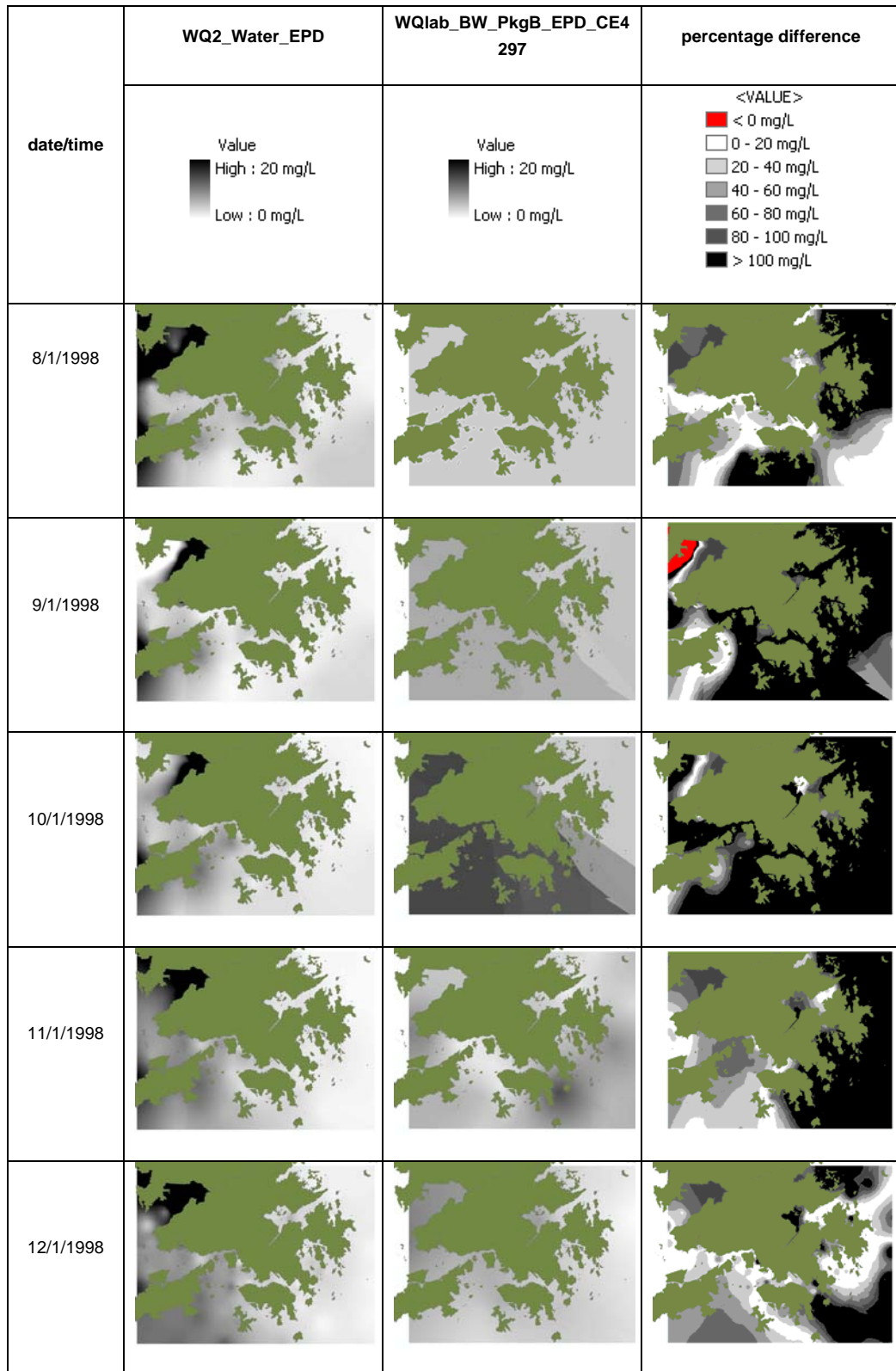


Figure 7.42 Predicted spatial layers for suspended solids for datasets WQ2_Water_EPD and WQlab_BW_PkgB_EPD_CE4297, and percentage difference.

7.6 Calibration and Verification of the Hydrodynamic-Water Quality Coupled Model

The integrated system merges field and model information into a common platform, thus allowing efficient calibration and verification of the hydrodynamic-water quality coupled model. Tidal elevation is selected in this example for demonstrating how model calibration can be carried out using the integrated system. In general, calibration process begins with forcing functions (e.g. tidal constituents) and physical parameters as they are entirely self-governing and therefore are the initial driving force of all physical processes of other variables (Chapra, 1997).

The existing model input contains two sets of tidal data, one for a dry season period (i.e. from 2/25/98 to 6/5/98) and the other for a wet season period (i.e. from 6/20/98 to 9/28/98). Using the *Find Tables* function (refer to Section 5.7), four measurement tables, namely, `tide_dry_CEDD_CE3296`, `tide_wet_CEDD_CE3296`, `tide_QUB_HKO`, and `tide_WAG_HKO`, are identified, and Table 7.6 summarizes the details for each of the tables. For both wet and dry season, model results can be verified against field data at seven locations as shown in Figure 7.43. Also displayed in the GIS interface is the model mesh grid. It is noted that none of these data stations coincide with the nodal points.

Table 7.6 Measurement tables selected for model calibration of tidal data.

measurement table	time period	stations	data source
<code>tide_dry_CEDD_CE3296</code>	2/25/1998 12:20:00 PM to 3/29/1998 12:30:00 PM	1, 3, 11, 12, 13	CEDD Project – Agreement no. 32/96
<code>tide_wet_CEDD_CE3296</code>	6/19/1998 2:50:00 PM to 7/20/1998 7:00:00 AM	1, 3, 11, 12, 13	CEDD Project – Agreement no. 32/96
<code>tide_QUB_HKO</code>	1/1/1995 1:00:00 AM to 3/1/2000 12:00:00 AM	QUB	HKO
<code>tide_WAG_HKO</code>	1/1/1995 1:00:00 AM to 3/1/2000 12:00:00 AM	HKO	HKO

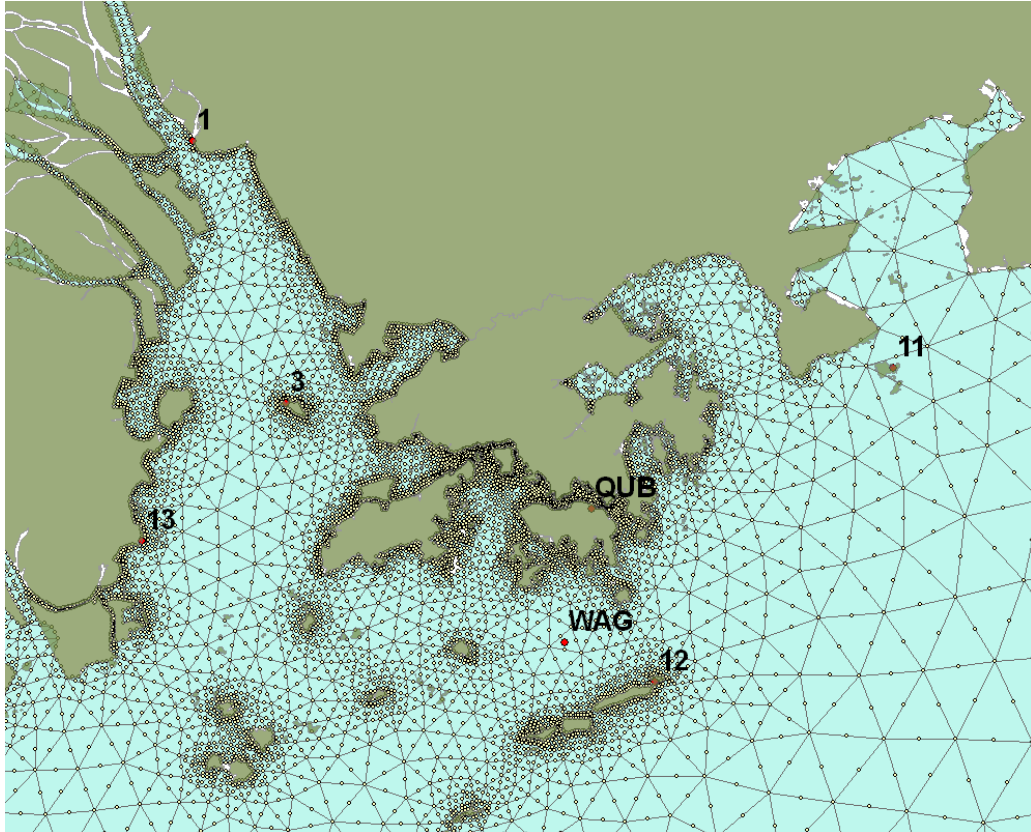


Figure 7.43 Tidal stations for model calibration and model mesh grid configuration.

To allow comparison of the field data with the model results, the mesh grids must be modified so that the location of each data station matches with a corner nodal point. Figure 7.44 shows the procedure for adjusting the nodal point for the WAG station. The nodal point is modified first by identifying the corner node closest to the data station, and then by moving the corner node to the position of the data station. Note that at step 3, the snapping environment allows the corner node point feature to “snap” precisely with the data station point feature. A similar nodal point adjustment procedure can be carried out for all other data stations.

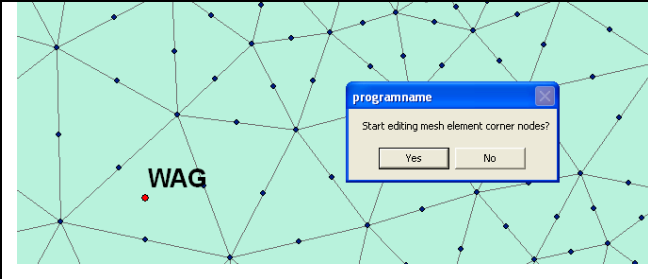
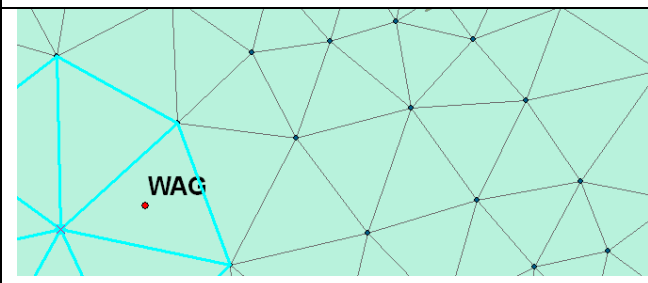
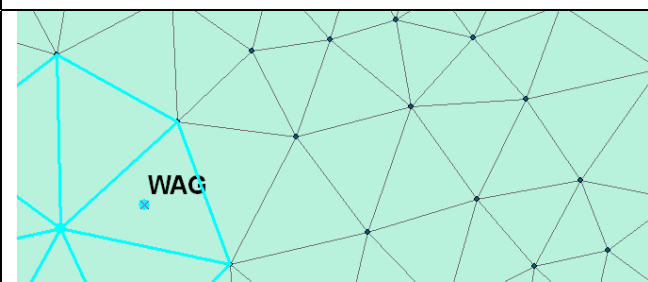
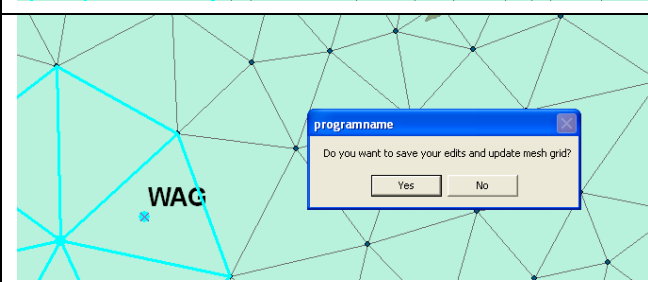
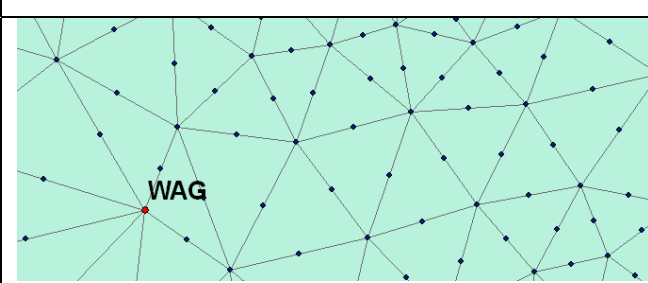
	1. Start edit session
	2. Select corner node for adjustment
	3. Move corner node to “snap” with data station
	4. Terminate edit session
	5. System performs update and displays the modified mesh grid configuration.

Figure 7.44 Procedure for adjusting nodal point for WAG station.

After modification of the mesh grids, the input files for mesh element and node coordinate can be updated (refer to Figure 6.4), and simulation can be carried out. Since each data station now coincides with a nodal point, the model results can be easily compared with the collected data using the time series display. The node number of the matching nodal points can be identified through the GIS interface. For example, as

shown in Figure 7.45, nodal number 5793 is identified as the matching nodal point for the WAG station. For calibration, the process of making adjustment to the model input of open boundary tidal data and running simulations can be repeated until the time series of the generated results conform well to those of the collected data.

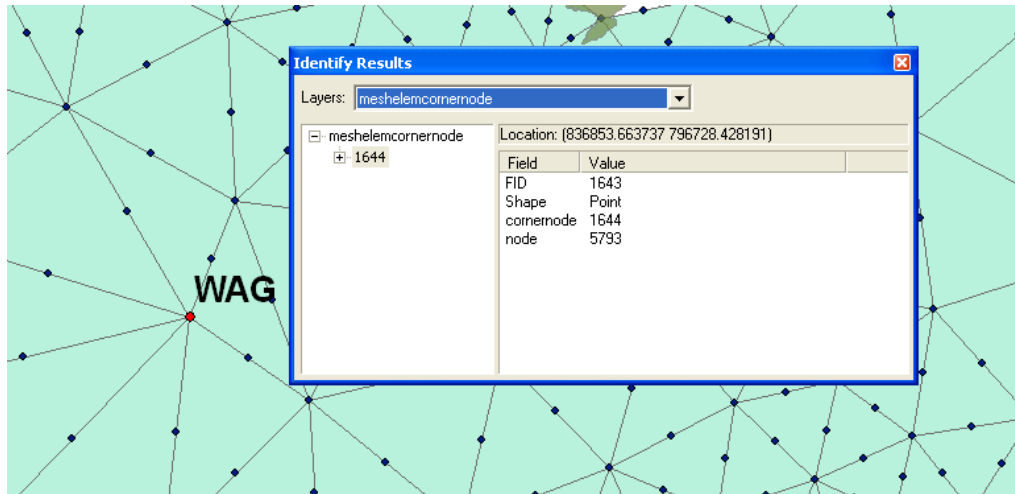


Figure 7.45 Identification of node number 5793 for WAG station.

The most significant aspect of applying the integrated system for calibration is that it enables easy comparisons of model results and field data using various forms of data display. While the time series display is used for tidal data in this example, other data displays such as spatial layer and profile can be applied for calibration of other parameters. When using time series and profile displays for calibration, adjustment must be made to the mesh grid to match a nodal point with each of the comparing data stations. For spatial layers, the model results can be interpolated into raster layers, and values can be extracted from the raster layers and compared with the field data.

7.7 Setting of Model Initial Conditions

There are two approaches for setting model initial conditions using PRE_WAGIS. One is to utilize the module as discussed in section 6.4.2 to extract data from an existing spatial layer and insert the data into the input table. Figure 7.46 shows a spatial layer of salinity generated using the tempo-spatial interpolation function (the Linear Spline for 1D interpolation and the IDW for spatial interpolation). This spatial layer is applied for setting model initial condition of salinity at layer number 1 (see Figure 7.47) using the *Set*

initial condition from spatial layer function. The resulted point spatial layer of salinity is shown in Figure 7.48, with the variation of salinity represented by the colour of the point features.



Figure 7.46 Tempo-spatial layer of salinity from measurement table WQ2_Water_EPD – November 1, 2003 – depth level: surface.

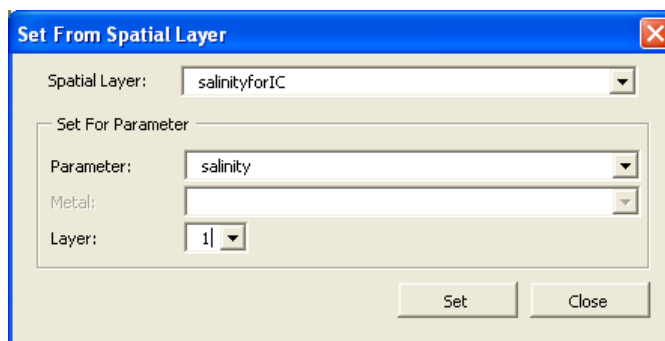


Figure 7.47 Dialog box for setting initial conditions for salinity – layer 1 from an existing layer.

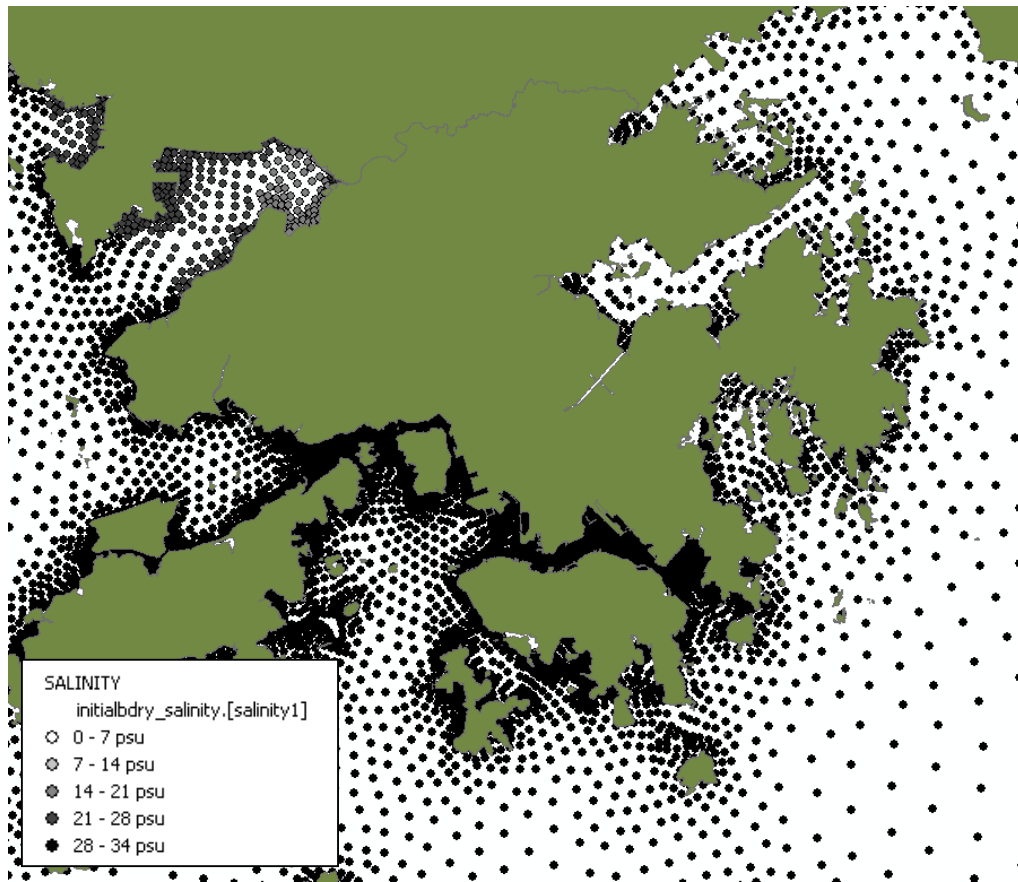


Figure 7.48 A spatial layer of salinity after setting initial condition from an existing layer.

Although this module is demonstrated as being an efficient way to make use of collected data for model input, there is a major limitation. The survey areas from which information is collected so far are bounded to a portion of the entire PRE (usually only for Hong Kong waters). Therefore, using the *set initial condition from spatial layer* function, data are extractable only for nodal points located within the extent of the input spatial layer. The second approach involves simply using the spatial layer as a reference. The numerical figures from the spatial layer can provide rough values (i.e. order of magnitude) for model input for the whole region.

7.8 Management of Wastewater Disposal

Wastewater consists primarily of domestic sewage from households, industrial wastewater from manufacturing and commercial facilities, as well as construction discharge from dredging activities. Domestic and industrial wastewater disposal is not of significant environmental concern for coastal water, as it is generally treated to remove toxic materials, organic matters, suspended solids, pathogenic micro-organisms, and

nutrients before discharging into the receiving water. However, construction dredged materials which are unsuitable for reclamation or other uses (for Hong Kong, dredge disposal totals to 31.3 million cubic metres in 2003) are released directly into the ocean (Hong Kong government, 2005).

When considering the management of marine dumping of dredged material, the most critical considerations are where the outfall should be located and when would be the best time to release the disposal. These two criteria should be chosen carefully to minimize disturbance to the aquatic environment. Dredged material can be broadly classified as either uncontaminated or contaminated (Klee, 1999). Uncontaminated dredged material, which consists of naturally occurring inorganic (e.g. sand, silt, clay, rock, and gravel) and organic matter, poses limited impacts on aquatic environment and thus can be disposed at a wide range of locations. For dredged material contaminated by pollutants from urban, agricultural and industrial activities, the environmental implication is considerably higher. The major environmental concerns of contaminated pollutants include sediment toxicity, turbidity, burial of benthos, and food web contamination. For example, in terms of turbidity, a high concentration not only reduces sunlight needed for plant photosynthesis, but also clogs respiratory systems of marine creatures. Possible considerations when selecting dumping sites may include:

1. The selected site should not be at locations with already high concentrations of pollutants such that the accumulated levels induce extreme impacts on the marine ecosystem.
2. The selected site should not be adjacent to coastal recreational regions to ensure the safety of the public.
3. The selected site should not be close to fish farm areas not only to prevent disastrous killing of fish, but also to protect public health as toxins may get into human body from fish consumption (i.e. web contamination).
4. The selected site should be at regions with fast water circulation such that intense levels of turbidity is diluted within a short time frame. Note timing also plays an important role in this criterion as the rate of water flow varies with time.

For the first consideration, the application of PRE_WAGIS may involve examining a spatial layer of turbidity concentration generated either from recently taken data or model results. Figure 7.49 shows a spatial layer of turbidity generated using the tempo-

spatial interpolation function (the Linear Spline for 1D interpolation and the IDW for spatial interpolation). Considering this spatial layer, Deep Bay should not be selected as a potential dredge dumping site because of its high turbidity level.



Figure 7.49 Tempo-spatial layer of turbidity from measurement table WQ2_Water_EPD – December 1, 2003 – depth level: surface.

For the second and third consideration, information on land or water use in coastal zones can be collected in the future to assist in identifying the environmental sensitive regions. The collected information can also be visualized using PRE_WAGIS for better spatial comprehension. For the last considerations, the best approach is to utilize the hydrodynamic/water quality coupled model to predict the variation of water flow with time and space, and to visualize the predicted results using PRE_WAGIS. Furthermore, model simulations can assist in understanding fate and transport of pollutants disposed at different times and locations, and thus allow better decisions in selecting dumping sites.

7.9 Summary

This chapter has demonstrated seven applications of PRE_WAGIS.

1. **Estimation of values at unknown points in space and time.** By combining 1D and spatial interpolation techniques, PRE_WAGIS can be applied for estimating values at unknown points in space and time. The example of examining *E. coli* at Repulse Bay on August 5, 2003 has shown that the beach is not suitable for swimming at the time.
2. **Evaluation of interpolation methods.** A set of parameters, including tidal level, current velocity (magnitude and direction), temperature, salinity, DO, turbidity, pH, chlorophyll a, total nitrogen, total phosphorus, BOD, and *E. coli*, have been selected for evaluation of both 1D and spatial interpolation methods. For time series, since tide, current speed, temperature, and salinity have daily and seasonal variations, they fit quite well with trigonometric or any high degree polynomial functions. For profile, a wide range of functions including polynomial, logarithmic, exponential, power are suitable for current speed and direction, temperature, salinity, and turbidity. In cases where the time series or profile does not exhibit any notable trends, the Spline – Linear or Natural Neighbour – method can be applied. The evaluation of the 2D interpolation methods has been carried out using the cross-validation analysis. However, there are not much definite correlation between hydrodynamic/water quality parameters and spatial interpolation methods. In general, most parameters fit best with either the Radius Basis Functions or the Kriging Method.
3. **Investigation of temporal and spatial trends.** A sample application has been carried out to demonstrate the functionality of the dynamic time series and section display tools. The parameter of interest is pH and the study region is within the Hong Kong waters. This example has shown that the two interactive data display tools are successful in capturing the movement of horizontal and vertical dispersions of acidic water over time.
4. **Assessment of quality of the collected data.** A brief example has been presented to show how PRE_WAGIS can be applied for assessing the quality of the collected data. This is achieved simply by comparing data of the same parameter taken within the same measurement period and water region. It has been shown that at areas where monitoring stations are scarce, the predicted spatial layers produce limited accuracy.

5. **Calibration and verification of the hydrodynamic-water quality coupled model.** The bridging of information from field and model into the GIS enables efficient calibration and verification of the hydrodynamic model. A simple example has been presented to demonstrate the procedure for calibrating tidal data. This involves first modifying the mesh grids to match the nodal nodes with the data stations, and then comparing the model results with the field data using the time series display.
6. **Setting of model initial conditions.** There are two approaches to apply the collected data for setting model initial conditions. One is to utilize the *Set Initial Condition from Spatial Layer* function, which extracts values from a created layer at nodal points and then updates the values in the model input database. The second method is simply using the spatial layer to provide rough numerical figures for model input.
7. **Management of wastewater disposal.** PRE_WAGIS can also be applied for managing wastewater disposal. PRE_WAGIS can be applied differently for the different possible considerations for selecting dumping sites. For example, the selected site should not be located at water regions with already high concentrations of pollutants, adjacent to coastal recreational regions, or close to fish farm. Examining the collected or predicted data in spatial context provides guidance in selecting dumping sites. For consideration in which timing of disposal is important, results for the model can be used for predicting the variation of water flow.

8 Development of an EIA Module for Water Quality Assessment

8.1 Application of GIS in EIA for Water Quality Evaluation

One of the main purposes of developing PRE_WAGIS is to provide a tool for environmentalists and decision makers to efficiently assess environmental impacts in spatial and temporal contexts. According to the Environmental Systems Research Institute, Inc. (1995), there are four types of questions, which can be answered, with the application of GIS:

1. What is where?
2. What spatial patterns exist?
3. What has changed since...?
4. What if?

These four questions offer general guidelines for developing an EIA module for assessing the coastal water quality in the PRE. The four approaches for conducting EIA in this study are: 1) identification of areas most vulnerable to environmental impact, 2) assessment of the relative importance of parameters, 3) investigation of temporal patterns and trends, and 4) prediction of future hydrodynamics and water quality.

In assessing environmental impacts on water quality, one of the most important aspects is the establishment of a well-quantifying system. An EIA module for water

quality evaluation is developed for the third component of PRE_WAGIS (see Figure 3.1). The EIA module measures the overall water quality based on the concept of WQI, and the *Map Algebra* operation function available from the ArcGIS Spatial Analyst extension (McCoy and Johnson, 2001) is applied for spatial evaluation of WQI.

8.1.1 WQI

The use of WQI is a simple practice to evaluate water quality. WQI integrates a selected set of measured parameters into a single unitless value (e.g. one number from 0 to 100, with 0 for the worst condition and 100 for the best condition) for water quality evaluation. Based on the WQI function, *Map Algebra* can be applied to combine raster layers of different parameters into a WQI raster layer (see Figure 8.1).

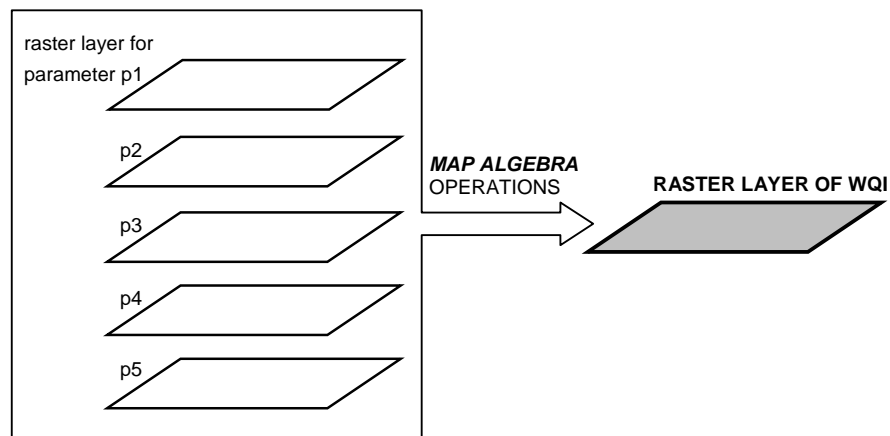


Figure 8.1 Application of *Map Algebra* operations for deriving a WQI spatial layer.

The calculation of WQI is based upon the use of aggregation functions. This involves first converting raw data of different units of measurement into unitless subindex values typically using rating curves, and then aggregating the subindex values into a single WQI (Cude, 2001).

8.1.2 Deriving WQI Using Aggregation Function

When calculating WQI, the first step is to identify the evaluating water quality variables and convert the water quality variables into unitless subindices using some sort of rating system. In this section, the variables and their respective rating curves included in this study are discussed. These assessing parameters correspond closely to those outlined in the water quality objectives (WQOs) for marine waters of Hong Kong from the

Environmental Protection Department (2003) of Hong Kong (see Table 8.1). The developed system allows users to choose part or all of these variables in their analysis.

Table 8.1 Summary of Water Quality Objectives (WQOs) for marine waters of Hong Kong – Environmental Protection Department (EPD) of Hong Kong.

Parameter	Water Quality Objective	Water Control Zone (WCZ)/ Part(s) of zone/ Subzone to which the WQOs applies
Dissolved Oxygen (bottom)	Not less than 2 mg/L for 90% samples	Marine waters of all WCZs except Tolo Harbour & Channel WCZ
Dissolved Oxygen (depth-averaged)	Not less than 4 mg/L for 90% samples	Marine waters of all WCZs except Tolo Harbour & Channel WCZ
Dissolved Oxygen (bottom)	Not less than 2 mg/L	Marine waters of all WCZs except Tolo Harbour & Channel WCZ
	Not less than 3 mg/L	Harbour Subzone in Tolo Harbour & Channel WCZ
	Not less than 4 mg/L	Channel Subzone in Tolo Harbour & Channel WCZ
Dissolved Oxygen (surface to 2m above bottom)	Not less than 4 mg/L	Harbour Subzone and Buffer Subzone in Tolo Harbour & Channel WCZ
Dissolved Oxygen (all depths)	Not less than 4 mg/L	Channel Subzone in Tolo Harbour & Channel WCZ
Nutrients	Annual mean depth-averaged inorganic nitrogen not to exceed 0.1 mg/L	Marine waters of Southern WCZ and Port Shelter WCZ
	Annual mean depth-averaged inorganic nitrogen not to exceed 0.3 mg/L	Marine waters of Mirs Bay WCZ, Junk Bay WCZ, North Western WCZ (Castle Peak Subzone)
	Annual mean depth-averaged inorganic nitrogen not to exceed 0.4 mg/L	Marine waters of Eastern Buffer WCZ, Western Buffer WCZ, Victoria Harbour WCZ
	Annual mean depth-averaged inorganic nitrogen not to exceed 0.5 mg/L	Marine waters of Deep Bay WCZ (Outer Subzone) and North Western WCZ (Whole zone except Castle Peak Subzone)
	Annual mean depth-averaged inorganic nitrogen not to exceed 0.7 mg/L	Marine waters of Deep Bay WCZ (Inner Subzone)
Unionised ammonia	Annual mean not to exceed 0.021 mg/L	All WCZs (whole zone) except Tolo Harbour & Channel WCZ
E. coli	Annual geometric mean not to exceed 610 cfu/100 mL	Secondary contact recreation subzones in Tolo Harbour & Channel WCZ, Southern WCZ, Port Shelter WCZ, Mirs Bay WCZ, Deep Bay WCZ, North Western WCZ, Western Buffer WCZ
	Annual geometric mean not to exceed 610 cfu/100 mL	Fish culture subzones in Tolo Harbour & Channel WCZ, Southern WCZ, Port Shelter WCZ, Junk Bay, Mirs Bay WCZ, Deep Bay WCZ, Eastern Buffer WCZ, Western Buffer WCZ
pH	To be in range 6.5 – 8.5, change due to waste discharge not to exceed 0.2	Marine waters of all WCZs except Tolo Harbour & Channel WCZ
	Change due to waste discharge not to be greater than ± 0.5	Harbour Subzone in Tolo Harbour & Channel WCZ
	Change due to waste discharge not to be greater than ± 0.3	Buffer Subzone in Tolo Harbour & Channel WCZ
	Change due to waste discharge not to be greater than ± 0.1	Channel Subzone in Tolo Harbour & Channel WCZ
Salinity	Change due to waste discharge not to exceed 10% of natural ambient level	All WCZs (Whole zone) except Tolo Harbour & Channel WCZ
	Change due to waste discharge not to be greater than $\pm 0.3\%$	Tolo Harbour & Channel WCZ
Temperature	Change due to waste discharge not to exceed 2 °C	All WCZs (Whole zone) except Tolo Harbour & Channel WCZ
	Change due to waste discharge not to exceed 1 °C	Tolo Harbour & Channel WCZ
Suspended solids	Waste discharge not to raise the natural ambient level by 30% nor cause the accumulation of suspended solids which may adversely affect aquatic communities	Marine waters of all WCZs except Tolo Harbour & Channel WCZ
Toxicants	Not to be present at levels producing significant toxic effect	All WCZs (Whole zone)
Chlorophyll-a	Not to exceed 20 mg/m ³ ($\mu\text{g/L}$) calculated as running arithmetic mean of 5 daily measurements for any location and depth	Harbour Subzone in Tolo Harbour & Channel WCZ
	Not to exceed 10 mg/m ³ ($\mu\text{g/L}$) calculated as running arithmetic mean of 5 daily measurements for any location and depth	Buffer Subzone in Tolo Harbour & Channel WCZ
	Not to exceed 6 mg/m ³ ($\mu\text{g/L}$) calculated as running arithmetic mean of 5 daily measurements for any location and depth	Channel Subzone in Tolo Harbour & Channel WCZ

8.1.2.1 Water Quality Variables and Rating Curves

Twelve water quality variables are included: DO, BOD, TN, ammonia nitrogen, TP, F. coli, pH, temperature, turbidity, suspended solids, toxicants, and chlorophyll. Numerous rating functions have been suggested in the literature on how these variables should be scored (Bhargava, 1983; Cude, 2001; Dinius, 1987; Liou et al., 2004; Prati et al., 1971; Schierow and Chesters, 1988; Silvia and Daniel, 2000; Smith, 1990; Stambuk-Giljanovic, 1999). Some are developed from expert opinions, while others are fitted based on environmental classification standards. The differences in these rating schemes are largely due the diverse natural conditions (physical, chemical, biological, and geological) that may exist at different water bodies, the intended water use, and the subjective opinions among different environmental groups. However, despite these discrepancies, there are certain general trends for the rating curves to follow for each specified parameter (e.g. water score decreases as concentration of toxicants increases, water score is the highest at pH of 6 to 8 and attenuates at lower and higher pH levels).

To date, no water quality scoring system has been developed for the PRE or Hong Kong waters. A selected set of curves taken from the literature are included in this EIA module for water quality evaluation (see Figures 8.2 to 8.13). Table 8.2 summarizes the list of water quality variables and their respective rating curves and equations. Note that the following descriptions of water quality parameters are referenced from Boyd (2000) and Chapman (1996).

Table 8.2 Summary of water quality variables and their respective rating curves included in the EIA module.

Variables	Equations	Source/ Applied Waters
dissolved oxygen	$DO_{\%} \leq 100\%$: $DO_c \leq 3.3 \text{ mg/L}$: $S = 10$ $3.3 \text{ mg/L} < DO_c < 10.5 \text{ mg/L}$: $S = -80.29 + 31.88 * DO_c - 1.401 * DO_c^2$ $10.5 \text{ mg/L} \geq DO_c$: $S = 100$ $100\% < DO_{\%} < 275\%$: $S = 100 * \exp((DO_{\%} - 100) * -1.197E-2)$ $275\% < DO_{\%}$: $S = 10$	Cude (2001) – Oregon's stream (US)
	$DO \leq 2 \text{ mg/L}$: $S = 0$ $2 \text{ mg/L} < DO \leq 3 \text{ mg/L}$: $S = -50 + 25 * DO$ $3 \text{ mg/L} < DO \leq 5.5 \text{ mg/L}$: $S = -29 + 18 * DO$ $5.5 \text{ mg/L} < DO \leq 6.5 \text{ mg/L}$: $S = -95 + 30 * DO$ $6.5 \text{ mg/L} < DO$: $S = 100$	Liou et al. (2004) - Taiwan
	$DO \leq 100\%$: $S = -4.113E-06 * DO^4 + 7.105E-04 * DO^3 - 2.616E-02 * DO^2 + 6.307E-01 * DO - 1.698E-01$ $DO > 100\%$: $S = 3.750E-05 * DO^4 - 1.758E-02 * DO^3 + 3.076E+00 * DO^2 - 2.386E+02 * DO + 7035$	Stambuk-Giljanovic (1999) - Dalmatia
	$0 \text{ mg/L} \leq DO \leq 16 \text{ mg/L}$: $S = 1.164E-02 * DO^4 - 4.108E-01 * DO^3 + 3.973E+00 * DO^2 - 7.833E-01 * DO + 5.382E+00$ note: DO in mg/L	Smith (1990) – New Zealand
	$S = 0.82 * DO + 10.56$ note: DO in %, assume average summer temperature of 20°C, low salt content, oxygen saturation of 9.2 mg/L	Dinius (1987)
biochemical oxygen demand	$BOD \leq 8 \text{ mg/L}$: $S = 100 * \exp(BOD * -0.1993)$ $8 \text{ mg/L} < BOD$: $S = 10$	Cude (2001) – Oregon's stream (US)
	$BOD \leq 3 \text{ mg/L}$: $S = 100$ $3 \text{ mg/L} < BOD \leq 4 \text{ mg/L}$: $S = 190 - 30 * BOD$ $4 \text{ mg/L} < BOD \leq 9 \text{ mg/L}$: $S = 98 - 7 * BOD$ $9 \text{ mg/L} < BOD \leq 15 \text{ mg/L}$: $S = 87.47 - 5.83 * BOD$ $15 \text{ mg/L} < BOD$: $S = 0$	Liou et al. (2004) - Taiwan
	$BOD \leq 16 \text{ mg/L}$: $S = 7.011E-04 * BOD^5 - 3.569E-02 * BOD^4 + 6.550E-01 * BOD^3 - 4.631E+00 * BOD^2 + 4.132E-01 * BOD + 1.002E+02$ $BOD > 16 \text{ mg/L}$: $S = 0$	Stambuk-Giljanovic (1999) - Dalmatia
	$0 \leq BOD \leq 12 \text{ mg/L}$: $S = 1.009E-03 * BOD^5 - 5.282E-02 * BOD^4 + 9.290E-01 * BOD^3 - 6.106E+00 * BOD^2 + 1.933E+00 * BOD + 9.986E+01$ $BOD > 12 \text{ mg/L}$: $S = 0$	Smith (1990) – New Zealand
total nitrogen	$N \leq 0.35 \text{ mg/L}$: $S = 152.13 * N^2 - 231.72 * N + 101.81$ $0.35 \text{ mg/L} < N \leq 1.37 \text{ mg/L}$: $S = -15.798 * N^3 + 56.504 * N^2 - 77.634 * N + 60.927$ $1.37 \text{ mg/L} < N < 3 \text{ mg/L}$: $S = 1.2102 * N^2 - 10.428 * N + 32.014$ $N > 3 \text{ mg/L}$: $S = 0$ (assumption made)	Stambuk-Giljanovic (1999) - Dalmatia
ammonia nitrogen	$N \leq 0.5 \text{ mg/L}$: $S = 100$ $0.5 \text{ mg/L} < N \leq 0.75 \text{ mg/L}$: $S = 160 - 120 * N$ $0.75 \text{ mg/L} < N \leq 3 \text{ mg/L}$: $S = 93.33 - 31.11 * N$ $3 \text{ mg/L} < N$: $S = 0$	Liou et al. (2004) - Taiwan
total phosphorus	$P \leq 0.25 \text{ mg/L}$: $S = 100 - 299.5 * P - 0.1384 * P^2$ $0.25 \text{ mg/L} < P$: $S = 10$	Cude (2001) – Oregon's stream (US)
	$P \leq 3 \text{ mg/L}$: $S = 2.833E+00 * P^3 - 1.300E+01 * P^2 - 6.833E+00 * P + 1.000E+02$ $3 \text{ mg/L} < P$: $S = -1.107E-02 * P^3 + 4.530E-01 * P^2 - 6.883 * P + 55.506$	Stambuk-Giljanovic (1999) - Dalmatia
faecal coliform	$FC \leq 50\#/100 \text{ mL}$: $S = 98$ $50\#/100 \text{ mL} < FC \leq 1600\#/100 \text{ mL}$: $S = 98 * \exp((FC-50) * -9.9178E-4)$ $1600\#/100 \text{ mL} < FC$: $S = 10$	Cude (2001) – Oregon's stream (US)
	$FC \leq 1\#/100 \text{ mL}$: $S = 100$ $1\#/100 \text{ mL} < FC \leq 5600\#/100 \text{ mL}$: $S = 100 - 10.67 * \log(FC)$ $5600\#/100 \text{ mL} < FC \leq 1000000\#/100 \text{ mL}$: $S = 60 - 26.64 * (\log(FC) - 3.75)$ $1000000\#/100 \text{ mL} < FC$: $S = 0$	Liou et al. (2004) - Taiwan
	$0 \leq FC \leq 10000$: $S = 6.1254E-01 * (\log(FC))^4 - 4.7376E+00 * (\log(FC))^3 + 5.9952E+00 * (\log(FC))^2 - 6.3106E+00 * \log(FC) + 1.0002E+02$	Smith (1990) – New Zealand

Table 8.2 Continued.

Variables	Equations	Source/ Applied Waters
pH	pH < 4: S = 10 4 ≤ pH < 7: S = 2.628 * exp(pH * 0.5200) 7 ≤ pH < 8: S = 100 8 < pH ≤ 11: S = 100 * exp((pH-8) * -0.5188) 11 < pH: S = 10	Cude (2001) – Oregon's stream (US)
	pH < 6: S = 0 6 ≤ pH ≤ 9: S = 100 9 < pH: S = 0	Liou et al. (2004) - Taiwan
	1 ≤ pH < 7: S = -9.77329E-02 * pH ⁵ + 1.77979E+00 * pH ⁴ - 1.13621E+01 * pH ³ + 3.37904E+01 * pH ² - 4.44242E+01 * pH + 2.05598E+01 7 ≤ pH ≤ 8: S = 4.65661E-10 * pH ⁴ - 1.39698.E-08 * pH ³ - 8.00000.E+00 * pH ² + 1.20000.E+02 * pH - 3.50000.E+02 8 < pH ≤ 12: S = 2.05250E-02 * pH ⁵ - 1.24165E+00 * pH ⁴ + 2.92382E+01 * pH ³ - 3.31367E+02 * pH ² + 1.77163E+03 * pH - 3.42383E+03	Smith (1990)
temperature	T ≤ 11°C: S = 100 11°C < T ≤ 29°C: S = 76.54 + 4.172*T - 0.1623*T ² - 2.0557E-3*T ³ 29°C < T: S = 10	Cude (2001) – Oregon's stream (US)
	T ≤ 38°C: S = 100 T > 38°C: S = 0	Liou et al. (2004) - Taiwan
	T ≤ 12°C: S = 100 12 °C < T ≤ 27.7 °C: S = -5.973E-03 * T ⁴ + 5.090E-01 * T ³ - 1.573E+01 * T ² + 2.012E+02 * T - 8.053E+02 T > 27.7°C: S = 0	Stambuk-Giljanovic (1999) - Dalmatia
	T ≤ 12.5°C: S = MIN(-2.798E-03 * T ⁴ + 7.821E-02 * T ³ - 8.967E-01 * T ² + 5.963E+00 * T + 8.006E+01, 100) 12.5 °C < T ≤ 22.5 °C: S = -1.067E-03 * T ⁴ + 4.800E-02 * T ³ - 6.333E-01 * T ² - 3.000E-01 * T + 1.340E+02 22.5 °C < T ≤ 30.0 °C: S = -1.4933E-01 * T ³ + 1.1440E+01 * T ² - 2.9927E+02 * T + 2.7230E+03 T > 30.0 °C: S = 10 (assumption made)	Smith (1990) – New Zealand
	TURB ≤ 5 NTU: S = 100 - 4 * TURB 5 NTU < TURB ≤ 20 NTU: S = 83.33 - 0.667 * TURB 20 NTU < TURB ≤ 30 NTU: S = 110 - 2 * TURB 30 NTU < TURB ≤ 50 NTU: S = 80 - TURB 50 NTU < TURB ≤ 120 NTU: S = 51.43 - 0.428 * TURB 120 NTU > TURB: S = 0	Liou et al. (2004) - Taiwan
0 NTU ≤ TURB ≤ 30 NTU: S = 1.755E-06 * TURB ⁴ - 1.261E-03 * TURB ³ + 1.033E-01 * TURB ² - 4.735E+00 * TURB + 1.011E+02 T > 30 NTU: TURB = 0 (assumption made) note: TURB in NTU	Smith (1990) – New Zealand	
suspended solids	SS ≤ 20 mg/L: S = 100 20 mg/L < SS ≤ 35 mg/L: S = 140 - 2 * SS 35 mg/L < SS ≤ 75 mg/L: S = 105 - SS 75 mg/L < SS ≤ 100 mg/L: S = 120 - 1.2 * SS 100 mg/L > SS: S = 0	Liou et al. (2004) - Taiwan
	0 ≤ SS ≤ 60 mg/L: S = 6.1914E-06 * SS ⁴ - 8.8874E-04 * SS ³ + 5.8025E-02 * SS ² - 2.9844E+00 * SS + 9.9188E+01 SS > 60 mg/L: S = 0 (assumption made) note: SS in mg/L	Smith (1990) – New Zealand
toxicants	R _i = C _i /S _i where C _i = substance with concentration (mg/L) S _i = maximum permissible concentration (mg/L) R _i ≤ 1: S = 100 - 100 * R _i R _i > 1: S = 0	Liou et al. (2004) - Taiwan
chlorophyll	S = MIN(-33.23 * log(Chl) + 81.39, 100)	Schierow and Chesters (1970) – North American Great Lakes

DO. Adequate level of DO is vital to all forms of aquatic life. While the optimal DO level is 100% saturation, too much DO is also a sign of unhealthy water. Extremely high levels of DO can be harmful to organisms and cause gas bubble disease. While the WQOs stipulate a minimum requirement of only 4 mg/L, a concentration of 5 mg/L is critical for the functioning and survival of biological communities and concentration below 2 mg/L may result in death of most fish. Furthermore, as DO level raises beyond saturation concentration, water quality is lowered.

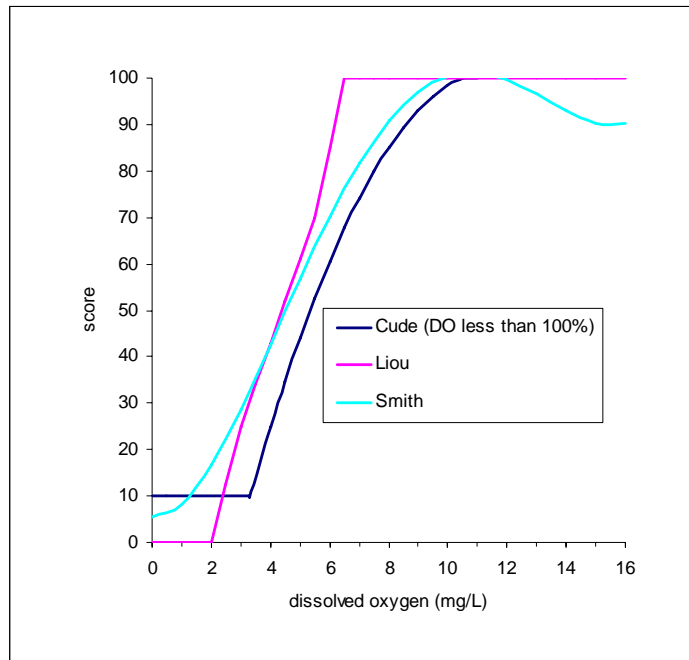


Figure 8.2 Rating curve for dissolved oxygen in mg/L.

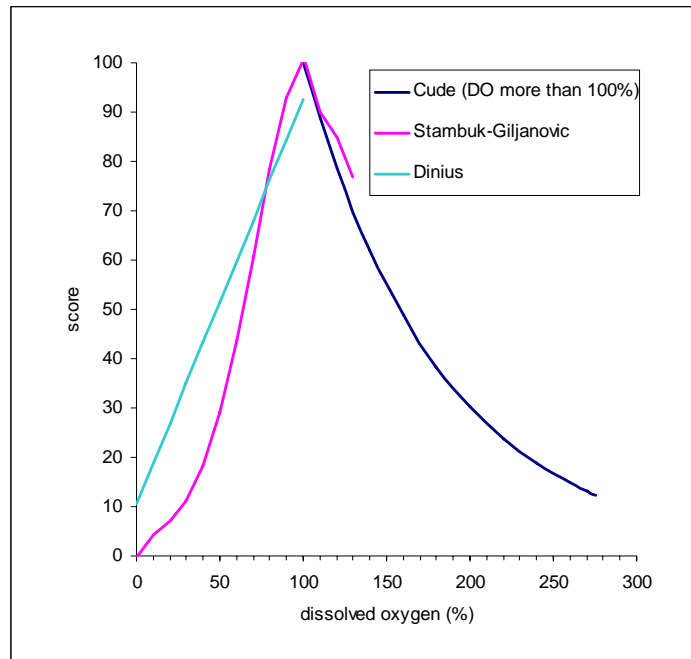


Figure 8.3 Rating curve for dissolved oxygen in %.

BOD. BOD is defined as the amount of dissolved oxygen consumed by aerobic microorganisms during the oxidation of organic matter, and thus is an indirect indicator of the amount of biodegradable organic matter present in water. Oxygen consumption during organic decomposition processes depletes the oxygen supply essential for other aquatic organisms. There is currently no minimum standard pertaining directly to BOD based on the WQOs. Unpolluted waters have typical BOD values of less than 2 mg/L, while receiving wastewaters may have values greater than 10 mg/L.

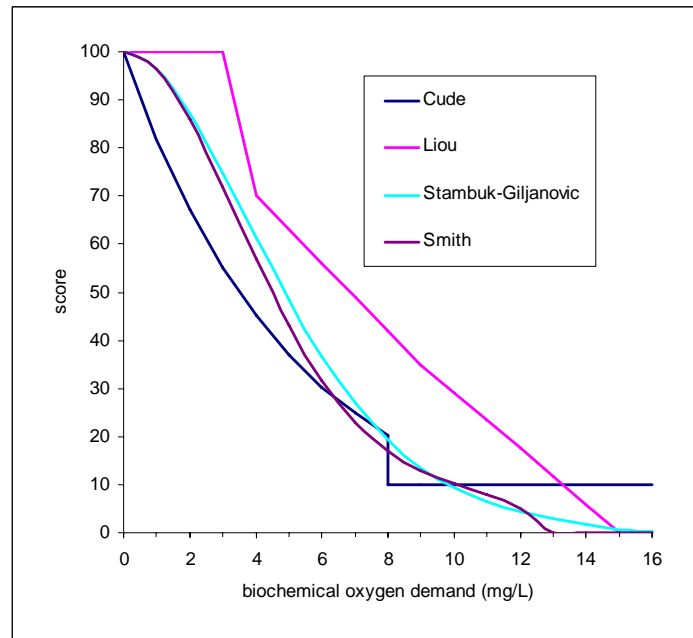


Figure 8.4 Rating curve for biochemical oxygen demand in mg/L.

Nutrients (nitrogen and phosphorus). Nitrogen and phosphorus are the major nutrients required for growth of marine plants and animals. Nitrogen occurs in several forms, including $\text{NH}_3\text{-N}$, $\text{NO}_3\text{-N}$ and $\text{NO}_2\text{-N}$, whereas phosphorus can exist as $\text{PO}_4\text{-P}$ or other inorganic and organic forms. Though a minimal quantity of nutrients is essential for aquatic growth, an excessive amount will simulate algal bloom, seize dissolved oxygen in the water required for other organisms, and possibly lead to eutrophication. While the WQOs specify maximum levels of 0.1 to 0.7 mg/L for inorganic nitrogen and 0.021 mg/L for unionised ammonia, there are no requirements identified for other nutrients. In general, unpolluted surface waters have small amounts of $\text{NH}_3\text{-N}$ less than 0.1 mg/L, $\text{NO}_3\text{-N}$ less than 5 mg/L, $\text{NO}_2\text{-N}$ less than 0.001 mg/L, and $\text{PO}_4\text{-P}$ less than 0.02 mg/L.

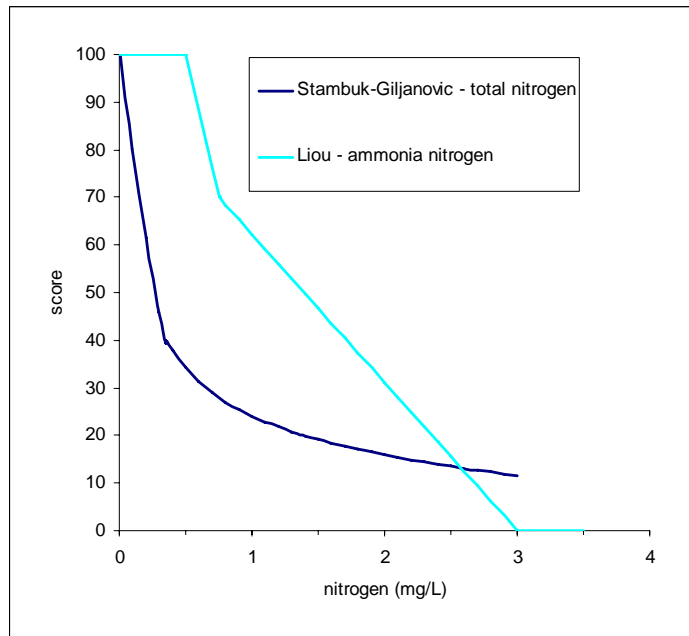


Figure 8.5 Rating curve for nitrogen in mg/L.

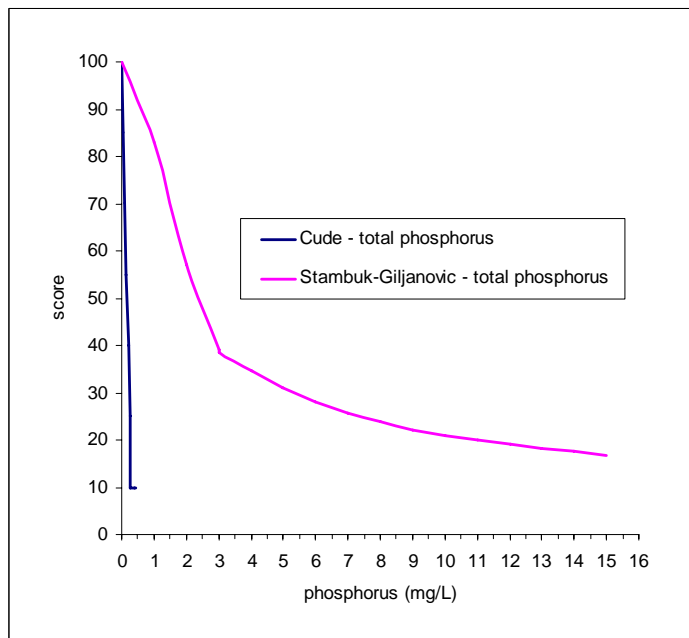


Figure 8.6 Rating curve for phosphorus in mg/L.

F. coli. Coliform bacteria exists in high numbers in human faecal and thus is an indicator of faecal contamination. The most common type of coliform is E. coli. Coliform bacteria in water for recreational and drinking purposes should be kept at minimal levels, as its presence is related to many waterborne pathogenic diseases such as typhoid fever, viral and bacterial gastroenteritis and hepatitis A. The WQOs suggest that

the annual geometric mean for *E. coli* must not exceed 610 cfu/100 mL. However, the typical standards is 1 cfu/100 mL for drinking water, 200 cfu/100 mL for body-contact recreation, 1000 cfu/100 mL for fishing and boating, and 2000 cfu/100 mL for domestic water supply.

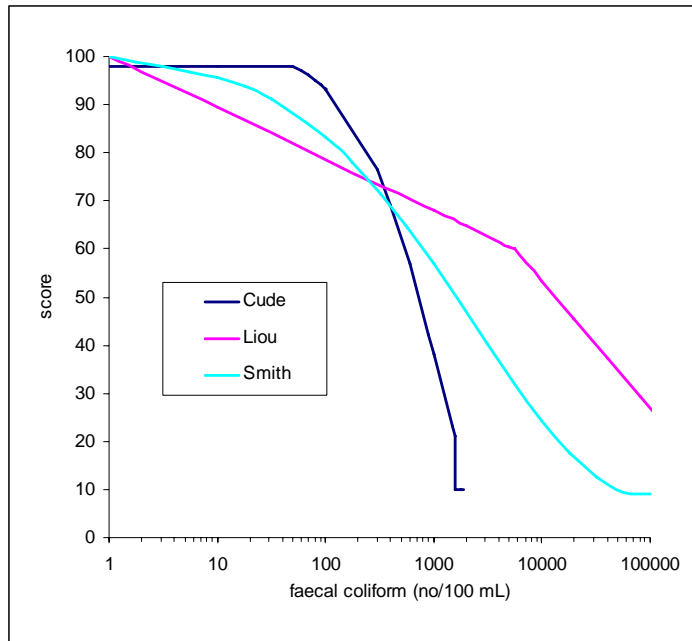


Figure 8.7 Rating curve for faecal coliform in no/100 mL.

pH. A pH range of 6.0 to 9.0 is essential for the protection of freshwater fish and other aquatic life. The most problematic effect of significant pH change is its indirect alternation of other aspects of water chemistry. For example, low pH levels can trigger toxicity of water by increasing solubility of heavy metals. According to the WQOs, the pH requirement for Hong Kong water is between 6.5 and 8.5.

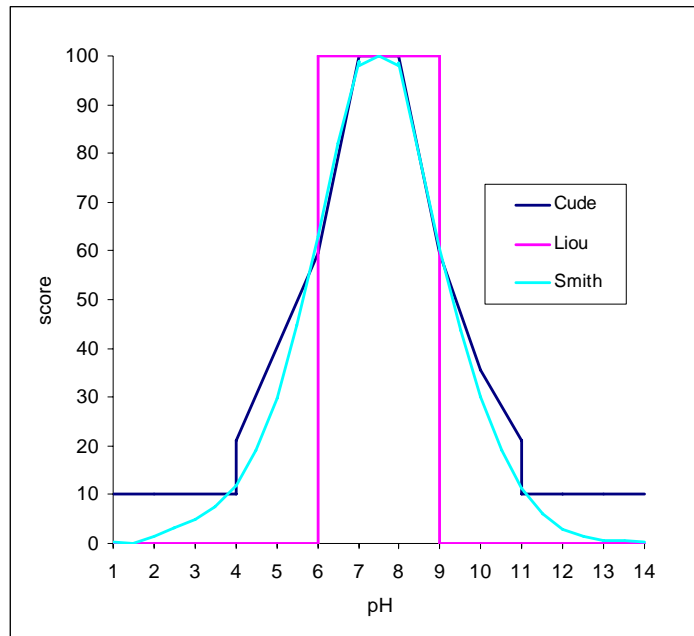


Figure 8.8 Rating curve for pH.

Temperature. There are many implications in which temperature affects biological and chemical quality of water. Increasing water temperature from thermal pollution generally increases the metabolic rates of aquatic organism, thus increasing oxygen consumption. The increase in growth rate of bacteria and phytoplankton in warmer water can lead to increase in turbidity, and algal bloom. The rate of chemical reaction also increases at higher temperature, which in turn affects biological activity. The WQOs only specify requirements for temperature change due to waste discharge, and have no stipulation on the maximum permissible temperature.

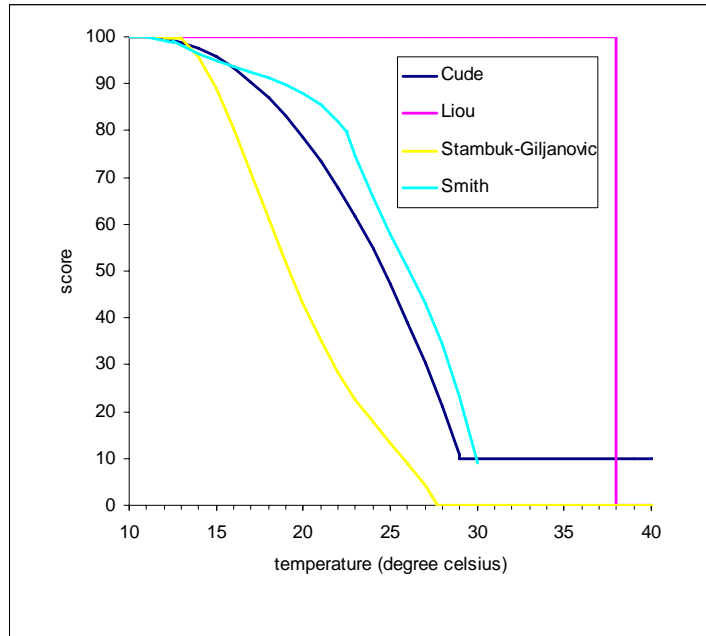


Figure 8.9 Rating curve for temperature in degree Celsius.

Suspended solids and turbidity. Turbid water is primarily due to the presence of suspended sediment in water. Suspended matter includes clays and silts, organic and inorganic matters, soluble organic compounds, algae, and faecal material. The WQOs only specify that the waste discharge should not raise the ambient level by more 30% and cause accumulation of suspended solids, which may adversely affect aquatic communities.

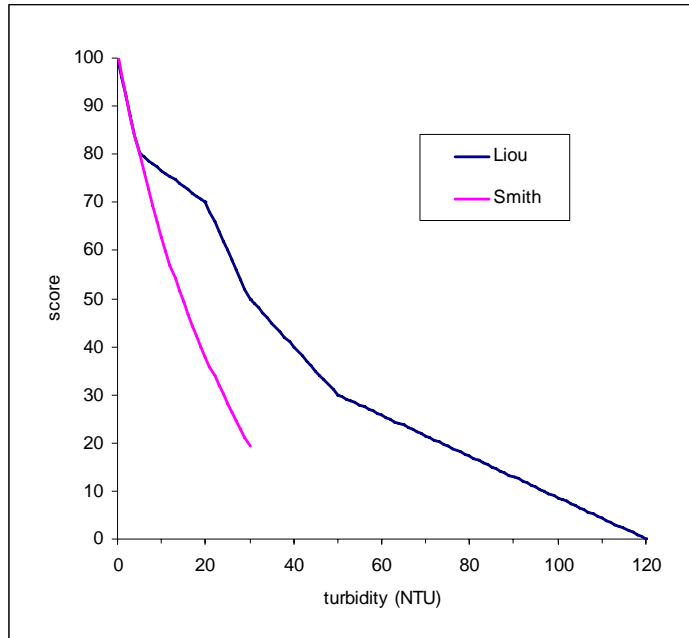


Figure 8.10 Rating curve for turbidity in NTU.

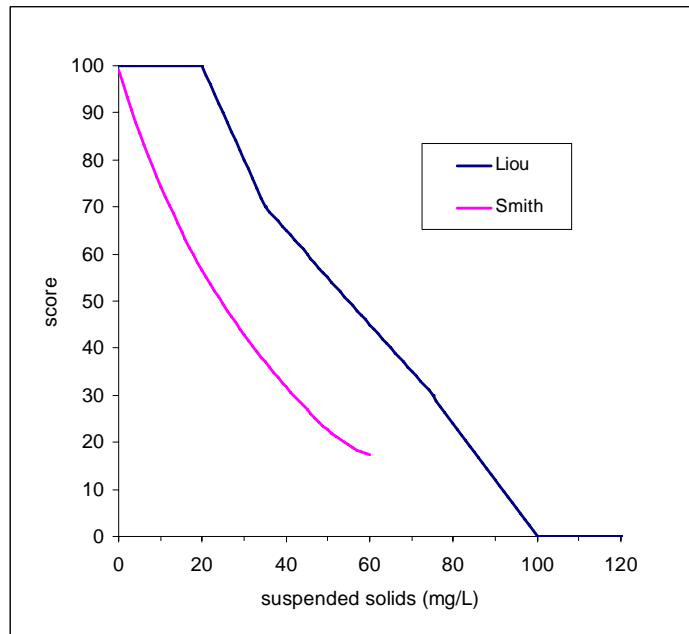


Figure 8.11 Rating curve for suspended solids in mg/L.

Toxicants. The toxic substances in waters include heavy metals such as cadmium, lead, chromium, copper, and zinc, and organic compounds such as pesticides. The WQOs only suggest that toxicants should not be present at levels producing significant toxic effect, but there are no quantitative criteria on toxicants.

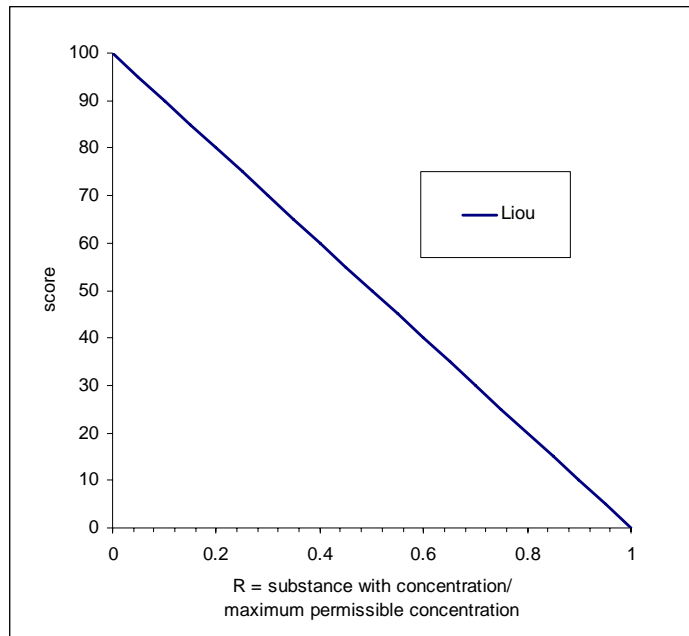


Figure 8.12 Rating curve for toxicants.

Chlorophyll. Chlorophyll, the green pigment used by plants in photosynthesis, is an indirect estimate of algal biomass and an indication of the trophic status of water body. The WQOs indicate the maximum levels of chlorophyll-a to be between 6 and 20 mg/m^3 depending on which WCZ. In general, low levels of chlorophyll of less than 2.5 mg/m^3 is classified as oligotrophic, whereas high levels of chlorophyll between 5 and 140 mg/m^3 indicate high nutrient content and eutrophic state.

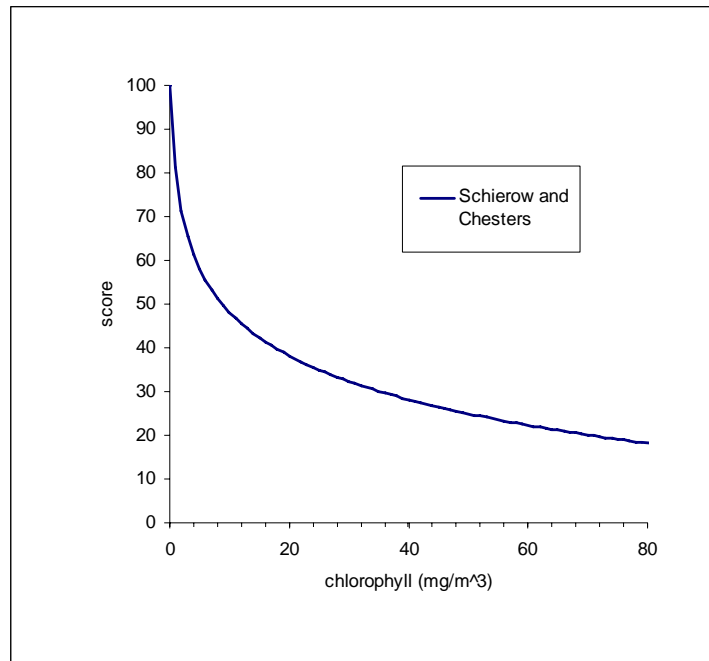


Figure 8.13 Rating curve for chlorophyll in mg/m^3 .

8.1.2.2 Aggregation Functions

Different forms of aggregation function in combining subindex scores into a single WQI have been proposed in the past two decades. Swamee and Tyagi (2000) has summarized a list of aggregation functions, suggested the ambiguity and eclipsing problems that exist in these functions, and then proposed a new form of aggregate function which sought solutions to these two problems. Table 8.3 provides a list of aggregation functions that are included in the EIA module for selection. The weighted arithmetic and geometric mean aggregation functions both suffer from the problem of eclipsing, that is, if one subindex has a poor quality, the aggregate result may not manifest an overall poor quality. The harmonic mean of square and the minimum operator aggregation functions have the problem of ambiguity, that is, the overall water quality may be heavily influenced by a single impaired subindex; and thus not provide a well-rounded picture of water quality. The last aggregation function given by Swamee and Tyagi (2000) has sought a balance between these two mathematical issues.

Table 8.3 Aggregation functions.

Aggregation Function	Equation	Remarks
Weighted Arithmetic Mean	$I = \sum_{i=1}^n w_i s_i$ <p>where I = water quality index; n = number of subindices; w_i = i-th weight; and s_i = i-th subindex</p> <p>The weights w_i indicates the relative importance of s_i, and they sum to unity:</p> $\sum_{i=1}^n w_i = 1$	<ul style="list-style-type: none"> • Problem of eclipsing, that is, if one subindex has a poor quality, the aggregated result may not show an overall poor quality
Weighted Geometric Mean	$I = \prod_{i=1}^n s_i^{w_i}$ <p>where I = water quality index; n = number of subindices; w_i = i-th weight; and s_i = i-th subindex</p>	<ul style="list-style-type: none"> • More sensitive to changes in individual variables than the arithmetic mean function • Problem of eclipsing, that is, when a near-zone weight is given to a low subindex, the aggregated result may not show an overall poor quality
Harmonic Mean of Square	$I = \sqrt{\frac{n}{\sum_{i=1}^n \frac{1}{s_i^2}}}$ <p>where I = water quality index; n = number of subindices; and s_i = i-th subindex</p>	<ul style="list-style-type: none"> • Allows the most impaired variable to give the greatest importance in computing the overall index • Problem of ambiguity, that is, the water an acceptable quality may be stated as unacceptable
Minimum Operator	$I = \min(s_1, s_2, s_3, \dots, s_n)$ <p>where I = water quality index; n = number of subindices; and s_i = i-th subindex</p>	<ul style="list-style-type: none"> • Problem of not providing an overall water quality index when one of subindices is significantly lower than the others
Swamee and Tyagi	$I = 100 * \left(1 - n + \sum_{i=1}^n \left(\frac{s_i}{100} \right)^{-1/k} \right)^{-k}$ <p>where I = water quality index; n = number of subindices; s_i = i-th subindex; and k = a positive constant between 0 and 1 As k approaches a near-zero value, the aggregation function becomes insensitive to all subindices except the lowest subindex (e.g. similar to the minimum operator). As k increases, the sensitivity of the aggregation function gradually increases. The recommended value for k is 0.4</p>	<ul style="list-style-type: none"> • Solved eclipsing and ambiguity problems

8.2 Identification of Areas Most Vulnerable to Environmental Impact

One of the most significant concerns in examining spatial trends in water quality data is to identify the locations subjected to the most severe environmental impacts (i.e. poorest water quality). A sample application of the EIA module is presented aiming to identify

the most vulnerable water region in Hong Kong. The selected dataset is obtained from the measurement table WQ2_Water_EPD, and the parameters included in this analysis are DO, BOD, total nitrogen, total phosphorus, F. coli, pH, temperature, turbidity, suspended solids and chlorophyll a. A set of spatial layers are generated using the tempo-spatial interpolation function (the Linear Spline for 1D and the kriging for spatial interpolation) for surface depth level on August 1, 2003.

Examining the spatial layers in Figure 8.14, Deep Bay, with no doubt, is identified as the most problematic water region. Deep Bay not only shows signs of low oxygen, but also possesses a high level of acidity, BOD, temperature, nutrients, turbidity, and suspended solids. Another region of environmental concern is the Western Buffer zone, which exhibits high concentration of both F. coli and chlorophyll a. The EIA module is applied to assess the extent of the water deteriorating condition using all five types of aggregation function.

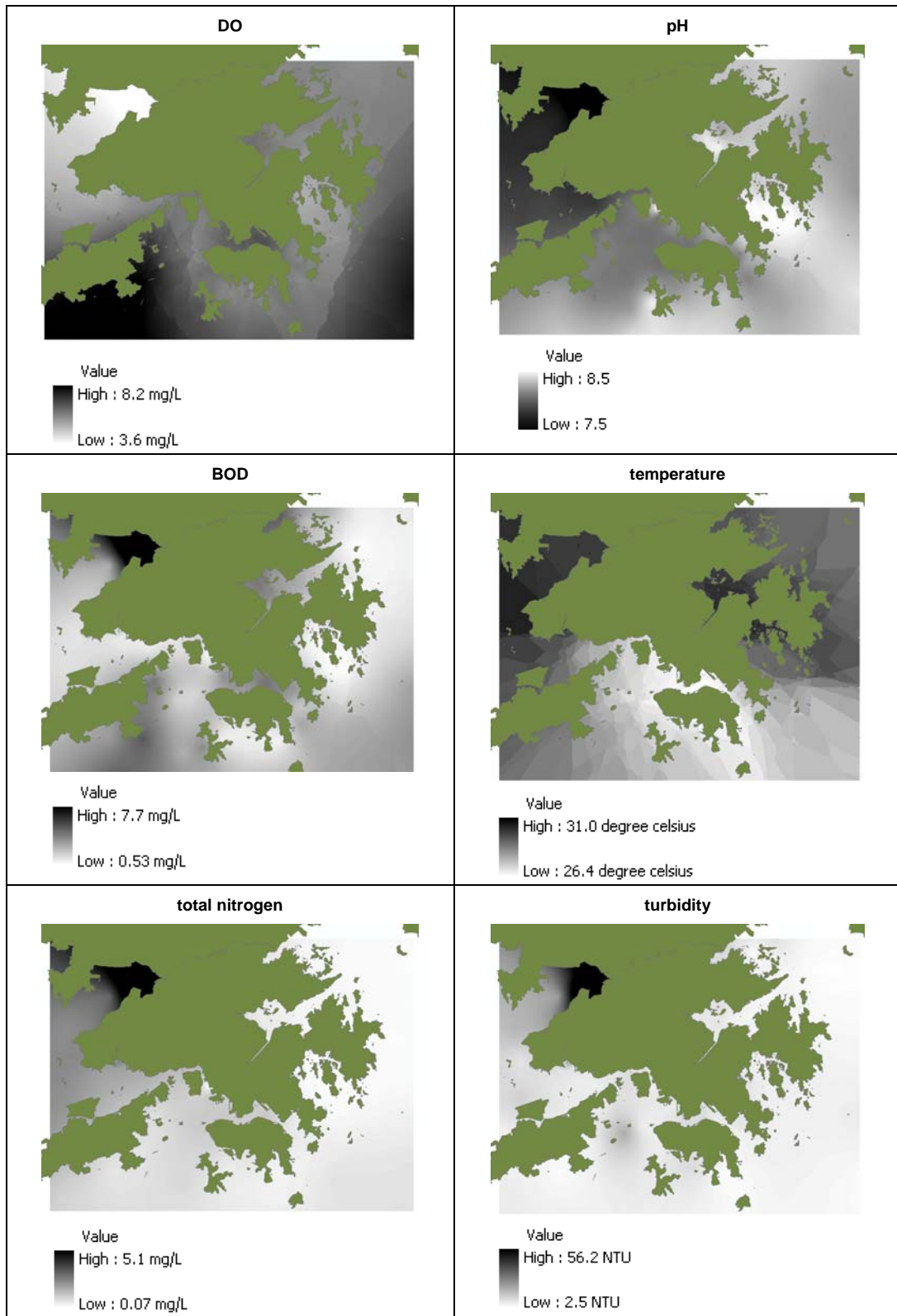


Figure 8.14 Tempo-spatial layers from measurement table WQ2_Water_EPD - August 1, 2003 – depth level: surface.

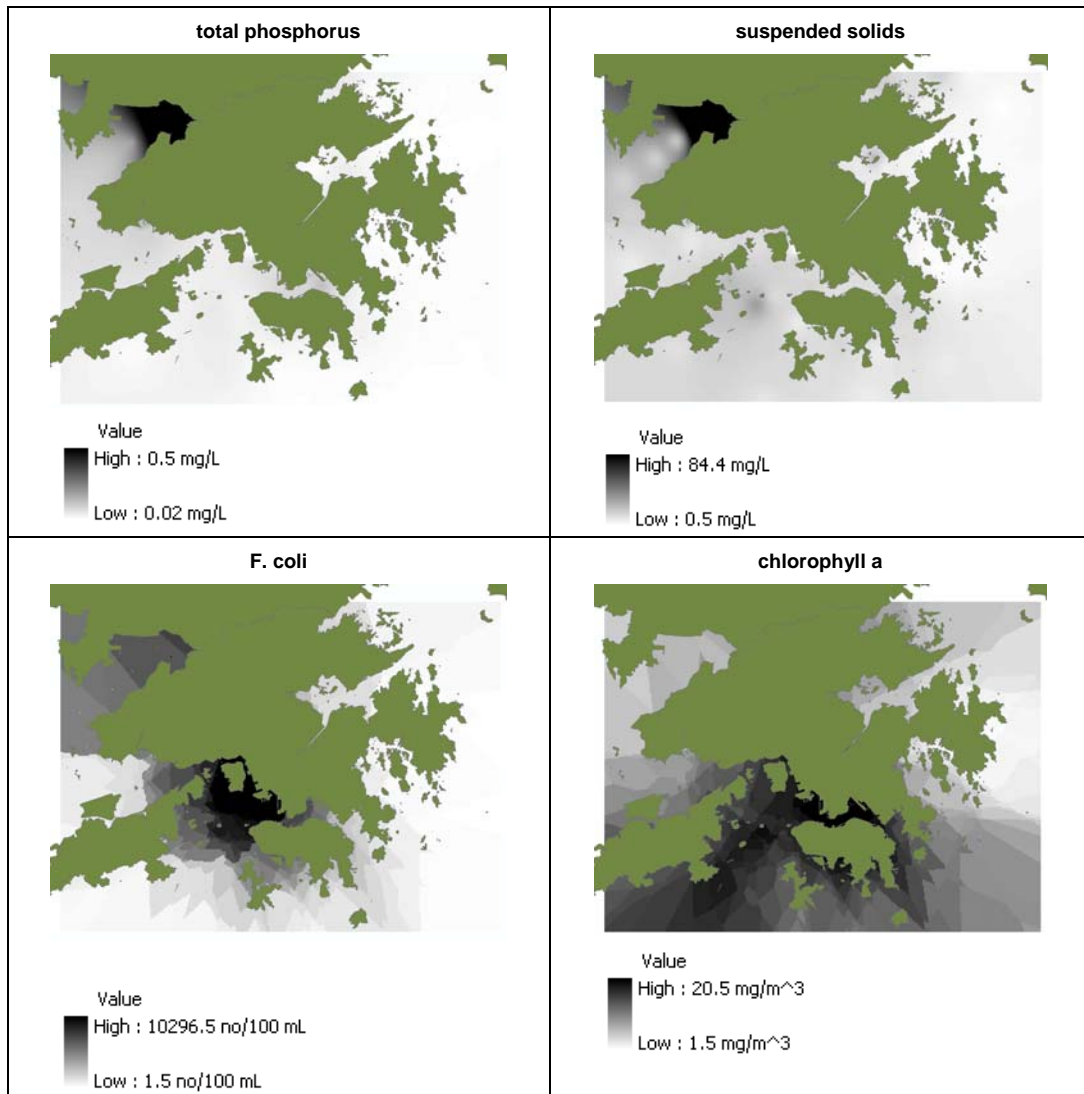


Figure 8.14. Continued.

Figure 8.15 shows the dialog box for creating a WQI spatial layer. The input process involves: 1) selecting the water quality parameters are to be included, their respective rating curve, raster layer, and weight if applicable (i.e. only for weighted arithmetic and geometric mean aggregation functions), and 2) selecting aggregation function type and entering the k value if the Swamee and Tyagi aggregation function is chosen. If *toxics* is selected for analysis, the input of *maximum permissible concentration* is also required. On the right of the dialog box is a display of rating curve in graphic format. The graph displays are included to enhance the user's decisions in selecting the rating curve for each parameter. Furthermore, there is an option to include the raster layers for the water quality sub-index in the output results.

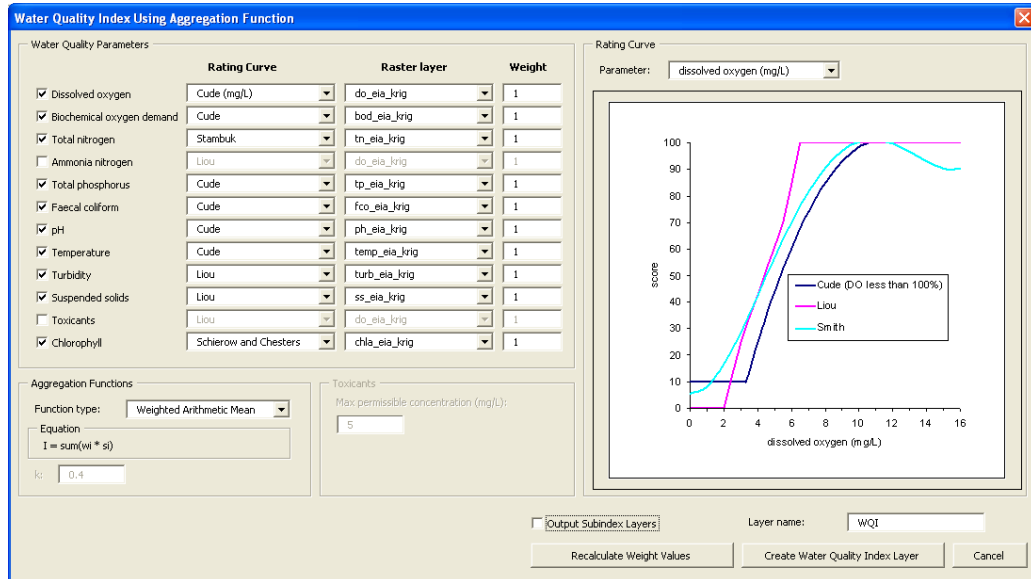


Figure 8.15 Dialog box for creating WQI layer.

In this analysis, all five types of aggregation function are applied for evaluation of WQI layers. For both the weighted arithmetic and geometric mean aggregation functions, equal weighting distribution is used (i.e. there are ten parameters, a weight of 0.1 for each parameter). For the Swamee and Tyagi aggregation function, k is set as the recommended value of 0.4. The selected rating curves for each parameter are summarized in Table 8.4, and the results of the generated WQI layers are shown in Figures 8.16 to 8.20.

Table 8.4 Selected rating curves for sample application.

parameter	rating curve
DO	Smith
BOD	Smith
total nitrogen	Stambuk
total phosphorus	Cude
F. coli	Liou
pH	Smith
temperature	Cude
turbidity	Liou
suspended solids	Liou
chlorophyll a	Schierow and Chesters



Figure 8.16 WQI spatial layer – August 1, 2003 - Weighted Arithmetic Mean.



Figure 8.17 WQI spatial layer - August 1, 2003 - Weighted Geometric Mean.

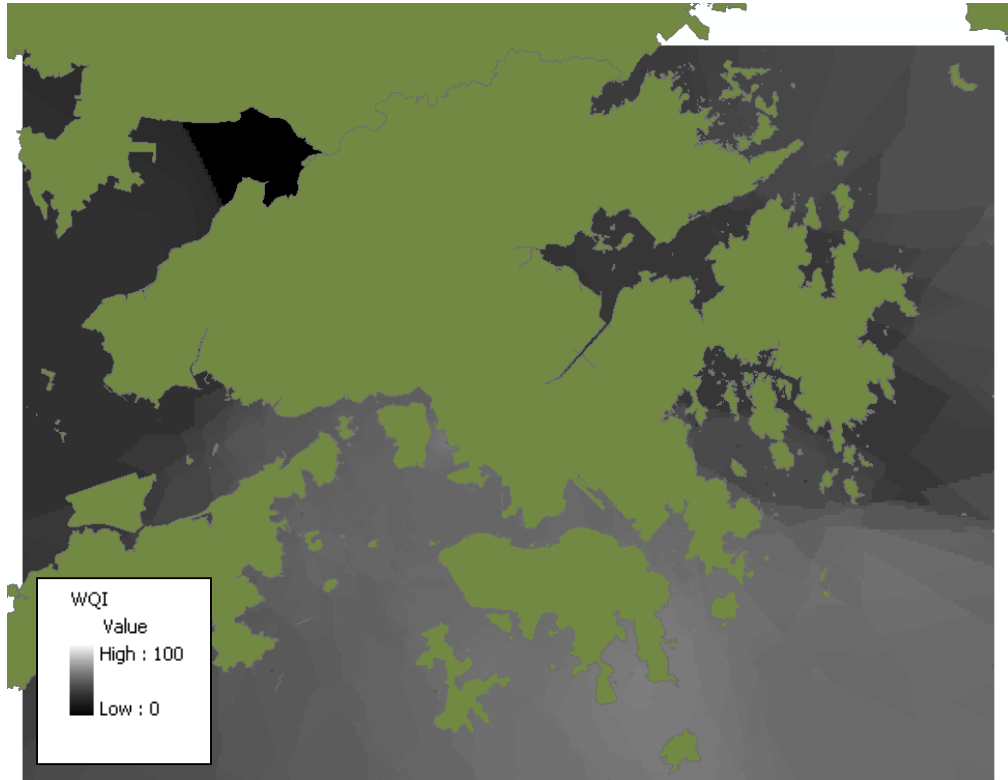


Figure 8.18 WQI spatial layer - - August 1, 2003 - Harmonic Mean of Square.



Figure 8.19 WQI spatial layer - - August 1, 2003 - Minimum Operator.

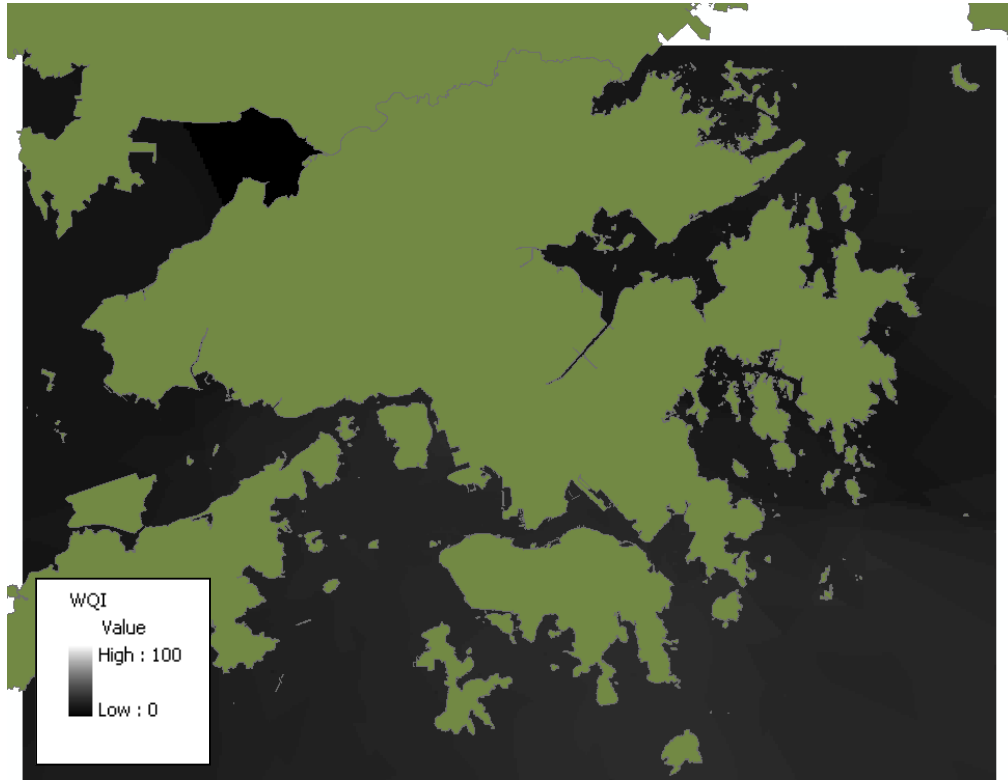


Figure 8.20 WQI spatial layer - - August 1, 2003 - Swamee and Tyagi.

As expected, all five spatial layers indicate relatively lower WQI values at the Deep Bay region. Table 8.5 summarizes the WQI results for different aggregation functions taken at a sample point at the upper end of Deep Bay. Both the weighted arithmetic and geometric mean aggregation functions show a much higher WQI of 37 and 9, respectively, while the other aggregation functions produce near-zero results. The more lenient results generated by the two methods may be due to the eclipsing problem as suggested by Swamee and Tyagi (2000). That is, the aggregation functions' inability to manifest overall poor quality condition from one low subindex value.

Table 8.5 WQI at sample location on upper end of the Deep Bay.

aggregation function	water quality index
weighted arithmetic mean	37
weighted geometric mean	9
harmonic mean of square	0
minimum operator	0
Swamee and Tyagi	0

For other water regions, there are distinct differences in the results generated from different aggregation functions. The weighted arithmetic and geometric mean

aggregation function show a much less severe condition for all other regions. Again, the failure of the aggregation function to capture poor quality condition of any of the parameters may have led to predictions of higher WQI values. The entire region scores relatively low values of WQI for spatial layers created using the minimum operator and Swamee and Tygai (2000) aggregation functions. The results generated by these two methods are governed strongly by the lowest subindex. Finally, despite the ambiguity problem suggested by Swamee and Tyagi (2000), the harmonic mean of square generates the most moderate WQI spatial layer. Within the Deep Bay region, the WQI ranges from 0 to 24, and at other locations, the value is at about 50.

8.3 Assessment of the Relative Importance of Parameters

The subindex layers can be examined to understand the role of each parameter in contributing the overall WQI. As seen in the dialog box as shown in Figure 8.15, the use of the *Output Subindex Layers* checkbox is to instruct the system to include outputting of the subindex spatial layers. The subindex spatial layers shown in Figure 8.21 to 8.30 are created based on the same sample application from the previous section.

It can be seen from examining these subindex spatial layers that the severe water quality conditions in Deep Bay are resulted from low values of the subindex of a wide range parameters, including DO, BOD, total nitrogen, total phosphorus, F. coli, temperature, turbidity, suspended solids, and chlorophyll a. This diversity of involved parameters does not come by surprise, as water quality variables are mutually dependent in affecting the overall condition. For other water regions, the major contributing parameters are total nitrogen and temperature. A notable point is the uniform distribution of high values of subindex in the temperature spatial layer. This may be due to the inappropriateness of applying the Cude temperature rating curve for Hong Kong waters. Since the Cude temperature rating curve has originally been designed for the Oregon's streams with lower median water temperature, its application for Hong Kong waters may predict relatively higher subindex values.

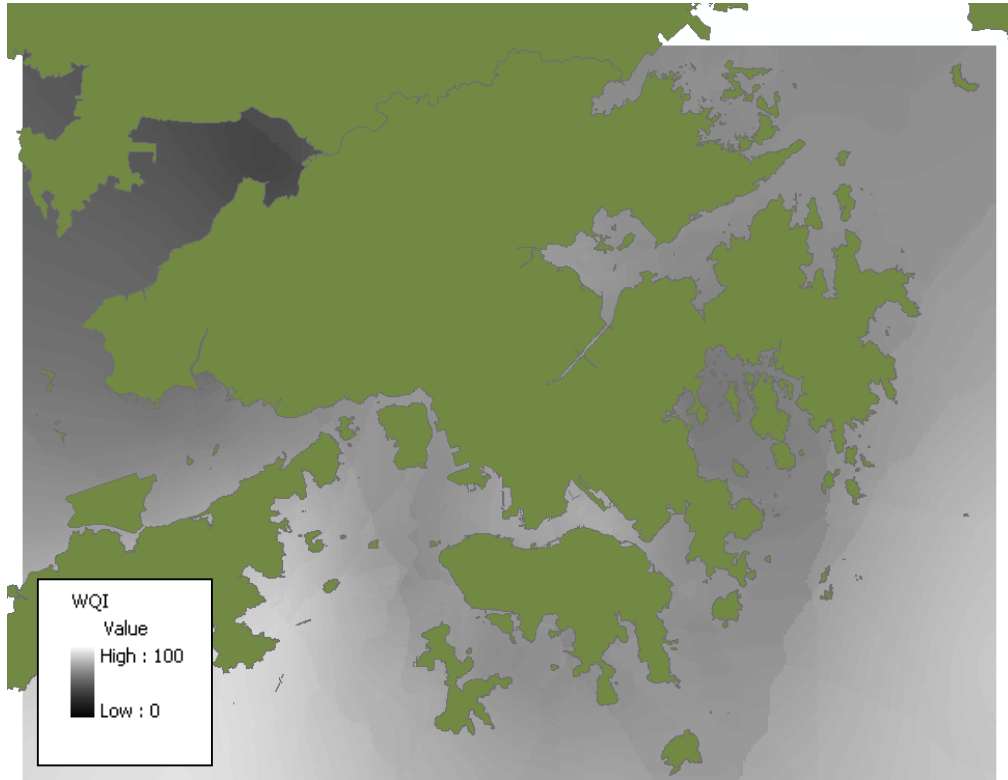


Figure 8.21 Water quality subindex spatial layer – August 1, 2003 – DO.



Figure 8.22 Water quality subindex spatial layer – August 1, 2003 – BOD.

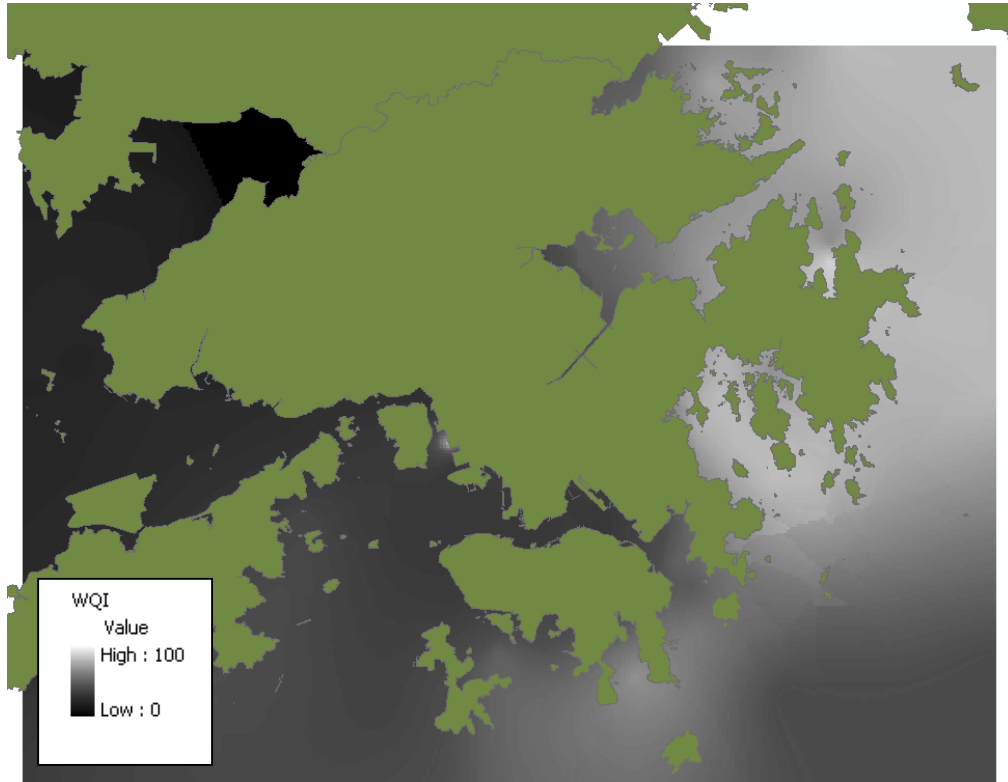


Figure 8.23 Water quality subindex spatial layer – August 1, 2003 – total nitrogen.



Figure 8.24 Water quality subindex spatial layer – August 1, 2003 – total phosphorus.



Figure 8.25 Water quality subindex spatial layer – August 1, 2003 – F. coli.



Figure 8.26 Water quality subindex spatial layer – August 1, 2003 – pH.

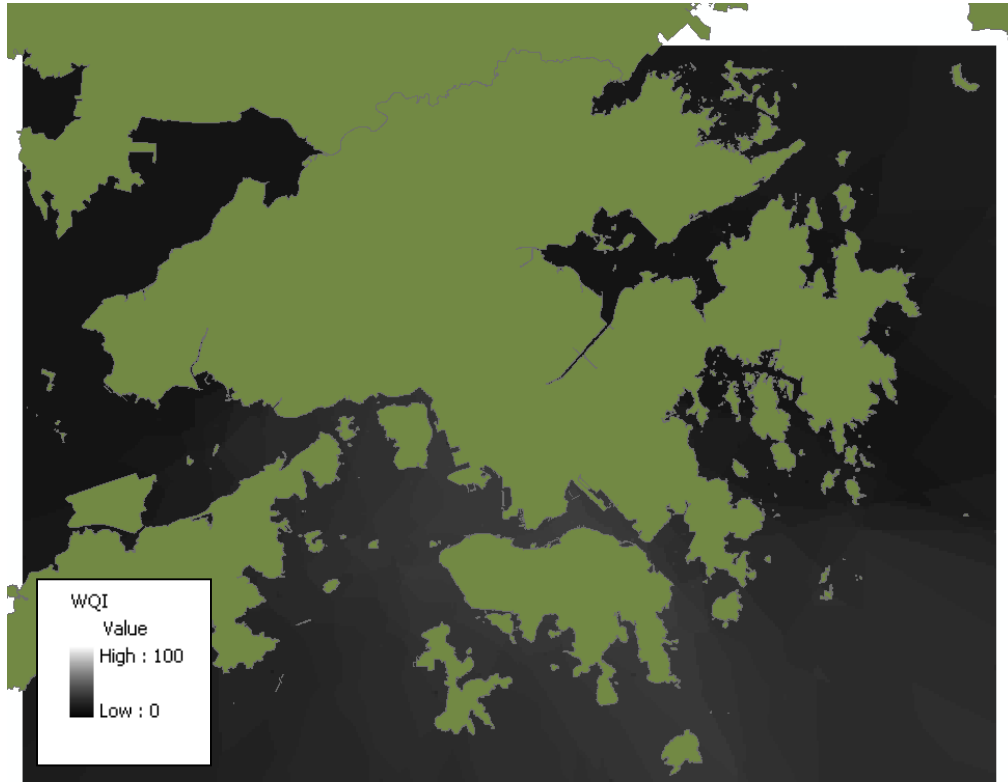


Figure 8.27 Water quality subindex spatial layer – August 1, 2003 – temperature.



Figure 8.28 Water quality subindex spatial layer – August 1, 2003 – turbidity.



Figure 8.29 Water quality subindex spatial layer – August 1, 2003 – suspended solids.



Figure 8.30 Water quality subindex spatial layer – August 1, 2003 – chlorophyll a.

8.4 Investigation of Temporal Patterns and Trends

To investigate the long-term temporal patterns and trends of the overall water quality of the Hong Kong waters, WQI spatial layers at different points in time can be generated and compared. In this example, two WQI spatial layers is created for each year from 1998 to 2003, one for the dry season (i.e. on February 1) and the other for the wet season (i.e. on August 1). The same rating curves from the sample application described in Section 8.2 are applied (see Table 8.4), and the harmonic mean of square aggregation function is used. The results are shown in Figures 8.31 to 8.44.

The results of the WQI spatial layers give little clear indication of the yearly variation of water quality. However, a significant difference between wet and dry seasons for all years is observed. Poor water quality condition is observed primarily within Deep Bay during the dry season, while the rest of the region has average quality at that time. Notably the entire Hong Kong waters has a low index value for the wet season.

To gain a more explicit understanding of the yearly change in water quality, numerical values are extracted from the WQI layers at several selected fixed stations. (see Figure 8.45). The extracted values are summarized in Tables 8.6 and 8.7 and are shown in graphical formats in Figures 8.46 and 8.47. All stations except DM2 indicate steady improvement in water quality during the dry season. The WQI increases continually from 50 in 1998 to greater than 80 in 2003. But, for wet season, most stations show variations of WQI between 20 and 60 from year to year. The WQI at station DM2 has kept almost constant at 0 during the six-year period for both wet and dry season, complying with the severely poor water quality condition at Deep Bay.



Figure 8.31 WQI spatial layer – February 1, 1998 – Harmonic Mean of Square.



Figure 8.32 WQI spatial layer – August 1, 1998 – Harmonic Mean of Square.

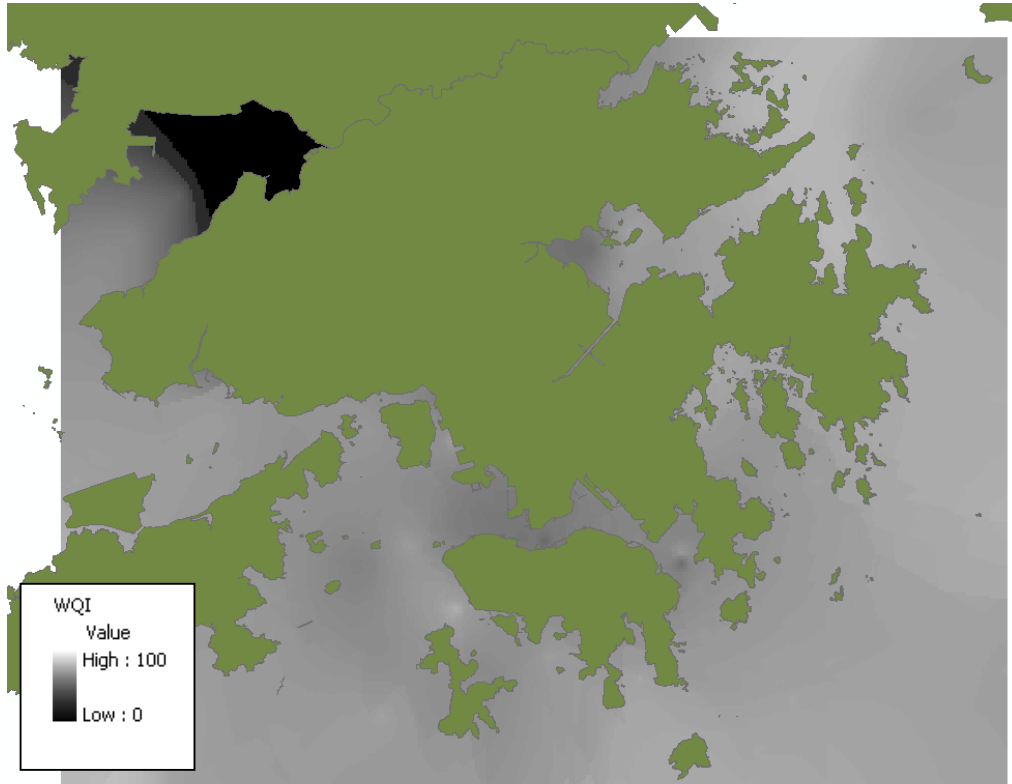


Figure 8.33 WQI spatial layer – February 1, 1999 – Harmonic Mean of Square.

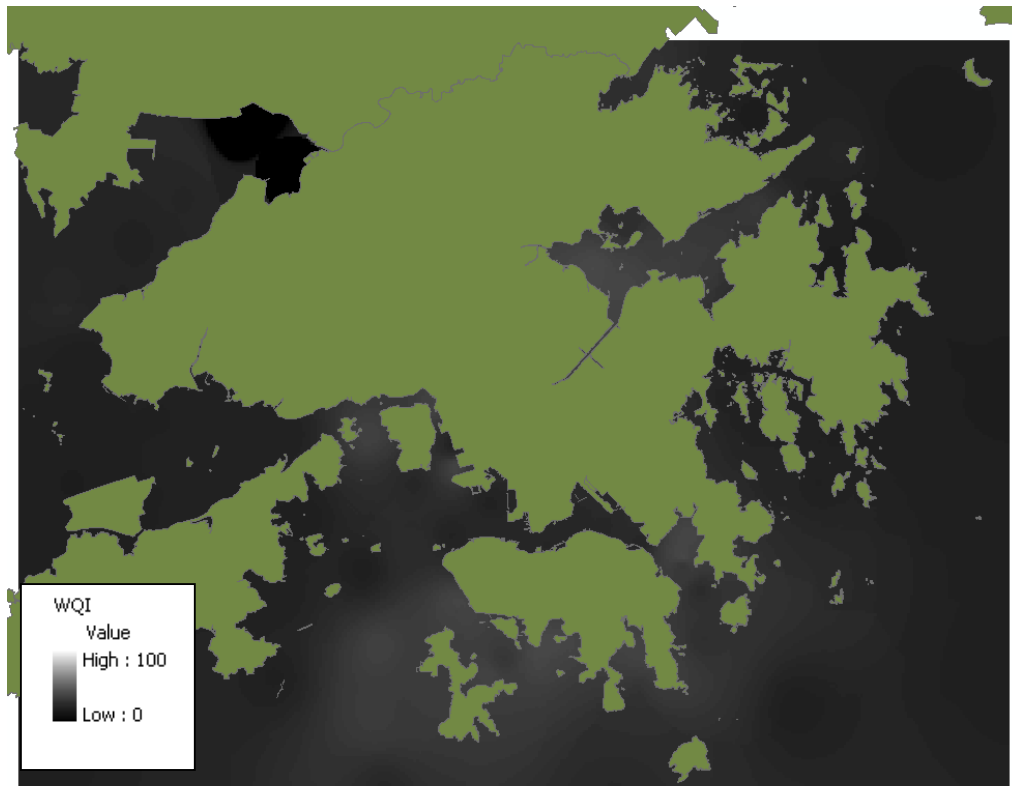


Figure 8.34 WQI spatial layer – August 1, 1999 – Harmonic Mean of Square.

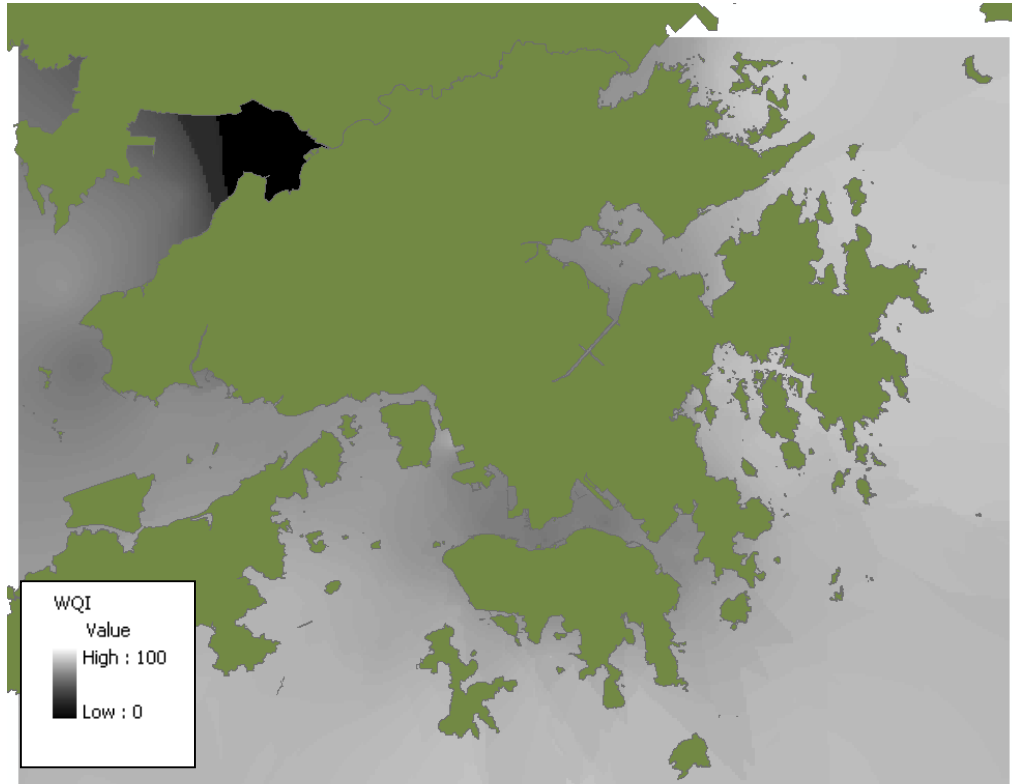


Figure 8.35 WQI spatial layer – February 1, 2000 – Harmonic Mean of Square.

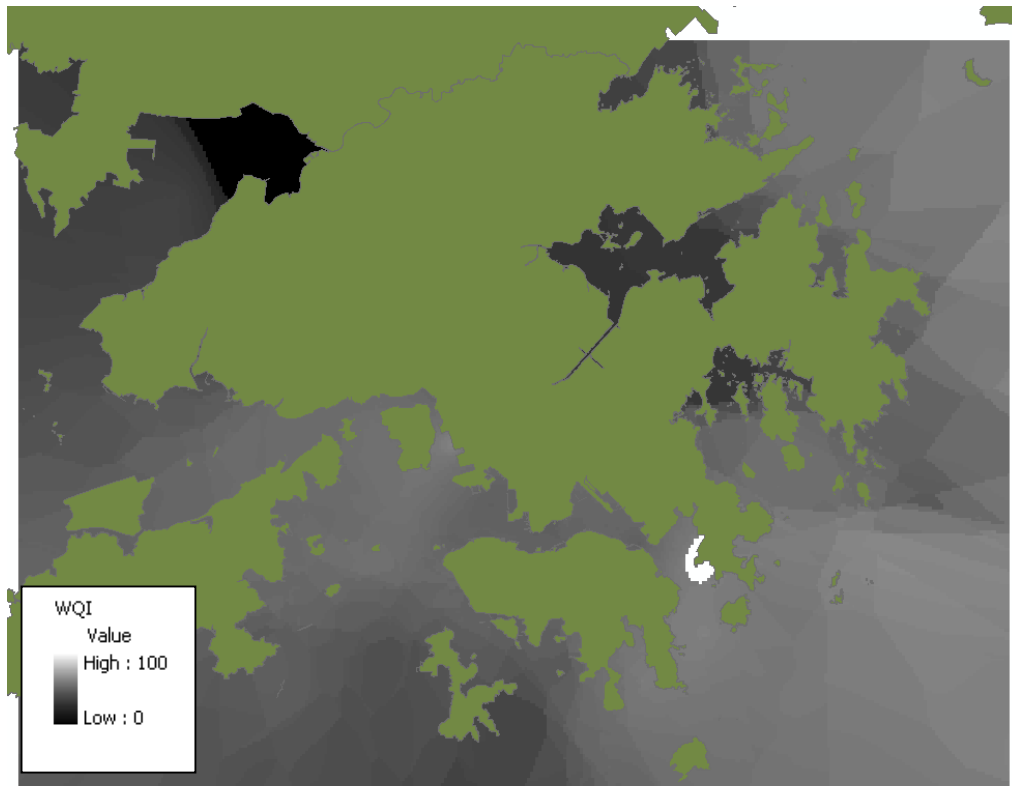


Figure 8.36 WQI spatial layer – August 1, 2000 – Harmonic Mean of Square.

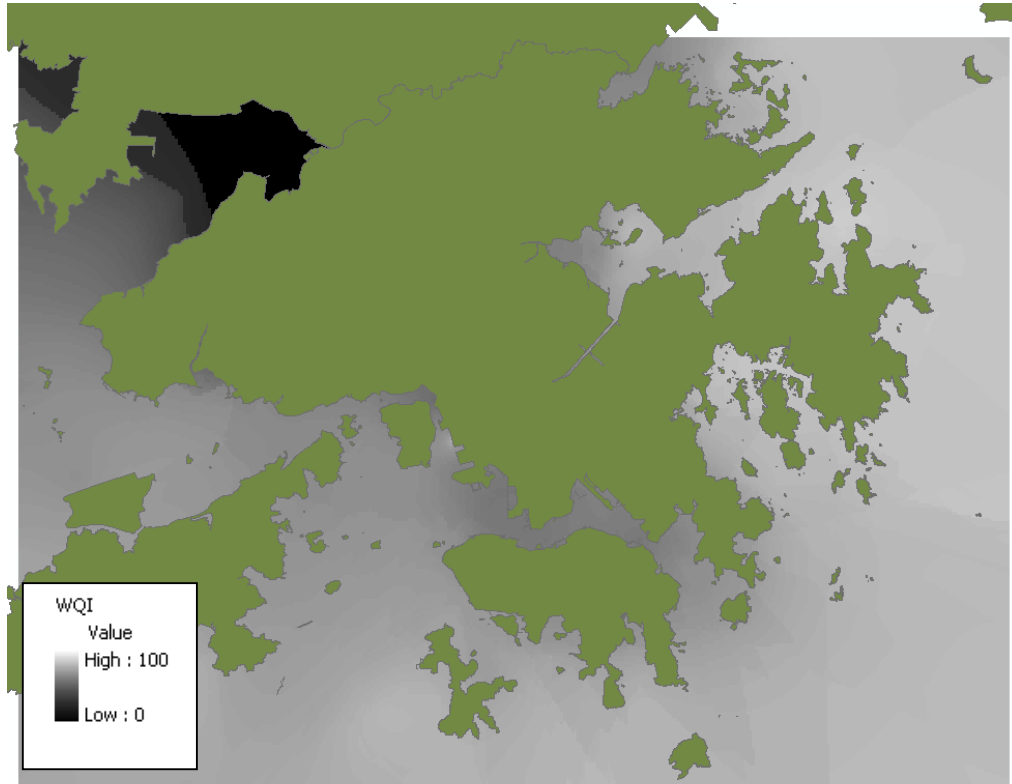


Figure 8.37 WQI spatial layer – February 1, 2000 – Harmonic Mean of Square.

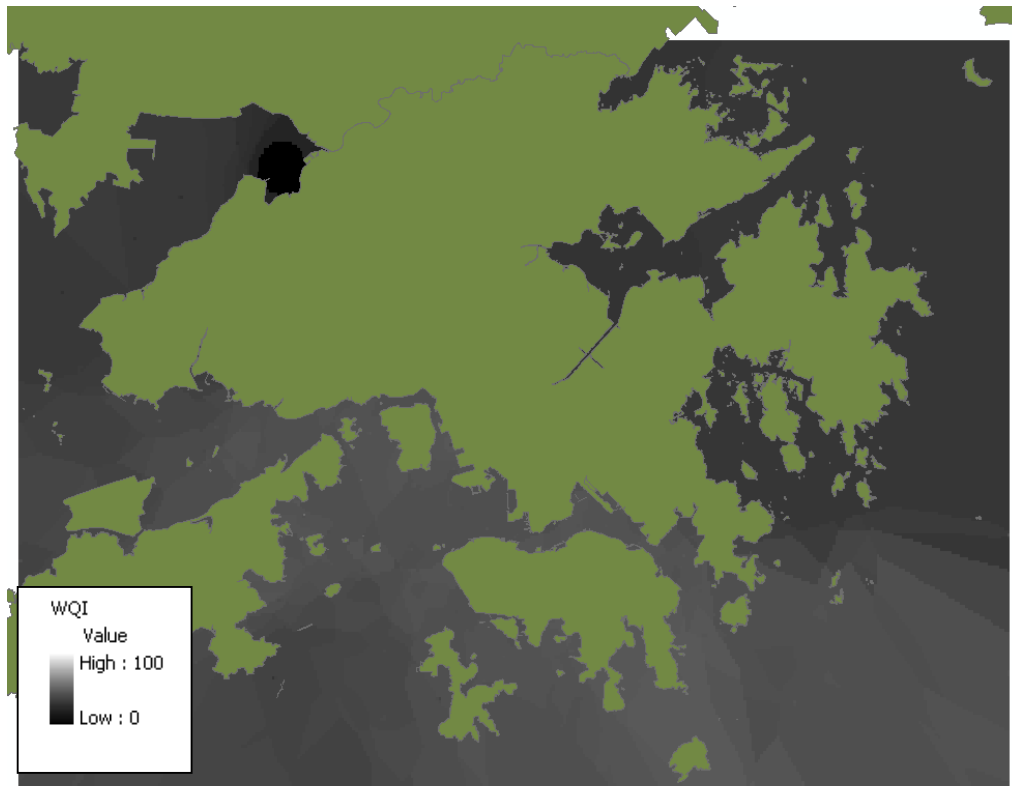


Figure 8.38 WQI spatial layer – August 1, 2000 – Harmonic Mean of Square.

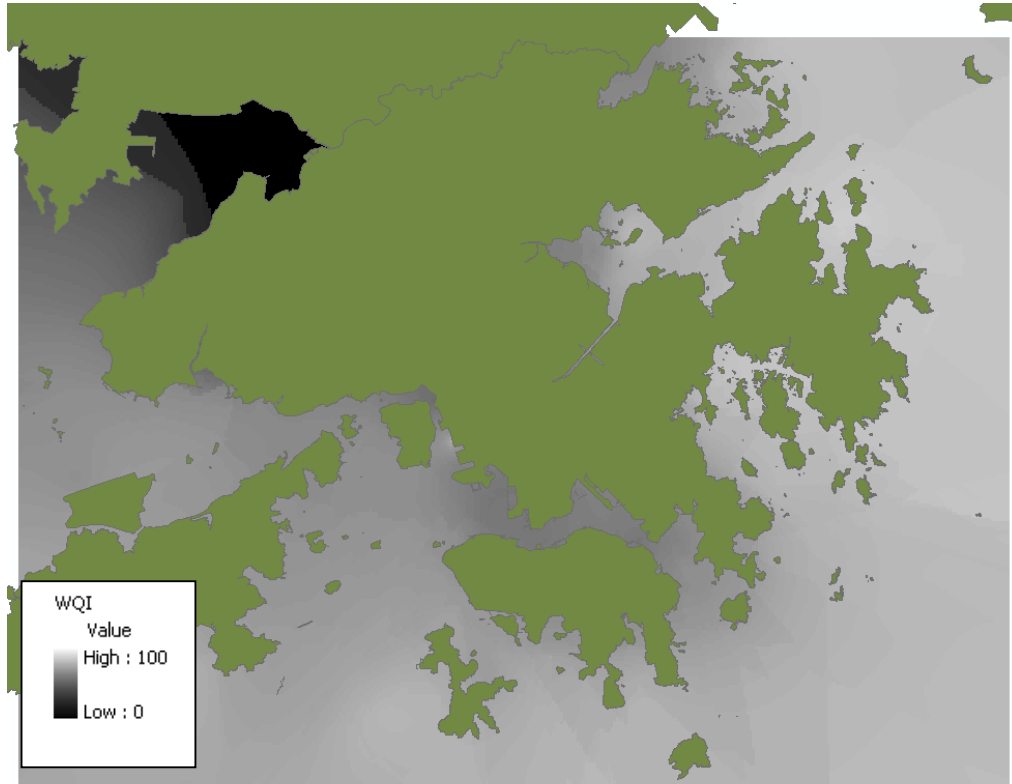


Figure 8.39 WQI spatial layer – February 1, 2001 – Harmonic Mean of Square.

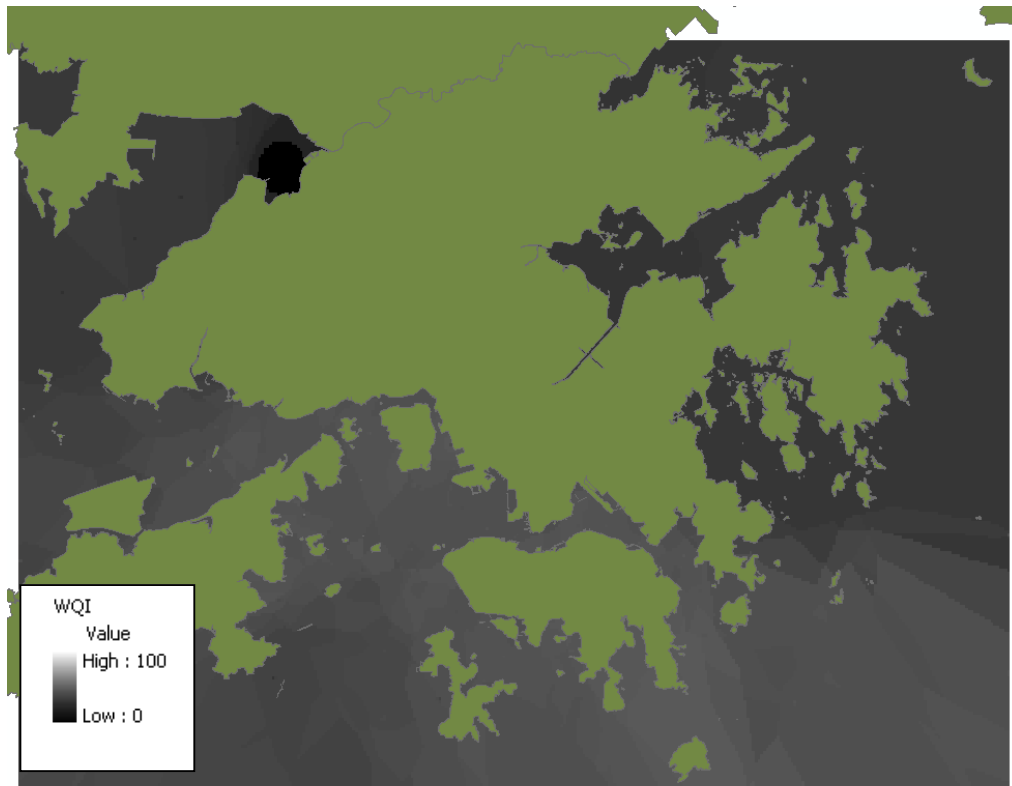


Figure 8.40 WQI spatial layer – August 1, 2001 – Harmonic Mean of Square.

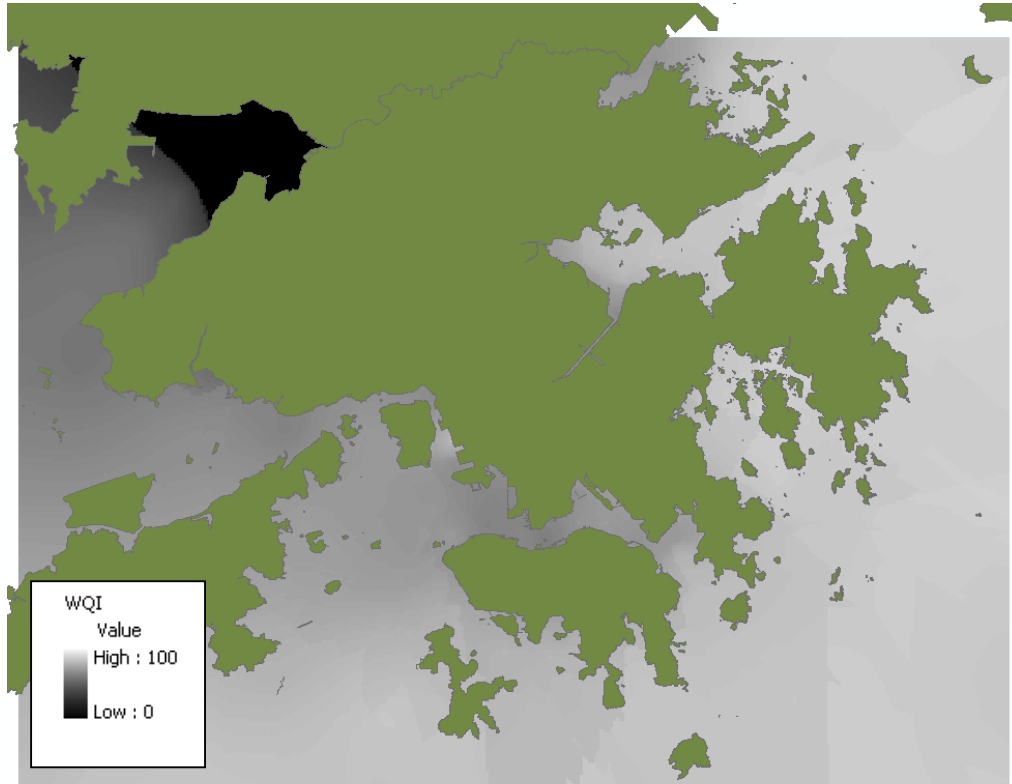


Figure 8.41 WQI spatial layer – February 1, 2002 – Harmonic Mean of Square.

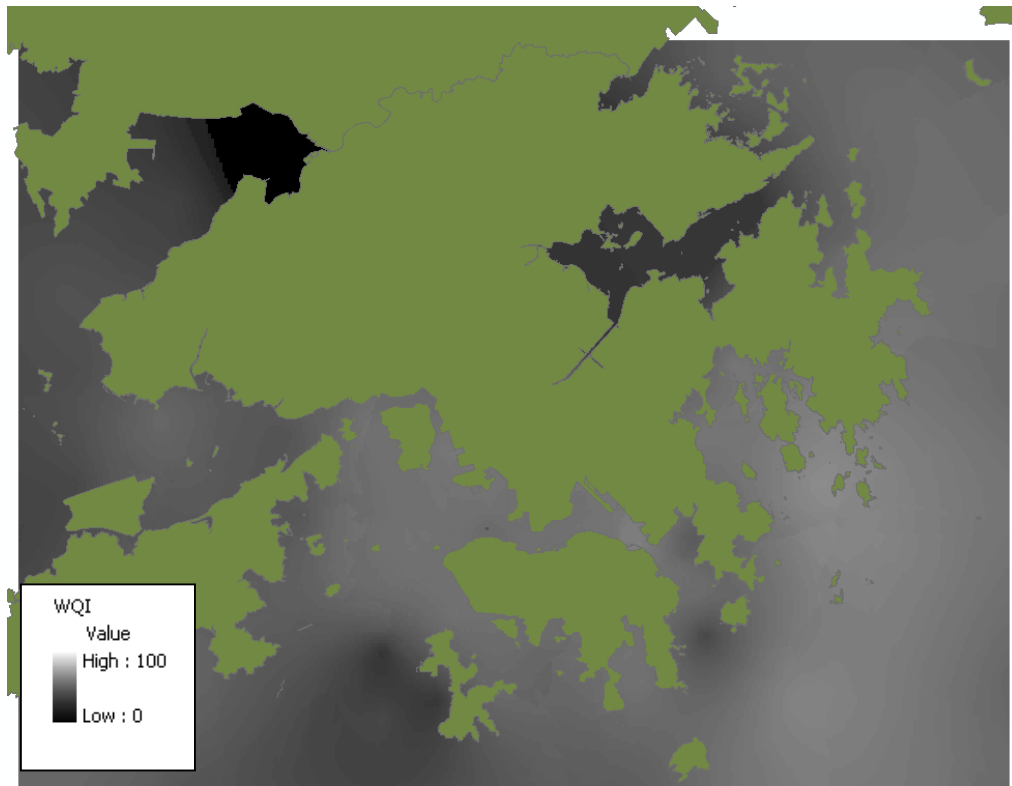


Figure 8.42 WQI spatial layer – August 1, 2002 – Harmonic Mean of Square.



Figure 8.43 WQI spatial layer – February 1, 2003 – Harmonic Mean of Square.

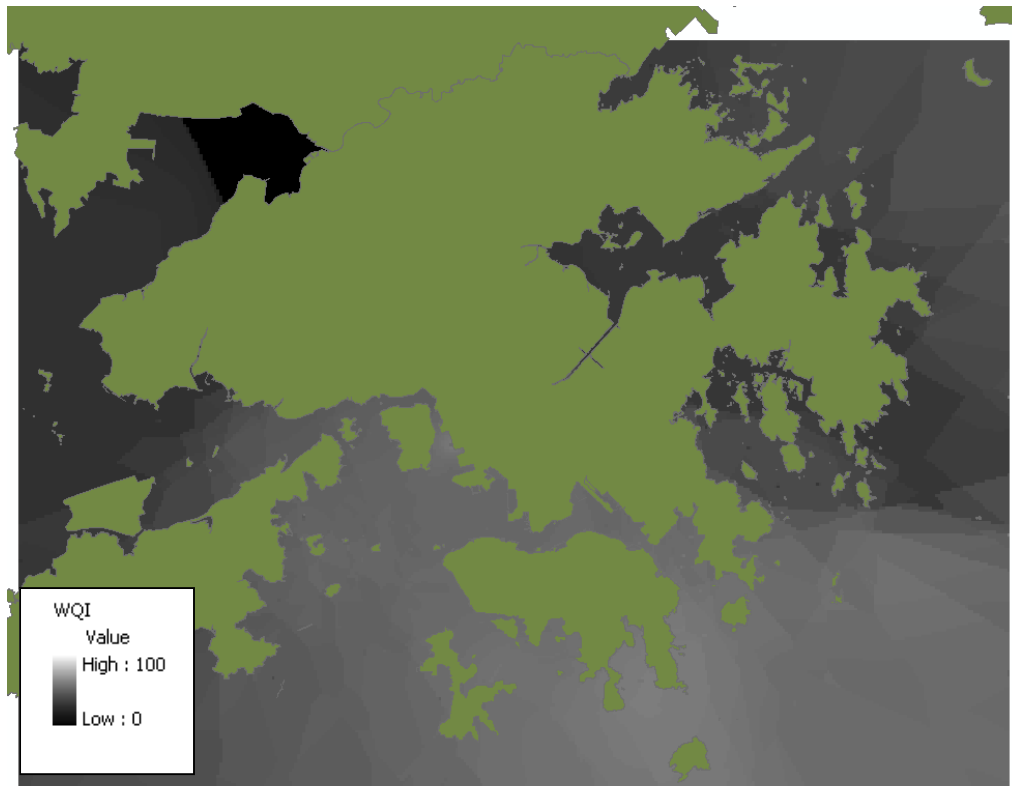


Figure 8.44 WQI spatial layer – August 1, 2003 – Harmonic Mean of Square.



Figure 8.45 Selected fixed stations for extracting values from WQI layers.

Table 8.6 WQI at selected fixed stations for dry season.

	DM2	NM2	SM12	WM3	SM3	TM6	PM8	MM8	MM14	MM5
2/1/1998	0	51	57	52	57	57	61	58	60	56
2/1/1999	0	71	69	64	67	69	70	73	76	71
2/1/2000	0	66	78	68	75	68	81	80	80	82
2/1/2001	0	67	71	65	72	75	80	78	81	81
2/1/2002	0	65	77	68	78	84	86	84	86	86
2/1/2003	0	72	78	67	80	80	88	84	86	84

Table 8.7 WQI at selected fixed stations for dry season.

	DM2	NM2	SM12	WM3	SM3	TM6	PM8	MM8	MM14	MM5
8/1/1998	0	31	48	49	49	50	30	51	53	28
8/1/1999	0	19	17	21	30	33	20	16	17	15
8/1/2000	0	51	48	56	46	29	54	58	61	59
8/1/2001	28	40	2	43	43	29	29	43	33	29
8/1/2002	0	46	44	55	53	29	60	62	56	54
8/1/2003	0	37	39	51	55	29	38	54	48	39

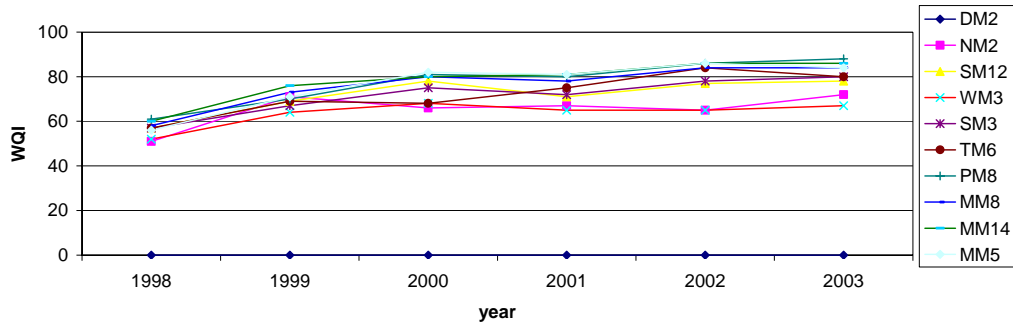


Figure 8.46 WQI at selected fixed stations for dry season (February 1).

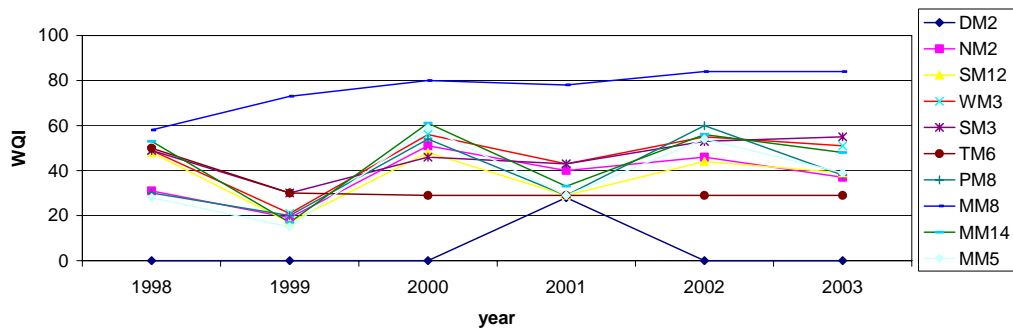


Figure 8.47 WQI at selected fixed stations for dry season (August 1).

8.5 Prediction of Future Hydrodynamics and Water Quality

The applications of the EIA module demonstrated in the previous sections are all based on historical data. The evaluation of WQI layer can further be extended using data generated from the numerical model. Creating WQI layers from predicted results can provide insights in the future water quality conditions in the PRE under different management scenarios and thus enhance decision-making in wastewater disposal. However, so far, the model is only capable of predicting two physical water quality parameters, namely, suspended solids and temperature. The model should be enhanced in the future to include the prediction of more water quality variables.

8.6 Summary

This chapter has discussed the third component of the integrated-GIS, an EIA module for water quality evaluation. The EIA module is developed based primarily on the concept of WQI, which combines a selected set of measured parameters into a single unitless value for water quality evaluation. Spatial layers, generated either from field or

model data, can be applied using the *Map Algebra* techniques to create a WQI spatial layer. Applying this EIA module with a dataset for Hong Kong waters, the four approaches for conducting EIA has been examined:

1. **Identification of areas most vulnerable to environmental impact.** The created WQI spatial layer allows the examination of water quality in spatial context. The results derived from the five different aggregation functions – weighted arithmetic mean, weighted geometric mean, harmonic mean of square, minimum operator, and Swamee and Tyagi (2000) – all have shown that Deep Bay is the area of the most significant environmental concerns.
2. **Assessment of the relative importance of parameters.** The EIA module also allows the inclusion of the subindex spatial layers as part of the output. It is found from examining the subindex spatial layers that a diversified range of parameters, including DO, BOD, total nitrogen, total phosphorus, E. coli, temperature, turbidity, suspended solids, and chlorophyll a, contributes the poor water quality condition at Deep Bay.
3. **Investigation of temporal patterns and trends.** The EIA module is further applied to investigate the long-term trend of WQI from 1998 to 2003, using the harmonic mean of square aggregation function. The generated results show a significant difference in the WQI spatial layers between the wet and dry seasons. During the dry season, the poor water quality condition is confined within Deep Bay, but in general, the water quality is improving steadily from year by year. For the wet season, the WQI for the entire Hong Kong waters is maintained at low values between 20 and 60.
4. **Prediction of future hydrodynamics and water quality.** While sample applications for the first three EIA approaches are carried out using historical data, the EIA module can be further applied using predicted results. The WQI layers created from model data will give insights into future water quality conditions in the PRE under different situations and thus enhance decision-making in coastal management.

9 Conclusions and Recommendations

9.1 Conclusions

In this study, the overall aim was to develop a GIS for handling coastal hydrodynamic and water quality information of the PRE, and thus to promote better management of this environmental concerning coastal water region. The system structure was based upon three main components, namely, data, model, and EIA. The following summarizes the main contributions of this project categorized under these three main components:

1. Data

- Hydrodynamic and water quality data were gathered and stored into a GIS database using MS Access software. The compilation of a GIS database not only enables efficient data querying and maintenance, but also allows the establishment of a direct linkage with the GIS for spatial display.
- A database metadata management framework utilizing object variables for defining data sources, datasets, and measurement tables and associated properties was implemented. This gives flexibility to add more data into the GIS database in the future.

- Though the advent of GIS technology undoubtedly has provided new ground for retrieval and display of spatial information, the 2D and static entity of GIS has asserted a great challenge for exploration of the 3D, dynamic marine regime. The developed data visualization techniques overcame this difficulty by supplementing the time series, profile, section, as well as dynamic displays.
- Another challenge of applying GIS technology in coastal environment is the typically sparsely-distribution of collected data in both space and time. To tackle this problem, interpolation functions - tempo-spatial and profile-spatial interpolation – combining spatial and 1D data-fitting techniques were incorporated into the system.

2. Model

- The GIS was coupled with a hydrodynamic-water quality numerical model using the *interface integration* method. This enables pre-processing and post-processing procedures to be carried out entirely within the GIS user interface.
- A separate database for storage of model input was compiled for the development of the pre-processing component. As for the database for field data, the compilation of a model input database was to facilitate a connection between the two systems. The developed modules for retrieval, editing, and display of model input not only saves time in preparation of input files, but has also linked field data for model input.
- A programming routine for model mesh grid was developed as part of the model pre-processing component. This module not only facilitates the generation of shapefiles resembling the mesh grid arrangement, but also allows minor adjustments to be made through the GIS interface window.
- The post-processing component included the development of a module for converting text-based files into DBF format. The attachment of DBF files to the GIS is demonstrated to be effective in maintaining performance of the system.
- The data visualization tools (i.e. spatial layer, time series, and profile displays) for model input and result were designed analogously to those for field data. Furthermore, the profile and section, and dynamic interactive display tools are equally applicable for visualization of model input and results.

3. EIA

- An EIA tool based on the concept of WQI and application of *Map Algebra* was implemented for evaluation of water quality. This module, for combining spatial layers of various water quality parameters into a single spatial layer of WQI, is targeted to provide a generalized index for water quality conditions. A wide selection of parameter rating curves and aggregation functions taken from the literature were incorporated into this module.
- A sample application using the EIA tool was carried out to evaluate the spatial and temporal trends of water quality in Hong Kong. It was found that Deep Bay has been suffering the worst water quality conditions over the past years, while other water regions indicated steady increases in WQI. The results suggested that the water quality problem in Deep Bay is largely caused by a number of parameters.

In conclusion, the newly developed integrated-GIS – PRE_WAGIS – is demonstrated as being an effective and versatile for coastal management, research, and decision-making. The system possesses a robust yet flexible structure. Each of the three components can be operated independently, yet together they act as an integrated whole for more inextricable analyses. There is a definable sense of parallelism in retrieval and display of field data, model input, and results, which enhances ease of usage of the user interface. Possible component-independent applications of the integrated system include estimation of values at unknown points in space and time, evaluation of the interpolation methods, and investigation of temporal and spatial trends. The bridging of field and model data supports interoperability of information for applications such as assessing quality of collected data, calibrating and verifying hydrodynamic model, and setting boundary conditions. Finally, the EIA module provides a straightforward approach for assessing environmental water quality impacts.

9.2 Recommendations

Whilst the work done in this thesis has established a solid framework for an integrated-GIS, additions and modifications can be made in a number of areas to improve system functionality:

- The collected data thus far are limited to text-based information. Remote sensing images could be acquired and added into the system. This will be useful for verification of field data, evaluation of the interpolated results, as well as

approximation of values outside survey regions. The types of remote sensing images that may be applicable in evaluating water quality parameters include microwave wavelengths, ultraviolet, infrared, and thermal. For example, it has been shown that suspended sediment and chlorophyll are correlated with the radiance of combinations of wave bands, while temperature can be detected using thermal remote sensing (Ritchie and Schiebe, 2000).

- Interactive tools were developed to support dynamic visualization of horizontal spatial layer as well as section display. The system methods for development of these two tools could be further applied for creating a dynamic section display. This will enhance the understanding of vertical movement of specified parameters in temporal context.
- There has been tremendous difficulty in acquiring coastal data in the China water regions due to China's strict policy on disclosure of information. Therefore, most data collected are limited to the Hong Kong waters. As China progressively opens up its informational barrier with the outside world, more field data could be obtained and placed into the system. This doubtlessly will deepen our understanding and enhance better management of the severe water quality conditions at the PRE.
- Since the hydrodynamic-water quality coupled model focuses primarily on solving physical processes in coastal environments, it is only capable of predicting various parameters such as suspended solids, metal concentration, and salinity. While the natural marine system is also controlled by chemical and biological processes, modification could be made to the model for predictions of other water quality parameters. This modification is essential to provide a comprehensive water quality overview based on predictive results.
- In the EIA module for water quality evaluation, the scoring of WQI is based principally on rating curves intended for other water bodies around the world. Though these rating curves offer approximate evaluation of WQI, their location-sensitiveness may not produce results for an accurate representation of the water quality conditions at the PRE. Therefore, the development of water quality rating curves for the Hong Kong or PRE regions is recommended.
- Instead of limiting the integrated-GIS to a single research sector, the software could be put forward for sharing with the other domains. The most effective and

convenient approach to achieve this would be by means of the World Wide Web. The ESRI offers a number of products for implementation of GIS on the internet. Future research may include selection of suitable software and studies to carry out the actual customization procedure. The final product of this internet-based GIS will not only facilitate efficient distribution of coastal information among environmental and engineering professionals, but will also increase the awareness of the general public of the coastal water issues in the PRE.

References

- Applied Science Associates, Inc. (2003a). COASTMAP Globally Re-locatable Integrated Coastal Ocean Monitoring and Modelling System. Retrieved November 1, 2004, from <http://www.coastmap.com/about.htm>
- Applied Science Associates, Inc. (2003b). HYDROMAP Hydrodynamic Modeling System. Retrieved November 1, 2004, from the World Wide Web: <http://www.appsci.com/hydromap/hydromap.htm>
- Applied Science Associates, Inc. (2003c). Suspended Sediment Exposure Model: SSDOSE. Retrieved November 1, 2004, from the World Wide Web: <http://www.appsci.com/ssdose/ssdose.htm>
- Applied Science Associates, Inc. (2003d). Suspended Sediment Exposure Model: SSFATE. Retrieved November 1, 2004, from the World Wide Web: <http://www.appsci.com/ssfate/ssfate.htm>
- Applied Science Associates, Inc. (2003e). WAVEMAP. Retrieved November 1, 2004, from the World Wide Web: <http://www.appsci.com/wavemap/wavemap.htm>
- Applied Science Associates, Inc. (2003f). WPMAP Water Quality Management and Analysis Package. Retrieved November 1, 2004, from the World Wide Web: <http://www.coastmap.com/about.htm>
- Bartlett, D. J. (1999). Working on the Frontiers of Science: Applying GIS to the Coastal Zone. In D. J. Wright, and D. J. Bartlett (Eds.), *Marine and Coastal Geographical Information Systems* (pp. 11-24). Philadelphia: Taylor & Francis.
- Bergamasco, A., De, N. L., Flindt, M. R., and Amos, C. L. (2003). Interactions and feedbacks among phytobenthos, hydrodynamics, nutrient cycling and sediment transport in estuarine ecosystems. *Continental Shelf Research*, 23, 1715-1741.
- Bernhardsen, T. (2002). *Geographic information systems: an introduction*. New York: John Wiley & Sons.
- Bhargava, D. S. (1983). Use of a water quality index for river classification and zoning of the Ganga River. *Environmental Pollution (Series B)*, 6, 51-67.
- Booth, B., and Environmental Systems Research Institute (2000). *Using ArcGIS 3D Analyst: GIS by ESRI*. Redlands, California: Environmental Systems Research.
- Boyd, C. E. (2000). *Water quality: an introduction*. Boston, Mass: Kluwer Academic Publishers.
- Burke, R. (2003). *Getting to Know ArcObjects: Programming ArcGIS with VBA*. Redlands, California: ESRI Press.
- Caeiro, S., Marco, P., Geoovaerts, P., Helena, C., and Sousa, S. (2003). Spatial sampling design for sediment quality assessment in estuaries. *Environmental Modelling & Software*, 18, 853-859.

- Chang, K. T. (2005). *Programming ArcObjects with VBA: a task-oriented approach*. Boca Raton, Florida: CRC Press.
- Chapman, D. (1996). *Water quality assessments: a guide to the use of biota, sediments, and water in environmental monitoring* (2nd ed.). London, New York: E&FN Spon.
- Chappell, D. (1996). *Understanding ActiveX and OLE*. Redmond, Washington: Microsoft Press.
- Chapra, S. C. (1997). *Surface water-quality modelling*. New York: McGraw-Hill.
- Chen, J. C., and Heinke, G. W. (2001). Pearl River Estuary Pollution Project Summary Report, Hong Kong University of Science and Technology.
- Chen, J. C., Lee, O. C. W., and Chan, W. M. (1999). Pearl River Estuary Pollution Project (PREPP) – An Integrated Approach. In *Proceedings of the 6th International Conference of Estuarine and Coastal Modelling*. New Orleans, USA.
- Clark, K. C. (2001). *Getting started with geographic information systems*. New Jersey, Upper Saddle River: Prentice Hall.
- Cude, C. (2001). Oregon water quality index: A tool for evaluating water quality management effectiveness. *Journal of American Water Resources Association*, 37, 125-137.
- Danish Hydraulic Institute (DHI). What is MIKE INFO Coast. Retrieved November 1, 2004, from <http://www.dhisoftware.com/mikeinfo/Description/index.htm>
- Delaney, J. (1999). *Geographical information systems: an introduction*. South Melbourne: Oxford University Press.
- Demers, M. N. (2000). *Fundamentals of geographic information systems*. New York: John Wiley & Sons.
- Dinius, S. H. (1987). Design of an index of water quality. *Water Resources Bulletin*, 23, 833-843.
- Environmental Modelling System, Incorporated. SMS 9.0 Overview. Retrieved June 14, 2006, from http://www.ems-i.com/SMS/SMS_Overview/sms_overview.html
- Environmental Protection Department (2003). *Marine water quality in Hong Kong in 2003*. Environmental Protection Department, Hong Kong.
- Environmental Systems Research Institute, Inc. (1995). *Understanding GIS: the ARC/INFO method: self-study workbook*. Redlands, California: Environmental Systems Research Institute, Inc.
- Environmental Systems Research Institute (2006, May 25). ArcView – Desktop GIS for Mapping, Data Integration, and Analysis. Retrieved June 14, 2006, from <http://www.esri.com/software/arcgis/arcview/index.html>
- French, D. P., and Reed, M. (1996). Integrated Environmental Impact Model and GIS for Oil and Chemical Spills. In M. F. Goodchild, L. T. Steyaert, B. O. Parks, C.

- Johnston, D. Maidment, M. Crane, and S. Glendinning (Eds.), *GIS and Environmental Modeling: Progress and Research Issues* (pp. 197-198). Fort Collins: GIS World Books.
- Goodwin, H., and Palerud, R. (2003). Arctic Coastal and Marine Environment Monitoring". In D. R. Green, and S. D. King (Eds.), *Coastal and Marine Geo-Information Systems: Applying the Technology to the Environment* (pp. 163-171). Boston: Kluwer Academic Publishers.
- Hartnett, M., and Nash, S. (2004). Modelling nutrient and chlorophyll a dynamics in an Irish brackish waterbody. *Environmental Modelling & Software*, 19, 47-56.
- Institute for the Environmental (IENV), the Hong Kong University of Science and Technology (HKUST) (2005). Pearl River Estuary Pollution Project.. Retrieved June 14, 2006, from <http://ccar.ust.hk/projects/PREPP/PREPP.html>
- Ip, S. F., and Wai, H. G. (1990). *Application of harmonic method to tidal analysis and prediction in Hong Kong*. Hong Kong: Hong Kong Royal Observatory.
- Jannasch, H. W., Honeyman, B. D., Balistrieri, L. S., and Murray, J. W. (1998). Kinetic of trace element uptake by marine particles. *Geochimica et Cosmochimica Acta*, 52, 567-577.
- Jiang, Y. (2003). *Three-dimensional numerical modelling of sediment and heavy metal transport in surface waters*. Unpublished PhD thesis, The Hong Kong Polytechnic University, Hong Kong, SAR China.
- Jiang, Y. W., Wai, O. W. H., Hong, H. S., and Li, Y. S. (2004). A Geographic Information System for Marine Management and its Application to Xiamen Bay, China. *Coastal Research*, 43, 254-264.
- Johnston, K., and Environmental Systems Research Institute (2001). *Using ArcGIS Geostatistical Analyst: GIS by ESRI*. Redlands, California: Environmental Systems Research Institute.
- Klee, G. A. (1999). *The coastal environment: toward integrated and marine sanctuary management*. New Jersey, Upper Saddle River: Prentice Hall.
- Lancaster, P., and Šalkauskas, K (1986). *Curve and surface: an introduction*. Academic Press, London.
- Li, Y., Brimicombe, A. J., and Ralphs, M. P. (2000). Spatial data quality and sensitivity analysis in GIS and environmental modelling: the case of coastal oil spills. *Computers, Environment and Urban Systems*, 24, 95-108.
- Liou, S. M., Lo, S. L., and Wang, S. H. (2004). *A generalised water quality index for Taiwan*. *Environmental Monitoring and Assessment*, 96, 35-52.
- Lucas, A. (2000). Representation of Variability in Marine Environmental Data. In D. J. Wright, and D. J. Bartlett (Eds.), *Marine and Coastal Geographical Information Systems* (pp. 53-74). Philadelphia: Taylor & Francis.
- Marsilli-Libelli, S., Caporali, E., Arrighi, S., and Becattelli, C. (2001). A georeferenced river quality model. *Water Science and Technology*, 43(7), 223-230.

- McCoy, J., and Johnston, K. (2001). *Using ArcGIS Spatial Analyst: GIS by ESRI*. Redlands, California: Environmental Systems Research Institute.
- Mellor, G. L., Oey, L. Y., and Ezer, T. (1998). Sigma coordinate pressure gradient errors and the seamount problem. *Journal of Atmospheric and Oceanic Technology*, 15, 1122-1131.
- Mellor, G. L., and Yamada, T. (1982). Development of a turbulence closure model for geophysical fluid problems. *Reviews of Geophysics and Space Physics*, 20(4), 851-875.
- Naoum, S., Tsanis, I. K., and Fullarton, M. (2003). A GIS pre-processor for pollutant transport modelling. *Environmental Modeling & Software*, 20, 55-68.
- Novalis, S. (1997). *Access 97 Macro & VBA Handbook*. San Francisco, California: Sybex.
- O'Brien, T. M., Pogge, S. J., and White, G. E. (1997). *Microsoft Access 97 Developer's Handbook*. Redmond, Washington: Microsoft Press.
- Pinho, J. L. S., Pereira Vieira, J. M., and Antunes do Carmo, J. S. (2004). Hydroinformatic environment for coastal waters hydrodynamics and water quality modelling. *Advances in Engineering Software*, 35, 205-222.
- Prati, L., Pavanello, R., and Pesarin, F. (1971). Assessment of surface water quality by a single index of pollution. *Water Research*, 5, 714-751.
- Press, W. H., Teukolsky, S. A., Vetterling, W. T., and Flannery, B. P. (1992) *Numerical Recipes in Fortran 77 The Art of Scientific Computing* (2nd ed.). Cambridge: Cambridge University Press.
- Puopolo, J. P. (1997). *Writing OLE controls: a practical and comprehensive approach*. New Jersey, Upper Saddle River: Prentice Hall PTR.
- Razavi, A. H. (2002). *ArcGIS Developer's Guide for VBA*. Clifton Park, New York: Thomson/Delmar Learning.
- Ritchie, J. C., and Schiebe, F. R.. (2000). Water Quality. In G. A. Schultz and E. T. Engman (Eds.), *Remote Sensing in Hydrology and Water Management* (pp. 287-303). Berlin: Springer.
- Robinson, C., and Simpson, A. (2001). *Mastering Access 2002*. San Francisco, California: Sybex.
- Runca, E., Bernstein, A., Postma, L., and Di Silvio, G. (1996). Control of macroalgae blooms in the Lagoon of Venice. *Ocean and Coastal Management*, 30(2-3), pp. 235-257.
- Schierow, L., and Chesters, G. (1988). Evaluation of the great lakes nearshore index. *Water Research*, 22, 269-277.
- Shamsi, U. M. (2002). *GIS Tools for Water, Wastewater and Stormwater System*. Reston: American Society of Civil Engineer.
- Silvia, F. P., and Daniel A. W. (2000). Use of water quality indices to verify the impact of cordoba city (argentina) on suquia river. *Water Research*, 34, 2915-2926.

- Smith, D. G. (1990). A better water quality indexing system for rivers and streams. *Water Research*, 24, 1237-1244.
- Stambuk-Giljanovic, N. (1999). Water quality evaluation by index in Dalmatia. *Water Research*, 33, 3423-3440.
- Swamee, P. K., and Tyagi, A. (2000). Describing water quality with aggregate index. *Journal of Environmental Engineering*, 126(5), 451 – 455.
- The Hong Kong Government (2005). Hong Kong Yearbook 2004. Retrieved November 1, 2005, from http://www.info.gov.hk/yearbook/2004/en/14_09.htm
- Tsanis, I. K., and Boyle S. (2001). A 2D Hydrodynamic/ Pollutant Transport GIS Model. *Advances in Engineering Software*, 32, 353-361.
- Tsanis, I. K., Noaum, S., and Fullarton, M. (2002). Coastal Modelling with a GIS Bathymetric Module. *Global Nest: The International Journal*, 4(1), 51-73.
- U.S. Environmental Protection Agency (2004a). BASINS. Retrieved November 1, 2004, from <http://www.epa.gov/waterscience/basins/basinsv3.htm>
- U.S. Environmental Protection Agency (2004b). AQUATOX. Retrieved November 1, 2004, from <http://www.epa.gov/waterscience/models/aquatox/about.html>
- Wai, O. W. H. *Sediment Transport in the Pearl River Estuary*. The Hong Kong Polytechnic University Department of Civil and Structural Engineering Retrieved June 14, 2006, from <http://www.cse.polyu.edu.hk/lab/PRE/SEDIMENT.htm>
- Wai, O. W. H., and Lu, Q. (2000). An efficient parallel model for coastal transport process simulation. *Advances in Water Resources*, 23, 747-764.
- Water Resources Environmental Information Systems Laboratory, Department of Civil Engineering, McMaster University. IDOR2D – A GIS Based Hydrodynamic Pollutant Transport Simulation Model. Retrieved November 1, 2004, from <http://www.eng.mcmaster.ca/water/pages/idor2d.html>
- Wright, D. J., and Goodchild, M. F. (1997). Data from the deep: implications for the GIS community. *International Journal of Geographical Information Science*, 11(6), 523-528.
- Yalin, M. S. (1977). *Mechanics of sediment transport*. Oxford: Pergamon.
- Zeiler, M. (2001). *Exploring ArcObjects: GIS by ESRI*. Redlands, California: Environmental Systems Research Institute.